CR 73276

AVAILABLE TO THE PUBLIC

BOEING

COMMERCIAL AIRPLANE DIVISION

AN ANALYSIS OF METHODS FOR PREDICTING THE STABILITY CHARACTERISTICS OF AN ELASTIC AIRPLANE

APPENDIX C
METHODS FOR PREDICTING STABILITY AND RESPONSE CHARACTERISTICS

By

Members of the Aerodynamics
and Structures Research Organizations

D6-20659-4

November 1968

Prepared Under Contract No. NAS 2-3662 by

The Boeing Company
Commercial Airplane Division
P. O. Box 707
Renton, Washington

for

AMES RESEARCH CENTER
NATIONAL AERONAUTICS AND SPACE ADMINISTRATION

TABLE OF CONTENTS

		Page
1.	INTRODUCTION	1
2.	SYMBOLS	6
3.	ASSUMPTIONS	20
4.	STATIC STABILITY CHARACTERISTICS	24
	4.1 Introduction	24
	4.2 Elevator and Stabilizer Trim Angles	29
	4.3 Stick-Speed Stability	33
	4.4 Longitudinal Control Per g	38
	4.5 Neutral and Maneuver Points	40
5.	DYNAMIC STABILITY ANALYSIS METHODS	45
	5.1 Introduction	45
	5.2 Roots of Characteristic Equations	45
	5.3 Time Histories	66
6.	DISCUSSION OF DYNAMIC STABILITY ANALYSIS RESULTS	75
	6.1 Introduction	75
	6.2 Longitudinal Dynamic Stability Characteristics	75
	6.3 Lateral-Directional Dynamic Stability Characteristics	100
7.	PARAMETRIC STUDIES	121
	7.1 Relative Importance of Rigid and Equivalent Elastic Derivatives	121
	7.2 Importance of Various Elastic Effects for Completely Elastic Airplane Mathematical Models	131
8.	SUPPORTING DATA AND RELATED MATERIAL	13.
	8.1 Introduction	133
	8.2 Rigid and Equivalent Elastic Stability Derivatives, Coefficients, and Inertial Properties	133
	8.3 Static Stability Data	187
	8.4 Rigid and Equivalent Elastic Longitudinal Dynamic Stability Data	200
	8.5 Rigid and Equivalent Elastic Lateral-Directional Dynamic Stability Data	219
	8.6 Parametric Study Data	233
9.	COMPLETELY ELASTIC AIRPLANE ANALYSIS	254
	9.1 Introduction	254
	9.2 707-320B Analysis	254
	9.3 SST Analysis	277

TABLE OF CONTENTS (Continued)

		Page
10.	CONCLUSIONS AND RECOMMENDATIONS	283
	10.1 Conclusions	283
	10.2 Recommendations	285
11.	REFERENCES	287

FIGURES

Figure	Title	Page
1	Boeing 707-320B General Arrangement	3
2	Typical SST General Arrangement	4
3	Effect of Mass Distribution on Elastic Neutral Point Shift — 72° SST	28
4	Trim Elevator, Rigid and Equivalent Elastic Airplanes — 707-320B	31
5	Trim Elevator, Rigid and Equivalent Elastic Airplanes — 30° SST	32
6	Stick-Speed Stability — 707-320B	35
7	Stick-Speed Stability — 707-320B	36
8	$d\delta E/dV$ Change in Elevator Angle with Velocity, Rigid versus Elastic Elastic Airplanes — 72° SST	37
9	Elevator Angle per g, $d\delta E/dn$ — 707-320B	41
10	Elastic Elevator Angle per g, $d\delta E/dn$ — 707-320B	42
11	Static Margin, Rigid versus Equivalent Elastic Airplanes	44
12	Applications of Dynamic Stability Criteria	46
13	Short Period Frequency and Damping, Rigid Airplane — 707-320B	78
14	Short Period Frequency and Damping, Rigid Airplane — 72° SST	79
15	Short Period Frequency for Rigid, Equivalent Elastic, and Completely Elastic Airplanes — SST	81
16	Short Period Damping for Rigid, Equivalent Elastic, and Completely Elastic Airplanes — SST	83
17	Variation of Short Period Frequency with Number of Modes — 30° and 42° SST	84
18	Variation of Short Period Frequency with Number of Modes — 72° SST	85
19	Variation of Short Period Damping with Number of Modes — 30° and 42° SST	86
20	Variation of Short Period Damping with Number of Modes — 72° SST	87
21	Typical Visual Display of Structural Mode Shape — Second Mode	89
22	Typical Visual Display of Structural Mode Shape — Fourth Mode	90
23	Variation of Short Period Frequency and Damping with Number of Elastic Modes — 707-320	91
24	Variation of Short Period Frequency and Damping with Number of Elastic Modes — 707-320	92

FIGURES (Continued)

Figure	Title	Page
25	Preliminary-Design-Type Data versus "Best" Well-Defined Elastic Model — 707-320B	93
26	Longitudinal Response to One Degree Out of Trim — 72° SST	96
27	Longitudinal Response — 707-320B	98
28	Longitudinal Response — 707-320B	99
29	Longitudinal Response, Lifting Surface Theory — 707-320B	101
30	Dutch Roll Damping, Rigid Airplane — 707-320B	102
31	Dutch Roll Frequency, Rigid Airplane — 707-320B	103
32	Dutch Roll Frequency and Damping, Rigid Airplane — 72° SST	104
33	Dutch Roll Damping Factor — 707-320B	106
34	Dutch Roll	107
35	Dutch Roll $\lvert \phi/\beta \rvert$ — 707-320B	108
36	Dutch Roll and Lateral Phugoid Frequency — 707-320B	110
37	Dutch Roll and Lateral Phugoid Damping — 707-320B	111
38	Dutch Roll Period and Damping, Rigid and Equivalent Elastic Airplanes — 72° SST	114
39	Rolling Convergence Mode, Rigid and Equivalent Elastic Airplanes — SST	115
40	Dutch Roll Motion Sideslip Angle, Rigid and Equivalent Elastic Airplanes — 707-320B	117
41	Dutch Roll Motion, Yaw and Roll Angles, Rigid and Equivalent Elastic Airplanes — 707-320B	118
42	Dutch Roll Motion, Structural Dynamic Analysis — 707-320B	120
43	Changes in Short Period Mode Characteristics Due to Variation in $C_{m_{\dot{\alpha}}}$ — 707-320B	125
44	Changes in Short Period Damping Due to Variations in $C_{m_{\dot{\alpha}}}$ — 30° and 42° SST	126
45	Changes in Short Period Damping Due to Variations in $C_{m_{\dot{\alpha}}}$ — 72° SST	127
46	Changes in Short Period Mode Due to Center-of-Gravity Shifts — 707-320B	128
47	Changes in Short Period Frequency Due to Center-of-Gravity Shifts and Dynamic Pressure — SST	129
48	Changes in Short Period Damping Due to Center-of-Gravity Shifts and Dynamic Pressure — SST	130
49	Comparison of Methods for Trim Elevator — 707-320B	188

FIGURES (Continued)

Figure	Title	Page
50	Comparison of Methods for Trim Elevator — 30° and 42° SST	189
51	Comparison of Methods for Trim Elevator — 72° SST	190
52	Comparison of Methods for Stick-Speed Stability — 707-320B and 30° SST	191
53	Comparison of Methods for Stick-Speed Stability — 42° and 72° SST	192
54	Comparison of Methods for Elevator Angle per g — 707-320B	193
55	Comparison of Methods for Elevator Angle per g — 30° and 42° SST	194
56	Comparison of Methods for Elevator Angle per g — 72° SST	195
57	Comparison of Methods for Neutral Point, Maneuver Point, and Static Margin — 707-320B	196
58	Comparison of Methods for Neutral Point, Maneuver Point, and Static Margin — 30° SST	197
59	Comparison of Methods for Neutral Point, Maneuver Point, and Static Margin — 42° SST	198
60	Comparison of Methods for Neutral Point, Maneuver Point, and Static Margin — 72° SST	199
61	Longitudinal Short Period Frequency Versus Damping — 707-320B	201
62	Longitudinal Short Period P_{SP}, $T_{1/2}$ and $C_{1/2}$ — 707-320B	202
63	Longitudinal Phugoid Frequency Versus Damping — 707-320B	203
64	Longitudinal Phugoid $T1/_2$ and T_2 — 707-320B	204
65	Longitudinal Phugoid P, $C_{1/_2}$, and C_2 — 707-320B	205
66	Longitudinal Short Period Frequency Versus Damping — 30° and 42° SST	206
67	Longitudinal Short Period Frequency Versus Damping — 72° SST	207
68	Longitudinal Short Period, Period — 30° and 42° SST	208
69	Longitudinal Short Period, Period — 72° SST	209
70	Longitudinal Short Period $T_{1/2}$ — 30° and 42° SST	210
71	Longitudinal Short Period $T_{1/2}$ — 72° SST	211
72	Longitudinal Short Period $C_{1/2}$ — SST	212
73	Longitudinal Phugoid Frequency Versus Damping — 30° and 42° SST	213
74	Longitudinal Phugoid Frequency Versus Damping — 72° SST	214

FIGURES (Continued)

Figure	Title	Page
75	Longitudinal Phugoid Period — SST	215
76	Longitudinal Phugoid $T_{1/2}$ and T_2 — 30° and 42° SST	216
77	Longitudinal Phugoid $T_{1/2}$ and T_2 — 72° SST	217
78	Longitudinal Phugoid $C_{1/2}$ and C_2 — 30° and 72° SST	218
79	Dutch Roll Frequency and Damping — 707-320B	220
80	Dutch Roll Period, $T_{1/2}$ and T_2 — 707-320B	221
81	Dutch Roll $C_{1/2}$ and C_2 — 707-320B	222
82	Rolling Convergence Roots and $T_{1/2}$ — 707-320B	223
83	Spiral Mode Roots and $T_{1/2}$ — 707-320B	224
84	Dutch Roll Frequency and Damping — SST	225
85	Dutch Roll Period — SST	226
86	Dutch Roll $T_{1/2}$ and T_2 — SST	227
87	Dutch Roll $C_{1/2}$ and C_2 — SST	228
88	Spiral Mode Roots — SST	229
89	Spiral Mode $T_{1/2}$ and T_2 — SST	230
90	Rolling Convergence Mode Roots — SST	231
91	Rolling Convergence Mode $T_{1/2}$ — SST	232
92	Changes in Short Period Mode Characteristics Due to Variations in $C_{m_{\dot{\alpha}}}$ — 707-320B	234
93	Changes in Phugoid Mode Characteristics Due to Variations in $C_{m_{\dot{\alpha}}}$ — 707-320B	235
94	Changes in Short Period Frequency Due to Varia ions in $C_{m_{\dot{\alpha}}}$ — SST	236
95	Changes in Short Period Damping Due to Variations in $C_{m_{\dot{\alpha}}}$ — 30° and 42° SST	237
96	Changes in Short Period Damping Due to Variations in $C_{m_{\dot{\alpha}}}$ — 72° SST	238
97	Changes in Real Root Due to Variations in $C_{m_{\dot{\alpha}}}$ — 30° and 42° SST	239
98	Changes in Phugoid Frequency Due to Variations in $C_{m_{\dot{\alpha}}}$ — 72° SST	240
99	Changes in Real Root Due to Variations in $C_{m_{\dot{\alpha}}}$ — 30° and 42° SST	241
100	Changes in Phugoid Damping Due to Variations in $C_{m_{\dot{\alpha}}}$ — 72° SST	242

FIGURES (Continued)

Figure	Title	Page
101	Changes in Dutch Roll Damping Due to Variations in $C_{n_{\dot{\beta}}}$ — 707-320B	243
102	Changes in Dutch Roll Frequency Due to Variations in $C_{n_{\dot{\beta}}}$ — 707-320B	244
103	Changes in Rolling Convergence Root Due to Variations in $C_{n_{\dot{\beta}}}$ — 707-320B	245
104	Changes in Spiral Mode Root Due to Variations in $C_{n_{\dot{\beta}}}$ — 707-320B	246
105	Changes in Dutch Roll Damping Due to Variations in $C_{n_{\dot{\beta}}}$ — 30° and 42° SST	247
106	Changes in Dutch Roll Frequency Due to Variations in $C_{n_{\dot{\beta}}}$ — 30° and 42° SST	248
107	Changes in Spiral Mode Roots Due to Variations in $C_{n_{\dot{\beta}}}$ — 30° and 42° SST	249
108	Changes in Rolling Convergence Roots Due to Variations in $C_{n_{\dot{\beta}}}$ — 30° and 42° SST	250
109	Typical Cantilever Stations for Airplane Components	256
110	Structural-Inertial Axis System Relationships	261
111	Schematic of Program Sequencing for SST Dynamic Analysis	282

TABLES

Table	Title	Page
1	Flight Conditions for Evaluation of Methods for Computing Stability and Response Characteristics of Rigid and Elastic Airplanes	5
2	Static Stability Requirements	25
3	Static Stability Calculations — General Results	27
4	Small Perturbation Equations of Motion in Stability Axes	48
5	Equations of Motion Mechanized in Small Perturbation Program	52
6	Characteristic Equations in Determinant Form	53
7	Equations of Arbitrary Motion (Stability Axes)	68
8	Dynamic Stability Calculations — General Results	76
9	Longitudinal Derivatives Used in Completely Elastic 707-320B Analysis	95
10	Lateral-Directional Derivatives Used in Analyses of Completely Elastic 707-320B	112
11	Dutch Roll Characteristics with Lift Growth for Truncated, Completely Elastic Airplane, 17 Modes (14 Elastic Modes) — 707-320B	116
12	Qualitative Assessment of $\dot{\alpha}$ Derivatives on Longitudinal Dynamics	123
13	Qualitative Assessment of $\dot{\beta}$ Derivatives on Lateral-Directional Dynamics	124
14	List of Tables of Derivatives and Coefficients Used in General Comparisons	134
15	Example Data Table	136
16	707-320B Longitudinal Derivatives and Coefficients Used in General Comparisons	137
17	SST Longitudinal Derivatives and Coefficients Used in General Comparisons	143
18	707-320B Lateral-Directional Derivatives Used in General Comparisons	156
19	SST Lateral-Directional Derivatives Used in General Comparisons	162
20	List of Tables of Derivatives and Coefficients Used in Special Comparisons	176
21	707-320B Longitudinal Derivatives and Coefficients Used in Special Comparisons	177
22	SST Longitudinal Derivatives and Coefficients Used in Special Comparisons	179

TABLES (Continued)

Table	Title	Page
23	Variation of Short Period and Phugoid Roots with $C_{L_{\dot{\alpha}}}$ for Study Airplanes	251
24	Changes in Lateral-Directional Characteristics Due to Variations in $C_{Y_{\dot{\beta}}}$ for Study Airplanes	252
25	Changes in Lateral-Directional Characteristics Due to Variations in $C_{\ell_{\dot{\beta}}}$ for Study Airplanes	253
26	Cantilever Mode Frequencies	259
27	Cantilever Vectors for Symmetrical Free-Free Modes	268
28	Cantilever Modes for Antisymmetrical Free-Free Modes	269

1. INTRODUCTION

This report has been prepared under NASA-Ames Contract NAS 2-3662, "An Analysis of Methods for Predicting the Stability Characteristics of an Elastic Airplane." The report consists of four volumes — a summary report and three appendixes. The summary report contains an overview of the complete report with pertinent final equations. It is meant to be complete in itself; however, the detailed derivations of equations and discussions of results are left to the appendixes. Appendix A contains a derivation of the equations of motion and a discussion of the stability criteria. Methods for evaluating stability derivatives are examined in app. B.

This volume presents and evaluates methods for calculating the stability and response characteristics of an elastic airplane and identifies those terms in the equations of motion which significantly affect these characteristics. The airplane equations of motion fall into two general categories:

(1) Small perturbation formulation (linear differential equations);

(2) Large perturbation formulation (nonlinear differential equations).

In applying these equations, three airplane mathematical models are treated. They evolve from the viewpoint of the degree of participation by airframe flexibility. When this flexibility participates dynamically in the form of additional motion variables (structural normal modes), the airplane is called "completely elastic." When the flexibility participates in a quasi-static manner, i.e., when structural deformations are in phase and in constant proportion with the loads, the airplane is called "equivalent elastic." "Residual flexibility" (see app. A, par. 6.3.6) represents a middle ground between completely elastic and equivalent elastic motion. When elasticity does not participate in the motion at all, the "rigid airplane" evolves.

Applications of stability criteria were discussed in app. A. These criteria were separated into two major types, static and dynamic. Static stability characteristics reflect the time-independent stability characteristics of equilibrium (steady-state) flight. Satisfaction of the static criteria can be determined by observing the signs of the stability derivatives. Typical stable conditions are $C_{m_\alpha} < 0$, $C_{n_\beta} > 0$, and $C_{D_u} > 0$. Other parameters that reveal more

information, sometimes slanted toward handling qualities, are items such as stick-speed stability, elevator angle per g, neutral point, and maneuver point. The variations in these parameters due to differences in derivative calculation techniques will be discussed in Sec. 4.

Dynamic stability comparisons and results are given in Sec. 6. Leading to this discussion, there exists a considerable amount of material concerning rigid airplane characteristics. Time history solutions are discussed in detail in ref. 51. Characteristic equations and associated roots, motion characteristics, and transfer functions can be found in refs. 4 and 36. For the completely elastic airplane, similar discussions may be found in refs. 5, 39, 58, and 74 through 76 along with some examples of application of residual flexibility (called residual stiffness in some of the references).

No such detailed treatments are found for the equivalent elastic airplane, but the techniques applicable to rigid airplane characteristics apply. Some special effects have been discussed briefly in refs. 4 and 51.

An almost complete parametric study of the influence of various derivatives on the roots of the rigid airplane characteristic equations for a particular study airplane can be found in ref. 36. Items not treated there are the effects of $\dot{\alpha}$ and $\dot{\beta}$ derivatives on the dynamic stability characteristics; these are investigated in Sec. 7. Some parametric studies for the elastic airplane undertaken in refs. 39 and 58 are also discussed in Sec. 7.

The airplanes studied were the Boeing 707-320B and a variable-sweep SST configuration at three sweep conditions. The general arrangements and pertinent geometric parameters for each airplane are illustrated in figs. 1 and 2. The study flight conditions are given in table 1.

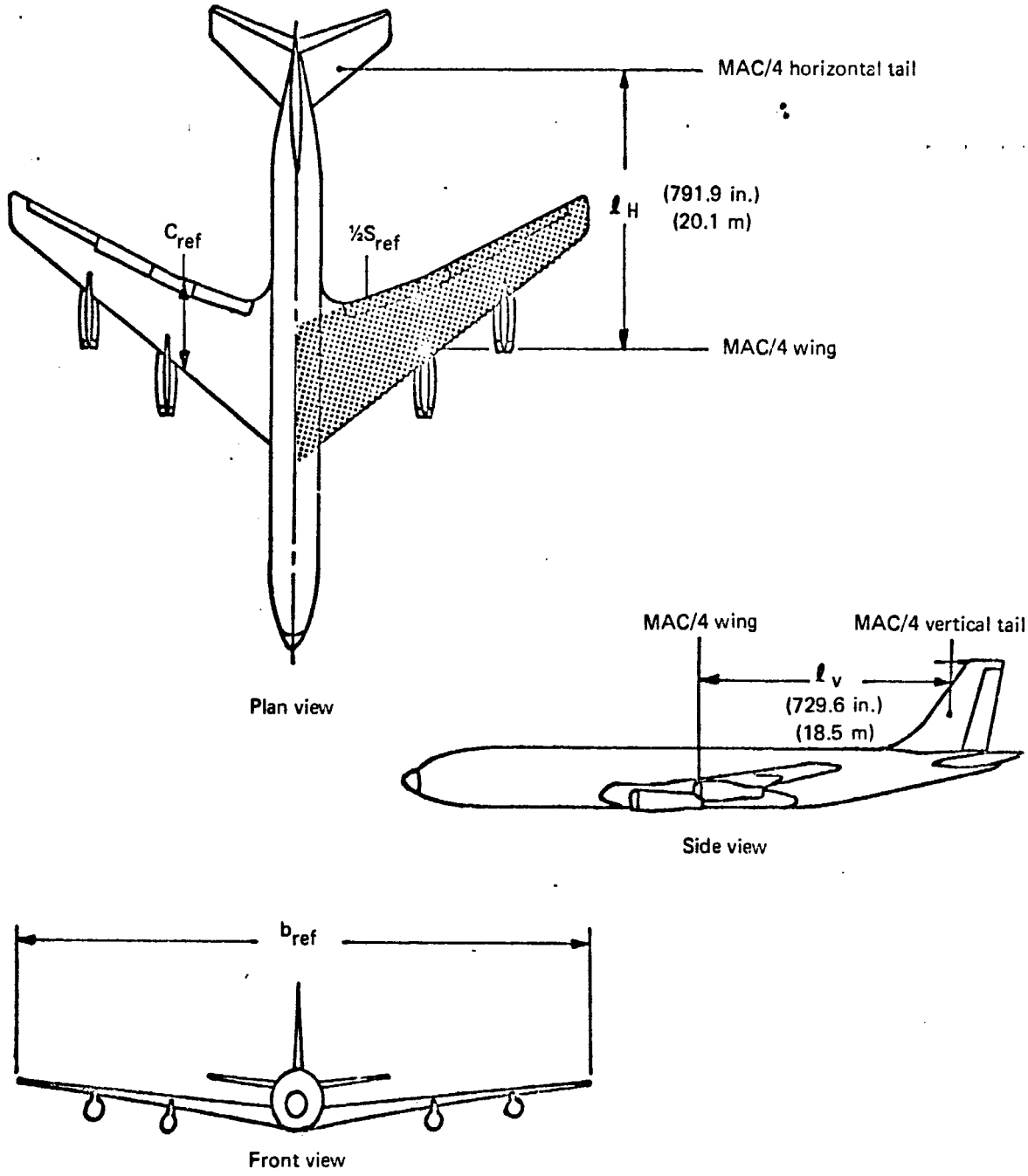

Leading edge sweep = 37.5°
Total wing area = S_{ref} = 2892 ft^2 (268.7 m^2)
Wing span = b_{ref} = 142 ft 5 in. (93.4 m)
Reference chord = C_{ref} = 272.3 in. (6.9 m)
Fuselage length = 145 ft 6 in. (44.35 m)

FIGURE 1. BOEING 707-320B GENERAL ARRANGEMENT

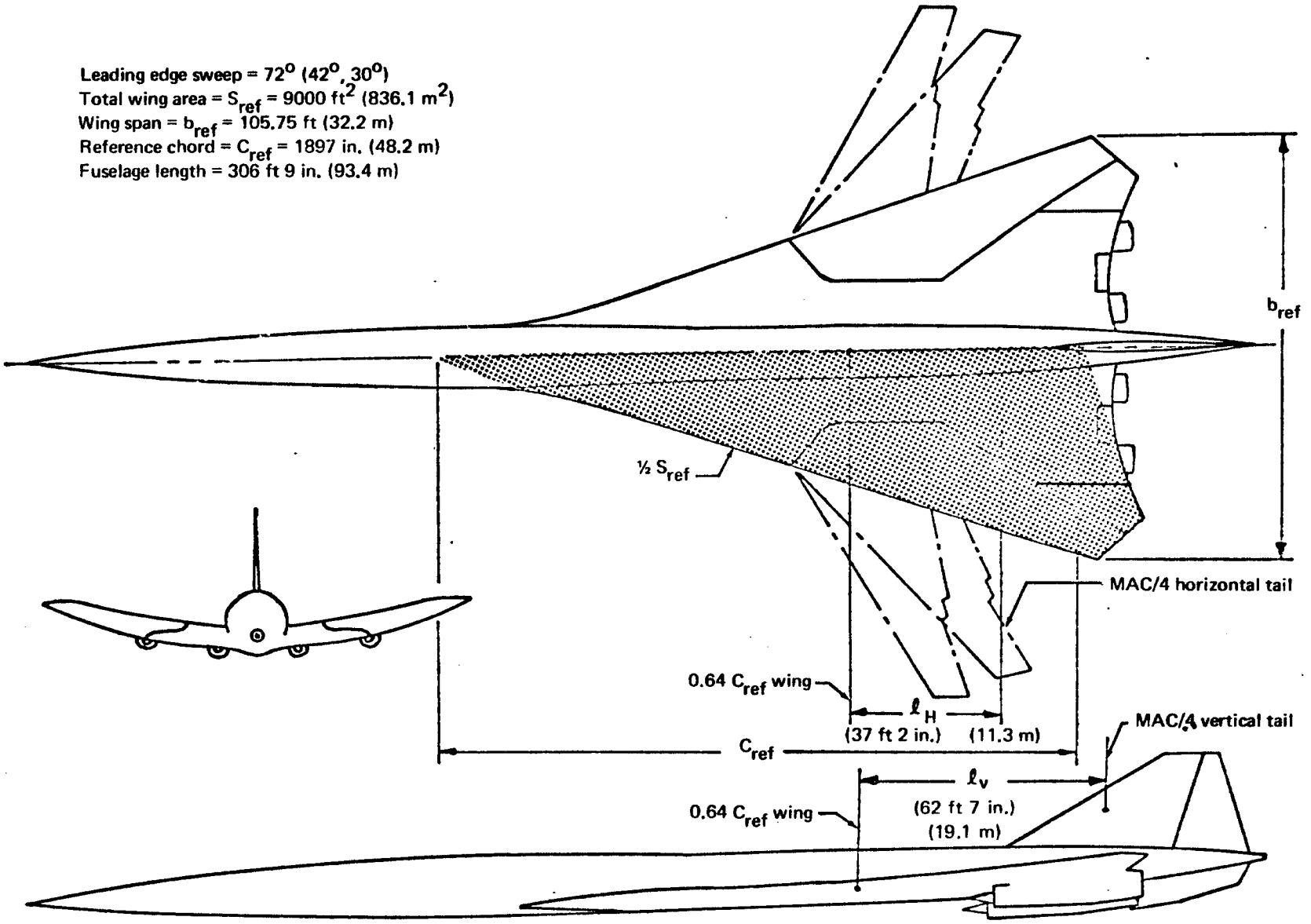

FIGURE 2. TYPICAL SST GENERAL ARRANGEMENT

TABLE 1. – FLIGHT CONDITIONS FOR EVALUATION OF METHODS FOR COMPUTING STABILITY AND RESPONSE CHARACTERISTICS OF RIGID AND ELASTIC AIRPLANES

Altitude		Dynamic pressure, $\bar{q}$		Reynolds number	Mach number	Weight		Wing leading edge sweep
ft	m	psf	N/m^2	$R_e \times 10^{-6}$		lb	N	
707-320B[a]								
10 000	3 050	66.7	3 194	31.0	0.255	268 000	1 192 064	
↓	↓	136.0	6 512	44.3	0.365	↓	↓	
↓	↓	306.0	14 651	66.5	0.548	↓	↓	
35 000	10 675	223.0	10 677	43.4 [b]	0.800	↓	↓	
↓	↓	251.0	12 018	46.1	0.850	↓	↓	
↓	↓	283.0	13 550	48.8	0.900	↓	↓	
SST[a]								
8 500	2 591	98	4 692	265.1	0.300	370 000	1 645 760	30°
9 500	2 896	260	12 449	413.5	0.500	↓	↓	↓
11 000	3 353	470	22 504	739.5	0.700	↓	↓	↓
32 500	9 906	98	4 692	206.9	0.500	675 000	3 002 400	42°
26 000	7 925	260	12 449	360.5	0.700	↓	↓	↓
23 500	7 163	470	22 504	502.9	0.900	↓	↓	↓
47 500	14 478	98	4 692	147.8 [c]	0.700	668 000	2 971 264	72°
37 000	11 278	260	12 449	314.1	0.900	↓	↓	↓
33 000	10 058	470	22 504	447.4	1.100	↓	↓	↓
30 000	9 144	750	35 910	586.9	1.300	520 000	2 312 960	↓
24 000	7 315	1300	62 244	824.9	1.500	↓	↓	↓
60 500	18 440	500	23 940	249.3	2.200	↓	↓	↓
49 000	14 935	1300	62 244	532.0	2.700	↓	↓	↓

[a] All conditions for clean airplane (gear up, flaps up)

[b] Based on C_{ref} = 6.92 m (22.7 ft)

[c] Based on C_{ref} = 48.19 m (158.1 ft)

2. SYMBOLS

This list includes the symbols found in the Summary and appendixes. In different technologies some of the symbols have different meanings. For example, ϵ means downwash angle to an aerodynamicist, but strain to a structural engineer. In these cases the several definitions have been listed after the symbol.

General

$\mathcal{AR}$	Aspect ratio, nondimensional
$[A]$	Steady aerodynamic influence coefficients matrix, meters^2/radian
$[\delta A]$	Unsteady aerodynamic influence coefficients matrix, meter^2-seconds/radian
$[A_1]$, $[A_2]$, $[A_3]$, $[A_4]$, $[A_5]$	Aerodynamic matrices, newtons, newton-meters
a	Root of characteristic equation, second^{-1}; lift curve slope, radian^{-1}
a_∞	Speed of sound, meters/second
$\bar{a}_v$	Vertical tail elastic to rigid lift ratio, nondimensional
$\ddot{\bar{a}}$	Acceleration, meters/second^2
b	Wingspan, meters
$C_{1/2}$	Cycles to damp to half amplitude, nondimensional
C_2	Cycles to double amplitude, nondimensional
C_D	Drag coefficient, $D/\bar{q}S$, nondimensional
C_{D_i}	Induced drag coefficient, $D_i/\bar{q}S$, nondimensional
C_L	Lift coefficient, $L/\bar{q}S$, nondimensional
C_ℓ	Rolling moment coefficient, $M_x/\bar{q}Sb$, nondimensional

C_m	Pitching moment coefficient, $M_y / \bar{q}S\bar{c}$, nondimensional
C_N	Normal pressure force coefficient, $N / \bar{q}S$, nondimensional
C_n	Yawing moment coefficient, $M_z / \bar{q}Sb$, nondimensional
C_p	Pressure coefficient, $(P - P_\infty)/\bar{q}_\infty$, nondimensional
C_T	Thrust coefficient, $T / \bar{q}S$, nondimensional
C_Y, C_y	Side force coefficient, $F_y / \bar{q}S$, nondimensional
$[C]$	Flexibility matrix with reference point fixed, meters/newton
$[C_o]$	Flexibility matrix with reference point fixed and with reference point rows and columns removed, meters/newton
$[\bar{C}]$	Flexibility matrix with reference point free, meters/newton
$[\bar{C}_R]$	Residual flexibility matrix, meters/newton
c	Wing chord, meters
c_R	Root chord, meters
$\bar{c}$	Mean aerodynamic chord, meters
c_{ref}	$\bar{c}$ for the 707 and c_R for the SST, meters
D	Drag, newtons
D_i	Induced drag, newtons
$[D]$	Transformation matrix from fluid to stability axis system, nondimensional
$\bar{d}$	Elastic displacement, meters
$\{d_i\}$	Column matrix of elastic displacement components at the i^{th} element, meters
$\{d_p\}$	Matrix of elastic displacement perturbation, meters
E	Total airplane perturbation energy, newton-meters; Young's modulus, newtons/meter^2; induced drag efficiency factor, nondimensional; energy, newton-meters

e	Internal energy density, newton-meters^4/kilogram
F	Energy decay parameter, nondimensional
$\vec{F}$	Force, newtons; surface stress vector, newtons/meter^2
$\{F\}$	Total force matrix, newtons
$\{F_A\}$	Aerodynamic force matrix, newtons
$[F_d]$	Flexibility matrix relating changes in panel centroid deflections to unit loads, meters/newton
$\{F_i\}$	Generalized forces at i^{th} element, arbitrary dimensions
$\{F_T\}$	Thrust force matrix, newtons
$[F_\theta]$	Flexibility matrix relating panel slopes to unit loads, radians/newton
f_{ij}	Aerodynamic influence coefficients (subsonic), newtons/radian
$\vec{f}$	Perturbation force, newtons; perturbation surface stress vector, newtons/meter^2
$\{f\}$	Perturbation force matrix, newtons
$\{f_A\}$	Aerodynamic perturbation force matrix, newtons
$\{f_T\}$	Thrust perturbation force matrix, newtons
G	Shear modulus, newtons/meter^2
GW	Gross weight, newtons
$\vec{G}$	Structural influence functions in diadic form with reference point free, meters^3/newton
g_{ij}	Aerodynamic influence coefficients (supersonic), newtons/radian
$\vec{g}$	Acceleration due to gravity, meters/second^2
$\vec{g}_i$	Unit base vector, nondimensional
	Altitude, meters; specific enthalpy, newton-meters/kilogram; center-of-gravity position, nondimensional

h_m	Maneuver point position, nondimensional
h_n	Neutral point position, nondimensional
$(h_n - h)$	Static margin, nondimensional
$\dot{h}_p$	Velocity of panel normal to the streamwise direction, meters/second
I_{xx}, I_{xy}, I_{xz} I_{yy}, I_{yz}, I_{zz}	Moments and products of inertia, kilogram-meters^2
[I], [I]	Identity matrix, nondimensional
i_H	Horizontal tail deflection, degrees
$\hat{i}, \hat{j}, \hat{k}$ $\underline{i}, \underline{j}, \underline{k}$	Unit base vectors, nondimensional
J	Torsional constant, meters^4/radian
K	Angular deflection at the exposed horizontal tail due to a unit load at the tail, radians/newton
K_{ij}	Structural stiffness coefficient, newtons/meter
K_N	Ratio of aircraft nose lift to aircraft wing lift, nondimensional
$K_{\dot{p}}$	Effective change in vertical tail angle of sideslip due to a unit change in rolling acceleration measured at the exposed vertical tail, degrees/radian/second^2
$K_{\dot{r}}$	Effective change in vertical tail angle of sideslip due to a unit change in yawing acceleration measured at the exposed vertical tail, degrees/radian/second^2
$K_{\ddot{y}}$	Effective change in vertical tail angle of sideslip due to a unit change in side acceleration measured at the exposed vertical tail, degrees/meter/second^2
$K'_{B(W)}$	Effect of lift carryover on the body due to the wing, nondimensional
$K'_{W(B)}$	Effect of lift carryover on the wing due to the body, nondimensional
[K]	Stiffness matrix with respect to fixed reference point, newtons/meter

$[K]_i$	Element stiffness matrix, newtons/meter
$[\bar{K}]$	Stiffness matrix with respect to free reference point, newtons/meter
$[\![\bar{K}]\!]$	Generalized stiffness matrix with free reference point, newtons/meter
k	Thermal conductivity, newton-meters/second-meter-degrees Celsius; elastic constant, newtons/meter^2; Strouhal number, nondimensional
$[K], [\![K]\!]$	Corrector matrix for influence coefficients, nondimensional
L	Lift, newtons
l	Moment arm, meters; characteristic length, meters; pressure difference across surface, newtons/meter^2
l_H	Wing $c_{ref}/4$ to horizontal tail $c_{ref}/4$, meters
l_v	Wing $c_{ref}/4$ to vertical tail $c_{ref}/4$, meters
l_1, l_2, l_3	Direction cosines, nondimensional
M	Mach number, nondimensional; mass of the airplane, kilograms
$\bar{M}$	Moment, meter-newtons
[M]	Inertial matrix, kilograms, kilogram-meters^2
$[\![M]\!]$	Generalized mass matrix, kilograms
m_1, m_2, m_3	Direction cosines, nondimensional
$\bar{m}$	Perturbation moment, meter-newtons
[m]	Mass matrix, kilograms
$[\![m]\!]$	Diagonal mass matrix, kilograms
N	Yawing moment, meter-newtons
$\bar{N}$	Normal force, newtons
	Load factor, nondimensional; number of elastically connected mass elements used to represent the airplane, nondimensional

n_1, n_2, n_3	Direction cosines of the normal surface, nondimensional
$\bar{n}$	Unit vector normal to the surface, nondimensional
$[n]$	Diagonal matrix of panel unit normal vectors, nondimensional
P	Period, seconds
P, Q, R	Components of the angular velocity $\bar{\omega}$ in the body axis system, radians/second
P_t	Total pressure, newtons/meter^2
$\{P\}$	Aerodynamic panel pressure forces, newtons
p	Static pressure, newtons/meter^2; roll rate, radians/second
p, q, r	Perturbation components of angular velocity $\bar{\omega}_p$ in the body axis system, radians/second
Q_i	Generalized force, arbitrary dimensions*
$\{Q\}$	Matrix of generalized aerodynamic and thrust forces, arbitrary dimensions*
q	Pitch rate, radians/second; rate of internal heat energy addition, newton-meters/second
q_i	Generalized coordinates, arbitrary dimensions*
$\bar{q}$	Dynamic pressure, newtons/meter^2
$\hat{q}$	Pitch rate, $qc_{ref}/2V_{c_1}$, nondimensional
$\{q\}$	Matrix of generalized coordinates, arbitrary dimensions*
$\{\tilde{q}\}$	Matrix of generalized coordinates of elastic free vibration, arbitrary dimensions*
$\{\tilde{\bar{q}}\}$	Cantilever eignvectors, nondimensional

*The units of a generalized force times the generalized coordinates must be newton-meters.

R	Universal gas constant, newton-meters/kilogram-degrees Kelvin; magnitude of position vector, meters; region of XY plane not covered by the airplane or wake, nondimensional
Re	Reynolds number, nondimensional
$\vec{R}$	Position vector at an initial instant of time, meters; body force per unit volume, newtons/meter^3
r	Reference distance, meters; magnitude of the position vector, meters
$\hat{r}$	Yaw rate component, $rb/2V_{c_1}$, nondimensional
$\vec{r}$	Position vector relative to the body axis system, meters; position vector relative to the fluid axis system, meters
$\vec{r}_o$	Position vector of the center of gravity relative to the fluid axis system, meters
$\vec{r}_s$	Position vector relative to the stability axis system, meters
$\vec{r}'$	Position vector relative to inertial space, meters
$\vec{r}'_o$	Position vector of the center of gravity relative to the inertial space, meters
$\vec{\bar{r}}_s$	Position vector in the undeformed airplane relative to the body axis system, meters
$\{r'_{o_p}\}$	Matrix of airplane position and orientation perturbations, meters, radians
S	Reference area, meters^2; airplane's projection on the XY plane, nondimensional
$[S]$	Diagonal matrix of panel areas, meters^2
s	Complex frequency function, 1/seconds
T	Kinetic energy, newton-meters; thrust, newtons; time, seconds
$\bar{T}$	Time to damp to ½ amplitude, seconds
T_2	Time to double the amplitude, seconds

$1/T_r$	Rolling convergence mode root, 1/seconds
$-1/T_s$	Spiral mode root, 1/seconds
t	Time, seconds; airfoil thickness, meters
t*	Nondimensionalizing time factor, seconds
U	Potential energy, newton-meters
U, V, W	Components of velocity $\vec{V}_c$ in the body axis system, meters/second
u, v, w	Perturbation components of the velocity in the body axis system, meters/second
u_i	Generalized coordinates, nondimensional
$\hat{u}$	Forward velocity component, u/V_{c_1}, nondimensional
$\{u\}, \{u_p\}$	Generalized elastic displacements, meters
V	Lyapunov function, nondimensional; volume, meters^3
V_E	Equivalent airspeed, meters/second
$\vec{V}_c$	Velocity vector of the airplane center of gravity, meters/second
$\vec{V}$	Velocity vector, meters/second
$\vec{V}_{c_p}$	Perturbation velocity vector of the airplane center of gravity meters/second
$\{V_p\}$	Matrix of airplane linear and rotational rate perturbations, meters/second, radians/second
$\{\dot{V}_p\}$	Matrix of airplane linear and rotational acceleration perturbations, meters/second^2, radians/second^2
W	Weight, newtons; airplane's wake projection on the XY plane, nondimensional
$\{X\}$	Matrix of panel centroid distances to the reference point, meters
X, Y, Z x, y, z	Body-fixed-axis system (app. A); fluid axis system (app. B)

X_B, Y_B, Z_B; x_B, y_B, z_B	Body-fixed-axis system
X_o, Y_o, Z_o	Axis system fixed to a material point
X', Y', Z'; x', y', z'	Earth-fixed-axis system
Y	Side force, newtons
$\lceil \Delta y \rfloor$	Matrix of spanwise panel widths, meters
Z_R	Vertical displacement of structural reference point, meters
$\{z\}$	Matrix of vertical displacements of each panel from equilibrium, meters
$[\ ]$	Square matrix
$\{\ \}$	Column matrix
$(\ )$	Row matrix
$\lceil \rfloor$	Diagonal matrix
$[\ ]^T, \{\ \}^T$	Transposed matrix
$[\ ]^{-1}$	Matrix inverse
$\|\|[\ ]\|\|$	Determinant of a matrix
$[0]$	All zero elements
$\{1\}$	Column matrix of ones
$[\![\ ]\!]$	"Jump" in enclosed quantity

Greek Symbols

α	Angle of attack, radians
α_R	Angular rotation of structural reference point, radians
α_{ref}	Angle between X body axis and $\bar{V}_{c_l}$, radians
$\{\alpha\}$	Matrix of panel slopes, radians

β	Angle of sideslip, radians
β^2	$(M^2 - 1)$, nondimensional
Γ	Circulation, meters^2/second
$\bar{\bar{\Gamma}}_o$	Structural influence functions with reference point fixed in diadic form, meters^3/newton
γ	Flight path angle, radians; ratio of specific heats for air, nondimensional
Δ	Finite change in some parameter, nondimensional
δ	Control surface deflection, radians; arbitrarily small number, nondimensional; Dirac's function, nondimensional; thickness ratio, nondimensional
$\{\delta\}$	Matrix of displacements relative to a space-fixed inertial system, meters
$\{\delta_s\}$	Matrix of flexible displacements relative to the structural axis system, meters
ϵ	Downwash angle, radians; arbitrarily small number, nondimensional; strain, meters/meter
ϵ_α	Change in downwash angle at the stabilizer per unit change in wing angle of attack, $\partial\epsilon/\partial\alpha$, radians/radian
ζ	Damping ratio, nondimensional; nondimensionalized coordinate, nondimensional; dummy variable, nondimensional
η	Efficiency factor, nondimensional; coordinate, nondimensional; dummy variable, nondimensional
Θ	Euler angle, radians
θ	Perturbed Euler angle, radians
Θ_s	Streamwise rotation of panel, radians
$\Theta_{ix}, \Theta_{iy}, \Theta_{iz}$	Node rotations, radians
$\dot{}$	Rate of change of Euler angle, radians/second

$\dot{\theta}_{ei}$	Rotational rate of paneled airplane about axis of rotation, radians/second
$\vec{\theta}$	Rigid-body rotation about center of gravity, radians
$[\dot{\theta}]$	Angle mode matrix, radians/meter
λ	Eigenvalue, nondimensional; taper ratio, nondimensional; bulk modulus, newtons/meter^2; Lame's constant, newtons/meter^2; sweep angle, degrees
λ_i	Roots of characteristic equation, 1/seconds
μ	Reduced mass parameter, nondimensional; Lame's constant, newtons/meter^2; extent of influence region, nondimensional
$\{\mu\}$	Cantilever mode shape matrix, nondimensional
$[\mu]$	Matrix of all cantilever modes, nondimensional
ν	Poisson's ratio, nondimensional
ξ,η,ζ	Coordinates, nondimensional; dummy variables, nondimensional
π	Constant, 3.14159. . ., nondimensional
ρ	Density, kilograms/meter^3
σ	Normal stress, newtons/meter^2; density ratio, nondimensional; real root of characteristic equation, 1/seconds
σ_R	Rotation of structural reference axis system, radians
σ_T	Rectilinear translation of structural reference axis system, meters
τ	Coefficient of viscosity, kilograms/meter-second; shear stress, newtons/meter^2; time, nondimensional
Φ	Total velocity potential, meters^2/second; Euler angle, radians
$[\Phi_n]$	Normalized natural free vibration modes of the airplane, nondimensional

ψ	Perturbation velocity potential, meters; perturbed Euler angle radians
$\dot{\phi}$	Rate of change of Euler angle, radians/second
$[\phi]$	Free-vibration mode shape matrix, nondimensional
$[\bar{\phi}]$	Rigid-body mode shape matrix, nondimensional
$\overline{\phi}$	Stress diadic, newtons/meter^2
$\overrightarrow{\phi_\alpha}$	Normal mode of generalized coordinate, nondimensional
φ	Velocity potential, nondimensional
$\varphi(t)$	Arbitrary positive function of time, arbitrary dimension
Ψ	Euler angle, radians
ψ	Perturbed Euler angle, radians
	Rate of change of Euler angle, radians/second
$\overline{\psi}$	Inertia diadic
Ω	Phase angle, radians
ω	Frequency, radians/second; imaginary part of a pair of complex roots, 1/seconds
ω_n	Undamped natural frequency, radians/second
$\overrightarrow{\omega_p}$	Perturbed angular velocity, radians/second

Subscripts

A	Aerodynamic; airplane; aileron
a	Aerodynamic
ac	Aerodynamic center
b	Body reference axis system

cg	Center of gravity
cp	Center of pressure
D	Dutch roll mode
E	Equivalent elastic (Formulation II); elevator
$\bar{E}$	Equivalent elastic (Formulation I)
Eff	Effective
EqEl	Equivalent elastic
exp	Experimental
F	Flutter
HB	Handbook methods
h ht	Horizontal tail
I	Inertia relief
l	Lower surface
L.E., LE	Leading edge
ls	Lifting surface theory method
P	Phugoid mode
R	Rigid; rudder
r	Rolling convergence root mode
S	Spiral root
sp	Short period
s	Stability axis system; spiral mode

sl	Sea level
t	Tip; total
u	Upper surface
v, vert, V.T.	Vertical tail
W	Wing
WB	Wing-body
WBT	Wing-body-tail
WT	Wind tunnel
0	At $\alpha = \delta_E = i_h = 0^o$; initial state
1	Steady state motion variables; trimmed condition
∞	Undisturbed condition

3. ASSUMPTIONS

Assumptions used in developing the equations and methods are listed here for reference. Where appropriate in the summary report, pertinent assumptions used in obtaining a result or equation are given. However, discussions of the assumptions as they come into the developments are given in the appendixes. Further descriptions and justifications are included in those discussions.

General Assumptions

- (G1) Airplane mass and mass distribution are constant with time
- (G2) No thermoelastic effects considered
- (G3) No electromagnetic effects considered
- (G4) Symmetric airplane
- (G5) Variation of air density with altitude is negligible
- (G6) No gust effects considered
- (G7) Gravitational forces on the field are negligible
- (G8) Small perturbation theory
- (G9) Large perturbation theory
- (G10) Origin of coordinate system is at the center of mass
- (G11) Arbitrary perturbations

Aerodynamic Assumptions

- (A1) Potential flow theory
- (A2) Thin body
- (A3) Slender body
- (A4) High aspect ratio
- (A5) Prandtl boundary layer approximation
- (A6) Perfect gas, thermally nonconducting and chemically nonreacting
- (A7) Isentropic flow
- (A8) Steady flow

(A9) Unsteady flow

(A10) Inviscid flow

(A11) Quasi-steady flow

(A12) Aerodynamic influence coefficients for nonzero sideslip

(A13) Continuum flow

(A14) No finite shock waves

(A15) Velocity field is irrotational

Structural Assumptions

(S1) Hooke's law applies

(S2) Only small strain and displacement gradients are considered

(S3) Structural damping is negligible

(S4) Structural perturbations can be represented by normal modes

(S5) Completely elastic math model of elastic airplane

(S6) Residual elastic math model of elastic airplane

(S7) Equivalent elastic math model of elastic airplane

(S8) Rigid math model of elastic airplane

(S9) Airplane displacement vector field is such that the center of gravity does not displace or rotate

(S10) X component of elastic deflection is negligible

(S11) Y component of elastic deflection is negligible

(S12) The structure can be adequately represented with beams

(S13) Inertia of each finite mass element about its center of gravity is negligible

Dynamic Assumptions

(D1)	Free flight only
(D2)	No spinning rotors
(D3)	Steady-state curvilinear flight
(D4)	Steady-state rotation is small
(D5)	Zero-lag thrust derivatives
(D6)	$C_{L_{\dot{\theta}}}$ is negligible
(D7)	$C_{Y_{\dot{p}_I}}$, $C_{Y_{\dot{r}_I}}$, $C_{\ell_{\ddot{Y}_I}}$, and $C_{n_{\ddot{Y}_I}}$ are negligible
(D8)	C_{D_q} is negligible
(D9)	Steady-state rectilinear motion
(D10)	Stick-fixed-and-unaugmented airplane
(D11)	Thrust perturbation forces are negligible
(D12)	Steady state, wings level, and zero sideslip
(D13)	Level flight (steady state)
(D14)	Linear aerodynamic stability derivatives
(D15)	Two-degree-of-freedom longitudinal motion

4. STATIC STABILITY CHARACTERISTICS

4.1 Introduction

The static stability characteristics of an airplane are strongly dependent on the individual stability derivatives and on how the stability derivatives combine. In this study three methods were used to determine the longitudinal derivatives that are used in the static stability analysis. They are shown in the following table together with a statement of applicability to rigid and equivalent elastic airplane representations. The calculation of these derivatives is the subject of app. B.

	Rigid airplane	Equivalent elastic airplane
(1) Computer, using lifting surface theory — aerodynamic influence coefficient method	Yes	Yes
(2) Handbook (combined with computer lifting surface theory for elastic calculation).	Yes	Yes
(3) Wind tunnel	Yes	Yes

The effects of the individual stability derivatives can be judged by comparing their sign with the static stability criteria of app. A and by noting the magnitude of the derivative. The sign of the derivative simply indicates whether the airplane is stable, unstable, or neutrally stable with respect to a certain motion variable. (Requirements for stable motion are summarized in table 2.) The magnitude of the derivative indicates the degree of stability or instability.

In addition to comparing certain stability derivatives with static stability criteria, the following static stability and control characteristics are usually investigated in an analysis:

(1) Elevator and stabilizer trim angles;

(2) Stick-speed stability;

(3) Elevator and stabilizer angles per g;

(4) Neutral point;

(5) Maneuver point.

TABLE 2. – STATIC STABILITY REQUIREMENTS

Observation (Appendix A)	
$C_{D_u} > 0$	$C_{\ell_p} < 0$
$C_{y_\beta} < 0$	$C_{m_q} < 0$
$C_{L_\alpha} > 0$	$C_{n_r} < 0$
$C_{n_\beta} > 0$	$C_{m_u} > 0$
$C_{m_\alpha} < 0$	$C_{\ell_\beta} < 0$

Calculation	
Stick-speed stability	$\frac{d\delta_{E_1}}{dV} > 0$ (see app. A)
Elevator angle per g	$\left.\frac{d\delta_{E_1}}{dn}\right\|_{V_{c_1}} < 0$ (see app. A)
Neutral point	Aft of aft c.g. limit (p. 78, ref. 4)
Maneuver point	Aft of aft c.g. limit (p. 59, ref. 4)

Applying this approach to the rigid airplane, the three methods listed above were compared. The stability derivatives used for the comparison are tabulated in par. 8.2. As is noted, in some cases a particular derivative for one of the methods was not available. For instance, no pitch rate derivatives were available from wind tunnel data; therefore, lifting surface values were used. Elastic stability characteristics were determined by using equivalent elastic stability derivatives of the Formulation II type (see app. B). These derivatives were generated by methods (1) and (2) listed above and are tabulated in par. 8.2.

Some flight test data were available to correlate theoretical predictions of longitudinal static stability. The data were obtained as part of the certification requirements for longitudinal stability and control for the model 707-320B airplane. Results for both maneuvering, $d\delta_E / dn$, and stick-speed stability, $d\delta_E/dV$, were obtained from these tests.

General results obtained from the static analysis are presented in table 3. Table 3 summarizes the accuracies obtained from lifting surface theory and handbook techniques in predicting the rigid airplane static stability and control characteristics when compared with wind tunnel predictions. Also shown is the relative effect of elasticity on the various static characteristics and the correlation of the limited amount of flight test data available with theoretical predictions. Although most of the substantiation of methods was for the rigid airplane, one could expect to obtain accuracies for the equivalent elastic similar to those for the rigid lifting surface method. The poor accuracy obtained for some configurations and characteristics is almost entirely due to poor prediction of the stability derivative C_{m_α}. Appendix B discusses the calculation of this derivative and the expected improvements to the lifting surface theory mechanization program to improve the prediction of C_{m_α}.

The mass distribution of an aircraft can strongly influence the static characteristics. Studies that investigated the effects of mass distribution were accomplished independently of the present study at The Boeing Company. An SST configuration similar to the study airplane was used. An example of the results of that study that illustrates the effects of mass distribution and dynamic pressure on the neutral point is shown in fig. 3.

TABLE 3. – STATIC STABILITY CALCULATIONS – GENERAL RESULTS

Stability and control characteristic	Relative accuracy of calculation method[a]: Computer lifting surface rigid and equivalent elastic				Relative accuracy of calculation method[a]: USAF Handbook			Relative effect of elasticity[b]		
	Sub			Super	Sub		Super	Sub		Super
	707		SST	SST	707	SST	SST			
	Rigid	E. E.	Rigid	Rigid	Rigid	Rigid	Rigid	707	SST	SST
δE_1	G	c	P	F	P	P	G	L	L	L
$d\delta E/dV$	G	G[d]	P	F	P	P	G	M	S	M
$d\delta E/dn$	G	G[d]	P	G	P	P	F	S	M	M
h_n	G	c	P	F	P	P	P	L	M	M
h_m	G	c	P	F	P	P	F	L	M	M

a. Reflects almost entirely ability to calculate derivative C_{m_α} and resulting effect on characteristic

G (good)— method compares favorably with wind tunnel predictions (exception allowed)

F (fair)— less favorable correlation with predictions

P (poor)— method does not compare favorably with predictions

b. L (large)— elasticity considered a significant effect

M (moderate)— elasticity considered moderately important; not quite as significant as differences due to stability calculation methods

S (small)— elasticity considered a minor change to stability characteristic; changes due to stability derivative calculation methods usually much more important

c. No data available

d. Correlation with flight test, but based on a very limited amount of data.

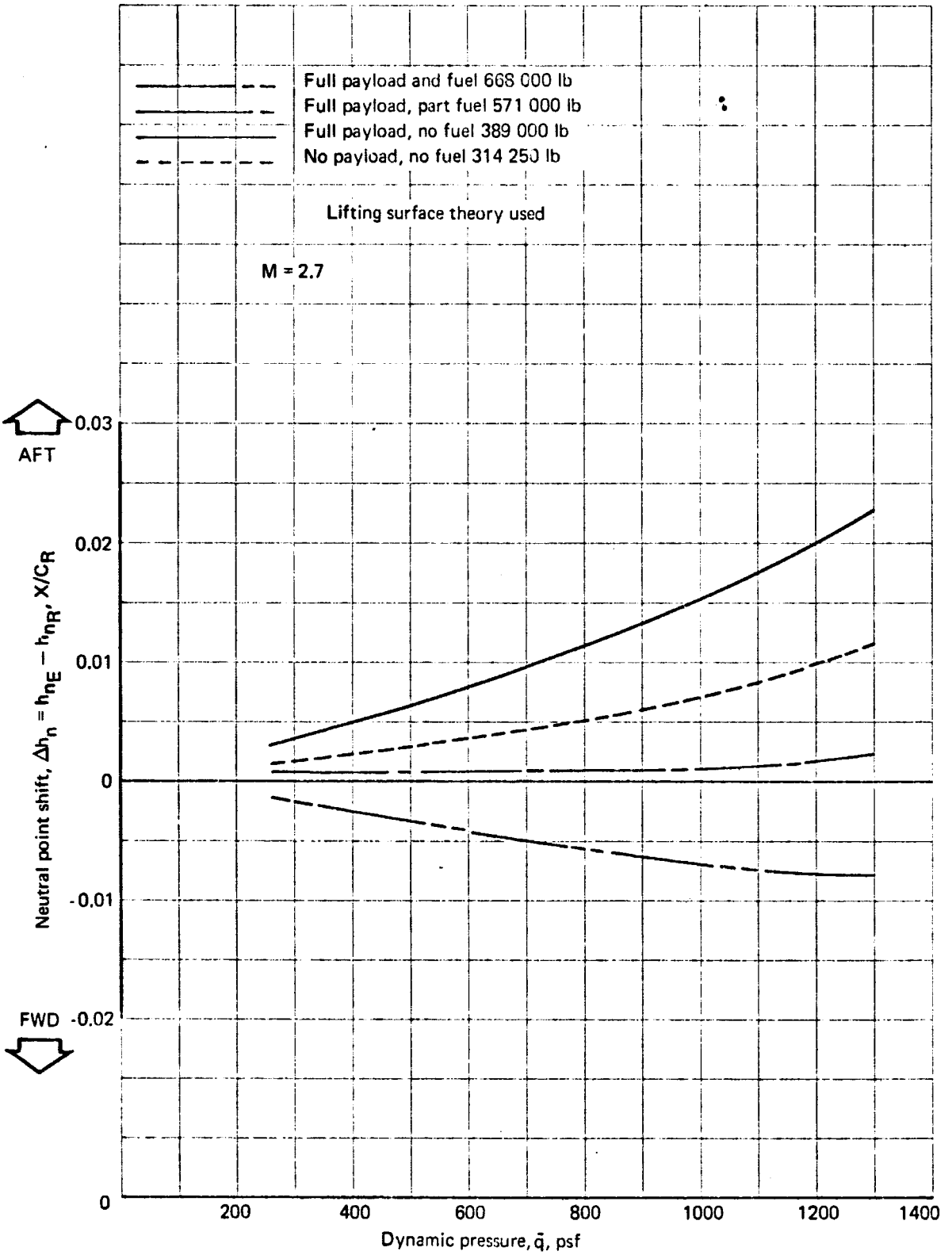

FIGURE 3. EFFECT OF MASS DISTRIBUTION ON ELASTIC NEUTRAL POINT SHIFT – 72° SST

Paragraphs 4.2 through 4.5 present the derivation of the equations used and the discussion of results in support of table 3. Section 4 presents only those data used for discussion. The complete set of static stability data supporting the conclusions of this section are shown in par. 8.3.

In several of the graphs that follow, data have been connected with curves. Strictly speaking, this should not be done for the SST flight conditions because several variables have changed between points. The connecting curves in these cases should, therefore, be considered as a visual aid only, and not be used to interpolate between data points.

4.2 Elevator and Stabilizer Trim Angles

For unaccelerated, straight and level flight the trim lift and pitching moment coefficient equations are (D12)

$$C_m = 0 = C_{m_o} + C_{m_\alpha}\alpha_1 + C_{m_{i_H}} i_{H_1} \tag{4.1}$$

and

$$C_{L_1} = \frac{W}{\bar{q}S_W} = C_{L_o} + C_{L_\alpha}\alpha_1 + C_{L_{i_H}} i_{H_1} \tag{4.2}$$

These equations obviously satisfy the case of an all-movable tail or imply a configuration choice of tail incidence. For a fixed horizontal stabilizer with elevators, the trim equations are

$$C_m = 0 = C_{m_o} + C_{m_\alpha}\alpha_1 + C_{m_{\delta_E}} \delta_{E_1} \tag{4.3}$$

and

$$C_{L_1} = \frac{W}{\bar{q}S_W} = C_{L_o} + C_{L_\alpha}\alpha_1 + C_{L_{\delta_E}} \delta_E \tag{4.4}$$

Solving equations (4.1) and (4.2) simultaneously for α_1 and i_{H_1}, the horizontal stabilizer to trim is given by

$$i_{H_1} = \frac{C_{L_\alpha} + C_{m_o} + C_{m_\alpha}[C_{L_1} - C_{L_o}]}{C_{m_\alpha} C_{L_{i_H}} - C_{m_{i_H}} C_{L_\alpha}} \tag{4.5}$$

Similarly, the elevator angle to trim is given by solving equations (4.3) and (4.4) as

$$\delta_{E_1} = \frac{C_{L_\alpha} C_{m_0} + C_{m_\alpha} [C_{L_1} - C_{L_0}]}{C_{m_\alpha} C_{L_{\delta_E}} - C_{m_{\delta_E}} C_{L_\alpha}} \qquad (4.6)$$

Representative δ_{E_1} results for the different calculation methods are shown in fig. 4 for the 707-320B and in fig. 5 for the 30° wing sweep SST. Paragraph 8.3 presents δ_{E_1} for all configurations and flight conditions used in this study. The coefficient C_{m_α} has a dominant effect; thus, the curves mainly reflect the ability to calculate C_{m_α} accurately. Generally speaking, for subsonic transports like the Boeing 707-320B lifting surface theory can predict δ_{E_1} with acceptable accuracy (using wind tunnel results as the standard for comparison).

Lifting surface theory, rigid and elastic, can be used to provide the increments in control deflections due to elasticity. The differences between the two handbook methods should not be used to deduce the increments in control due to elasticity. This is because these two methods are based on different techniques and, consequently, the results show differences due to both technique and elasticity.

The static characteristics based upon derivatives calculated by an elastic handbook method (combined with lifting surface theory data) can, however, be compared to the elastic lifting surface theory values. This comparison shows our ability to calculate individual elastic derivatives and the resulting static characteristics without the benefit of a computer program that handles complete wing-body-tail configurations for the elastic airplane. Appendix B should be consulted for details concerning the calculation of the elastic handbook stability derivatives. For the trim elevator results under discussion here, we see that the elastic handbook method compares quite well with the elastic lifting surface method.

For less conventional configurations it is recommended at the present time that only wind tunnel predictions of stability derivatives be relied upon for the rigid airplane and that desired elastic corrections be obtained by using the computer program. This can be done by ratioing the computed elastic to rigid values. For example:

$$C_{m_{\alpha_{EL.}}} = C_{m_\alpha}\Big|_{W.T.} \cdot \left.\frac{C_{m_{\alpha\ ELASTIC}}}{C_{m_{\alpha\ RIGID}}}\right|_{\text{computed}}$$

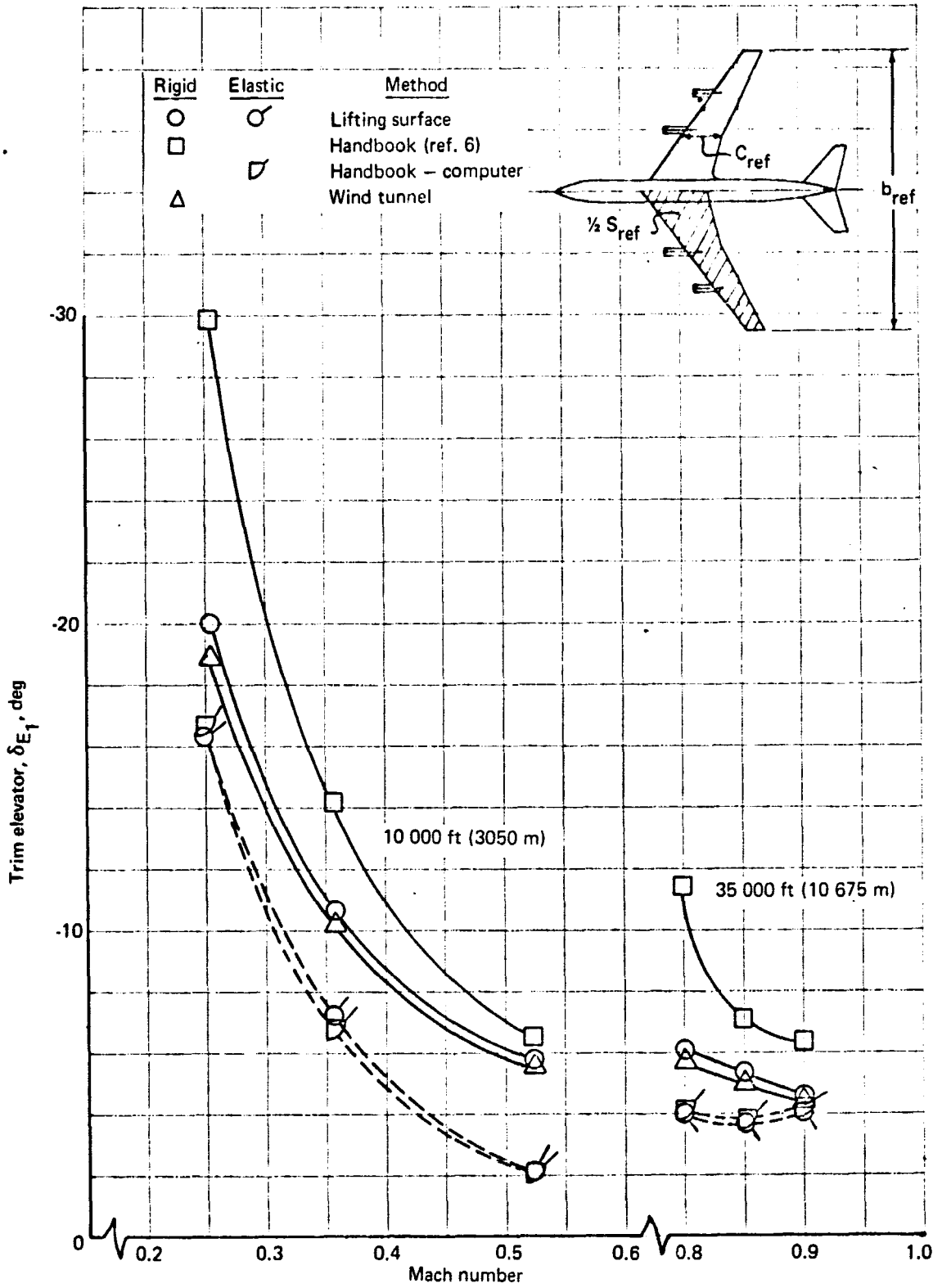

FIGURE 4. TRIM ELEVATOR, RIGID AND EQUIVALENT ELASTIC AIRPLANES – 707-320B

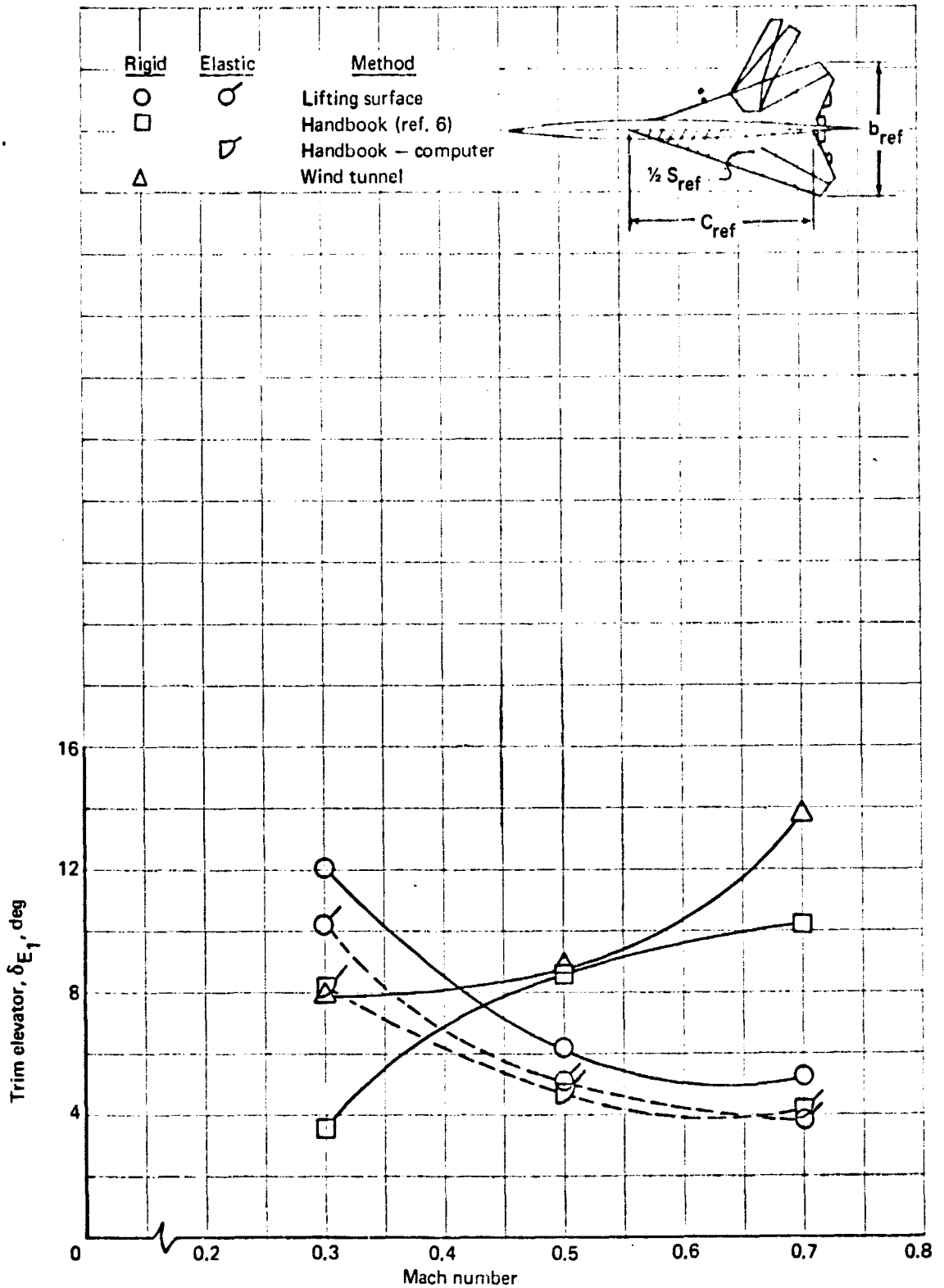

FIGURE 5. TRIM ELEVATOR, RIGID AND EQUIVALENT ELASTIC AIRPLANES – 30° SST

or, if there are large variations in the individual values, it may be more accurate to use incremental corrections such as

$$C_{m_{\alpha_{Eq.El.}}} = C_{m_\alpha}\Big|_{W.T.} + \left(C_{m_{\alpha_E}} - C_{m_{\alpha_R}}\right)_{\text{computed}}$$

This latter method is substantiated in app. B in conjunction with the discussion of the elastic SST wind tunnel model results.

4.3 Stick-Speed Stability

The elevator angle to trim, δ_{E_1}, depends on both dynamic pressure and Mach number, $\delta_{E_1} = \delta_{E_1}(\bar{q}, M)$. Therefore,

$$\frac{d(\delta_E)}{dV}_{n=1} = \frac{\partial(\delta_E)_1}{\partial \bar{q}}\frac{\partial \bar{q}}{\partial V} + \frac{\partial \delta_{E_1}}{\partial M}\frac{dM}{dV} = \rho V_{C_1}\frac{\partial \delta_{E_1}}{\partial \bar{q}} + \frac{1}{a}\frac{\partial \delta_{E_1}}{\partial M} \qquad (4.7)$$

G5 D12

Substituting equation (4.6) into (4.7) and carrying out the indicated differentiation, the following is obtained for the equivalent elastic airplane:

$$\begin{aligned}\frac{d(\delta_E)}{dV}\Big|_E = \frac{1}{C_{m_\alpha}C_{L_{\delta_E}} - C_{m_{\delta_E}}C_{L_\alpha}}\Bigg[&\Bigg\{C_{L_\alpha}\frac{\partial C_{m_0}}{\partial \bar{q}} + C_{m_0}\frac{\partial C_{L_\alpha}}{\partial \bar{q}} \\ &- C_{m_\alpha}\left(\frac{C_{L_1}}{\bar{q}} + \frac{\partial C_{L_0}}{\partial \bar{q}}\right) + \left(C_{L_1} - C_{L_0}\right)\frac{\partial C_{m_\alpha}}{\partial \bar{q}} \\ &- \delta_{E_1}\left(C_{m_\alpha}\frac{\partial C_{L_{\delta_E}}}{\partial \bar{q}} + C_{L_{\delta_E}}\frac{\partial C_{m_\alpha}}{\partial \bar{q}} - C_{m_{\delta_E}}\frac{\partial C_{L_\alpha}}{\partial \bar{q}} - C_{L_\alpha}\frac{\partial C_{m_{\delta_E}}}{\partial \bar{q}}\right)\Bigg\}\rho V_{C_1} \\ &+\Bigg\{\frac{\partial C_{m_\alpha}}{\partial M}\left(C_{L_1} - C_{L_0}\right) - C_{m_\alpha}\frac{\partial C_{L_0}}{\partial M} + C_{L_\alpha}\frac{\partial C_{m_0}}{\partial M} + C_{m_0}\frac{\partial C_{L_\alpha}}{\partial M} \\ &- \delta_{E_1}\left(\frac{\partial C_{m_\alpha}}{\partial M}C_{L_{\delta_E}} + C_{m_\alpha}\frac{\partial C_{L_{\delta_E}}}{\partial M} - C_{L_\alpha}\frac{\partial C_{m_{\delta_E}}}{\partial M} - C_{m_{\delta_E}}\frac{\partial C_{L_\alpha}}{\partial M}\right)\Bigg\}\frac{1}{a}\Bigg]\end{aligned} \qquad (4.8)$$

For the rigid airplane all variations with dynamic pressure vanish, i.e., $\frac{\partial C_{m_0}}{\partial \bar{q}} = \frac{\partial C_{L_1}}{\partial \bar{q}} = 0$, etc. The following simpler equation is then obtained:

$$\left.\frac{d\delta_E}{dV}\right|_R = \frac{1}{C_{m_\alpha} C_{L_{\delta_E}} - C_{m_{\delta_E}} C_{L_\alpha}} \left[\frac{-\partial C_{m_\alpha} C_{L_1}}{V} \right.$$

$$+ \left\{ \frac{\partial C_{m_\alpha}}{\partial M} (C_{L_1} - C_{L_0}) - C_{m_\alpha} \frac{\partial C_{L_0}}{\partial M} + C_{L_\alpha} \frac{\partial C_{m_0}}{\partial M} \right.$$

$$+ C_{m_0} \frac{\partial C_{L_\alpha}}{\partial M} - \delta_{E_1} \left(\frac{\partial C_{m_\alpha}}{\partial M} C_{L_{\delta_E}} + C_{m_\alpha} \frac{\partial C_{L_{\delta_E}}}{\partial M} \right.$$

$$\left. \left. \left. - C_{L_\alpha} \frac{\partial C_{m_{\delta_E}}}{\partial M} - C_{m_{\delta_E}} \frac{\partial C_{L_\alpha}}{\partial M} \right) \right\} \frac{1}{a} \right] \qquad (4.9)$$

The expressions for $d(i_H)/dV$ are the same as equations (4.8) and (4.9), with δ_E replaced by i_H in all terms.

Appendix A refers to stick-speed stability as a handling-qualities parameter. A stable gradient of elevator displacement versus speed is defined there as one for which $d(\delta_E)/dV \mid n = 1 > 0$. A comparison of values of $\frac{d(\delta_E)}{dV}$ predicted from lifting surface theory stability derivatives is made with a flight test value in fig. 6. The one flight test value agrees well with the theoretical prediction. As shown in fig. 7 a stable gradient of $d(i_H)/dV$ is predicted for the rigid 707-320B with good correlation between lifting surface theory and wind tunnel predictions. However, for the equivalent elastic airplane an unstable gradient is shown at the high Mach numbers. Figure 8 illustrates the correlation of methods for the rigid and elastic airplane stick-speed stability for the 72° sweep SST. For this configuration we see that the USAF Handbook produces derivatives that give generally better results than lifting surface theory. The elastic effect can be significant, but depends to a large extent on the flight conditions.

As is noted in fig. 7 for $d(i_H)/dV$, a large discrepancy is shown between the handbook and the other two methods at the higher Mach numbers for the rigid airplane. The opposite trend with Mach number shown by the handbook method is due to the large dropoff in the value of C_{m_α} and C_{L_α} after the force-break Mach number is reached. In other words, the derivatives $\partial C_{m_\alpha}/\partial M$ and $\partial C_{L_\alpha}/\partial M$ are predicted by the handbook to be much larger in the transonic region than either the wind tunnel or lifting surface theory would predict. For $M < M_{fb}$ the term $\frac{1}{a} \frac{\partial(i_H)}{\partial M}$ of equation (4.7) written for the stabilizer is insignificant. Therefore, a good approximation for these subsonic Mach numbers would be

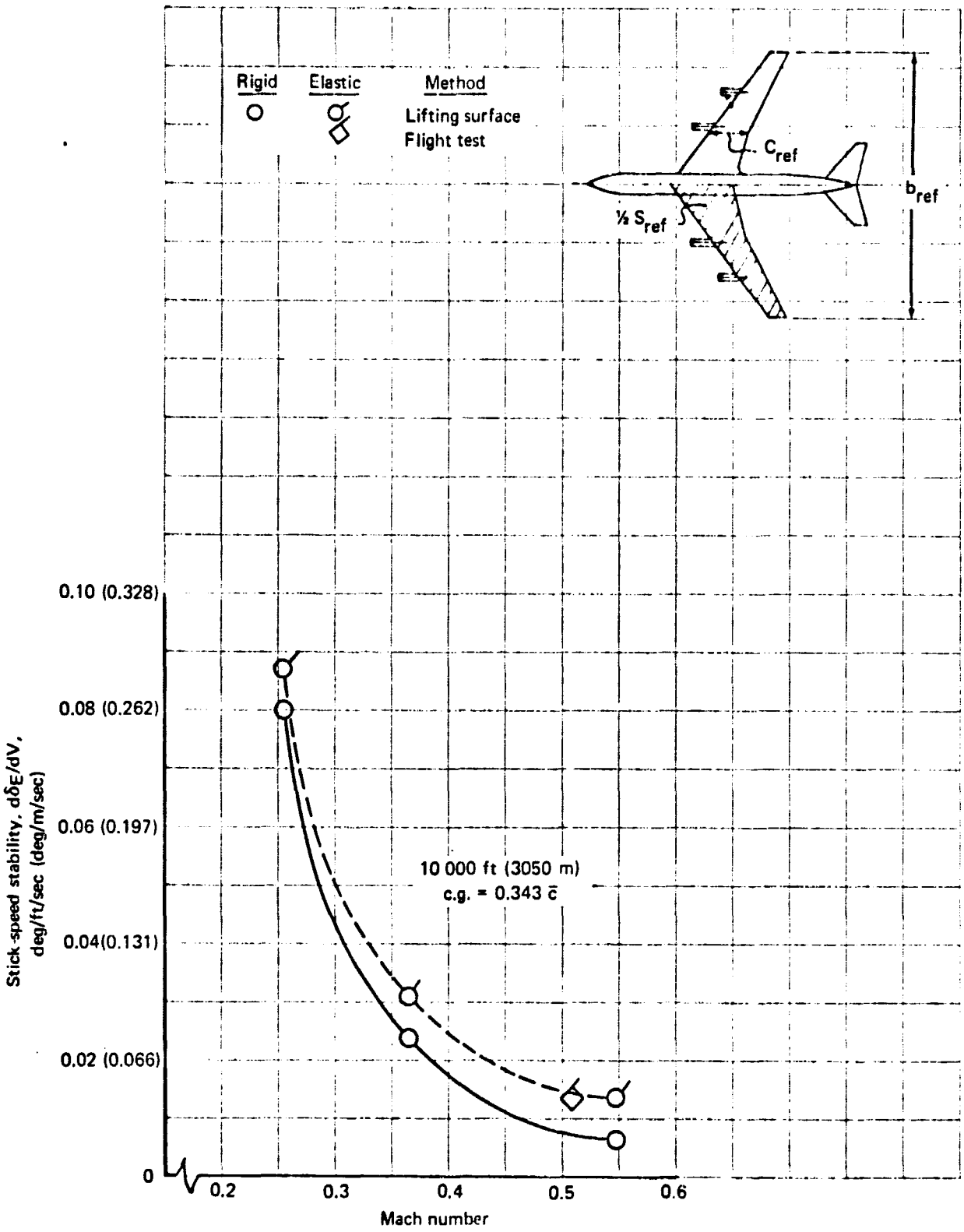

FIGURE 6. STICK-SPEED STABILITY – 707-320B

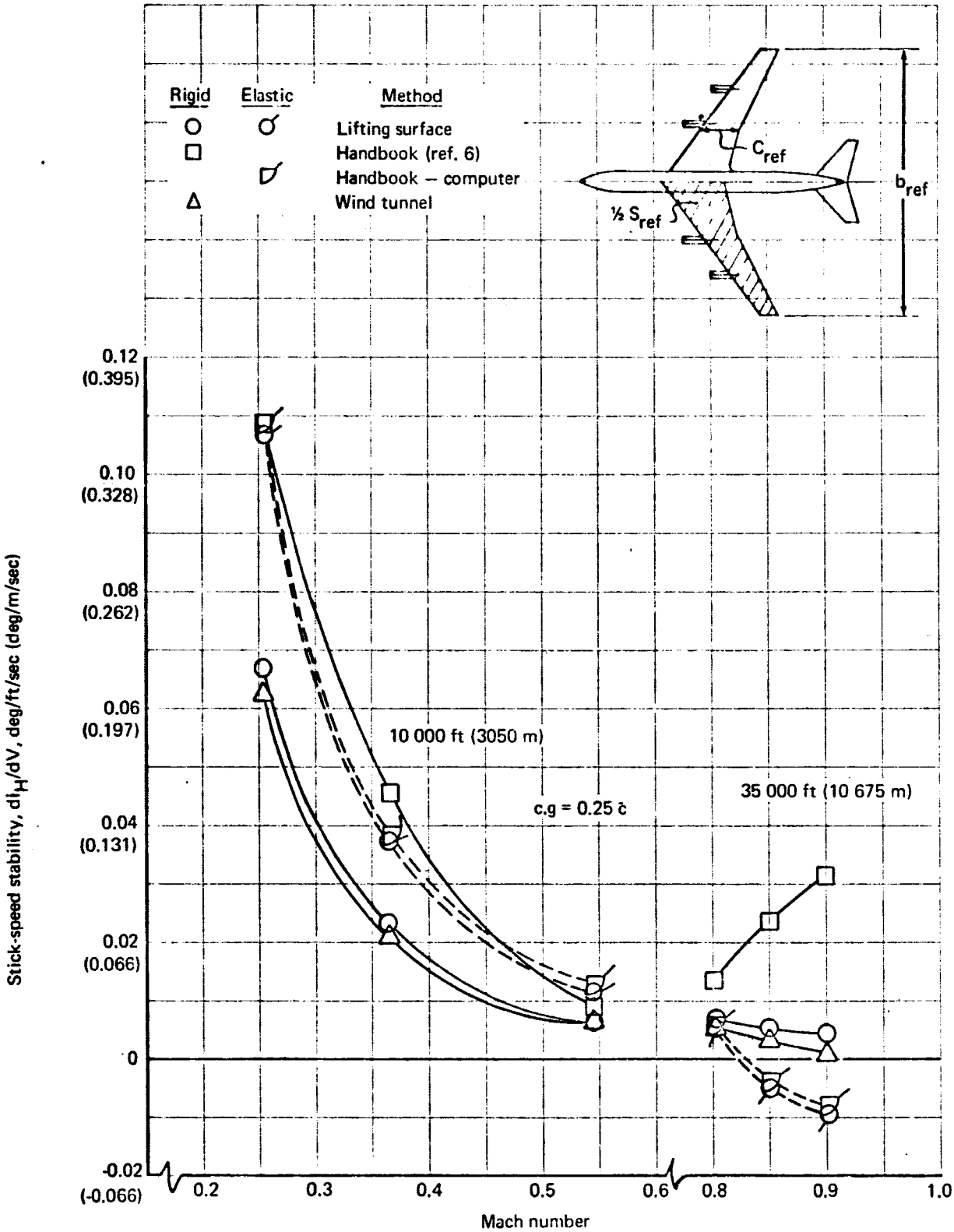

FIGURE 7. STICK-SPEED STABILITY – 707-320B

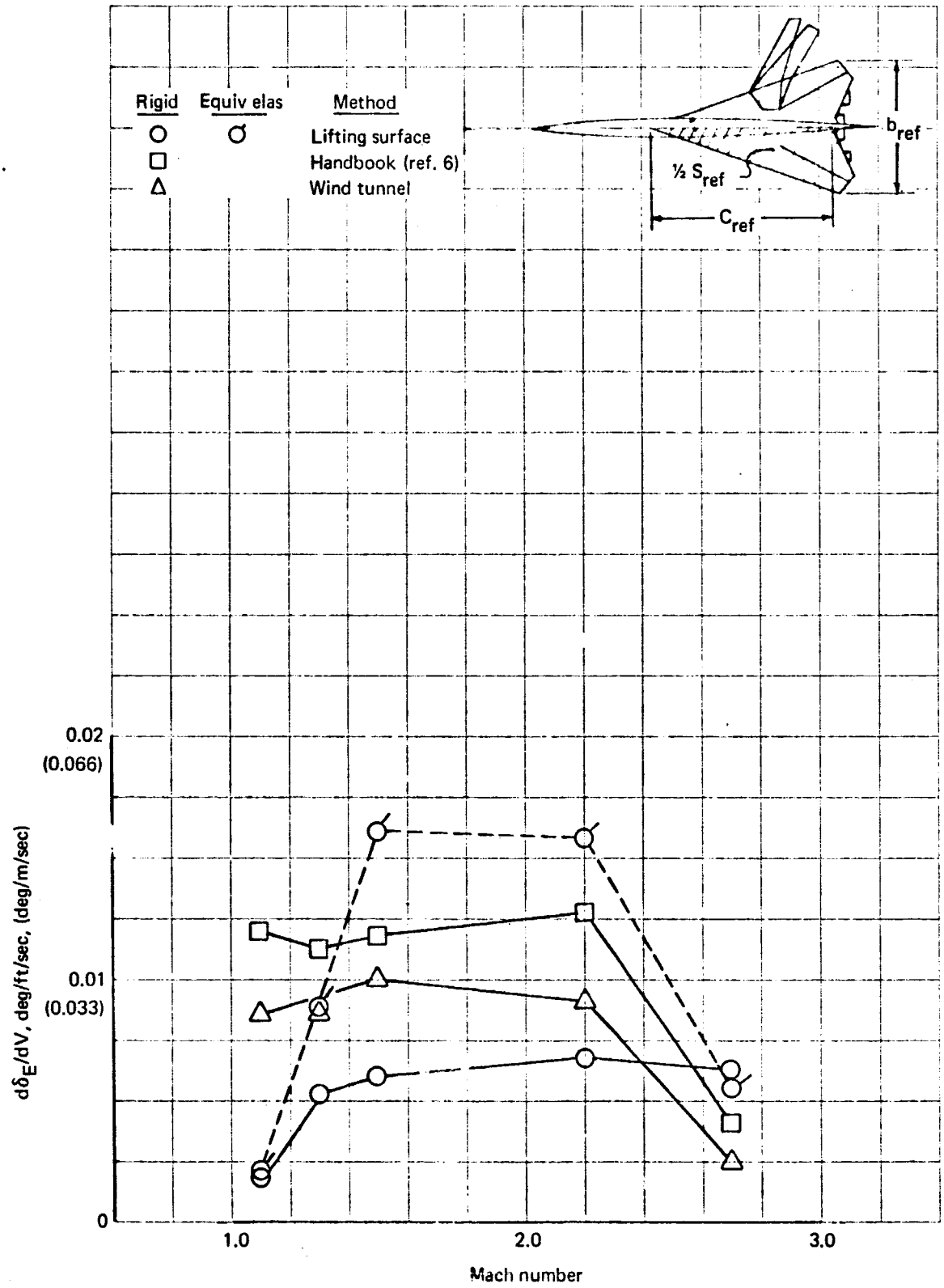

FIGURE 8. $d\delta_E/dV$ CHANGE IN ELEVATOR ANGLE WITH VELOCITY, RIGID VERSUS ELASTIC AIRPLANES – 72° SST

$$\frac{d(i_H)}{dV} = \frac{-2C_{m_\alpha} C_{L_1}}{V(C_{m_\alpha} C_{L_{i_H}} - C_{m_{i_H}} C_{L_\alpha})} \qquad (4.10)$$

It is recommended that wind tunnel derivatives be used to calculate stick-speed stability for the rigid airplane, and that desired elastic effects be determined using lifting surface theory computer methods.

Paragraph 8.3 presents the stick-speed stability data for all configurations and flight conditions of this study.

4.4 Longitudinal Control Per g

Lift and pitching moment coefficients for a steady pullup are given by

(D3)

$$C_m = C_{m_o} + C_{m_\alpha}\alpha + C_{m_{\delta_E}}\delta_E + C_{m_q}\frac{q\bar{c}}{2V_{c_1}}$$

$$C_L = C_{L_o} + C_{L_\alpha}\alpha + C_{L_{\delta_E}}\delta_E + C_{L_q}\frac{q\bar{c}}{2V_{c_1}}$$

Now defining α_1 and δ_{E_1}, as the straight and level steady-state flight conditions, then due to the pullup

$$\Delta C_m = C_{m_\alpha}\Delta\alpha + C_{m_{\delta_E}}\Delta\delta_E + C_{m_q}\frac{q\bar{c}}{2V_{c_1}} \qquad (4.11)$$

$$\Delta C_L = C_{L_\alpha}\Delta\alpha + C_{L_{\delta_E}}\Delta\delta_E + C_{L_q}\frac{q\bar{c}}{2V_{c_1}} \qquad (4.12)$$

However, $\Delta C_m = 0$ (steady, symmetrical pullup), so that from equation (4.11),

$$\Delta\delta_E = -\frac{C_{m_\alpha}\Delta\alpha + C_{m_q}\frac{q\bar{c}}{2V_{c_1}}}{C_{m_{\delta_E}}} \qquad (4.13)$$

From equation (4.12),

$$\Delta\alpha = \frac{1}{C_{L_\alpha}}\left(\Delta C_L - C_{L_{\delta_E}}\Delta\delta_E - C_{L_q}\frac{q\bar{c}}{2V_{c_1}}\right)$$

Also,

$$\Delta C_L = \frac{\Delta L}{\bar{q}S_W} = \frac{nW - W}{\bar{q}S_W} = (n-1)C_{L_1}$$

Therefore,

$$\alpha = \frac{1}{C_{L_\alpha}}\left[(n-1)\,C_{L_1} - C_{L_{\delta_E}}\Delta\delta_E - C_{L_q}\frac{q\bar{c}}{2V_{c_1}}\right] \tag{4.14}$$

Substituting equation (4.14) into (4.13) and solving for $\Delta\delta_E$ yields, after reducing,

$$\Delta\delta_E = -\frac{(n-1)C_{L_1}C_{m_\alpha} - C_{L_q}C_{m_\alpha}\frac{q\bar{c}}{2V_{c_1}} + C_{m_q}C_{L_\alpha}\frac{q\bar{c}}{2V_{c_1}}}{C_{L_\alpha}C_{m_{\delta_E}} - C_{m_\alpha}C_{L_{\delta_E}}}$$

For a steady pullup, a $q = \frac{(n-1)\,g}{V}$, which gives

$$\Delta\delta_E = -\frac{(n-1)\left(C_{m_\alpha}C_{L_1} - C_{m_\alpha}C_{L_q}\frac{g\bar{c}}{2V_{c_1}^2} + C_{m_q}C_{L_\alpha}\frac{g\bar{c}}{2V_{c_1}^2}\right.}{C_{L_\alpha}C_{m_{\delta_E}} - C_{m_\alpha}C_{L_{\delta_E}}}$$

Finally, an expression for elevator angle per g results:

$$\left.\frac{\Delta\delta_{E_1}}{n-1}\right|_{V_{c_1}} = \left.\frac{d(\delta_{E_1})}{dn}\right|_{V_{c_1}} = -\frac{C_{m_\alpha}C_{L_1} + \frac{q\bar{c}}{2V_{c_1}^2}\left(C_{L_\alpha}C_{m_q} - C_{m_\alpha}C_{L_q}\right)}{C_{L_\alpha}C_{m_{\delta_E}} - C_{m_\alpha}C_{L_{\delta_E}}} \tag{4.15}$$

The derivation for trim stabilizer per g is identical to that previously given for $\frac{d\delta_E}{dn}$ and would yield

$$\left.\frac{d(i_H)}{dn}\right|_{V_{c_1}} = -\frac{C_{m_\alpha}C_{L_1} + \frac{q\bar{c}}{2V_{c_1}^2}\left(C_{L_\alpha}C_{m_q} - C_{m_\alpha}C_{L_q}\right)}{C_{L_\alpha}C_{m_{i_H}} - C_{m_\alpha}C_{L_{i_H}}} \tag{4.16}$$

Equations (4.15) and (4.16) hold for both rigid and equivalent elastic airplanes. As with the other static stability characteristics, the derivative C_{m_α} was found to have the largest influences for the configurations investigated. Except for the 30° wing sweep SST configuration, all cases have their best correlation between lifting surface theory and wind tunnel predictions. The derivative $d\delta_E/dn$ is a negative quantity for all cases except where the c.g. is aft of the maneuver point, which is to be expected. A stable gradient of elevator displacement versus load factor is defined in app. A as one that satisfies

$$\left.\frac{d(\delta_{E_1})}{dn}\right|_{V_{c_1}} < 0 \tag{4.17}$$

It was noted that the terms containing the pitch rate derivatives in equation (4.15) were insignificant for the 707-320B, but not for the SST configurations. A good approximation to equation (4.15) for large subsonic type transports would then be

$$\frac{d(\delta_E)}{dn} = \frac{-\,C_{m_\alpha} C_{L_1}}{C_{L_\alpha} C_{m_{\delta_E}} - C_{m_\alpha} C_{L_{\delta_E}}} = \frac{-\,C_{L_1}(h - h_n)}{C_{m_{\delta_E}} - C_{L_{\delta_E}}(h - h_n)} \quad (4.18)$$

For a rougher approximation for the 707-320B, the following equation will suffice

$$\frac{d(\delta_E)}{dn} = -\frac{C_{m_\alpha} C_{L_1}}{C_{L_\alpha} C_{m_{\delta_E}}} \quad (4.19)$$

Equation (4.19) is acceptable for the 707-320B because $C_{m_\alpha} C_{L_{\delta_E}}$ is ten percent or less than the term $C_{L_\alpha} C_{m_{\delta_E}}$ for all flight conditions. Therefore, it is seen that elevator angle per g is approximately proportional to C_{m_α} for the 707-320B. Figure 9 shows $d\delta_E/dn$ for this airplane. The handbook method gave the largest values of the stability derivative C_{m_α} and, consequently $d\delta_E/dn$ was much larger than that shown by the other two methods.

The effect of elasticity is seen to be small for this stability characteristic. It has the effect of an increase in the stable gradient of elevator displacement versus load factor. The effect of elasticity on $d\delta_E/dn$ for the SST configurations is quite small also (see par. 8.3). Figures 54, 55, and 56 show the results for the rigid airplane for all configurations. The comparison of flight test results for the 707-320B with the theoretical prediction obtained by using lifting surface theory stability derivatives is shown in fig. 10. In general, the correlation of lifting surface theory and flight test data is seen to be quite good.

4.5 Neutral and Maneuver Points

The neutral point, h_n, is defined as that c.g. position for which $\partial C_{m_\alpha} / \partial_\alpha = 0$. It was calculated from the expression

$$h_n = h - \frac{C_{m_\alpha}}{C_{L_\alpha}} \quad (4.20)$$

where h is the c.g. position.

(D14) Equation (4.20) is derived in ref. 4 as equation (2.3.3). This expression is only valid for small angles of attack in the linear range.

The maneuver point is defined as that c.g. position for which $d\delta_E/dn = 0$. If either equation (4.15) or (4.16) is rewritten for the maneuver point and if we let $C_{m_\alpha} = C_{L_\alpha}(h - h_n)$, the following is the result:

$$(h_m - h_n) C_{L_1} + \frac{g\bar{c}}{2V_{c_1}^2}\left[C_{m_q} - (h_m - h_n) C_{L_q}\right] = 0 \quad (4.21)$$

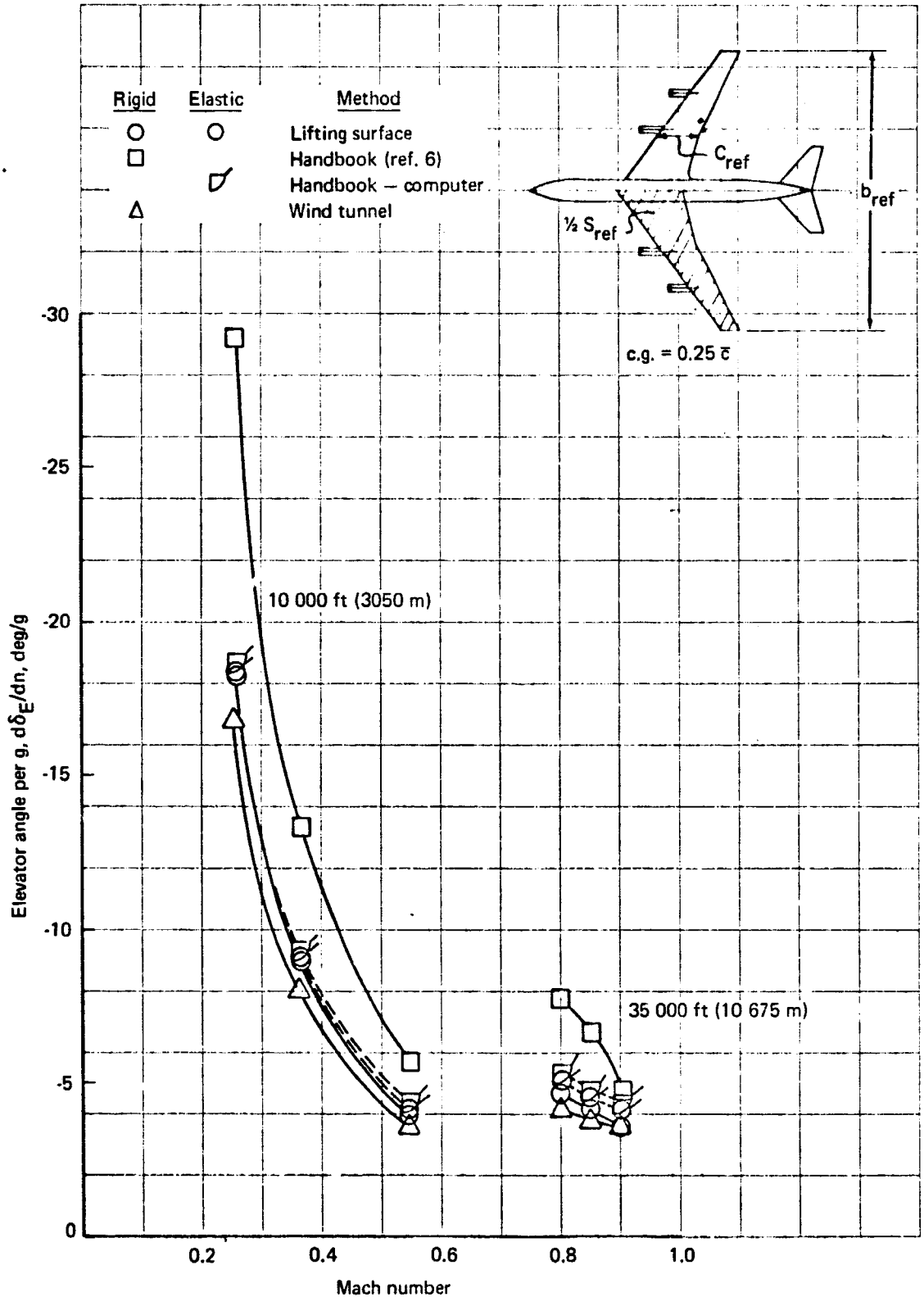

FIGURE 9. ELEVATOR ANGLE PER g, $d\delta_E/dn$ –707-320B

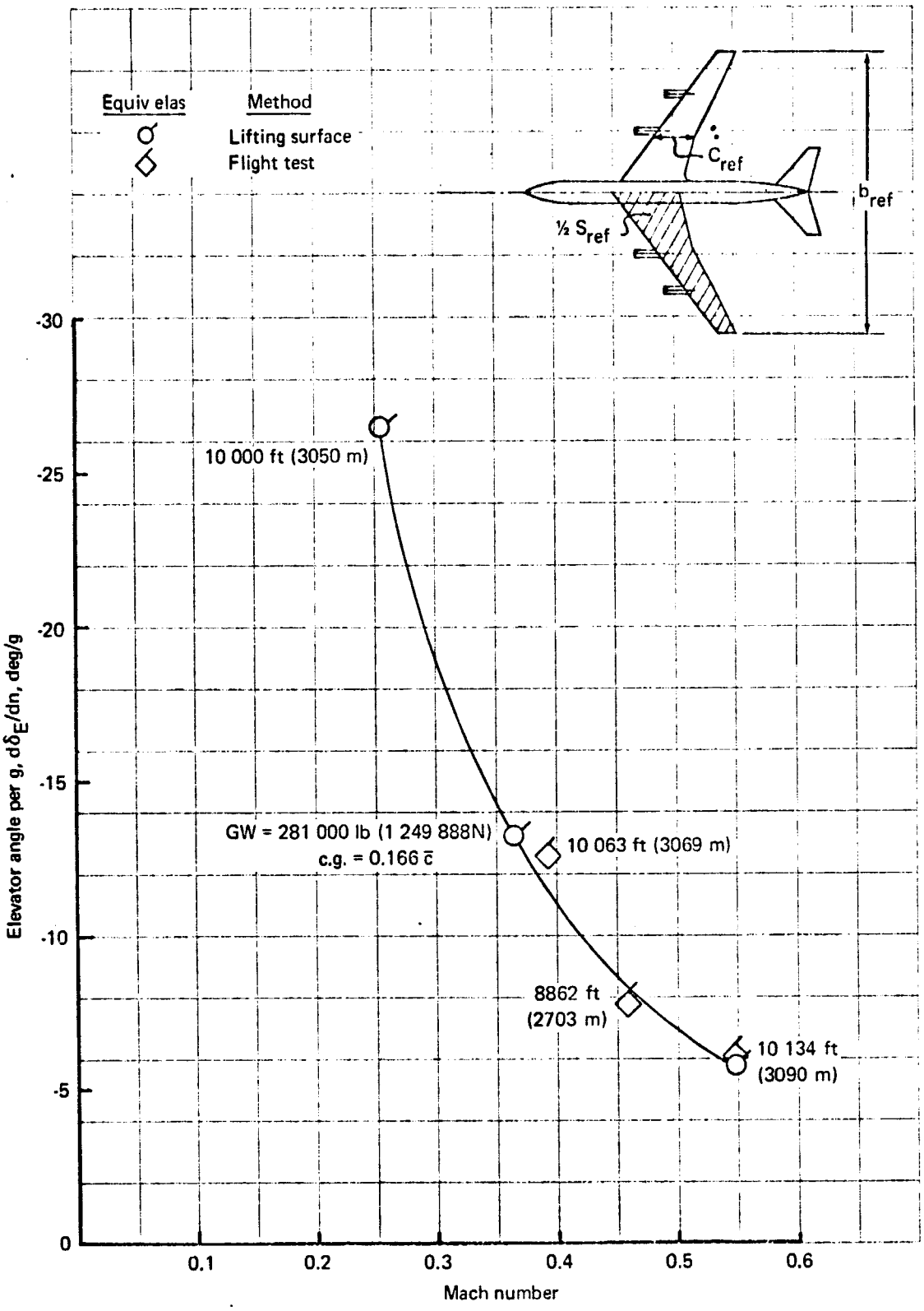

FIGURE 10. ELASTIC ELEVATOR ANGLE PER g, $d\delta_E/dn$ – 707-320B

Let $C_{L_1} = \frac{mg}{\bar{q}Sw} = \frac{2mg}{\rho Vc_1^2 Sw}$ in equation (4.21) and simplify. This yields an expression for the maneuver point

$$h_m = h_n - \frac{C_{m_q}}{\frac{4m}{\rho S_w \bar{c}} - C_{L_{\dot{q}}}} \quad (4.22)$$

Except for the 30° SST configuration, the best correlation with wind tunnel data is given by lifting surface theory for the neutral point. The static margin, $h_n - h$, is shown in figure 11 for both the 707-320B and the 30° sweep SST. As can be seen, lifting surface theory would be quite acceptable for the 707-320B, but for the 30° SST wind tunnel data would have to be used. The rather significant difference between the rigid wind tunnel data and rigid lifting surface data for the 30° SST is due to differences in C_{m_α}. Only a minor change in representing the pressure distribution can affect C_{m_α}. The small discrepancy in pressure distribution used in the lifting surface representation (discussed in detail in app. B) is sufficient to produce the differences shown in the data. Elasticity is seen to have the effect of a forward shift in neutral point (i.e., a smaller static margin) for the 707-320B and an aft shift for the 30° sweep SST.

As pointed out in the introduction to Sec. 4, the mass distribution can have significant effects on the static characteristics of an airplane. A study performed during the course of the SST development and independent of the present study investigated the mass effects. An example of the results of that study is shown in fig. 3. As can be seen, the shift in the neutral point due to elasticity can be either stabilizing or destabilizing depending on the mass distribution. Lifting surface theory methods were used in the analysis.

The correlation of the three methods for the maneuver point calculations is similar to that shown by the neutral point comparisons because of the effect of C_{m_α}. All the results are shown in par. 8.3. In general, lifting surface values compare most favorably with wind tunnel data. For the 707-320B there is a forward shift in maneuver point due to elastic effects; however, for many of the SST flight conditions analyzed there is a slight aft shift. The effect of the stability derivative C_{L_q} on the maneuver point is negligible for both the equivalent elastic and rigid airplanes.

Figures 57 through 60 present the complete set of data for the rigid and equivalent elastic airplanes for all configurations for the neutral point, static margin, and the maneuver point.

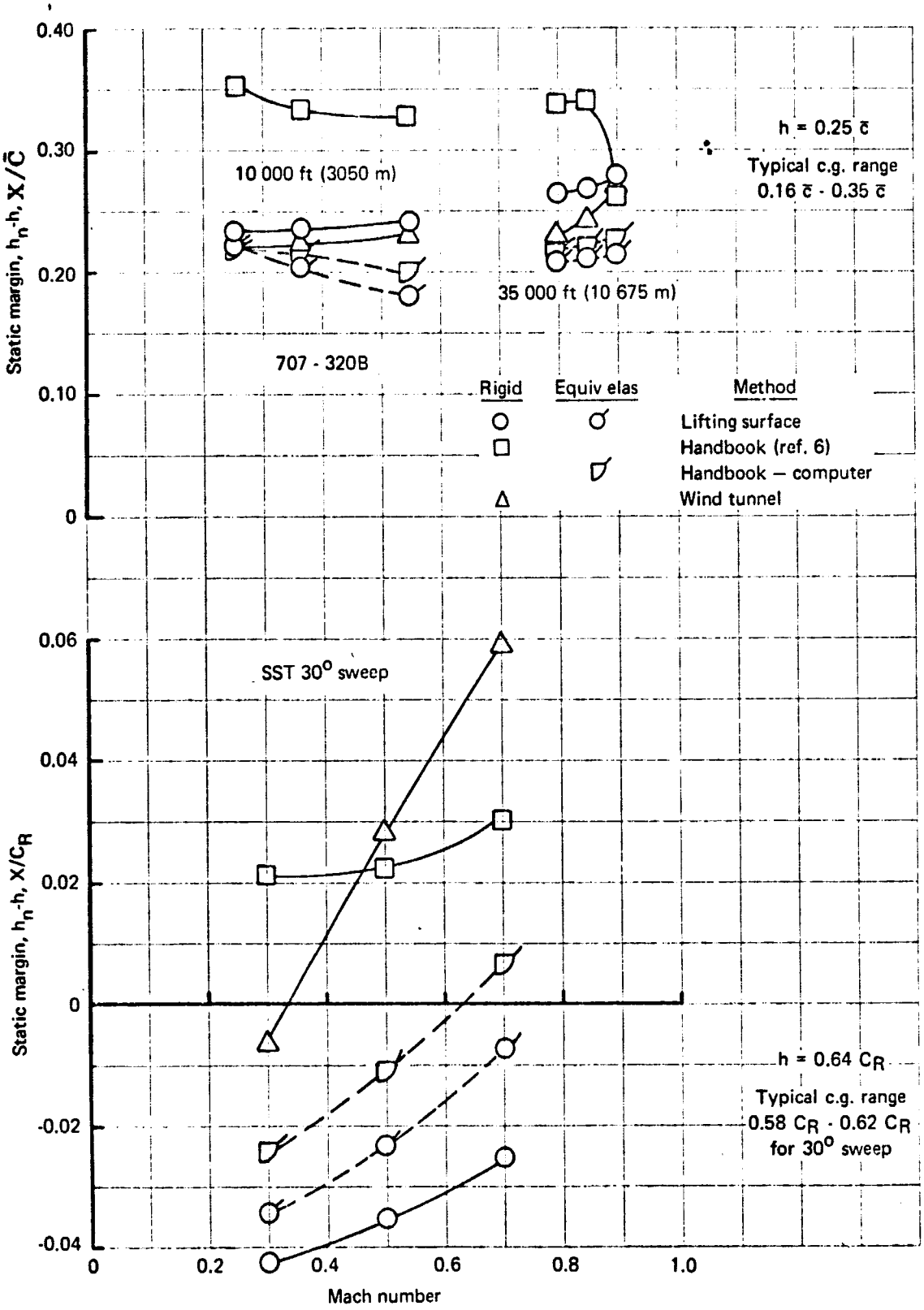

FIGURE 11. STATIC MARGIN – RIGID VERSUS EQUIVALENT ELASTIC AIRPLANES

5. DYNAMIC STABILITY ANALYSIS METHODS

5.1 Introduction

This section presents methods for determining and illustrating dynamic stability characteristics. Dynamic stability criteria that separate motions into the categories of stable, neutrally stable, and unstable are given in app. A. Four sets of stability criteria are discussed in that volume; they are the criteria relative to characteristic equation methods, time history methods, energy decay methods and methods based on the direct method of Lyapunov. Of these, only characteristic equation methods and time history methods are adequately mechanized. Further, of the characteristic equation methods, only the method for the roots of the characteristic equations is mechanized. Thus, two methods, roots of the characteristic equations and time histories, were used to obtain and analyze the predicted dynamic stability characteristics of the study airplanes. Figure 12 indicates how the calculation methods and dynamic stability criteria relate.

5.2 Roots of Characteristic Equations

Airplane equations of motion can be reduced to a set of linear second-order differential equations with constant coefficients when dynamic behavior can be approximated by assuming that motion perturbations relative to the steady state are small. These equations are called small perturbation equations of motion and are amenable to generating characteristic equations whose roots can be examined to determine motion characteristics. (G8)

The dynamic stability criteria of all characteristic equation roots in app. A are:

If the airplane equations of motion are linear and autonomous*, then the airplane stability behavior is said to be:

- stable, if the real parts of the roots of the characteristic equation are all negative;

*Autonomous equations do not contain time explicitly.

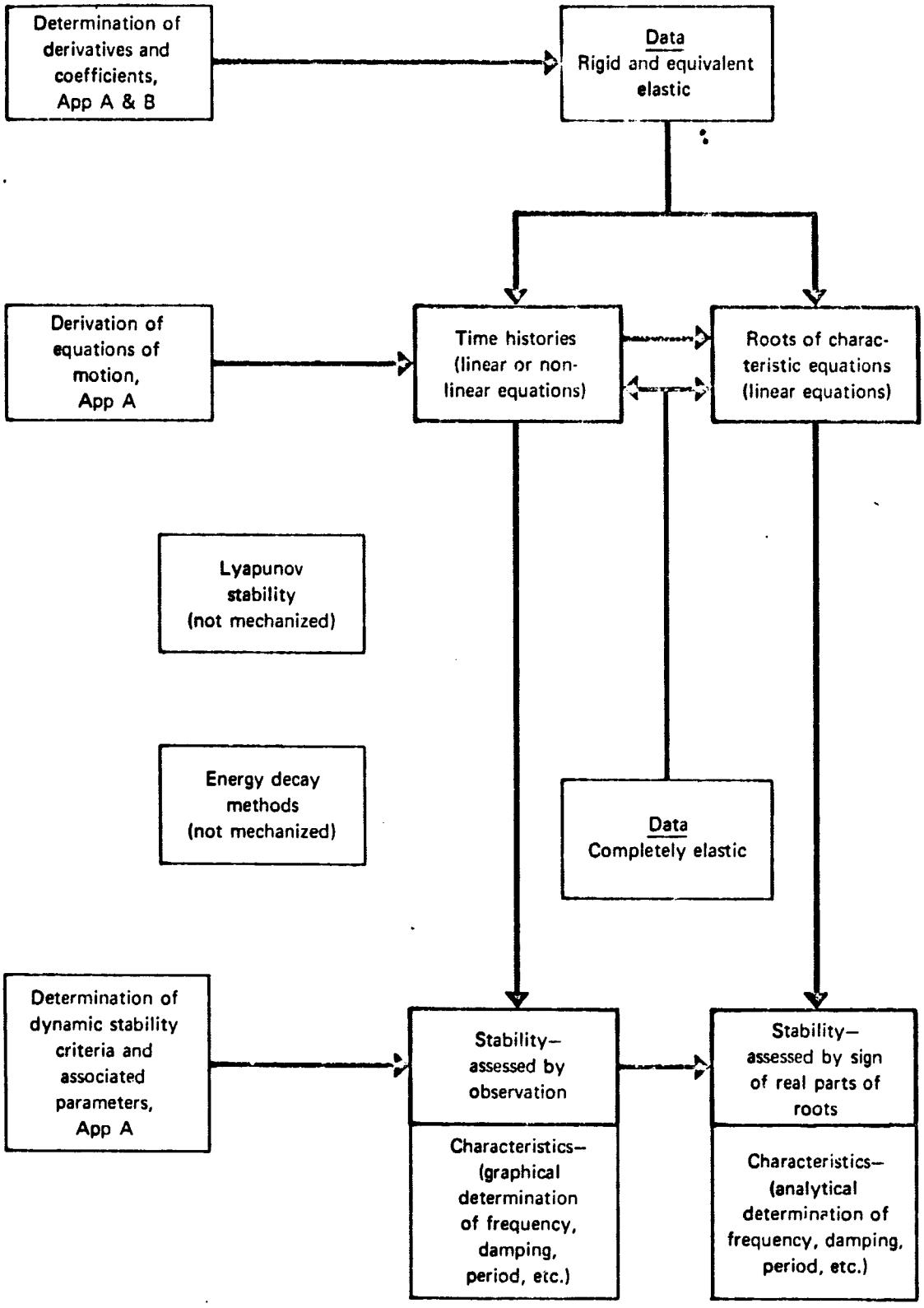

FIGURE 12. APPLICATIONS OF DYNAMIC STABILITY CRITERIA

- neutrally stable, if one or more roots of the characteristic equation has zero real parts and the remaining roots have all-negative real parts;
- unstable, if at least one root of the characteristic equation has a positive real part.

These criteria can be satisfied by inspection, i.e., by checking the sign or absence of the real parts of the roots. However, these yes-no-type stability answers relate very little information about airplane motion characteristics. Some of the parameters that can be deduced from the roots and that are more physically oriented than just the roots themselves are discussed below.

5.2.1 Rigid and equivalent elastic mathematical models. — The rigid airplane small perturbation longitudinal and lateral-directional equations of motion for steady, rectilinear flight developed in app. A are repeated in table 4 in a somewhat revised matrix form for discussion purposes. As was discussed in app. A, it is possible to take the Laplace transformation of the equations of motion and solve for the roots of the resulting characteristic equations. However, the program that generated the roots and associated data in this study uses a different technique. This program will be referred to as the "small perturbation program." The equations in table 4 can be put into the form used in the small perturbation program through a series of assumptions and substitutions combined with a good deal of algebraic manipulation. The assumptions and substitutions are listed below.

(1) Straight and level flight gives the following:

$$
\begin{aligned}
M_g &= W = \bar{q} S_w C_{L_1} \qquad \text{(D9)} \\
Q_1 &= 0 \qquad \text{(D12)} \\
\theta_1 &= 0 \Rightarrow \dot{\phi} = p \qquad \text{(D13)} \\
\dot{\theta} &= q
\end{aligned}
\tag{5.1}
$$

(2) Thrust effects are negligible.

$$
\begin{aligned}
C_{T_{x_\alpha}} &\approx 0 \\
C_{T_{z_u}} &\approx 0 \\
C_{T_{z_\alpha}} &\approx 0 \qquad \text{(D11)}
\end{aligned}
\tag{5.2}
$$

TABLE 4. – SMALL PERTURBATION EQUATIONS OF MOTION IN STABILITY AXES

a. Longitudinal

$$\begin{bmatrix} 1 & \frac{\bar{q}S_w\bar{c}}{2MV_{c_1}^2}C_{D_{\dot{u}}} & 0 & 0 \\ 0 & 1-\frac{\bar{q}S_w\bar{c}}{2MV_{c_1}^2}C_{L_{\dot{u}}} & 0 & 0 \\ 0 & -\frac{\bar{q}S_w\bar{c}^2}{2I_{YY_1}V_{c_1}}C_{m_{\dot{u}}} & 1 & 0 \\ 0 & 0 & 0 & 1 \end{bmatrix} \begin{Bmatrix} \dot{u} \\ \dot{\alpha} \\ \dot{q} \\ \dot{\theta} \end{Bmatrix}$$

Assumptions required:

G1-6 G8 G10

D1 D2 D5 D6 D9 D13 D14

S1 S2 S5 S10 S11

$$= \begin{bmatrix} \frac{\bar{q}S_w}{MV_{c_1}}[(C_{T_{X_u}}-C_{D_u})+2(C_{T_{X_1}}-C_{D_1})] & -Q_1V_{c_1}+\frac{\bar{q}S_w}{M}(C_{T_{X_\alpha}}-C_{D_\alpha}+C_{L_\alpha}) & -\frac{\bar{q}S_w\bar{c}}{2MV_{c_1}}C_{D_q} & -g\cos\theta_1 \\ \frac{Q_1}{V_{c_1}}+\frac{\bar{q}S_w}{MV_{c_1}^2}[(C_{T_{Z_u}}-C_{L_u})+2(C_{T_{Z_1}}-C_{L_1})] & \frac{\bar{q}S_w}{MV_{c_1}}(C_{T_{Z_\alpha}}-C_{L_\alpha}-C_{D_1}) & 1-\frac{\bar{q}S_w\bar{c}}{2MV_{c_1}^2}C_{L_q} & -\frac{g}{V_{c_1}}\sin\theta_1 \\ \frac{\bar{q}S_w\bar{c}}{I_{YY_1}V_{c_1}}(C_{T_{m_u}}+C_{m_u}) & \frac{\bar{q}S_w\bar{c}}{I_{YY_1}}(C_{T_{m_\alpha}}+C_{m_\alpha}) & \frac{\bar{q}S_w\bar{c}^2}{2I_{YY_1}V_{c_1}}C_{m_q} & 0 \\ 0 & 0 & 1 & 0 \end{bmatrix} \begin{Bmatrix} u \\ \alpha \\ q \\ \theta \end{Bmatrix}$$

TABLE 4. – SMALL PERTURBATION EQUATIONS OF MOTION IN STABILITY AXES (CONCLUDED)

b. Lateral-directional

$$\begin{bmatrix} 1 - \frac{\bar{q}Sb}{2MV_{c_1}^2} C_{Y_{\dot\beta}} & 0 & 0 & 0 \\ -\frac{\bar{q}Sb^2}{2V_{c_1} I_{xx_{1_S}}} C_{l_{\dot\beta}} & 1 & -\frac{I_{xz_{1_S}}}{I_{xx_{1_S}}} & 0 \\ -\frac{\bar{q}Sb^2}{2V_{c_1} I_{zz_{1_S}}} C_{n_{\dot\beta}} & -\frac{I_{xz_{1_S}}}{I_{zz_{1_S}}} & 1 & 0 \\ 0 & 0 & 0 & 1 \end{bmatrix} \begin{Bmatrix} \dot\beta \\ \dot p \\ \dot r \\ \dot\phi \end{Bmatrix}$$

Assumptions required:

D1 D2 D5 D6 D7 D9 D13 D14
G1-6 G8 G10
S1 S2 S5 S10

$$= \begin{bmatrix} \frac{\bar{q}S_w}{MV_{c_1}} C_{Y_\beta} & \frac{\bar{q}Sb}{2MV_{c_1}^2} C_{Y_p} & \frac{\bar{q}Sb}{2MV_{c_1}^2} C_{Y_r} - 1 & \frac{g}{V_{c_1}} \cos\theta_1 \\ \frac{\bar{q}Sb}{I_{xx_{1_S}}} C_{l_\beta} & \frac{I_{xz_{1_S}}}{I_{xx_{1_S}}} Q_1 + \frac{\bar{q}Sb^2}{2V_{c_1} I_{xx_{1_S}}} (C_{T_{l_p}} + C_{l_p}) & \frac{I_{yy_{1_S}} - I_{zz_{1_S}}}{I_{xx_{1_S}}} Q_1 + \frac{\bar{q}Sb^2}{2V_{c_1} I_{xx_{1_S}}} C_{l_r} & 0 \\ \frac{\bar{q}Sb}{I_{zz_{1_S}}} C_{n_\beta} & \frac{I_{xx_{1_S}} - I_{yy_{1_S}}}{I_{zz_{1_S}}} Q_1 + \frac{\bar{q}Sb^2}{2V_{c_1} I_{zz_{1_S}}} C_{n_p} & -\frac{I_{xz_{1_S}}}{I_{zz_{1_S}}} Q_1 + \frac{\bar{q}Sb^2}{2V_{c_1} I_{zz_{1_S}}} C_{n_r} & 0 \\ 0 & 1 & \tan\theta_1 & Q_1 \tan\theta_1 \end{bmatrix} \begin{Bmatrix} \beta \\ p \\ r \\ \phi \end{Bmatrix}$$

$$C_{T_{z_1}} \approx 0$$

$$C_{T_{m_u}} \approx 0$$

$$C_{T_{m_\alpha}} \approx 0$$

$$\frac{\partial T}{\partial u} \approx 0 \Rightarrow -C_{T_{x_u}} - 2C_{T_{x_1}} \approx 0$$

(3) The following substitutions are made.

$$\mu = \frac{M}{\rho S w \ell}$$

$$\ell = \begin{cases} \frac{\bar{c}}{2} & \text{longitudinal equations} \\ \frac{b}{2} & \text{lateral-directional equations} \end{cases}$$

$$t^* = \frac{\ell}{V c_1}$$

$$i_A = \frac{I_{xx}}{\rho S w \ell^3}$$

$$i_B = \frac{I_{yy}}{\rho S w \ell^3}$$

$$i_C = \frac{I_{zz}}{\rho S w \ell^3}$$

$$i_E = \frac{I_{xz}}{\rho S w \ell^3} \qquad (5.3)$$

$$\hat{u} = \frac{u}{V c_1}$$

$$\hat{r} = \frac{rb}{2V c_1} = \frac{r\ell}{V c_1}$$

(4) Rather than the Laplace transformation a differential operator notation is used.

$$D = t^* \frac{d}{dt}$$

(5) The conventional elevator (δ_E), aileron (δ_A), and rudder (δ_R) control terms are added.

$$C_{z_{\delta_E}} \quad C_{m_{\delta_E}}$$

$$C_{Y_{\delta_A}} \quad C_{Y_{\delta_R}}$$

$$C_{\ell_{\delta_A}} \quad C_{\ell_{\delta_R}}$$

$$C_{n_{\delta_A}} \quad C_{n_{\delta_R}}$$

(6) The effect of pitch rate on drag, C_{D_q}, is negligible. (D8)

Using items (1) through (6), the equations presented in table 5 are obtained. These equations are similar to those in ref. 4, with slightly different derivative nomenclature. Some modifications to these equations are required to handle the equivalent elastic airplane model. For example, those accelerations affecting inertia relief in the lateral-directional modes are $\ddot{y}_I$, $\dot{p}$, and $\dot{r}$. Inertia relief due to these accelerations is affected by letting

$$
\begin{aligned}
M &\rightarrow M' = M - C_{Y_{\ddot{Y}_I}} \bar{q} S_W \\
I_{xx} &\rightarrow I'_{xx} = I_{xx} - C_{\ell_{\dot{p}_I}} \bar{q} S_{wb} \\
I_{zz} &\rightarrow I'_{zz} = I_{zz} - C_{n_{\dot{r}_I}} \bar{q} S_{wb} \\
I_{xz} &\rightarrow I'_{xz} = \frac{I''_{xz} + I'''_{xz}}{2} \\
&= \frac{1}{2}\left[\left(I_{xz} + C_{\ell_{\dot{r}_I}} \bar{q} S_{wb}\right) + \left(I_{xz} + C_{n_{\dot{p}_I}} \bar{q} S_{wb}\right)\right]
\end{aligned}
\tag{5.4}
$$

In addition, the following effects were not included:

$$C_{Y_{\dot{p}_I}} \; , \; C_{Y_{\dot{r}_I}} \; , \; C_{\ell_{\ddot{Y}_I}} \; , \; C_{n_{\ddot{Y}_I}} \qquad \text{(D7)}$$

These terms could not be accounted for due to limitations in the current technique. However, this is not a major discrepancy for the study airplanes. It is shown in app. B that these terms are very small.

Thus, the characteristic equation with the indicated rigid/equivalent elastic definitions evolves as indicated in table 6a. This equation is a result of the requirement that (for $\delta_A = \delta_R = 0$)

$$\left[A(D)\right]\{x\} = \{0\} \tag{5.5}$$

has nontrivial solutions, i.e.,

$$\{x\} = \begin{Bmatrix} \beta \\ \varphi \\ \hat{r} \end{Bmatrix} \neq \{0\}$$

Frequency, damping, and related data were obtained from the equation in table 6a. Appropriate rigid and equivalent elastic input data to this equation are tabulated in par. 8.2.

TABLE 5. – EQUATIONS OF MOTION MECHANIZED IN SMALL PERTURBATION PROGRAM

$$\begin{bmatrix} (2\mu - C_{y_{\dot\beta}})D - C_{y_\beta} & -(C_{y_p}D + C_{L_\epsilon}) & (2\mu - C_{y_r}) \\ -(C_{l_\beta} + C_{l_{\dot\beta}}D) & i_A D^2 - C_{l_p}D & -(i_E D + C_{l_r}) \\ -(C_{n_\beta} + C_{n_{\dot\beta}}D) & -(i_E D^2 + C_{n_p}D) & i_C D - C_{n_r} \end{bmatrix} \begin{Bmatrix} \beta \\ \phi \\ \psi \end{Bmatrix} = \begin{bmatrix} C_{y_{\delta_A}} & C_{y_{\delta_R}} \\ C_{l_{\delta_A}} & C_{l_{\delta_R}} \\ C_{n_{\delta_A}} & C_{n_{\delta_R}} \end{bmatrix} \begin{Bmatrix} \delta_A \\ \delta_R \end{Bmatrix}$$

$$\begin{bmatrix} 2\mu D + C_{D_u} + 2C_{D_1} & C_{D_{\dot\alpha}} - C_{L_2} & C_{L_1} \\ C_{L_u} + 2C_{L_1} & (2\mu + C_{L_{\dot\alpha}})D + (C_{L_\alpha} + C_{D_1}) & -(2\mu - C_{L_q})D \\ -C_{m_u} & -(C_{m_{\dot\alpha}}D + C_{m_\alpha}) & i_B D^2 - C_{m_q}D \end{bmatrix} \begin{Bmatrix} \hat{u} \\ \alpha \\ \theta \end{Bmatrix} = \begin{Bmatrix} 0 \\ C_{z_{\delta_E}} \\ C_{m_{\delta_E}} \end{Bmatrix} \delta_E$$

Assumptions required:

D1 D2 D5-9 D11 D13 D14
G1-6 G8 G10
S1 S2 S5 S10

TABLE 6. – CHARACTERISTIC EQUATIONS IN DETERMINANT FORM

a. Lateral-directional

$$\begin{vmatrix} (2\mu - C_{y_{\dot\beta}})D - C_{y_\beta} & -(C_{y_p}D + C_{L_1}) & (2\mu - C_{y_r}) \\ -(C_{l_\beta} + C_{l_{\dot\beta}}D) & i_A D^2 - C_{l_p}D & -(i_E D + C_{l_r}) \\ -(C_{n_\beta} + C_{n_{\dot\beta}}D) & -(i_E D^2 + C_{n_p}D) & i_C D - C_{n_r} \end{vmatrix} = 0$$

where: $\mu = M/\rho S_w \ell$; $M = W/g$; $\ell = b/2$

$D = t^* d/dt$; $t^* = \ell / V_{C_1}$

Note: For the equivalent elastic airplane, $C_{y_{\dot p_I}}$, $C_{y_{\dot r_I}}$, $C_{l_{\ddot y_I}}$, $C_{n_{\ddot y_I}}$ are not accounted for.

Rigid airplane S8	Equivalent elastic airplane S3 & S7
All derivatives are conventional rigid derivatives.	Derivatives include elastic effects due to aerodynamic loading (Formulation I) and would have $\bar{E}$ subscripts.
$i_A = I_{xx}/\rho S_w \ell^3$	$i_A = (I_{xx} - C_{l_{\dot p_I}} \bar q S_w b)/\rho S_w \ell^3$
$i_C = I_{zz}/\rho S_w \ell^3$	$i_C = (I_{zz} - C_{n_{\dot r_I}} \bar q S_w b)/\rho S_w \ell^3$
$i_E = I_{xz}/\rho S_w \ell^3$	$i_E = \dfrac{(I_{xz} + \frac{1}{2} C_{l_{\dot r_I}} \bar q S_w b + \frac{1}{2} C_{n_{\dot p_I}} \bar q S_w b}{\rho S \ell^3}$
W = Actual gross weight = W_1	$W = g(M - C_{y_{\ddot y I}} \bar q S_w)$; $M = W_1/g$

Assumptions required: D1 D2 D5 D7 D11 G1 – 6 G10 S1 S2 S5

and

$$R_1 = \emptyset_1 = \beta_1 = 0$$

TABLE 6. -- CHARACTERISTIC EQUATIONS IN DETERMINANT FORM (CONCLUDED)

b. Longitudinal

$$\begin{vmatrix} 2\mu D + C_{D_u} + 2C_{D_1} & C_{D_\alpha} - C_{L_1} & \dot{C}_{L_1} \\ C_{L_u} + 2C_{L_1} & (2\mu + C_{L_{\dot\alpha}})D + (C_{L_\alpha} + C_{D_1}) & -(2\mu - C_{L_q})D \\ -C_{m_u} & -(C_{m_{\dot\alpha}}D + C_{m_\alpha}) & i_B D^2 - C_{m_q} D \end{vmatrix} = 0$$

where:

$$\mu = M/\rho S_w \ell; \quad M = W/g; \quad \ell = \bar{c}/2$$

$$D = t^* d/dt; \quad t^* = \ell / V_{c_1}$$

Note: For the equivalent elastic airplane, $C_{L_{\ddot\theta_I}}$ and all $\dot{u}_I$ are not accounted for.

Rigid airplane S8	Equivalent elastic airplane S7
All derivatives are conventional rigid derivatives. $i_B = I_{yy}/\rho S_w \ell^3$ W = Actual airplane weight	Derivatives include elastic effects due to both aerodynamic and inertial loading (Formulation II) and would have E subscripts. $i_B = (I_{yy} - C_{m_{\dot\theta_E}} \bar{q} S_w \bar{c})/\rho S_w \ell^3$ W = Actual airplane weight

Assumptions required:

(D1) (D2) (D5) (D7) (D11) (G1 - 6) (G10) (S1) (S2) (S5) and

$R_1 = \phi_1 = \beta_1 = C_{T_{m1}} + C_{m_1} = 0$

The longitudinal equations also require consideration of three accelerations. These are $\dot{u}$, $\dot{w}/V_{c_1} = \dot{\alpha}$, and $\dot{q} = \ddot{\theta}$. Elastic deformations in the airplane x-direction are usually small and, hence, those deformations due to $\dot{u}$ are ignored. The effects of $\dot{\alpha}$ do not completely specify the load factor conditions. In particular, the perturbation load factor is given by (S10)

$$n_p = -\left(\frac{\dot{W}}{g} - \frac{V_{c_1} q}{g} + \theta \sin\theta_1\right)$$

as is shown in app. B. However, as indicated in equation (5.1), $\theta_1 = 0$, yielding

$$n_p = -\left(\frac{\dot{W}}{g} - \frac{V_{c_1} q}{g}\right) \tag{5.6}$$

Adding load factor terms with proper nondimensionalizing scale factors, the second matrix equation in table 5 may be rewritten to account for inertia relief due to load factor perturbations. However, since current applications of lifting surface theory (influence coefficient methods) allow the implicit treatment of inertia relief, called Formulation II in app. B, it was decided that derivatives that include inertia relief would be used.

The effects due to $\ddot{\theta}$ cannot be treated explicitly. To treat $C_{L_{\ddot{\theta}_I}}$ in the equation form of the second equation in table 5, it is necessary to have a D^2 term (D6) in the second row, third column of the [A(D)] matrix. This is not currently available. The other major effect, $C_{m_{\ddot{\theta}_I}}$, can be treated by modifying the pitch inertia term, i_B. This effect is discussed in app. B and identified as using

$$I_{yy_{EFF}} = I_{yy_I} - C_{m_{\ddot{\theta}_I}} \bar{q} S_w \bar{c} \tag{5.7}$$

where

$$C_{m_{\ddot{\theta}_I}} = \partial C_m / \partial \ddot{\theta}_I$$

For the longitudinal equations, the characteristic equation in determinant form with rigid/equivalent elastic definitions is given in table 6b.

The expanded form of the characteristic equations given in table 6 for the small perturbation equations of motion written in the parameter λ is

$$A\lambda^4 + B\lambda^3 + C\lambda^2 + D\lambda + E = 0 \tag{5.8}$$

where the coefficients A through E are determined by the case (longitudinal or lateral-directional). This is obtained by assuming the solutions

$$\text{Longitudinal mode} \quad \begin{cases} \hat{u} = \hat{u}_o e^{\lambda t/t^*} \\ \alpha = \alpha_o e^{\lambda t/t^*} \\ \theta = \theta_o e^{\lambda t/t^*} \end{cases} \tag{5.9}$$

or

$$\text{Lateral-directional mode} \quad \begin{cases} \beta = \beta_o e^{\lambda t/t^*} \\ \phi = \phi_o e^{\lambda t/t^*} \\ \hat{r} = \hat{r}_o e^{\lambda t/t^*} \end{cases} \tag{5.10}$$

and substituting these into the equations in the form of (5.5). After carrying out the differentiation, $e^{\lambda t/t^*}$ can be eliminated, leaving

$$\left[A(\lambda)\right]\{x_o\} = \{0\} \tag{5.11}$$

where $[A(\lambda)]$ is identical with $[A(D)]$ for $\lambda = D$. The solutions $\lambda'_i = \lambda_i / t^*$, $i = 1, 2, 3, 4$ of the fourth-order polynomial (5.8), are the "roots of the characteristic equation." Since a rather complete discussion of the coefficients A through E and the occurrence and significance of various combinations of real and complex roots may be found in refs. 4 and 36, it is not repeated here. The coefficients are, however, presented below. For the characteristic equation:

$$A\lambda^4 + B\lambda^3 + C\lambda^2 + D\lambda + E = 0$$

longitudinal coefficients are as follows.

$$A = 2\mu i_B (2\mu + C_{L_{\dot{\alpha}}})$$

$$B = 2\mu i_B \left[(C_{L_\alpha} + C_{D_t}) + (C_{D_u} + 2C_{D_t})\right] + i_B C_{L_{\dot{\alpha}}} (C_{D_u} + 2C_{D_t}) + 2\mu (C_{L_q} C_{m_{\dot{\alpha}}} - C_{m_q} C_{L_{\dot{\alpha}}}) - 4\mu^2 (C_{m_{\dot{\alpha}}} + C_{m_q})$$

$$C = i_B [(C_{Du} + 2C_{D_1})(C_{L\alpha} + C_{D_2}) - (C_{D\alpha} - C_{L_1}) C_{Lu}]$$
$$- 2\mu [C_{mq} (C_{L\alpha} + C_{D_2}) - C_{m\alpha} C_{Lq} + (C_{mq} + C_{m\dot{\alpha}})(C_{Du} + 2C_{D_1})]$$
$$- 4\mu^2 C_{m\alpha} - (C_{Du} + C_{D_2})(C_{mq} C_{L\dot{\alpha}} - C_{Lq} C_{m\dot{\alpha}})$$
$$- 2i_B C_{L_2} (C_{D\alpha} - C_{L_1})$$

$$D = -2C_{L_2}^2 C_{m\dot{\alpha}} - 2\mu [C_{m\alpha} (C_{Du} + 2C_{D_1}) - C_{mu} (C_{D\alpha} - C_{L_1})$$
$$- C_{L_2} C_{mu}] + (C_{Du} + 2C_{D_1}) [C_{m\alpha} C_{Lq} - C_{mq} (C_{L\alpha} + C_{D_2})]$$
$$- (C_{D\alpha} + C_{L_1})(C_{mu} C_{Lq} - C_{mq} C_{Lu})$$
$$+ C_{L_2} (C_{mu} C_{L\dot{\alpha}} - C_{Lu} C_{m\dot{\alpha}}) + 2 C_{L_2} C_{mq} (C_{D\alpha} - C_{L_1})$$

$$E = C_{L_2} [C_{mu} C_{L\alpha} - C_{m\alpha} (C_{Lu} + 2C_{L_2})]$$

Lateral-directional coefficients are as follows.

$$A = (2\mu - C_{y\dot{\beta}})(i_A i_C - i_E^2)$$

$$B = C_{y\beta} (i_E^2 - i_A i_C) - (2\mu - C_{y\dot{\beta}}) [i_A C_{nr} + i_C C_{lp} + i_E (C_{np} + C_{lr})]$$
$$- C_{yp} (i_C C_{l\dot{\beta}} + i_E C_{n\dot{\beta}}) + (2\mu - C_{yr})(i_E C_{l\dot{\beta}} + i_A C_{n\dot{\beta}})$$

$$C = C_{y\beta} [i_A C_{nr} + i_C C_{lp} + i_E (C_{np} + C_{lr})]$$
$$+ (2\mu - C_{y\dot{\beta}})(C_{lp} C_{nr} - C_{np} C_{lr}) - C_{L_1} (i_C C_{l\dot{\beta}} + i_E C_{n\dot{\beta}})$$
$$- C_{yp} (i_C C_{l\beta} + i_E C_{n\beta} - C_{nr} C_{l\dot{\beta}} + C_{lr} C_{n\dot{\beta}})$$
$$+ (2\mu - C_{yr})(i_E C_{l\beta} + i_A C_{n\beta} + C_{np} C_{l\dot{\beta}} - C_{lp} C_{n\dot{\beta}})$$

$$D = C_{y\beta} (C_{np} C_{lr} - C_{lp} C_{nr})$$
$$- C_{L_1} (i_C C_{l\beta} + i_E C_{n\beta} - C_{nr} C_{l\dot{\beta}} + C_{lr} C_{n\dot{\beta}})$$
$$+ C_{yp} (C_{l\beta} C_{nr} - C_{n\beta} C_{lr}) + (2\mu - C_{yr})(C_{l\beta} C_{np} - C_{n\beta} C_{lp})$$

$$E = C_{L_1} (C_{l\beta} C_{nr} - C_{n\beta} C_{lr})$$

The systems analysis analogies used for airplane characteristic equations lead to the conventional "mode" definitions which follow. First, for longitudinal equations (for two complex pairs of roots):

$$((\lambda')^2 + 2\zeta_p \omega_{n_p} \lambda' + \omega_{n_p}^2)((\lambda')^2 + 2\zeta_{sp} \omega_{sp} \lambda' + \omega_{n_{sp}}^2) = 0$$

where: p is the phugoid mode

sp is the short period mode

$\omega_{n_p} < \omega_{n_{sp}}$

the roots are

$$\lambda'_{1,2} = \sigma_p \pm j\omega_p$$

$$\lambda'_{3,4} = \sigma_{sp} \pm j\omega_{sp}$$

$-\zeta_{p(sp)} \omega_{n_{p(sp)}} = \sigma_{p(sp)}$ is the real part of the phugoid (short period) root pair

$\omega_{n_{p(sp)}} \sqrt{1 - \zeta^2_{p(sp)}} = \omega_{p(sp)}$ is the imaginary part of the phugoid (short period) root pair

$\zeta_{p(sp)}$ is the phugoid (short period) damping ratio

$\omega_{n_{p(sp)}}$ is the phugoid (short period) undamped natural frequency

Second, for lateral-directional equations (for one complex pair and two real roots):

$$((\lambda')^2 + 2\zeta_D \omega_{n_D} \lambda' + \omega_{n_D}^2)(\lambda' + \tfrac{1}{T_r})(\lambda' + \tfrac{1}{T_s})^* = 0$$

where D is the Dutch roll mode

r is the rolling convergence root

s is the spiral root

$\frac{1}{T_r} > \frac{1}{T_s}$ the roots are

$$\lambda'_{1,2} = \sigma_D \pm j\omega_D$$

$$\lambda'_{3,4} = -\tfrac{1}{T_r}, \; -\tfrac{1}{T_s} = \sigma_3, \sigma_4$$

$-\zeta_D \omega_{n_D} = \sigma_D$ is the real part of the Dutch roll root pair

$\omega_{n_D} \sqrt{1 - \zeta_D^2} = \omega_D$ is the imaginary part of the Dutch roll root pair

ζ_D is the Dutch roll damping ratio

ω_{n_D} is the Dutch roll undamped natural frequency

*Sometimes the term $(\lambda' + 1/T_s)$ is written $(\lambda' - 1/T_s)$

The relationship between the damping factor, ζ, undamped natural damping, σ, and damped frequency, ω, is illustrated in the diagram below.

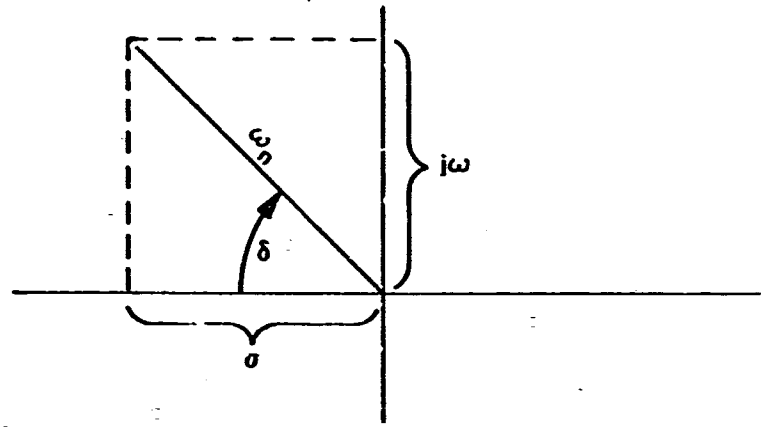

$$\sigma = -\zeta\omega_n$$
$$\zeta = -\cos\zeta$$
$$\omega = \omega_n(1-\zeta^2)^{\frac{1}{2}}$$

Assume that there are two complex pairs of roots that result from the solution of the rigid or equivalent elastic longitudinal characteristic equation. The real-time solution for α will then have the form

$$\alpha = e^{\sigma_p t}\sin(\omega_p t - \rho_1) + e^{\sigma_{sp} t}\sin(\omega_{sp} t - \rho_2) \qquad (5.12)$$

where α_1 and α_2 are constants determined by initial conditions.

One pair of roots, the highest frequency pair, determines the short period mode. The "damped frequency" is given by

$$\omega_{sp} \sim \text{radians/second}$$

The "period" is given by

$$P_{sp} = \frac{2\pi}{\omega_{sp}} \text{ seconds/cycle}$$

"Time to damp to half amplitude" for $\sigma_{sp} < 0$ may be deduced from

$$\alpha = (1/2)\alpha_1$$

which requires that

$$e^{\sigma_{sp} T_{\frac{1}{2}}} = 1/2$$

yielding

$$T_{1/2} = \frac{1}{\sigma_{sp}} \ln\left(\frac{1}{2}\right) \text{ seconds} \qquad (5.13)$$

For $\sigma_{sp} > 0$, "time to double amplitude" is given by

$$T_2 = \frac{1}{\sigma_{sp}} \ln(2) \text{ seconds} \qquad (5.14)$$

"Cycles to damp to half amplitude" is given by

$$C_{\frac{1}{2}} = \frac{T_{\frac{1}{2}}}{P_{sp}} = \frac{\omega_{sp} T_{\frac{1}{2}}}{2\pi} \text{ cycles} \qquad (5.15)$$

and "cycles to double amplitude" by

$$C_2 = \frac{T_2}{P_{sp}} = \frac{\omega_{sp} T_2}{2\pi} \text{ cycles} \qquad (5.16)$$

These parameters apply also to the longitudinal phugoid mode, the lateral-directional Dutch roll mode and, in some cases, a lateral phugoid mode when the lateral-directional characteristic equation yields two pairs of complex roots. Graphic presentation techniques for the various parameters and their relationship to stability are illustrated in the following sketch.

5.2.2 Completely elastic airplane. — For the completely elastic airplane a less restricted approach is required than that used for the rigid and equivalent elastic cases. This involves a mathematical model that will account for the structural dynamic motions of the airplane explicitly or by use of a residual flexibility formulation in addition to the rigid-body degrees of freedom. This is accomplished by using a model with the option of including or excluding structural degrees of freedom, thus giving a system with an arbitrary number of variables. The airplane has, then, the usual six degrees of freedom plus an arbitrary number of degrees of freedom that involve the structural dynamics.

Depending on the type of problem to be solved and the degree of accuracy required, the engineer has a choice as to the number of variables (degrees of freedom) to include in any one analysis. Note that this is a considerable departure from the philosophy of the well-defined, six rigid-body degrees of

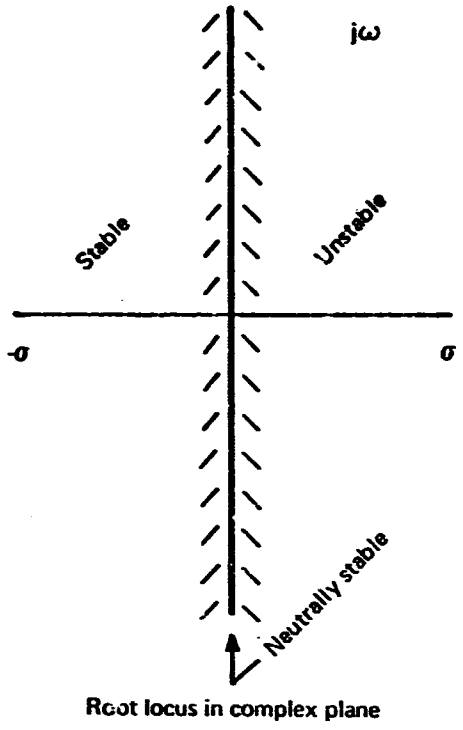

Root locus in complex plane

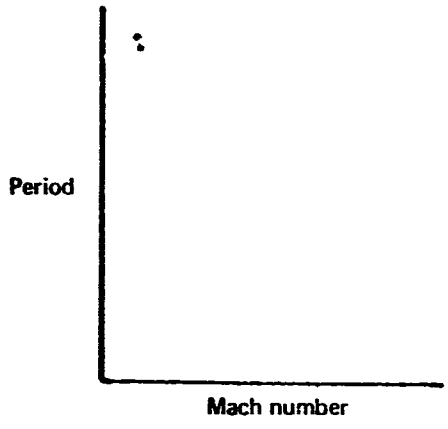

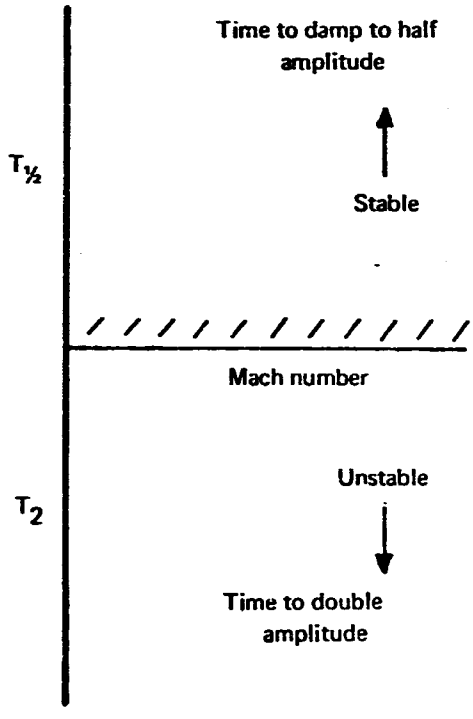

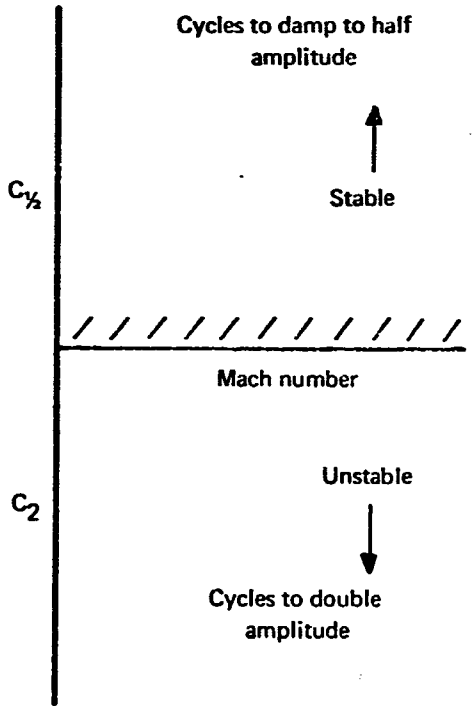

freedom associated with the rigid and equivalent elastic mathematical models previously discussed.

The equations of motion that represent both rigid body and internal motion are developed in app. A and are repeated here combined into a single matrix expression as

$$[a]\{\ddot{q}\} + [B]\{\dot{q}\} + [C]\{q\} = \{0\} \tag{5.17}$$

where $\{q\}$ is the column matrix of rigid-body plus elastic motion variables. Expressions for the coefficients [a], [B], and [C] are presented in app. A for a residual flexibility formulation and for the case where all elastic degrees of freedom participate dynamically. For the latter case, i.e., the completely elastic airplane, the coefficient [a] represents the generalized mass, [B] includes the aerodynamic damping, and [C] the generalized stiffness and generalized displacement-dependent aerodynamic coefficients.

Taking the Laplace transformation of equation (5.17) yields

$$\left[[a]S^2 + [B]S + [C]\right]\{q(S)\} = \{0\} \tag{5.18}$$

Note that from the definition of perturbation variables [q],

$$\{q(t=0)\} = \{\dot{q}(t=0)\} = \{0\}$$

which will have nontrivial solutions [q] only if

$$\left|\left[[a]S^2 + [B]S + [C]\right]\right| = 0 \tag{5.19}$$

The characteristic equation (5.19) then yields a determinant with elements $a_{ij}S^2 + B_{ij}S + C_{ij}$. When equation (5.19) is expanded, it yields a polynomial of degree $\leq 2n$, where n is the order of the determinant. The roots of this polynomial are the roots of the characteristic equation (5.19). These roots are obtained using an eigenvalue approach. The general solution is as follows:

The matrices [a], [B], and [C], square matrices of order n, are input as the coefficients of powers of S. In the program used at Boeing, the matrix equation (5.19) is reduced to an eigenvalue problem such as

$$S\{x\} = [D]\{x\} \tag{5.20}$$

where

$$\{x\} = \begin{Bmatrix} \dot{y} \\ q \end{Bmatrix} \; ; \quad \{y\} = S\{q\}$$

$$[D] = \begin{bmatrix} [0] & [I] \\ [a]^{-1}[B] & [a]^{-1}[C] \end{bmatrix}$$

The eigenvalues of [D] are then obtained using the "QR" technique described in refs. 37 and 38.

The mechanization described above is adequate for the current linear equation formulation of the completely elastic airplane. However, if nonlinear characteristics are to be considered, the current mechanized eigenvalue approach would not be adequate.

5.2.3 Approximate solutions. — Approximate solutions for rigid airplane frequency and damping characteristics have long been in existence. It is assumed that the approximate solutions also apply to the equivalent elastic mathematical model because of its similarity to the rigid model.

An extensive discussion of approximate characteristics, transfer functions, etc., can be found in ref. 36. For a two-degree-of-freedom (α and θ) longitudinal short period mode approximation, the expressions for frequency and damping are:

$$\omega_{n_{SP}} \approx \left[M_q Z_w - V_{c_1} M_w \right]^{1/2} \tag{5.21}$$

and

$$\zeta_{SP} \approx \frac{-(V_{c_1} M_{\dot{w}} + Z_w + M_q)}{2\omega_{n_{SP}}} \tag{5.22}$$

where

$$M_q = \frac{\bar{q} S \bar{c}^2}{2 V_{c_1} I_{YY_1}} C_{m_q}$$

$$Z_w = \frac{\bar{q} S}{M V_{c_1}} \left(-C_{L_\alpha} - C_{D_1} \right) = \frac{\bar{q} S}{M V_{c_1}} C_{Z_\alpha}$$

$$M_w = \frac{\bar{q} S \bar{c}}{V_{c_1} I_{YY_1}} C_{m_\alpha}$$

$$M_{\dot{w}} = \frac{\bar{q} S \bar{c}^2}{2 V_{c_1}^2 I_{YY_1}} C_{m_{\dot{\alpha}}}$$

Data in both refs. 4 and 36 show these to be accurate expressions for certain rigid airplanes when compared with the exact quartic solution of equation (5.8) for longitudinal equations. These expressions have been considered in the light of the study airplanes and the data are discussed in par. 6.2.

The longitudinal phugoid mode can also be approximated by two degrees of freedom, u and θ. Approximate frequency and damping expressions for the phugoid are:

$$\omega_{n_p} \approx \left[- Z_u g / V_{c_1} \right]^{\frac{1}{2}} \tag{5.23}$$

and

$$\zeta_p \approx - \frac{X_u}{2 \omega_{n_p}} \tag{5.24}$$

where

$$Z_u = \frac{\bar{q} S}{M V_{c_1}} \left(- C_{L_u} - 2 C_{L_1} \right) = \frac{\bar{q} S}{M V_{c_1}} C_{Z_u}$$

$$X_u = \frac{\bar{q} S}{M V_{c_1}} \left(- C_{D_u} - 2 C_{D_1} \right) = \frac{\bar{q} S}{M V_{c_1}} C_{X_u}$$

The accuracy of these phugoid expressions is also discussed in par. 6.2.

A set of approximate expressions for the lateral-directional modes is given in ref. 36. The Dutch roll, rolling convergence, and spiral modes are given as

$$\omega_{n_D} \approx \left(N_\beta \right)^{\frac{1}{2}} \tag{5.25}$$

$$\zeta_D \approx \frac{- Y_v - L_p - N_r - \frac{1}{T_s} - \frac{1}{T_r}}{2 \left(N_\beta \right)^{\frac{1}{2}}} \tag{5.26}$$

(or a less complicated expression

$$\zeta_D \approx \frac{-N_r}{2(N_\beta)^{1/2}} \tag{5.27}$$

which, together with equation (5.25) gives good results in some cases)

$$\frac{1}{T_r} \approx -\frac{Y_v L_p N_r + L_p N_\beta + \frac{g}{V_{c_1}} L_\beta}{N_\beta} \tag{5.28}$$

$$\frac{1}{T_s} \approx \frac{\frac{g}{V_{c_1}}(N_\beta L_r - L_\beta N_r)}{Y_v L_p N_r + L_p N_\beta + \frac{g}{V_{c_1}} L_\beta} \tag{5.29}$$

where

$$N_\beta = \frac{\bar{q} S b}{I_{zz_1}} Cn_\beta$$

$$Y_v = \frac{\bar{q} S}{M V_{c_1}} Cy_\beta$$

$$L_p = \frac{\bar{q} S b^2}{2 V_{c_1} I_{xx_1}} C_{\ell_p}$$

$$N_r = \frac{\bar{q} S b^2}{2 V_{c_1} I_{zz_1}} Cn_r$$

$$L_r = \frac{\bar{q} S b^2}{2 V_{c_1} I_{xx_1}} C_{\ell_r}$$

$$L_\beta = \frac{\bar{q} S b}{V_{c_1} I_{xx_1}} C_{\ell_\beta}$$

The reduced expression for Dutch roll damping (5.27) follows from a one-degree-of-freedom approximation. Generally, the accuracy of equation (5.27) is configuration dependent and, therefore, unreliable. The merits of using equations (5.25) and (5.27) are illustrated in par. 6.3. The complexity of equations (5.28) and (5.29) make their use almost ineffectual when compared with the use of the small perturbation program. These expressions for $1/T_r$ and $1/T_s$ were not used in this study.

Similarity between the rigid and equivalent elastic mathematical models implies that the approximate expressions could also be used for equivalent elastic cases with some minor redefinitions of terms involved.

Some studies have been made for the completely elastic airplane from the viewpoint of approximate transfer functions. In "Analytical Study of Approximate Longitudinal Transfer Functions for a Flexible Airframe" (ref. 39) some approximate frequency and damping expressions were obtained for rigid-body modes with one and two elastic modes for three dissimilar configurations. It is apparent from the study that the form and accuracy of approximate expressions are sensitive to configuration, number of elastic modes being considered, and dynamic pressure. The treatment of special problems for known significant isolated elastic effects appears to be in the approximation category. The availability, speed, and versatility of digital computer techniques tends to preclude the use of approximate expressions for solving general problems in elastic airplane dynamics.

5.3 Time Histories

The stability criteria for time history methods are those given in app. A as follows.

If the motions of an airplane following a disturbance from steady-state flight are determined by a time history (integration), then the stability behavior is said to be:

- stable, if the motions remain in proximity to the steady state;
- neutrally stable, if the motions are undamped and oscillatory about some steady state;
- unstable, if the motions diverge from the steady state either linearly, exponentially, oscillatorily, or in any combination.

If the disturbance is temporary, then the reference steady state is the initial steady state. If it is permanent — for example, a step elevator change — then the reference steady state is a different one determined by the new equilibrium flight conditions. These criteria are utilized in Sec. 6 where analysis results are discussed and illustrated.

5.3.1 Rigid and equivalent elastic time history solutions. — The time history technique for rigid and equivalent elastic models is essentially that written for the rigid airplane. This mechanized solution will subsequently be referred to as the "rigid-body, six-degree-of-freedom program" even though it is also used for equivalent elastic solutions. The equations of motion solved by the rigid-body, six-degree-of-freedom program, as described in app. A, are the "equations of arbitrary motion."

These equations* are shown in table 7. The program used in generating the time histories for rigid and equivalent elastic airplanes numerically integrates these six equations. The Euler angles in these equations, θ and ϕ, are developed from the direction cosines that relate the earth-fixed axes and body axes. If the body axes are described by the unit vectors ($\vec{i}_B$, $\vec{j}_B$, $\vec{k}_B$) and the earth-fixed axes by ($\vec{i}_1$, $\vec{j}_1$, $\vec{k}_1$), the relation between the two sets is given in terms of the Euler angles by

$$\vec{i}_B = \vec{i}_1(\cos\psi\cos\theta) + \vec{j}_1(\sin\psi\cos\theta) - \vec{k}_1\sin\theta$$

$$\vec{j}_B = \vec{i}_1(\cos\psi\sin\theta\sin\phi - \sin\psi\cos\phi) + \vec{j}_1(\sin\psi\sin\theta\sin\phi + \cos\psi\cos\phi) + \vec{k}_1(\cos\theta\sin\phi) \tag{5.30}$$

$$\vec{k}_B = \vec{i}_1(\cos\psi\sin\theta\cos\phi + \sin\psi\sin\phi) + \vec{j}_1(\sin\psi\sin\theta\cos\phi - \cos\psi\sin\phi) + \vec{k}_1(\cos\theta\cos\phi)$$

or rewritten in terms of direction cosines

$$\vec{i}_B = \vec{i}_1 l_1 + \vec{j}_1 l_2 + \vec{k}_1 l_3$$

$$\vec{j}_B = \vec{i}_1 m_1 + \vec{j}_1 m_2 + \vec{k}_1 m_3 \tag{5.31}$$

$$\vec{k}_B = \vec{i}_1 n_1 + \vec{j}_1 n_2 + \vec{k}_1 n_3$$

*Used here in the body axis system.

TABLE 7. – EQUATIONS OF ARBITRARY MOTION (STABILITY AXES)

$$
\begin{Bmatrix} \dot{u} \\ \dot{v} \\ \dot{w} \\ \dot{p} \\ \dot{q} \\ \dot{r} \end{Bmatrix} =
\begin{Bmatrix}
rv - qw - g\sin\theta + \frac{F_{Axs}}{M} + \frac{F_{Txs}}{M} \\
pw - ru + g\cos\theta\sin\phi + \frac{F_{Ays}}{M} + \frac{F_{Tys}}{M} \\
qu - pv + g\cos\theta\cos\phi + \frac{F_{Azs}}{M} + \frac{F_{Tzs}}{M} \\
\frac{I_{xz_{1s}}}{I_{xx_{1s}}}\dot{r} + \frac{I_{xz_{1s}}}{I_{xx_{1s}}}pq + \frac{I_{yy_{1s}} - I_{zz_{1s}}}{I_{xx_{1s}}}qr + \frac{M_{Axs}}{I_{xx_{1s}}} + \frac{M_{Txs}}{I_{xx_{1s}}} \\
\frac{I_{xz_{1s}}}{I_{yy_{1s}}}(r^2 - p^2) + \frac{I_{zz_{1s}} - I_{xx_{1s}}}{I_{yy_{1s}}}pr + \frac{M_{Ays}}{I_{yy_{1s}}} + \frac{M_{Tys}}{I_{yy_{1s}}} \\
\frac{I_{xz_{1s}}}{I_{zz_{1s}}}\dot{p} - \frac{I_{xz_{1s}}}{I_{zz_{1s}}}qr + \frac{I_{xx_{1s}} - I_{yy_{1s}}}{I_{zz_{1s}}}pq + \frac{M_{Azs}}{I_{zz_{1s}}} + \frac{M_{Tzs}}{I_{zz_{1s}}}
\end{Bmatrix}
$$

Assumptions required:

D1

G1 G2 G3 G5 G6 G10

S1 S2 S3 S5 S8 S7 S10 S11

Differentiation of each of the direction cosines yields:

$$\dot{\ell}_1 = m_1 R - n_1 Q \qquad \dot{\ell}_2 = m_2 R - n_2 Q \qquad \dot{\ell}_3 = m_3 R - n_3 Q$$

$$\dot{m}_1 = n_1 P - \ell_1 R \qquad \dot{m}_2 = n_2 P - \ell_2 R \qquad \dot{m}_3 = n_3 P - \ell_3 R \tag{5.32}$$

$$\dot{n}_1 = \ell_1 Q - m_1 P \qquad \dot{n}_2 = \ell_2 Q - m_2 P \qquad \dot{n}_3 = \ell_3 Q - m_3 P$$

By calculating the direction cosine rates at the midpoint of the time interval, angular displacements are estimated in a linear fashion for the new time intervals.

The Euler angles are calculated from the following:

$$\begin{aligned} \theta &= \sin^{-1}(-\ell_3) = \tan^{-1}\left(\frac{-\ell_3}{\sqrt{1-\ell_3^2}}\right) \\ \phi &= \sin^{-1}\left(\frac{m_3}{\cos\theta}\right) \\ \psi &= \sin^{-1}\left(\frac{\ell_2}{\cos\theta}\right) \end{aligned} \tag{5.33}$$

For this technique, the equations in table 7 can be nonautonomous. Thrust forces and moments may be input as explicit functions of time. Also, aerodynamic forces and moments due to controls may be explicit functions of time.

The forces and moments expressed as functions of force coefficients and dynamic pressure are:

$$\begin{aligned} F_{A_{X_S}} &= \left[C_{1_X} + C_{2_X} + \cdots\right] \bar{q} S \\ M_{A_{X_S}} &= \left[\bar{C}_{1_X} + \bar{C}_{2_X} + \cdots\right] \bar{q} S b \\ M_{A_{Y_S}} &= \left[\bar{C}_{1_Y} + \bar{C}_{2_Y} + \cdots\right] \bar{q} S \bar{c} \end{aligned} \tag{5.34}$$

The coefficients may be functions of several arguments, e.g., $C_{1_X} = C_{1_X}(\alpha, \beta, M)$. Therefore, the coefficients may be represented in a linear or nonlinear fashion as desired. The aerodynamic forces and moments are then of the form:

$$\frac{F_{A_{X_S}}}{\bar{q}S} = -C_D = C_{1_x}(\alpha,\beta,M) + C_{2_x}(\alpha,M,\delta_A) + C_{3_x}(\alpha,M,\delta_E) + C_{4_x}(\alpha,M,\delta_R) + \left[C_{5_x}(\alpha,M,q)\right]\frac{q\bar{c}}{2V_{c_1}} \quad (5.35)$$

$$\frac{M_{A_{X_S}}}{\bar{q}S} = C_\ell = \bar{C}_{1_x}(\alpha,\beta,M) + \bar{C}_{2_x}(\alpha,M,\delta_A) + \bar{C}_{3_x}(\alpha,M,\delta_R) + \left[\bar{C}_{4_x}(\alpha,M,p)\right]\frac{pb}{2V_{c_1}} + \left[\bar{C}_{5_x}(\alpha,M,r)\right]\frac{rb}{2V_{c_1}} + \left[\bar{C}_{6_x}(\alpha,M,\dot{\beta})\right]\frac{\dot{\beta}b}{2V_{c_1}} \quad (5.36)$$

In equation (5.36), $C_{l_x}(\alpha, \beta, M)$ corresponds to the C_{ℓ_β} derivative and may be represented in a completely nonlinear manner as a function of α, β, and Mach number. The coefficient $\bar{C}_{4_x}$ is the usual roll-damping derivative C_{ℓ_p} and, if desired, may be represented in the three-dimensional tables as a function of α, Mach number, and roll rate, p. All the usually important aerodynamic forces and moments may be represented in the six force and moment equations, two of which are shown in equations (5.35) and (5.36). Negligible derivatives such as $C_{x_{\dot{\gamma}}}$ and $C_{y_{\delta_a}}$ have been neglected. Nonlinear aerodynamic cross-coupling may be represented if desired, e.g., C_{D_β}, C_{m_β}, and C_{L_β}.

For the time histories generated here, the aerodynamic coefficients were (D14) of a linear nature as tabulated in par. 8.2, for both the rigid and equivalent elastic airplanes. Some equivalent elastic characteristics were accounted for by using Formulation II derivatives for the longitudinal equations and Formulation I derivatives for the lateral-directional equations. Mass and inertial properties are modified by $\ddot{y}$, $\dot{p}$, and $\dot{r}$ in the lateral-directional equations and I_{yy} is modified by $\ddot{\theta}$. The exact techniques were given by equations (5.4) and (5.7). A detailed discussion of representing inertia relief implicitly (Formulation II) can be found in app. B. The thrust forces and moments, $F_{T_{i_S}}$ and $M_{T_{i_S}}$, were assumed to be constant for the time histories of Sec. 6. The thrust was equal to that needed for steady, unaccelerated flight.

The particular disturbances applied to the airplane are noted with the respective time history plots in Sec. 6.

The equations in table 7 can be described as six simultaneous, first-order differential equations with variable coefficients. An explicit solution of these equations is not possible. The approximate solution devised will not be discussed. The method involves a linear approximation with one iteration (quasi-linearization). The method can best be discussed in detail following a brief outline of the approach. The solution of the equations for the first time increment is as follows.

(1) Equate velocities and displacements at t- 1 to velocities and displacements at t

$$u_{t-1} = u_t \quad , \quad x_{t-1} = x_t$$

(2) Calculate forces and moments at t-1

$$F_{x_{t-1}} = F(u_{t-1}, x_{t-1})$$

(3) Calculate linear and angular accelerations at t-1

$$\dot{u}_{t-1} = \left(\frac{F_x}{m} - QW + RV \right)\Big|_{t-1}$$

(4) Estimate linear and angular velocities at t, assuming the accelerations at t-1 are constant across the time interval Δt

$$u_t = u_{t-1} + \dot{u}_{t-1} \Delta t$$

(5) Estimate linear and angular displacements at t based on linear variation of velocities

$$x_t = x_{t-1} + \frac{1}{2}(u_t + u_{t-1})\Delta t$$

(6) Calculate forces and moments from velocities and displacements at t

$$F_{x_t} = F(u_t, x_t)$$

(7) Calculate linear and angular accelerations at t from estimates of forces and velocities at t

$$\dot{u}_t = \left(\frac{F_x}{m} - QW + RV \right)\Big|_t$$

(8) Calculate linear and angular velocities at t from linear variation of accelerations across the interval Δt

$$u_t = u_{t-1} + \frac{1}{2}(\dot{u}_t + \dot{u}_{t-1})\,\Delta t$$

(9) Calculate linear and angular displacement at t from linear variation of velocities across interval Δt

$$x_t = x_{t-1} + \frac{1}{2}(u_t + u_{t-1})\,\Delta t$$

(10) Advance time by the increment Δt and return to the first step and repeat the cycle.

$$t = t + \Delta t$$

The integration technique described above is applied to each of the six degrees of freedom. Following the method, values are computed for U, V, and W by using the equation in table 7 for $\dot{U}$, $\dot{V}$, and $\dot{W}$. From these velocities the following additional parameters are calculated.

$$V_C = \sqrt{u^2 + V^2 + W^2} \tag{5.37}$$

$$\alpha = \tan^{-1}\left(\frac{W}{u}\right)$$

$$\beta = \sin^{-1}\left(\frac{V}{V_C}\right)$$

Similarly, using this same technique the body axis angular rates (P, Q, R) are developed by using the equations in table 7 for $\dot{P}$, $\dot{Q}$, and $\dot{R}$. The body axis angular rates are used in the computation of the direction cosine-rates, equation (5.32), as well as being given as program output. A sufficient body of information is given for each time increment as computer output to generate complete time histories of the motion.

The rigid-body, six-degree-of-freedom program has the capability to analyze handling-qualities problems. Part of the basic program output is the velocity (Up, Vp, Wp) and acceleration ($\dot{U}p$, $\dot{V}p$, $\dot{W}p$) at the pilot's station. Also, because engine thrust may be input separately for each engine as an explicit function of time, the program has the capability to analyze engine-out-type time history solutions.

5.3.2 Completely elastic time history solutions. — The time history solutions for the completely elastic airplane equations of motion (see Sec 9) for this study were obtained using a special programming language called MIMIC. This special technique is documented in ref. 40. The time histories are merely the time-dependent analog of the frequency-dependent equation (5.18), with initial conditions (equilibrium conditions) to which the perturbations are added along with a disturbance to excite the system. The scheme is simple. From the equilibrium conditions and the disturbance, the accelerations are calculated, e.g.,

$$\ddot{q}_i = \ddot{q}_i\left(\{\ddot{q}\}, \{\dot{q}\}, \{q\}\right) \qquad i = 1, 2, \cdots, n \tag{5.38}$$

These are integrated by making the statements

$$\dot{q}_i = \mathrm{INT}\left(\ddot{q}_i, \dot{q}_i(0)\right) = \dot{q}_i(0) + \int \ddot{q}\, dt \qquad i = 1, 2, \cdots, n \tag{5.39}$$

and further by

$$q_i = \mathrm{INT}\left(\dot{q}_i, q_i(0)\right) = q_i(0) + \int \dot{q}_i\, dt \qquad i = 1, 2, \cdots, n \tag{5.40}$$

Included as a subroutine in the MIMIC program is a Runge-Kutta numerical integration technique which accomplishes the integrations (5.39) and (5.40). This approach is easy for the engineer since the programs are then physically oriented. However, as one might expect, the easier the program is to write, for a given problem, the more time is required to execute it.

As was mentioned already, this solution is an analog of the frequency-dependent equation (5.18). Indeed, aside from errors inherent in the numerical integration technique, there should be no difference between the MIMIC solutions and those obtained from the explicit expression

$$\{q\} = \mathcal{L}^{-1}\left(\left[[a]s^2 + [B]s + [C]\right]^{-1}\{q_0\}\right)$$

where $\mathcal{L}^{-1}$ indicates the inverse Laplace transformation.

6. DISCUSSION OF DYNAMIC STABILITY ANALYSIS RESULTS

6.1 Introduction

The preceding section consisted of a discussion of the techniques used to calculate the dynamics. This section presents the results of applying these techniques. The primary analysis tool was the characteristic equation method. Time history solutions were generated to obtain a graphic presentation of the motion variables. No attempt was made to investigate nonlinear aerodynamic or dynamic effects with the time history methods. The approximate expressions for frequency and damping discussed in the last section were evaluated for the study airplanes by comparing the results obtained with the exact quartic solution roots.

General results obtained from the dynamic analyses are presented in table 8. Table 8 summarizes the accuracies obtained from lifting surface theory and handbook techniques in predicting the rigid airplane dynamic characteristics when compared with wind tunnel stability derivative predictions. The relative effect of elasticity on the various dynamic characteristics is noted, as well as the approximate number of elastic modes needed for an accurate analysis. In addition, the usefulness of approximate formulas for predicting frequency and damping is summarized. Paragraph 8.2 should be consulted for details of the derivatives used in an individual method.

Paragraphs 6.2 and 6.3 present only those figures used to support the discussion there. A great deal of supplementary dyna[illegible]ability data generated for the rigid and equivalent elastic study airp[illegible]es may be found in pars. 8.4 and 8.5.

6.2 Longitudinal Dynamic Stability Characteristics

6.2.1 Roots of the longitudinal characteristic equations. — Characteristic equation methods were applied to the study airplanes at the study flight conditions given in table 1. The rigid and equivalent elastic airplanes were analyzed for all conditions given in table 1. The completely elastic airplane was analyzed at only selected flight conditions from this table. The rigid and equivalent elastic derivatives, coefficients, and inertial properties used in each case are

TABLE 8. – DYNAMIC STABILITY CALCULATIONS–GENERAL RESULTS

	Relative accuracy of calculation method[a]										Relative effect of elasticity[b]			Approx. no. of elastic modes for accurate comp. elastic results		
	Computer lifting surface for long. modes; NACA TR 1098 for lat.-dir. modes[c]			Handbook quartic solution				Approx. eqs. (accuracy or usefulness)[d]								
	Sub		Super	Sub			Super	Sub		Super	Sub		Super	Sub		Super
	707 Rigid	SST Rigid	SST Rigid	707 Rigid	E. E.	SST Rigid	SST Rigid	707	SST	SST		SST	SST	707	SST	SST
Longitudinal																
Short period: frequency	G	P	G	F	e.	P	G	G	G	G	S	S	S	10	20	15
damping	G	P	G	G	e.	F	F	G	G	G	S	M	S	10	15	15
Phugoid: frequency	F	P	G	F	e.	P	P	P	P	P	M	S	L	Not done		
damping	F	P	F	P	e.	P	P	P	P	P	M	M	L			
Lateral-directional																
Dutch roll: frequency	G	G	No method	F	p[f]	F	F	F	P	F	S	S	M	15	?	?
damping	F	F	No method	P	p[f]	F	F	F	P	P	M	L	L	12	?	?
Roll mode: damping	F	G	No method	F	e.	G	G	Not done (quartic solution more efficient)			S	S	S	Not done		
Spiral mode: damping	F	G	No method	P	e.	F	P				M	M	S			

a. G (good) - method compares favorably with wind tunnel predictions (exception allowed)
F (fair) - less favorable correlation with predictions
P (poor) - method does not compare favorably with predictions

b. L (large)- elasticity considered a significant effect
M (moderate) - elasticity considered moderately important; not quite as significant as differences due to stability derivative calculation methods
S (small)- elasticity considered a minor change to stability characteristic; changes due to stability derivative calculation methods usually much more important

c. No lifting surface theory method mechanized for lateral-directional derivatives

d. Compared to rigid and equivalent elastic quartic solution

e. No data available

f. Based on comparison with flight test data

tabulated in par. 8.2. The frequency, damping, period, and time to damp to half or double amplitude were determined from the quartic equation (5.8) for the rigid and equivalent elastic airplanes. The dynamic stability comparison of the latter two mathematical models for various sets of stability derivatives for the short period and phugoid modes are all presented in par. 8.4. These data tend to reflect the good and bad correlation evident in the derivative comparisons of app. B. A summary of the results is given in table 8. The following section illustrates and discusses primarily that rigid and equivalent elastic data for those conditions at which the corresponding completely elastic airplane was analyzed.

The short period characteristics of the 707-320B and SST at 72° leading edge sweep were also calculated using the approximate expressions for frequency and damping given in the previous section. The approximate expressions were applied to the derivatives obtained from rigid airplane lifting surface theory, and the results are plotted in figures 13 and 14 where they are compared with the quartic solution, short period data. The data show that the differences between the approximate solutions and quartic solutions for one set of derivatives are small when compared with the differences in the data due to variations in the derivative calculation techniques. These data illustrate the significant effect of the accuracy of the derivatives on the short period characteristics as opposed to the relative insensitivity to solution approximations. Thus, it is observed that derivative accuracy will be of primary importance in determining the short period characteristics.

The approximate expressions for the phugoid frequency and damping are not very accurate as compared with the short period cases. This is mainly due to their small values and sensitivity to small changes in the derivatives.

The derivative C_{m_α} is often credited with too much significance in determining the short period characteristics. In many cases it dominates the expressions determining the short period frequency and damping (equations (5.21) and (5.22), but only when it is quite large. Also, a small, positive value of C_{m_α} for some of the subsonic SST cases (using lifting surface methods) did not yield an unstable short period mode. This again raises the question of the requirement of static stability that $C_{m_\alpha} < 0$.

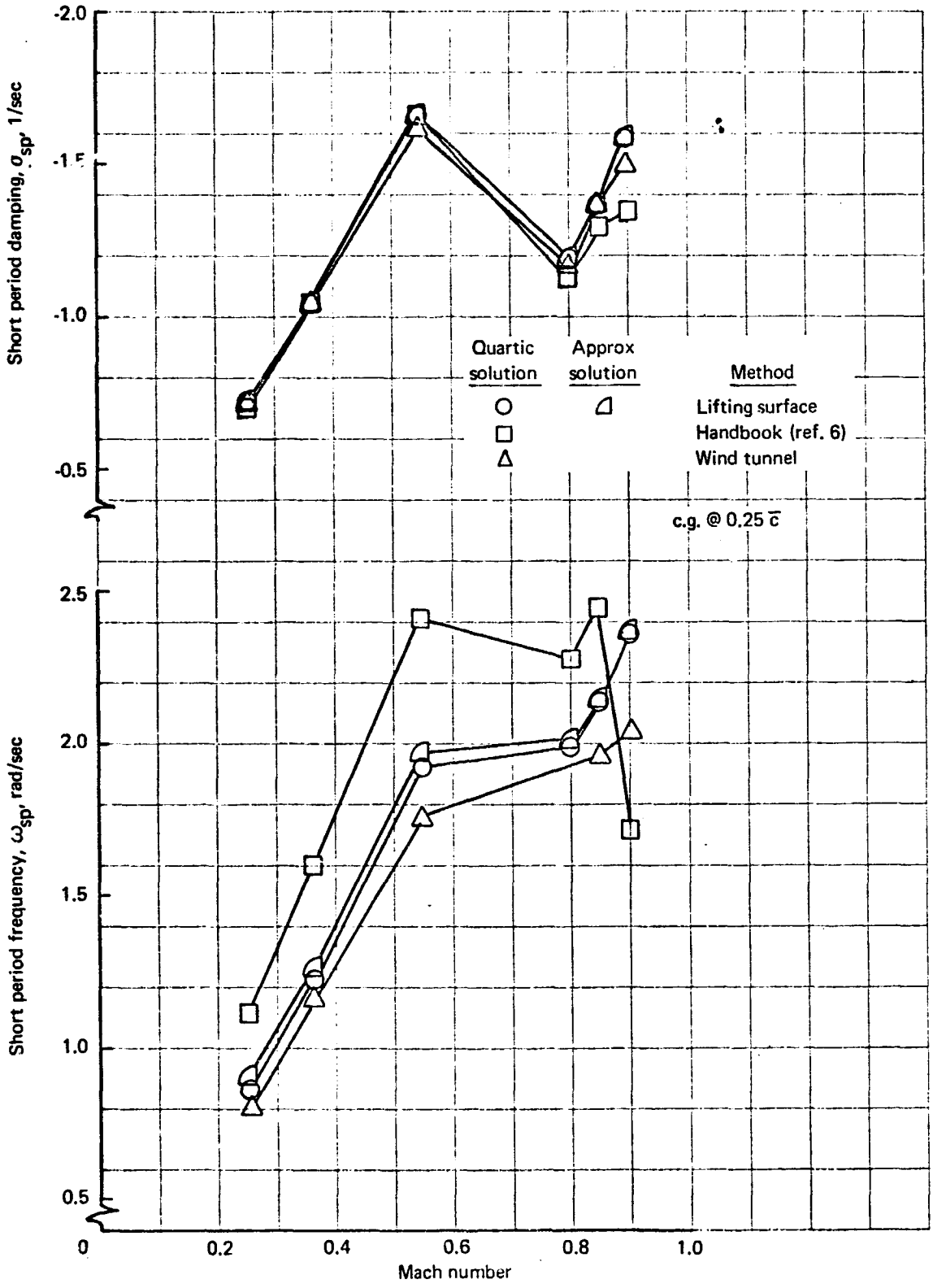

FIGURE 13. SHORT PERIOD FREQUENCY AND DAMPING, RIGID AIRPLANE – 707-320B

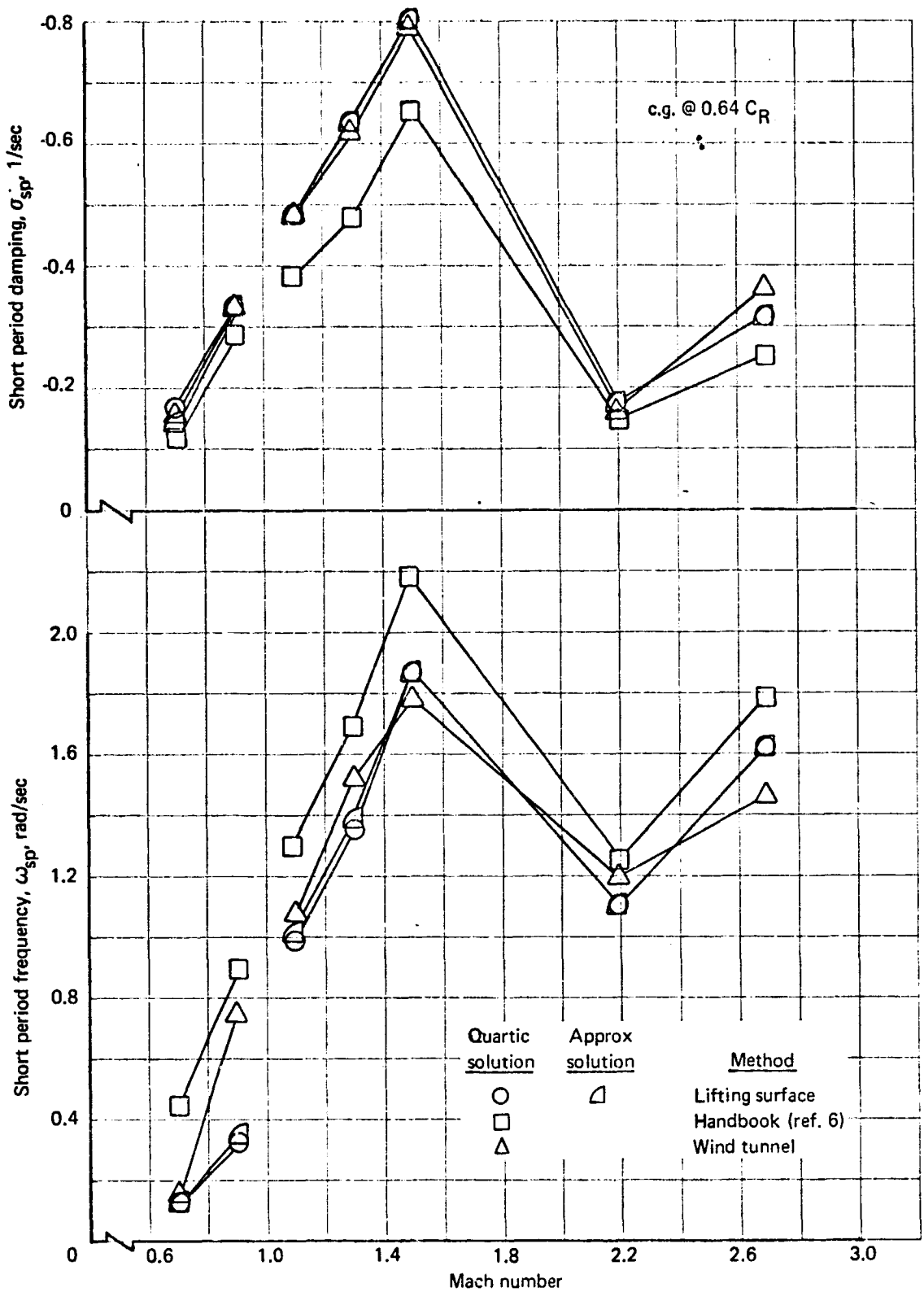

FIGURE 14. SHORT PERIOD FREQUENCY AND DAMPING, RIGID AIRPLANE – 72° SST

It is again pointed out that the data in figs. 13 and 14 are designed to illustrate the rigid airplane short period characteristic sensitivity to derivatives and insensitivity to calculation techniques. This trend carries somewhat into the elastic models. This is illustrated in the data presented in fig. 15. These data show the variations in short period frequency for four distinct but similar mathematical models. The similarity lies in the use of aerodynamic influence coefficients (lifting surface methods) and structural influence coefficients. The differences are more detailed. Three rigid-body degrees of freedom, α , θ, and u, are used for the rigid and equivalent elastic data (labeled "lifting surface"), with the derivatives $C_{m_{\dot{\alpha}}}$ and $C_{m_{\ddot{\theta}_I}}$ included. Two rigid-body degrees of freedom, α and θ, were used for the completely elastic airplane without the derivatives $C_{m_{\dot{\alpha}}}$ and $C_{m_{\ddot{\theta}_I}}$. The latter has been labeled as a "truncated" model because of the way it is handled. The rigid-body modes are representative of a two-degree-of-freedom rigid airplane. The elastic modes are included as additional degrees of freedom up to some desired cutoff point where all of the remaining elastic modes are ignored completely. This has been called "truncated, completely elastic" data. The 2 x 2 is a rigid model and the 22 x 22 is two rigid-body modes with the first 20 lowest frequency elastic modes.

The effect of $C_{m_{\ddot{\theta}_I}}$ for the equivalent elastic airplane was handled as discussed in app. B, i.e., it was used to modify the pitch inertia and, hence, implies an effective frequency change (equation (5.21)) in the fashion

$$\omega_{n_{sp}} \propto \frac{1}{\sqrt{I_{yy}}} = \frac{1}{\sqrt{I_{yy_s} - C_{m_{\ddot{\theta}_I}} \bar{q} S_w \bar{c}}}$$

All of these subtle differences did not appear to have pronounced effects on the data credibility, as fig. 15 illustrates. However, it can be observed that the addition of dynamically participating elastic modes has much less effect on the short period frequency (2 x 2 versus 22 x 22 modes) than does the static-elastic type of correction (3 x 3, rigid versus equivalent elastic). The effect of dynamic pressure is also illustrated in figure 15 at Mach 2.7. It appears that an increase in $\bar{q}$ at that condition has an overall stiffening effect as observed by comparing the elastic increments between the comparable models.

The worst correlation in fig. 15 is as good as the best variable derivative in comparison in fig. 14. This again emphasizes the need for an accurate set of basic aerodynamic data for the rigid-body modes.

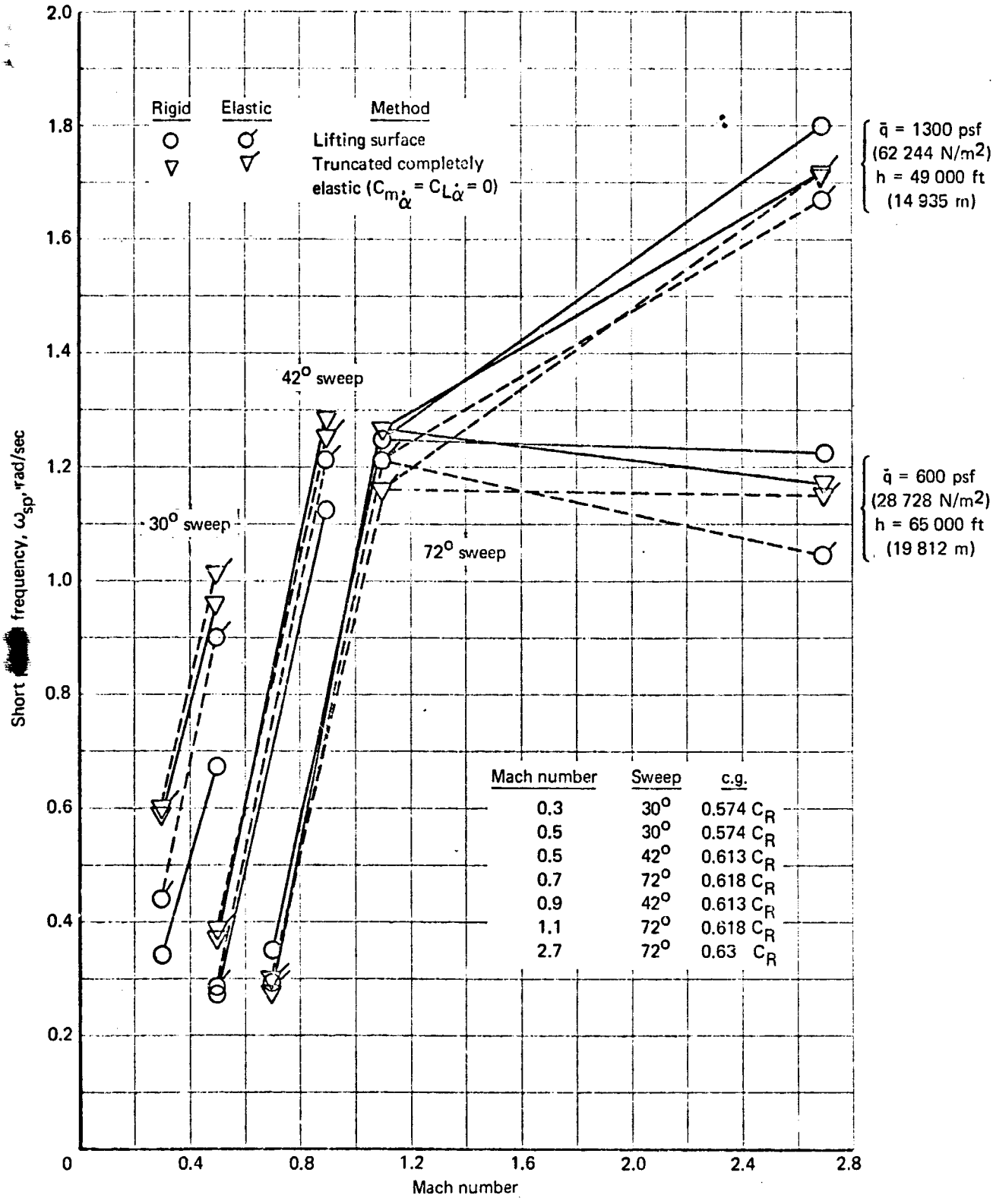

FIGURE 15. SHORT PERIOD FREQUENCY, RIGID, EQUIVALENT ELASTIC, AND COMPLETELY ELASTIC AIRPLANES – SST

The damping associated with the short period frequency just discussed is presented in fig. 16. The largest discrepancies are mostly attributable to using $Cm_{\dot{\alpha}}$ derivatives for the 3 x 3 rigid and equivalent elastic cases and not using these derivatives for the truncated, completely elastic formulation. Increments in damping due to elasticity between rigid versus equivalent elastic and also 2 x 2 versus 22 x 22 are small compared with the differences due to $C_{m_{\dot{\alpha}}}$. (Both $Cm_{\dot{\alpha}}$ and $C_{L_{\dot{\alpha}}}$ are treated in the parametric studies in par. 7.1.)

A particularly disturbing quality of the data in figs. 15 and 16 is the lack of consistency in the effects of elasticity. For example, the truncated, completely elastic data show increases, decreases, and no changes in both frequency and damping. Also, the change between rigid and equivalent elastic shows increases in frequency for 30° and 42° leading edge sweep and decreases at 72° sweep. This precludes making any general statements as to the overall effects of elasticity. This inconsistency is even more evident in figs. 17 and 18, where the undamped natural frequency is presented for the SST at various sweep and flight conditions. In each case shown, the effect of adding elastic degrees of freedom (generalized coordinates) is illustrated.

In general, the frequency increased when the two lowest frequency elastic modes were added, and then decreased when the next sets of two were added out to eight total modes. From there on adding modes had rather unpredictable effects, except that in all cases the frequency tends to approach a constant value as more modes are added beyond 12. The apparent inconsistency is that the constant value is not always less than or more than the rigid 2 x 2.

The damping factors for the same SST cases are presented in figs. 19 and 20. The data show the same consistency of trend up to eight total modes, as did the frequency data. However, the damping factor in all cases settles to a constant value less than the rigid 2 x 2 as more modes are added.

It is observed that elastic effects on the dynamics, as found here, are not very significant but were more significant in the static trim considerations discussed in Sec. 4 and illustrated in detail in par. 8.3.

It would be convenient to assign names to the free-free structural vibration modes used in the SST analysis. The engineer could then call out the modes by name and determine exactly what type of motion was being included in the

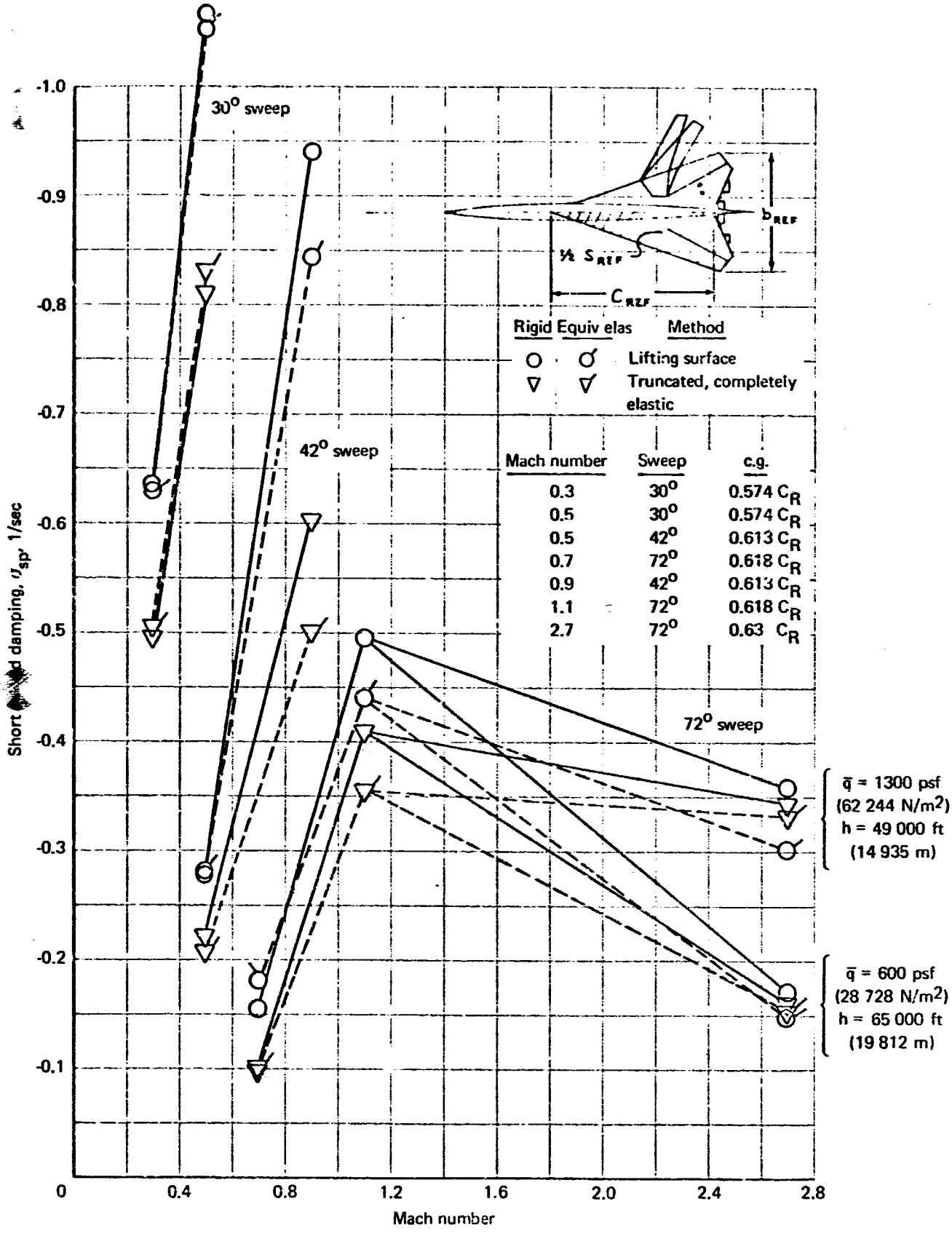

FIGURE 16. SHORT PERIOD DAMPING, RIGID, EQUIVALENT ELASTIC AND COMPLETELY ELASTIC AIRPLANES – SST

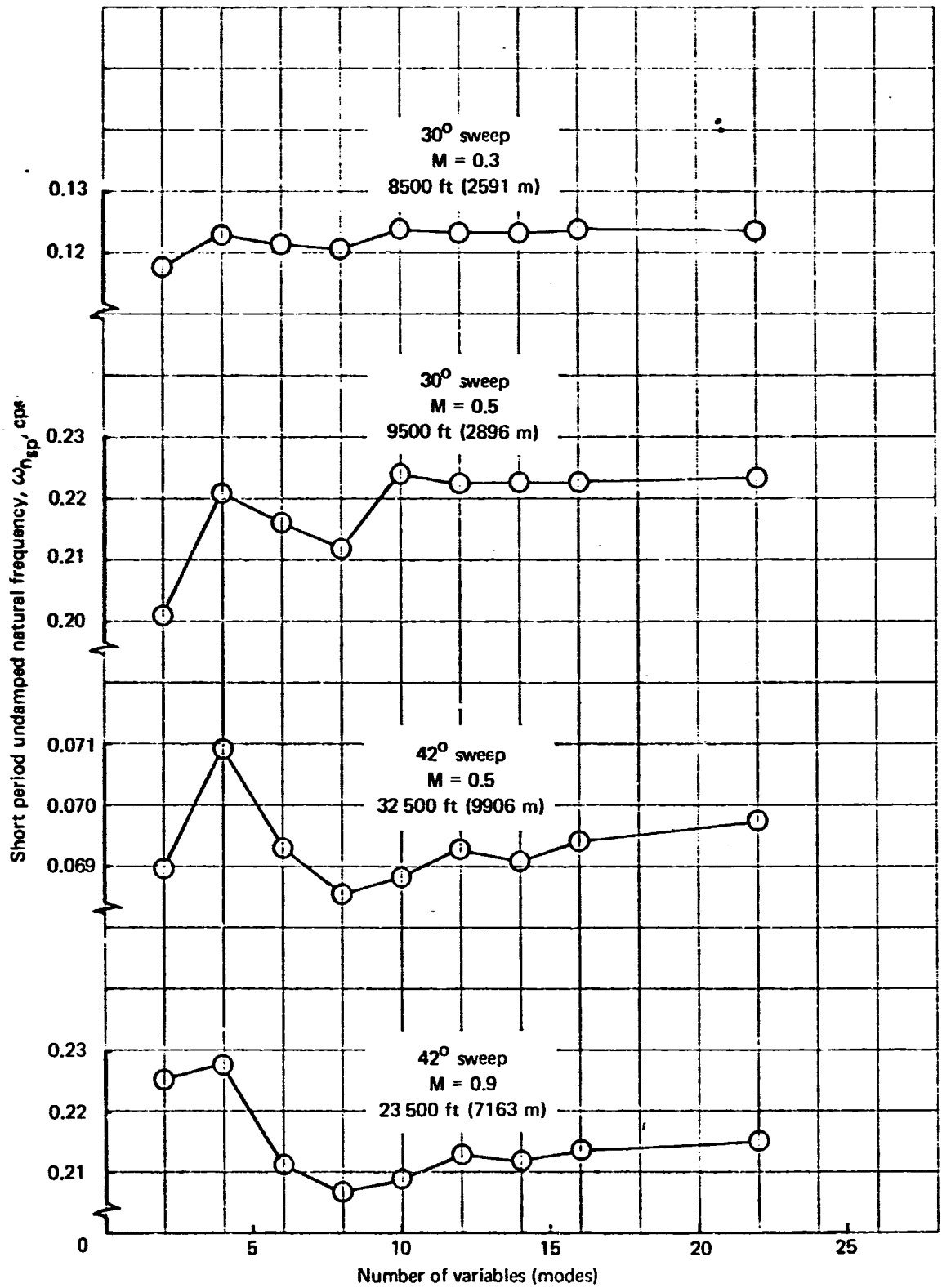

FIGURE 17. VARIATION OF SHORT PERIOD FREQUENCY WITH NUMBER OF MODES – 30° AND 42° SST

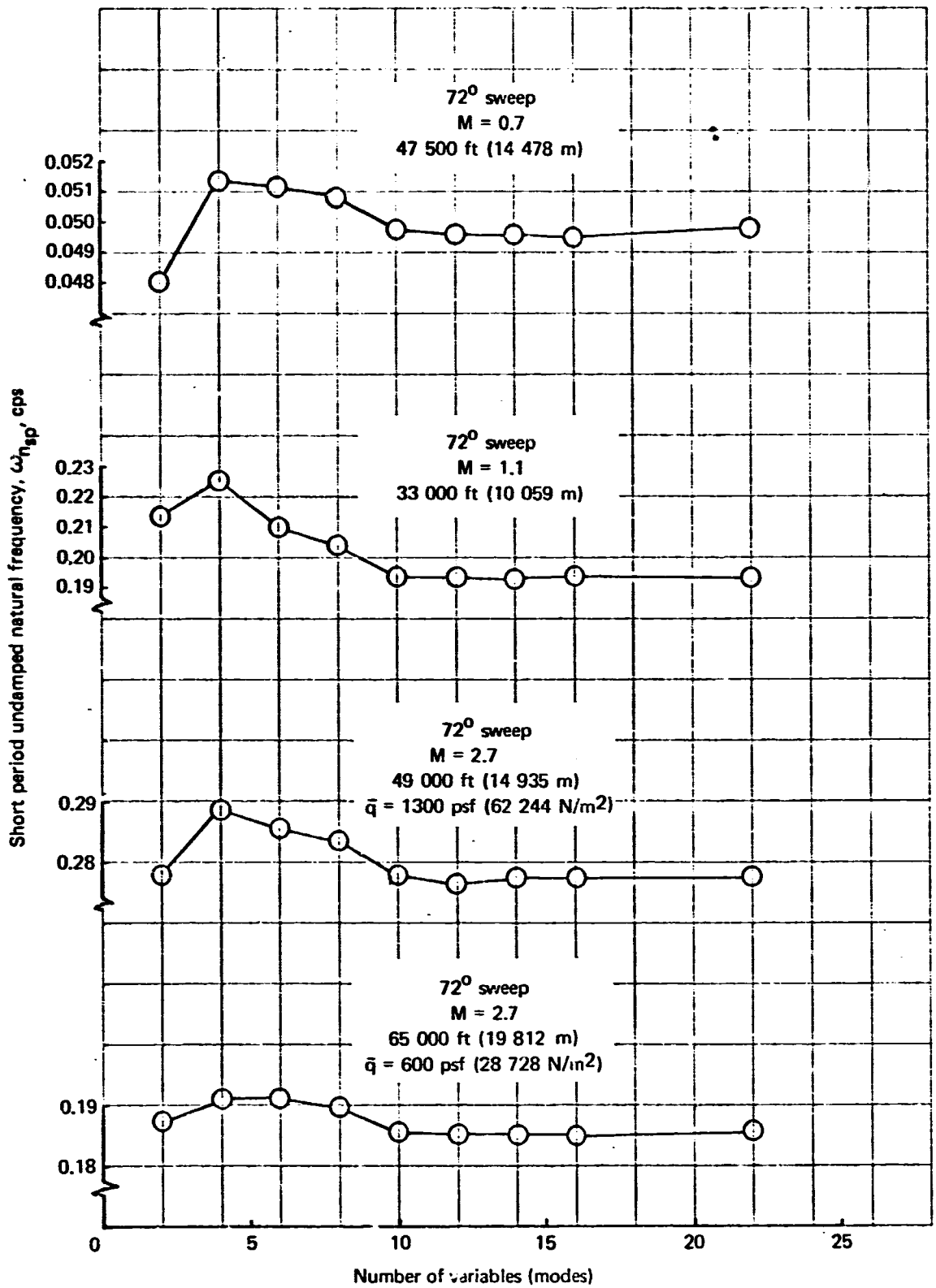

FIGURE 18. VARIATION OF SHORT PERIOD FREQUENCY WITH NUMBER OF MODES – 72° SST

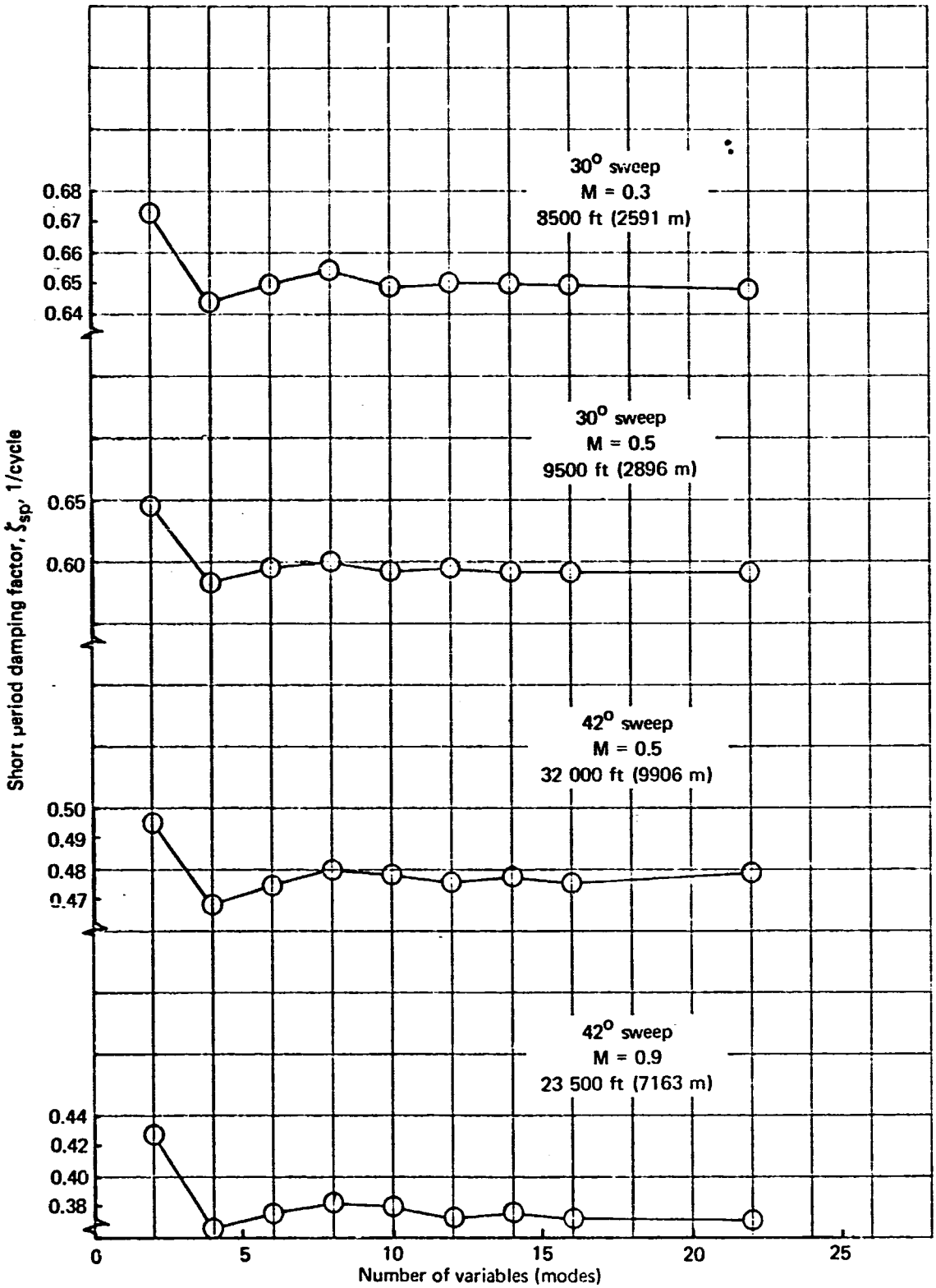

FIGURE 19. VARIATION OF SHORT PERIOD DAMPING WITH NUMBER OF MODES – 30° AND 42° SST

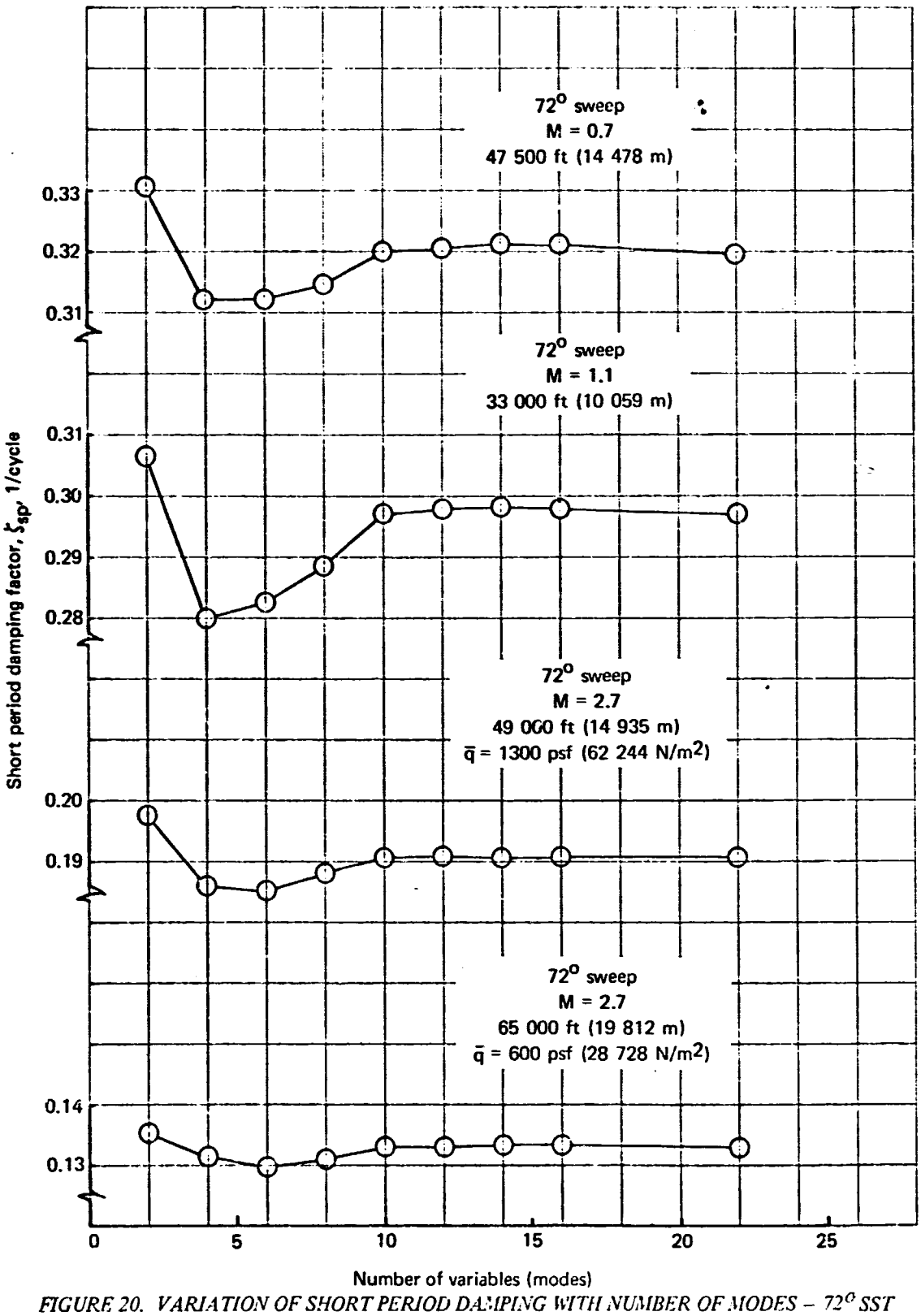

FIGURE 20. VARIATION OF SHORT PERIOD DAMPING WITH NUMBER OF MODES – 72° SST

analysis. Unfortunately, it is not very meaningful to assign names to the natural modes of motion of the SST, since the wing, tail, and body all participate in each mode. Because the free-free modes are all coupled motion and cannot be accurately described by words, it is necessary to represent each mode in some type of graphical form to determine the type of motion involved in each mode shape. Figures 21 and 22 are typical examples of visual displays used to study the types of motion participating in each structural mode.

The initial trends for less than 12 modes, shown for the SST configurations, also appear in the 707-320B data. This can be seen in figs. 23 and 24 where similar data are shown. Note that dominant effects are listed in the figures.

The technique of coupling cantilever modes (as was done for the 707-320B) to obtain free-free modes lends itself to quick determination of the type of structural deformation that dominates each free-free mode. The determination is based on identifying the largest element of the cantilever vector from which the free-free modes are computed. Figures 23 and 24 show the variations in the short period roots due to adding free-free modes to the equations of motion. Each root has associated with it an identification of the largest element of the cantilever vector that was used in computing the free-free mode just added. Note that when the first mode is added there is an increase in short period frequency and a decrease in damping. The first free-free mode is dominant by the lowest frequency, wing-bending mode. As additional modes are included, the effect on the short-period roots can be observed. The essential consideration here is that the important deformations be reflected in the modes that are included in the analysis.

Large differences can exist between a preliminary-design-type study and a relatively well-defined, completely elastic airplane analysis. This is illustrated in fig. 25 where rigid and equivalent elastic data using lifting surface derivatives (supplemented by handbook data) are compared with the completely elastic formulation. The aerodynamic influence coefficients for the completely elastic airplane were obtained from a lifting line mechanization using experimental pressure distributions. Note that increments in damping due to elasticity are much less than differences due to the approaches used. The culprit here is again $C_{m_{\dot{\alpha}}}$.

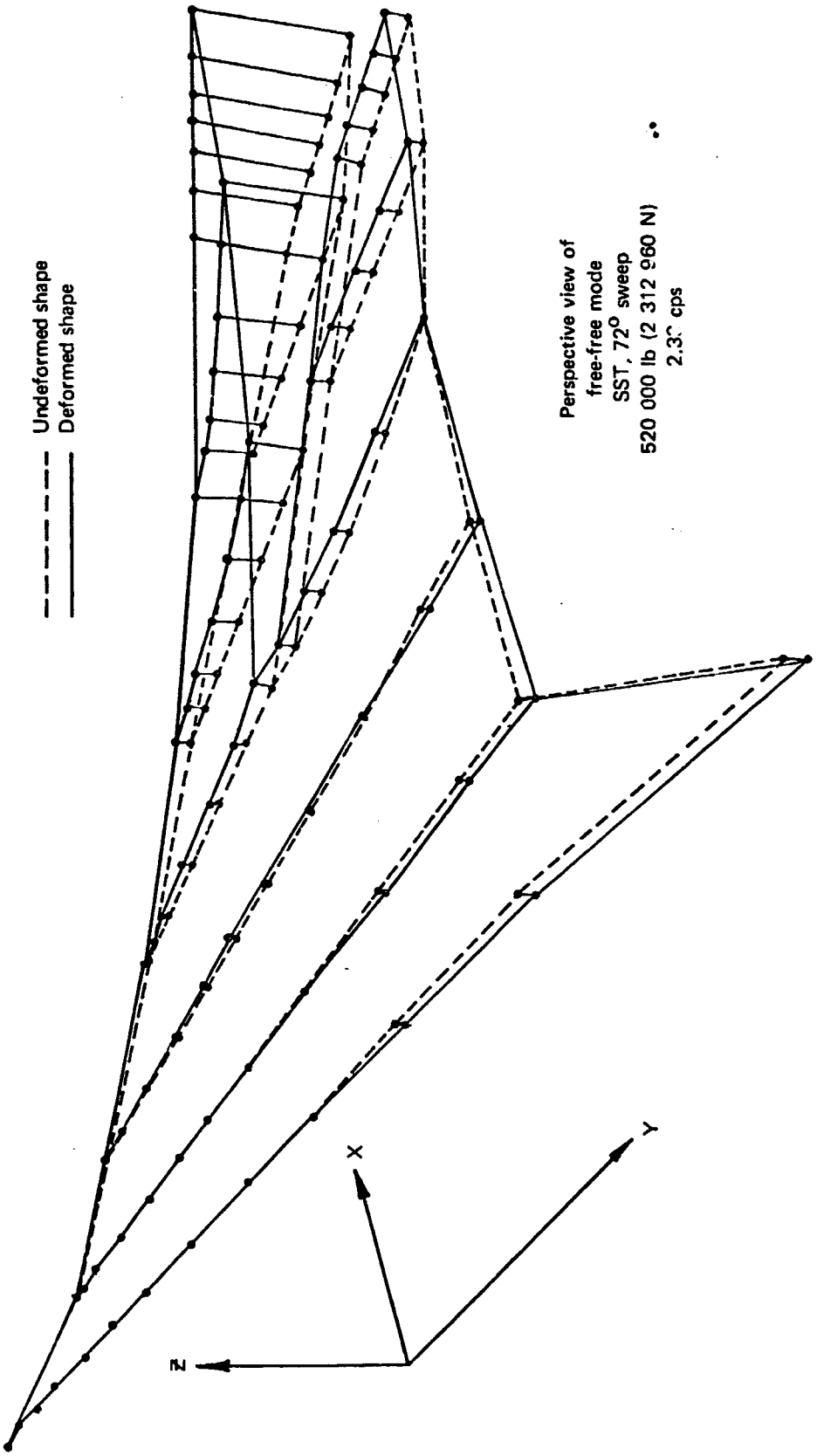

FIGURE 21. TYPICAL VISUAL DISPLAY OF STRUCTURAL MODE SHAPE - SECOND MODE

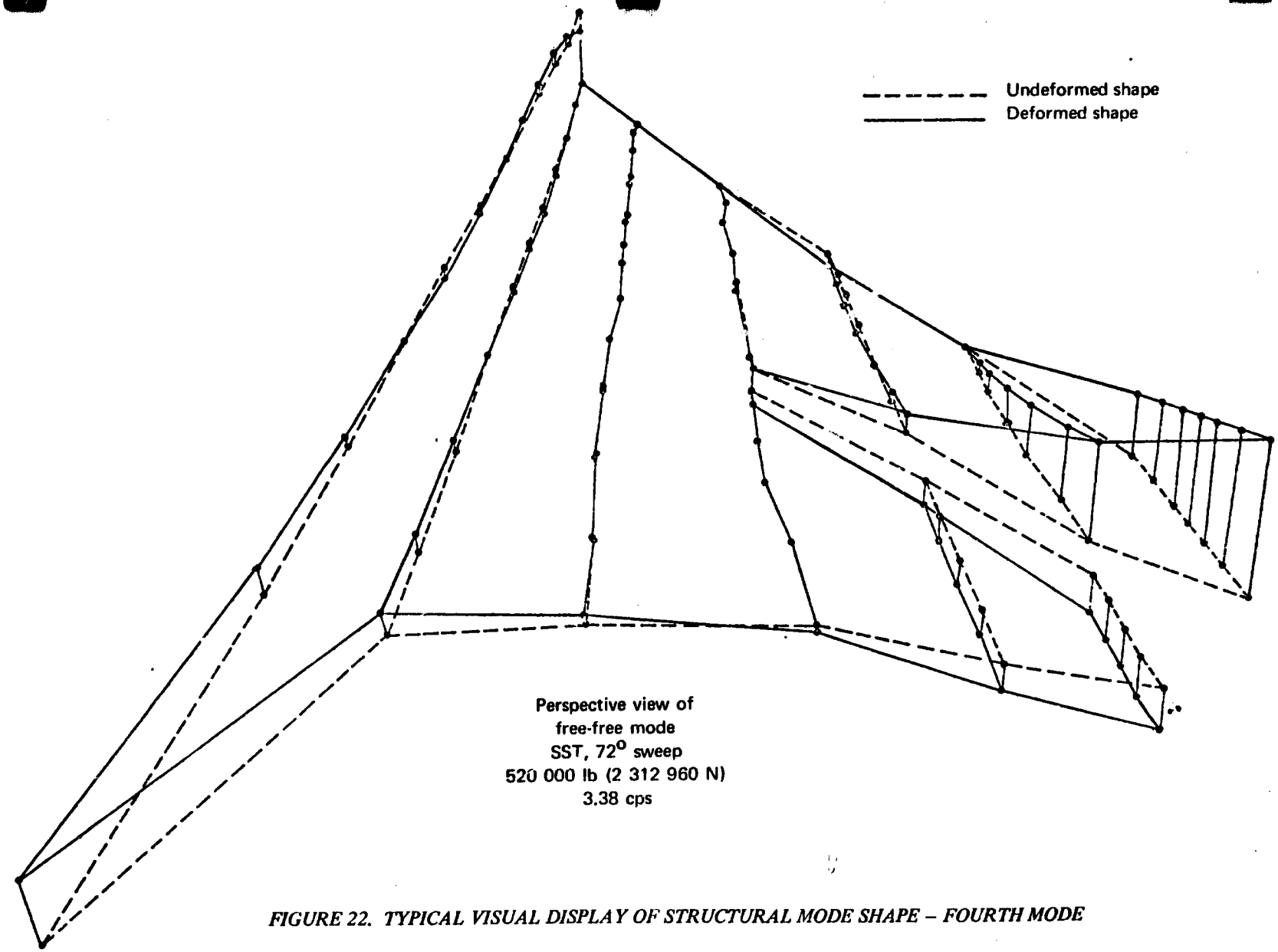

FIGURE 22. TYPICAL VISUAL DISPLAY OF STRUCTURAL MODE SHAPE – FOURTH MODE

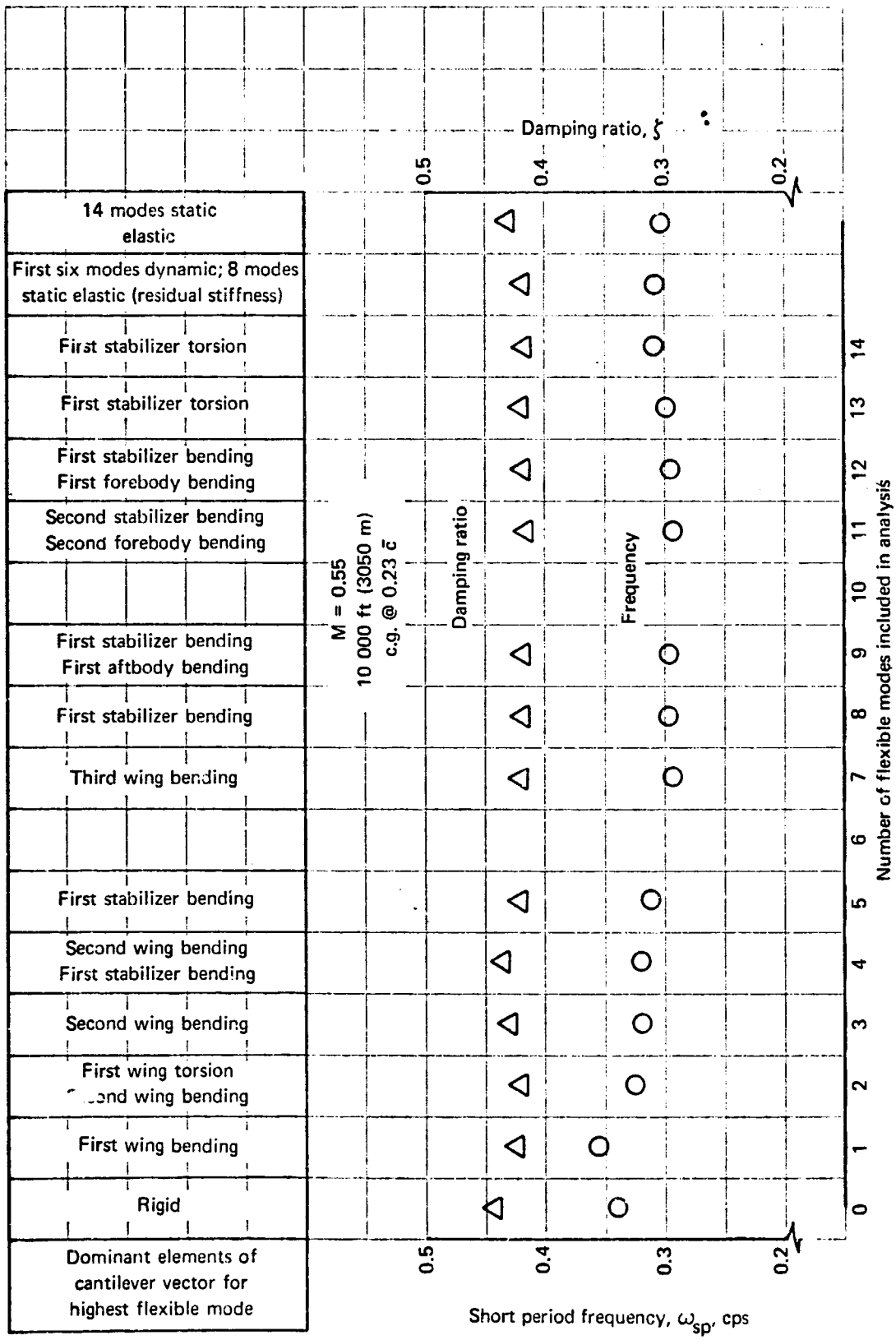

FIGURE 23. VARIATION OF SHORT PERIOD FREQUENCY AND DAMPING WITH NUMBER OF ELASTIC MODES – 707-320B

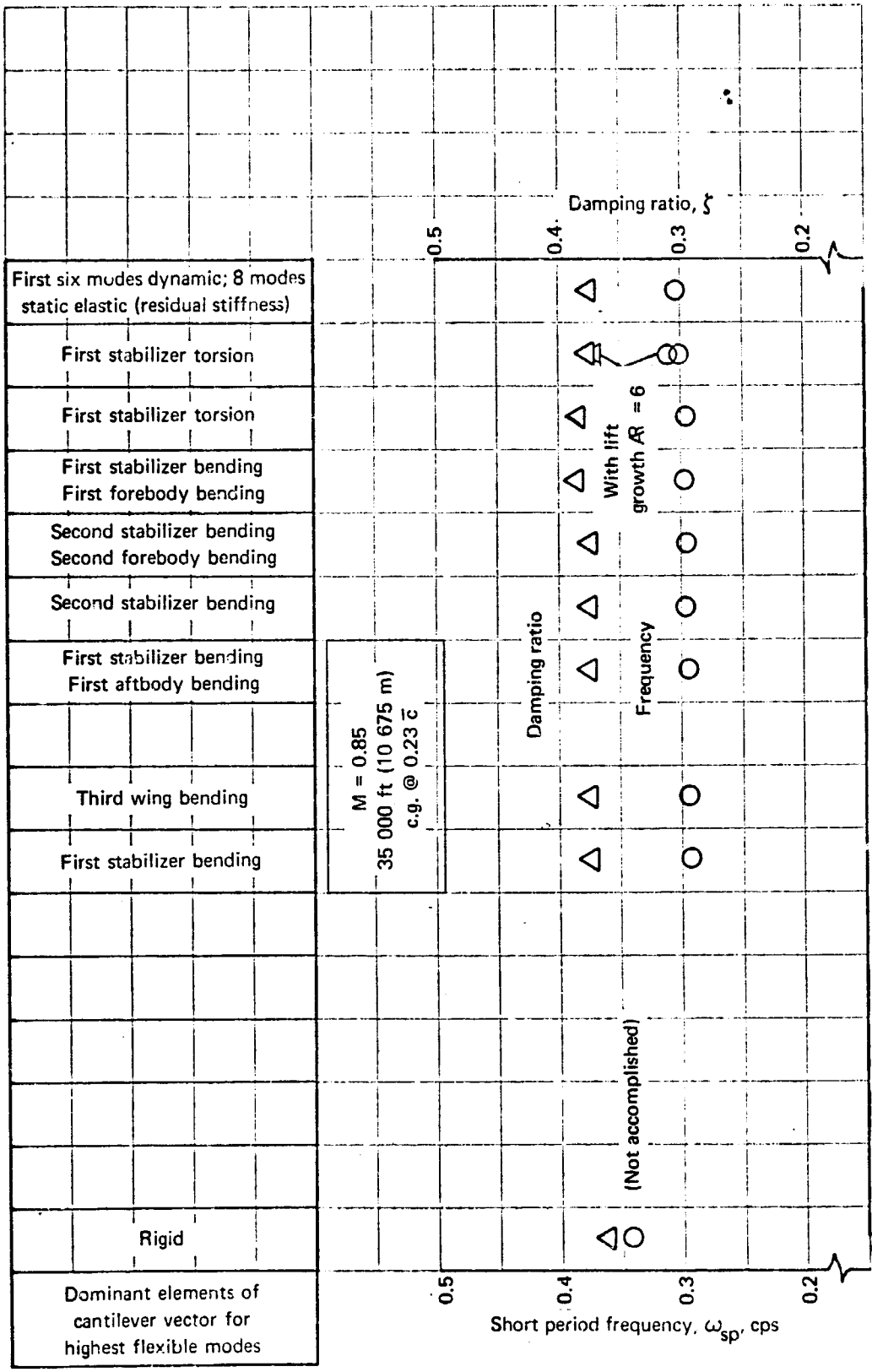

FIGURE 24. VARIATION OF SHORT PERIOD FREQUENCY AND DAMPING WITH NUMBER OF ELASTIC MODES – 707-320B

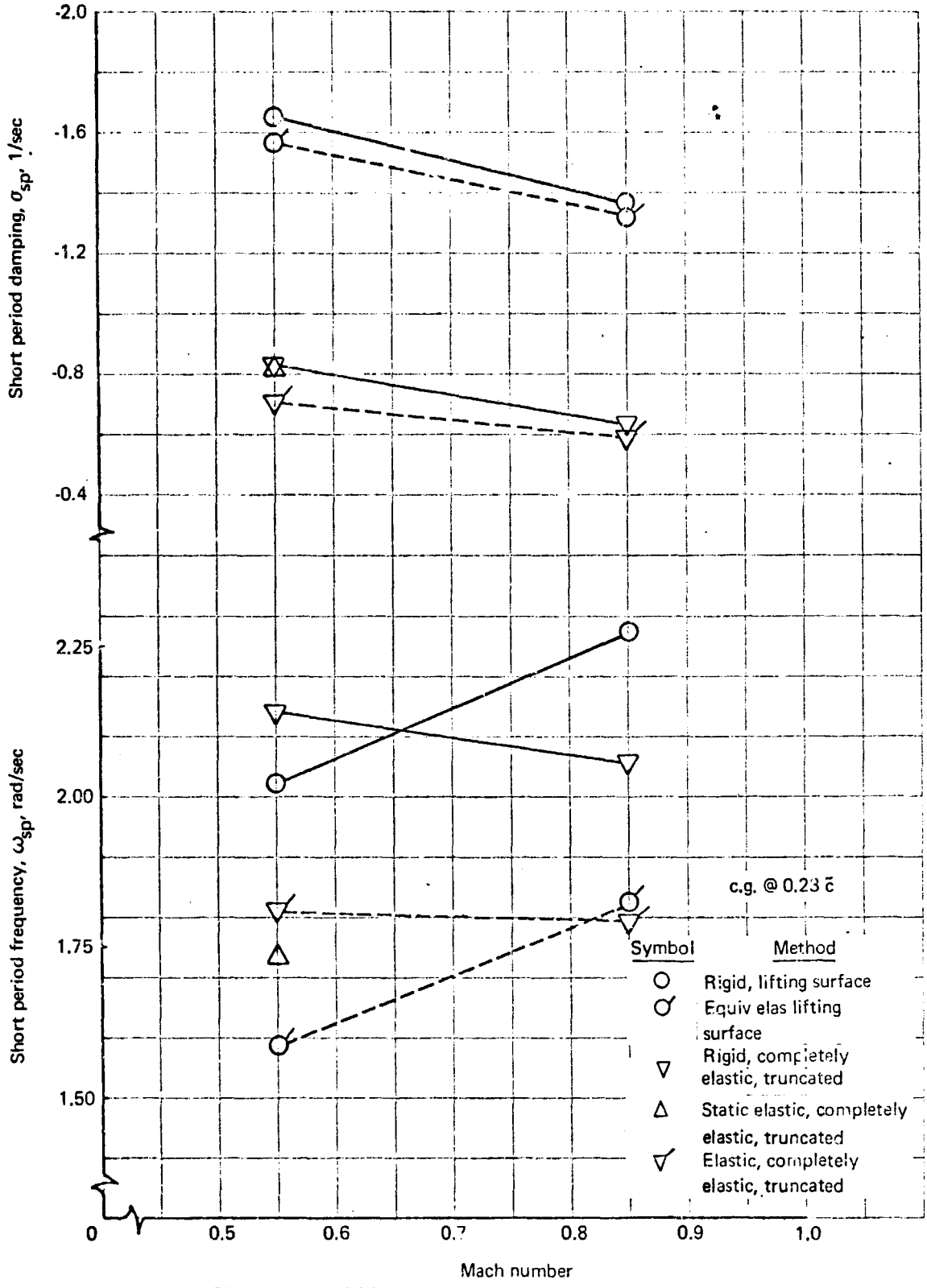

FIGURE 25. PRELIMINARY-DESIGN-TYPE DATA VERSUS 'BEST' WELL-DEFINED ELASTIC MODEL – 707-320B

The frequency data show ball-park-type correlation for the rigid or elastic airplane, and the changes due to elasticity for consistent approaches are also roughly the same.

The longitudinal stability derivatives used in the completely elastic 707-320B analysis are listed in table 9. The rigid derivatives are shown, together with elastic corrections from all modes treated as static elastic. The formulation of static elastic equations is presented in par. 9.2. The rigid and equivalent elastic derivatives for the 707-320B used in the comparisons of fig. 25 are given in table 21 of par. 8.2.

The primary effect of lift growth (Wagner effect) is to alter the transient response of the system. This can be verified by an examination of the roots of the rigid-body modes, those calculated with lift growth versus those calculated without lift growth (figs. 24). The inclusion of lift growth tends to reduce the real part of the roots (a reduction in damping) leaving the imaginary part essentially unaltered. The lift growth functions are sensitive to planform details and Mach number, and the number of available functions is so limited that calculation of precise effects is precluded in the absence of a complete unsteady aerodynamic formulation. Solutions with the available lift growth functions can, at best, be interpreted as sensitivity indicators. Section 9 discusses the lift growth functions that were used and the manner in which they were incorporated into the equations of motion.

6.2.2 Longitudinal time histories. — Examples of the use of the six-degree-of-freedom program and MIMIC for longitudinal time histories are presented in this section.

Longitudinal time histories are shown for the following conditions:

(1) SST, M = 2.70, 49 000 ft

(2) 707-320B, M = 0.548, 10 000 ft

Figure 26 shows the results for an SST 72° wing sweep configuration at M = 2.70. As can be seen, the equivalent elastic airplane mathematical model utilizing aerodynamic lifting surface theory produces slightly larger pitch amplitudes than the other models. Specific reasons for this are not apparent, because all stability derivatives varied between the rigid and equivalent elastic

TABLE 9. – LONGITUDINAL DERIVATIVES USED IN COMPLETELY ELASTIC 707-720B ANALYSIS

Derivatives*	Values for M = 0.55		M = 0.85
	Rigid	14 modes as static elastic	Rigid
C_{L_α}	5.36	4.86	6.8
C_{m_α}	-1.44	-1.44	-1.66
$C_{L_{\hat{q}}}$	13.9	12.35	14.9
$C_{m_{\hat{q}}}$	-17.18	-14.73	-19.52

*All derivatives are nondimensional and are for angles measured in radians

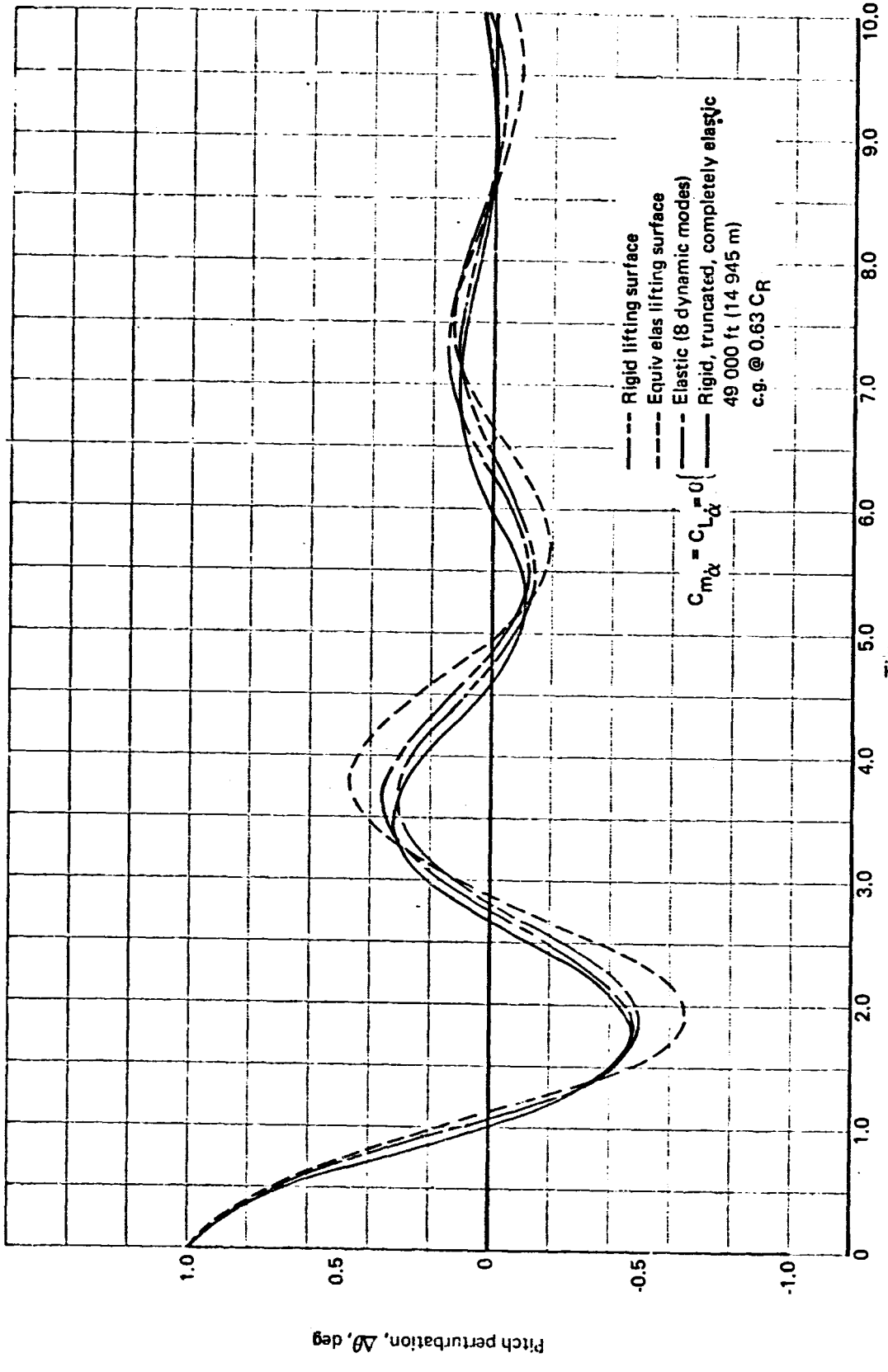

FIGURE 26. LONGITUDINAL RESPONSE TO ONE DEGREE OUT OF TRIM – 72^{D}SST

models except the $\dot{\alpha}$ derivatives; also, the equivalent elastic pitch inertia, $I_{yy_{eq\ el}}$, was approximately 27 percent larger than that used for the rigid mathematical model. There is not a great deal of difference between the rigid model and the completely elastic mathematical model with eight dynamic modes. The frequencies and amplitudes are very nearly equal. For all mathematical models the time history of the pitch perturbation shows a stable motion. For this particular configuration and flight condition the rigid mathematical model would probably be satisfactory to describe the short period longitudinal dynamics for stability and control purposes.

The response of the 707-320B to an elevator pulse is shown in fig. 27 for three mathematical models. The rigid model corresponds to the truncated, completely elastic model resulting in the use of a 2 x 2 matrix. The inclusion of 14 dynamic modes in a static elastic manner results in the greatest pitch amplitudes. If four modes are allowed to participate dynamically, the result is an effective increase in the damping as reflected in the decrease of amplitude.

The same control derivatives were used to perturb the rigid and equivalent elastic lifting surface theory mathematical models. The resulting time histories are shown in fig. 28 along with the rigid response from the truncated, completely elastic analysis. As can be seen, there is a large difference in the damping between the two rigid models. This is apparently due to the differences in treating the stability derivatives, C_{m_q} and $C_{m_{\dot{\alpha}}}$. For the curve labeled "lifting surface theory" in fig. 28, C_{m_q} and $C_{m_{\dot{\alpha}}}$ were obtained from aerodynamic lifting surface theory and the USAF Stability and Control Handbook, respectively. The rigid curve produced from the completely elastic analysis used a C_{m_q} derivative obtained from a generalized forces approach, while no $\dot{\alpha}$ derivatives were used. The same results are shown in fig. 25 where the frequency and damping obtained from the roots of the characteristic equation are presented.

The maximum pitch amplitudes in figs. 26 through 28 are found for those mathematical models for which the forces are considered quasi-static; that is, the forces and deflections are in phase. The equivalent elastic and static elastic models are both of the preceding type.

Figures 27 and 28 illustrate the response to an elevator pulse with the control derivatives the same for all mathematical models. Therefore, these

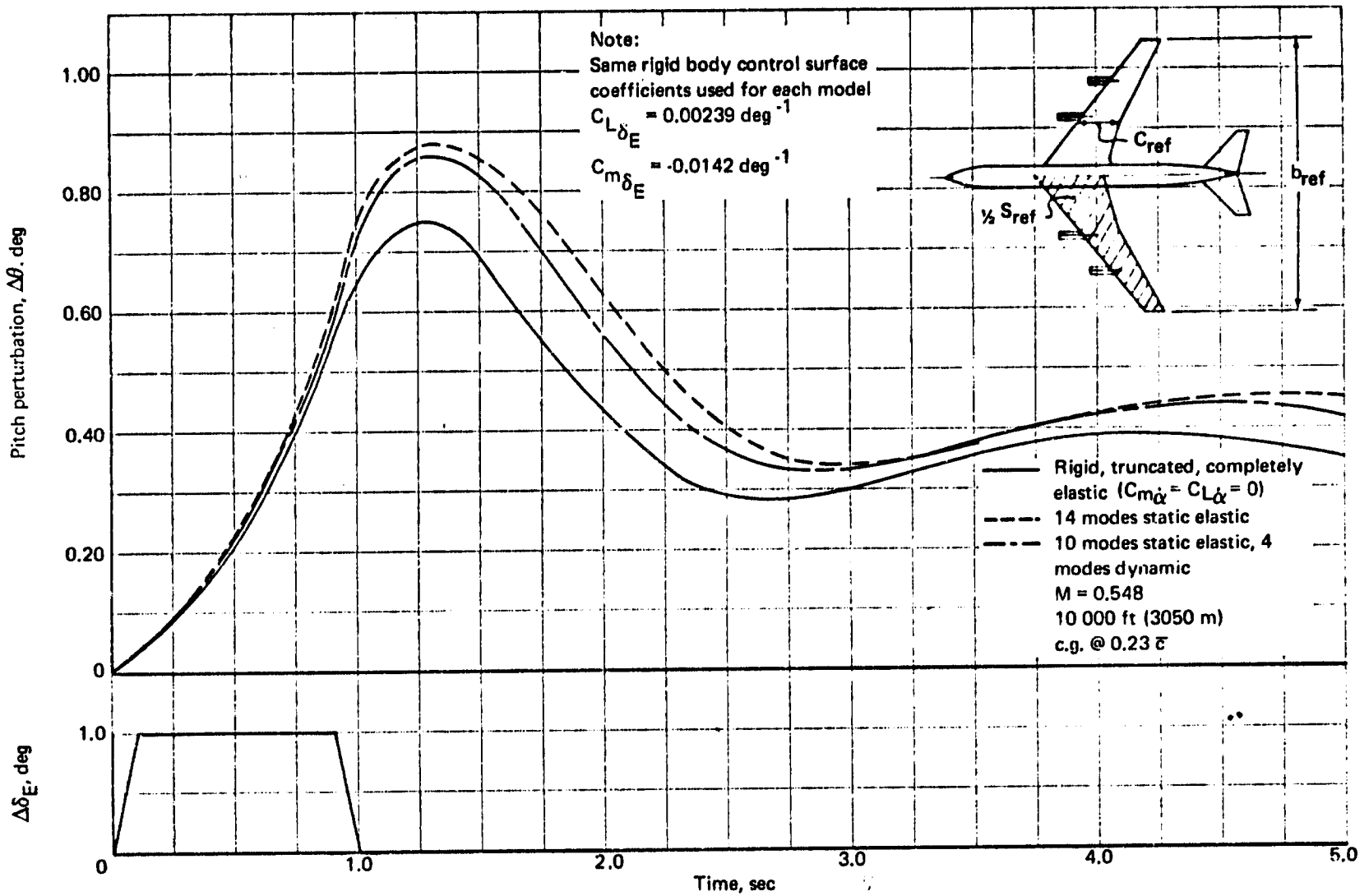

FIGURE 27. LONGITUDINAL RESPONSE – 707-320B

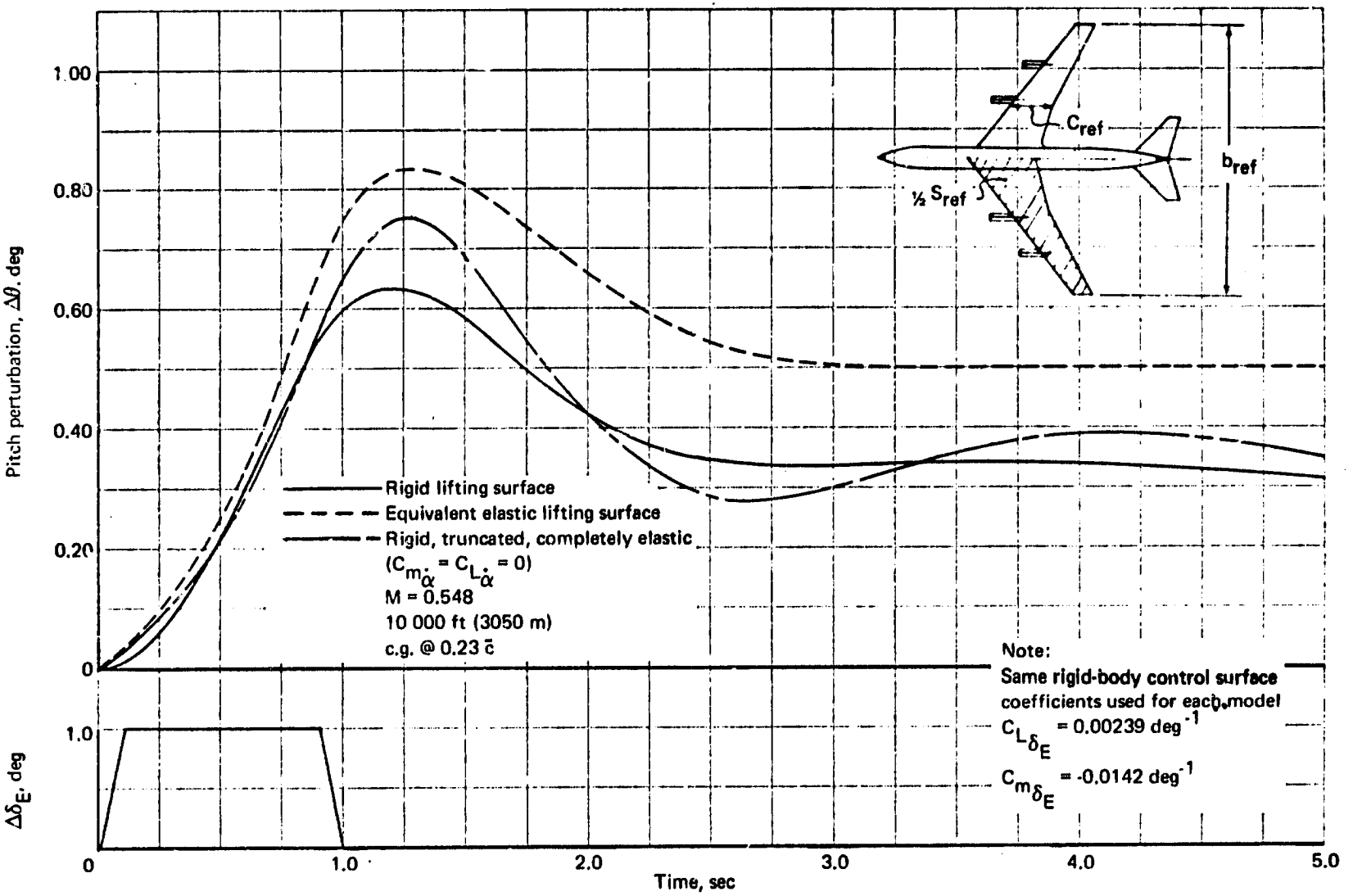

FIGURE 28. LONGITUDINAL RESPONSE – 707-320B

time histories show differences due to stability derivatives. If the effects of elasticity are included in the elevator control derivatives, the resulting response reflects this input. Figure 29 presents the 707-320B longitudinal response to an elevator pulse using rigid and equivalent elastic lifting surface theory for the control as well as the stability derivatives. The most notable difference between the motion shown in fig. 29 and that in fig. 28 is that the equivalent elastic pitch response is now smaller than the rigid response. The opposite result occurs if the same control inputs are applied to the rigid and elastic airplanes. The true response of the airplane is shown only when the control derivatives are altered to reflect the elasticity of the structure.

6.3 Lateral-Directional Dynamic Stability Characteristics

6.3.1 Roots of the lateral-directional characteristic equations. — Lateral-directional stability characteristics were determined for the rigid and equivalent elastic study airplanes at the flight conditions given in table 1 using the characteristic equation method (small perturbation program). The rigid and equivalent elastic derivatives, coefficients, and inertial properties used in obtaining the data are tabulated in par. 8.2 and the detail results are illustrated in par. 8.5. The frequency, damping, period, time to damp to half or double amplitude, and cycles to damp to half or double amplitude were determined from the quartic equation (5.8) and are all presented in par. 8.5. These results generally reflect the good and bad correlation evident in the derivative comparisons in app. B. The rigid and equivalent elastic data presented and discussed in this section are primarily those used to compare with the results of the completely elastic airplane analysis. A lateral-directional analysis of the latter type was performed for the 707-320B airplane only.

The Dutch roll characteristics for the 707-320B and SST at 72° leading edge sweep were also calculated using the approximate expressions for frequency and damping given in Sec. 5. The approximate expressions were applied to the wind tunnel derivatives for the rigid airplane. The results are plotted in figs. 30 through 32, where they are compared with the various quartic solutions. The data show that the accuracy of the approximate formulas depends greatly on the type of configuration. The 707-320B data show, except for one flight condition, that the differences between the approximate solutions and quartic

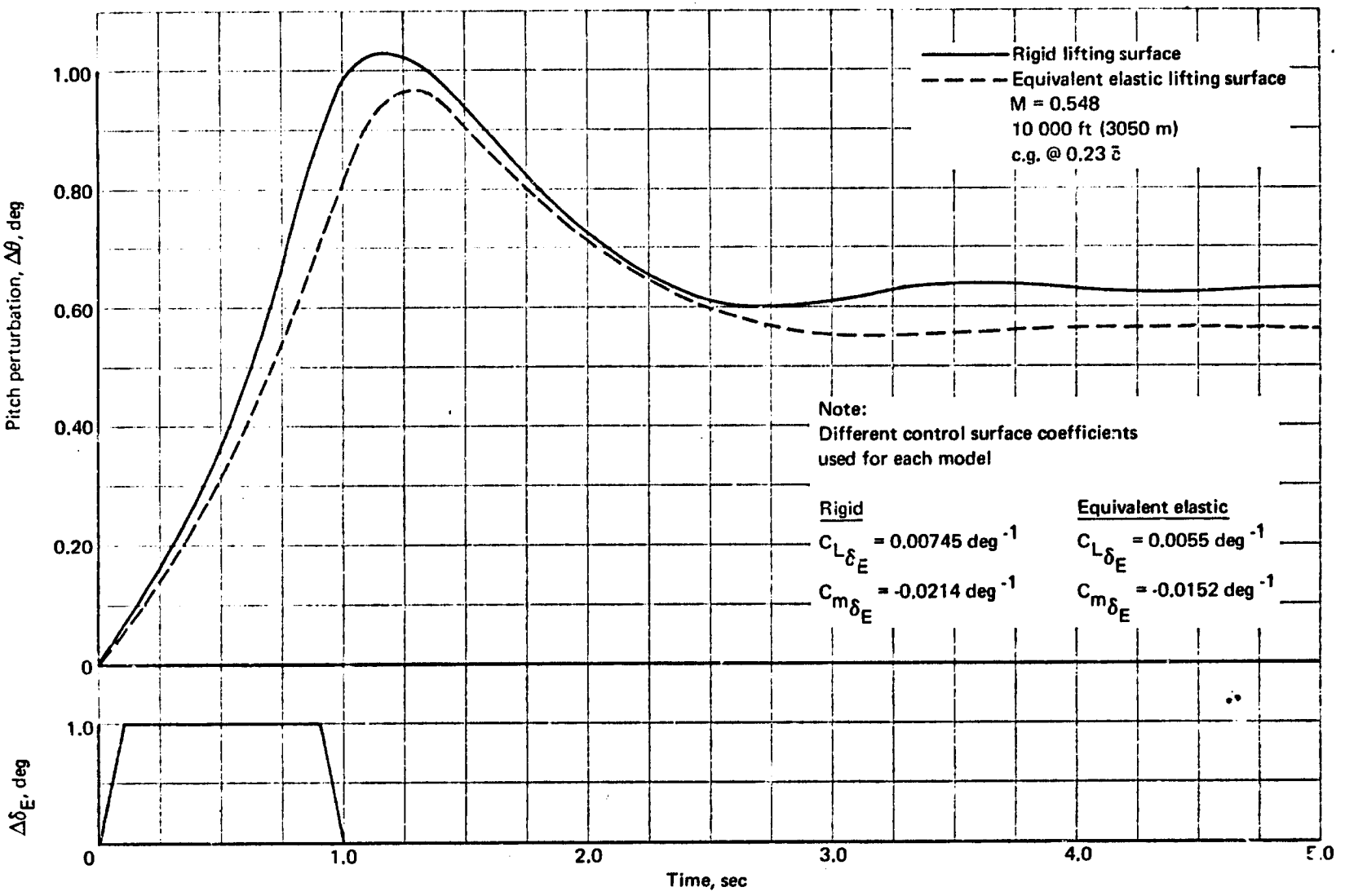

FIGURE 29. LONGITUDINAL RESPONSE, LIFTING SURFACE THEORY – 707-320B

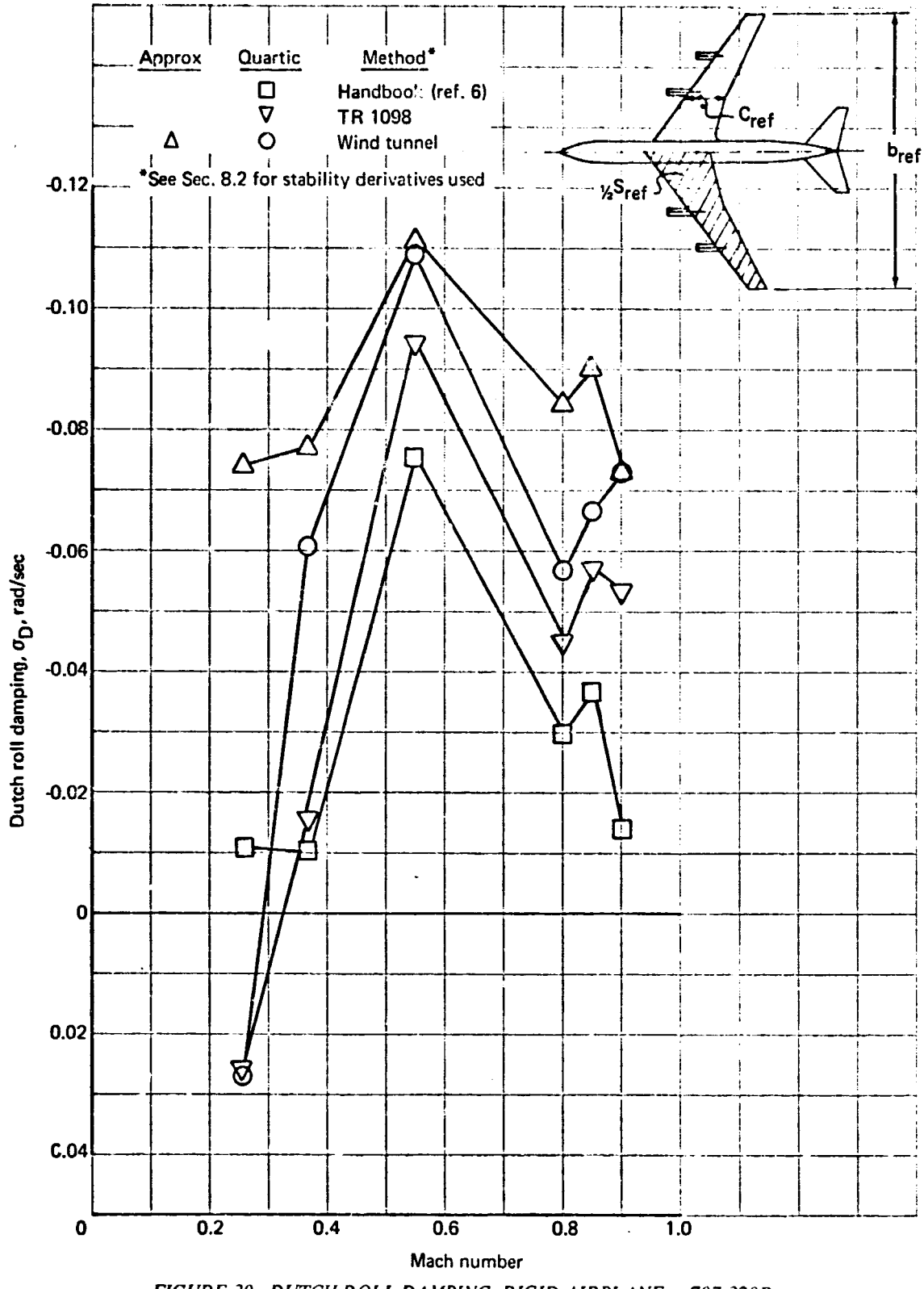

FIGURE 30. DUTCH ROLL DAMPING, RIGID AIRPLANE – 707-320B

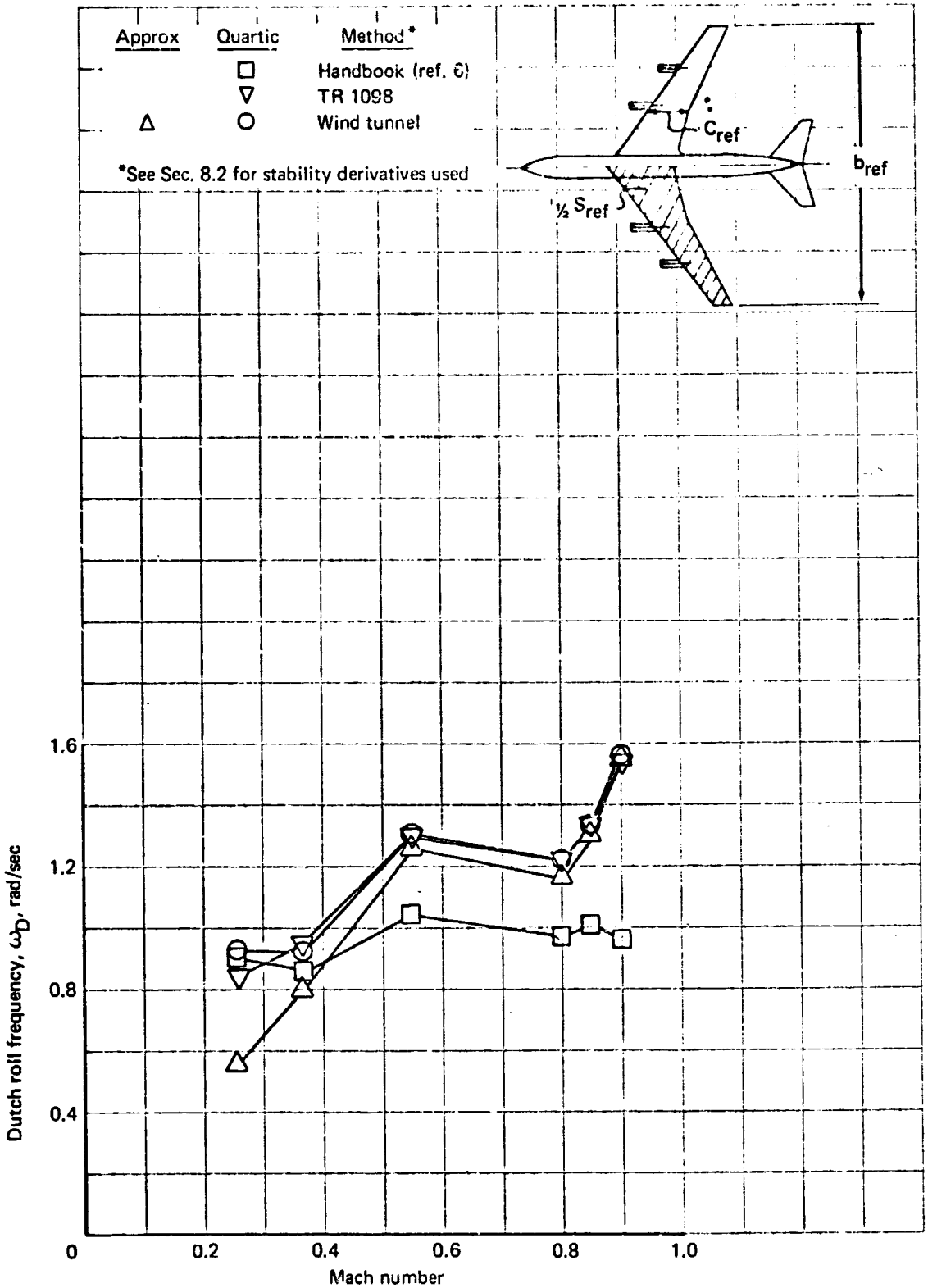

FIGURE 31. DUTCH ROLL FREQUENCY, RIGID AIRPLANE – 707-320B

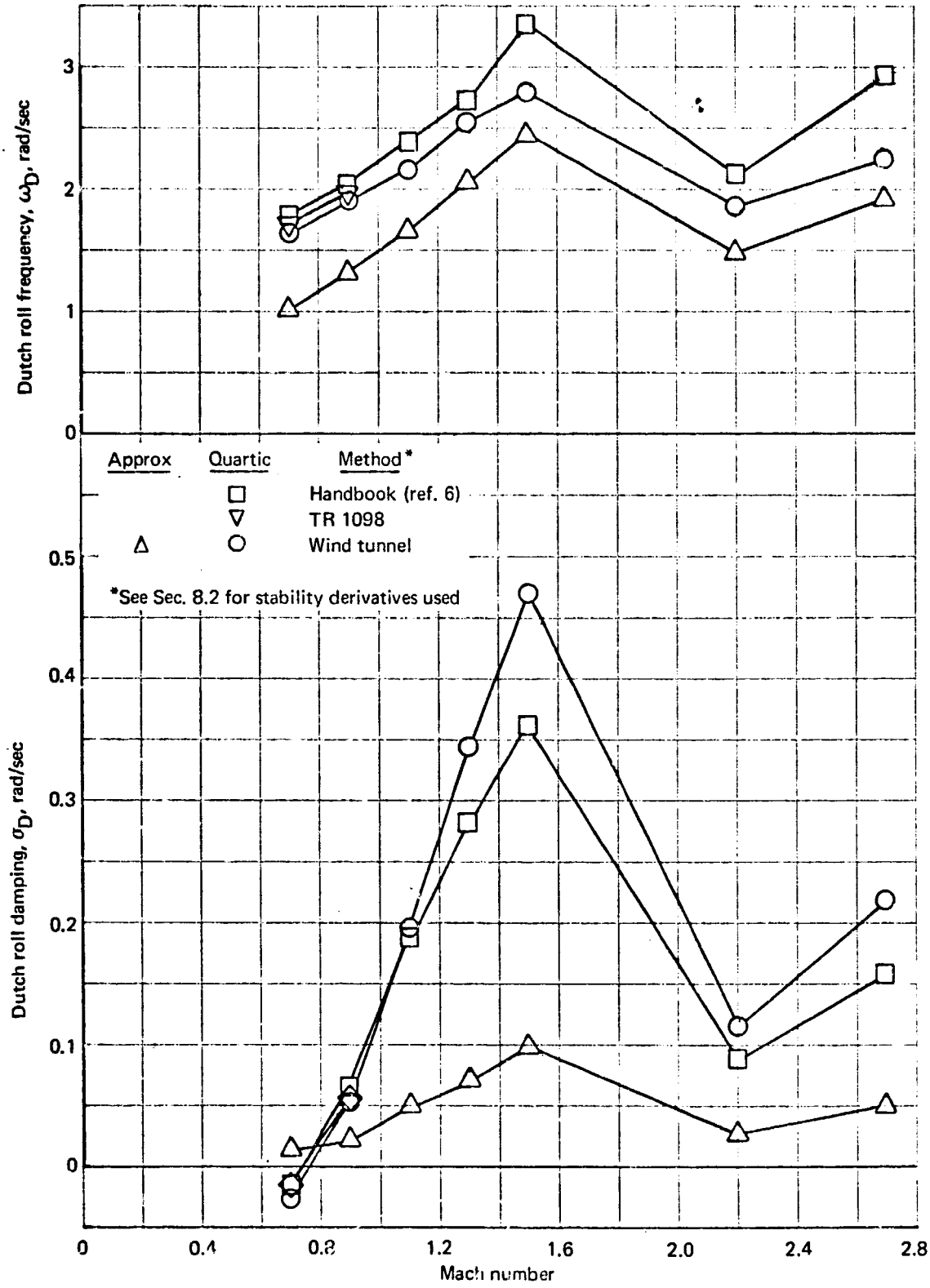

FIGURE 32. DUTCH ROLL FREQUENCY AND DAMPING, RIGID AIRPLANE – 72° SST

solutions for one set of derivatives are small or of the same order as the differences in the data due to variations in the derivative calculation techniques. These data illustrate that for the 707-320B the effect of accuracy of the derivatives on the Dutch roll characteristics is usually a more important consideration than the approximate formula. On the other hand, the SST data show that the approximate expressions (equations (5.25) and (5.27)) give results that generally differ considerably from the quartic solution. This is true especially for the damping. It must be noted that the equations used were for a one-degree-of-freedom approximation. The three-degree-of-freedom approximation may have given better results, but the complexity of the expression for the damping reduces its usefulness. Therefore, because of the unreliable nature of the simple approximate equations for the lateral-directional modes and the availability and speed of computer programs for solving the roots of the quartic equation, the engineer should make use of these programs.

Comparisons of the 707-320B Dutch roll characteristics calculated by use of the rigid wind tunnel and equivalent elastic handbook derivatives are made with flight test data and the results of the completely elastic airplane analysis in figs. 33 through 35. Appendix B contains a detailed discussion of the equivalent elastic handbook stability derivative calculation. As pointed out in app. B, a value for the aftbody bending parameter, $\bar{K}_\beta = 56.1 \times 10^{-8}$ rad/lb, was used in the initial calculations. A value of $\bar{K}_\beta = 21.0 \times 10^{-8}$ would be more realistic. Appendix B illustrates the difference in the elastic lateral-directional derivatives due to this parameter. As shown there, the differences in the derivatives due to aftbody bending are small compared to the effect of vertical tail flexibility. The dynamic stability characteristics illustrated here in app. C were calculated with $\bar{K}_\beta = 56.1 \times 10^{-8}$, and only very small differences would be noted if $\bar{K}_\beta = 21.0 \times 10^{-8}$ had been used. The poor correlation shown in figs. 33 through 35 between the equivalent elastic handbook method and the flight test data is primarily due to the following (which are discussed in app. B):

(1) The vertical tail flexibility was calculated to be somewhat high;

(2) The handbook technique developed for the equivalent elastic analysis has deficiencies and needs more development.

The data of figs. 33 through 35 show that for stability and control purposes a static elastic analysis would probably be sufficient to estimate the Dutch roll

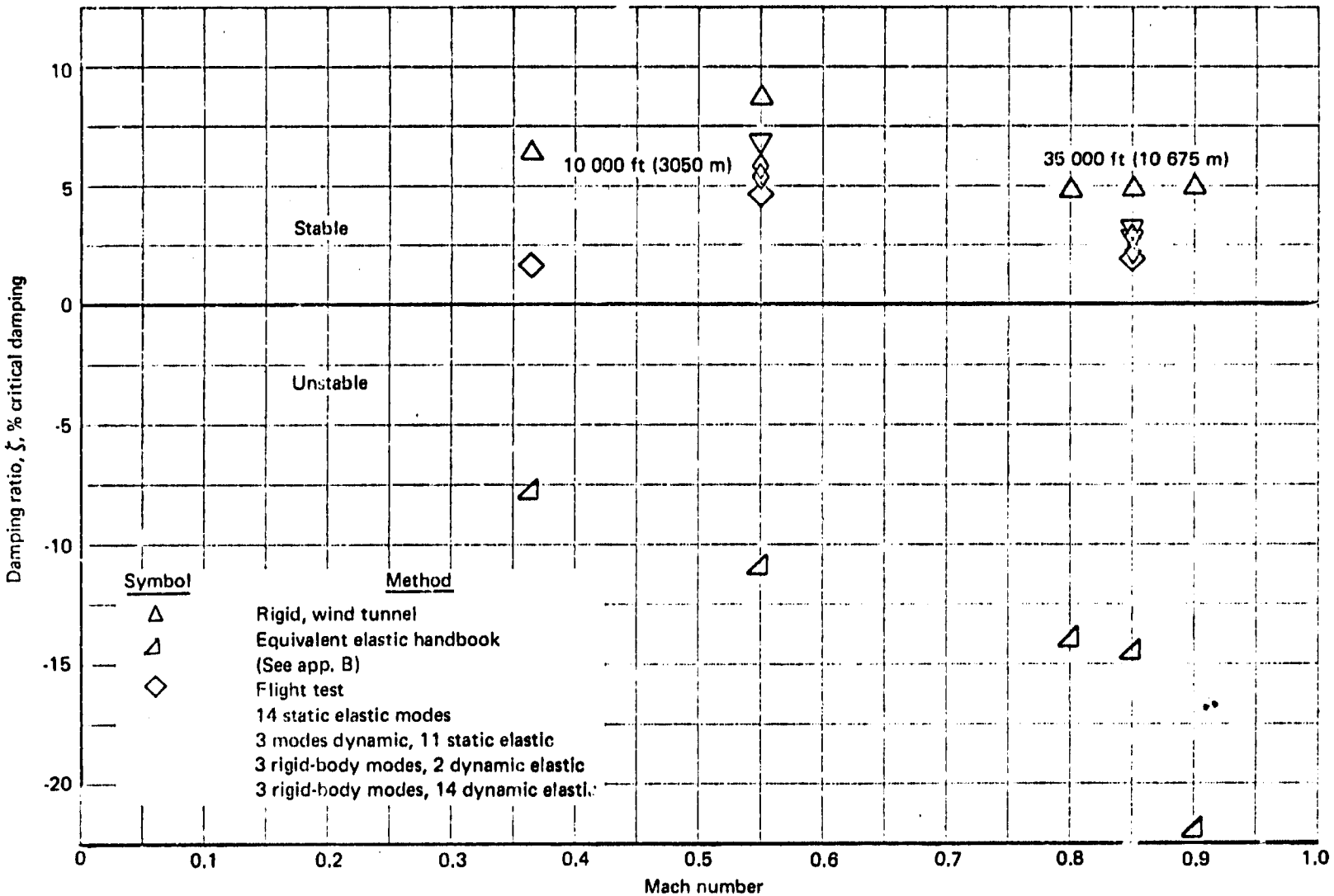

FIGURE 33. DUTCH ROLL DAMPING FACTOR – 707-320B

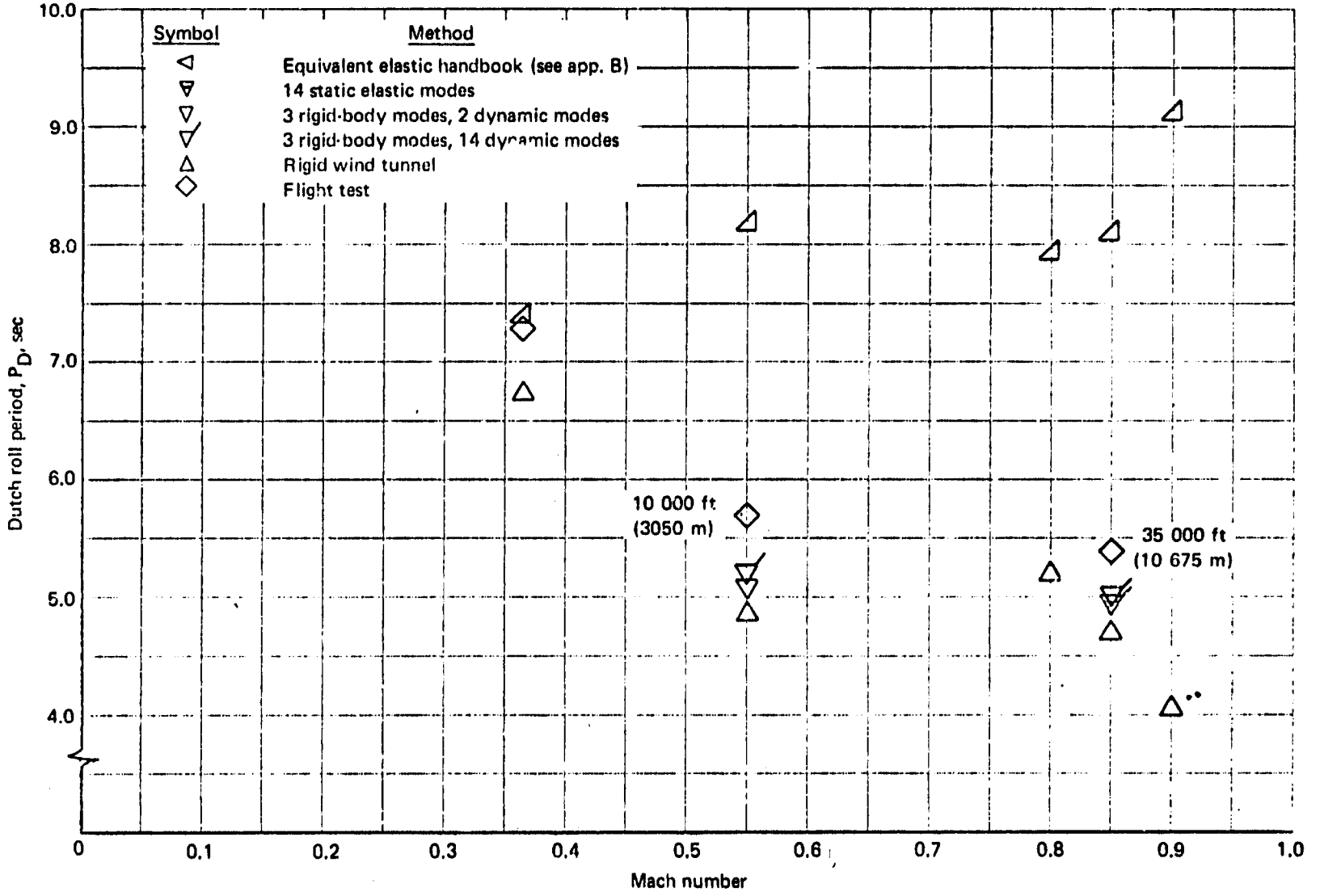

FIGURE 34. DUTCH ROLL PERIOD – 707-320B

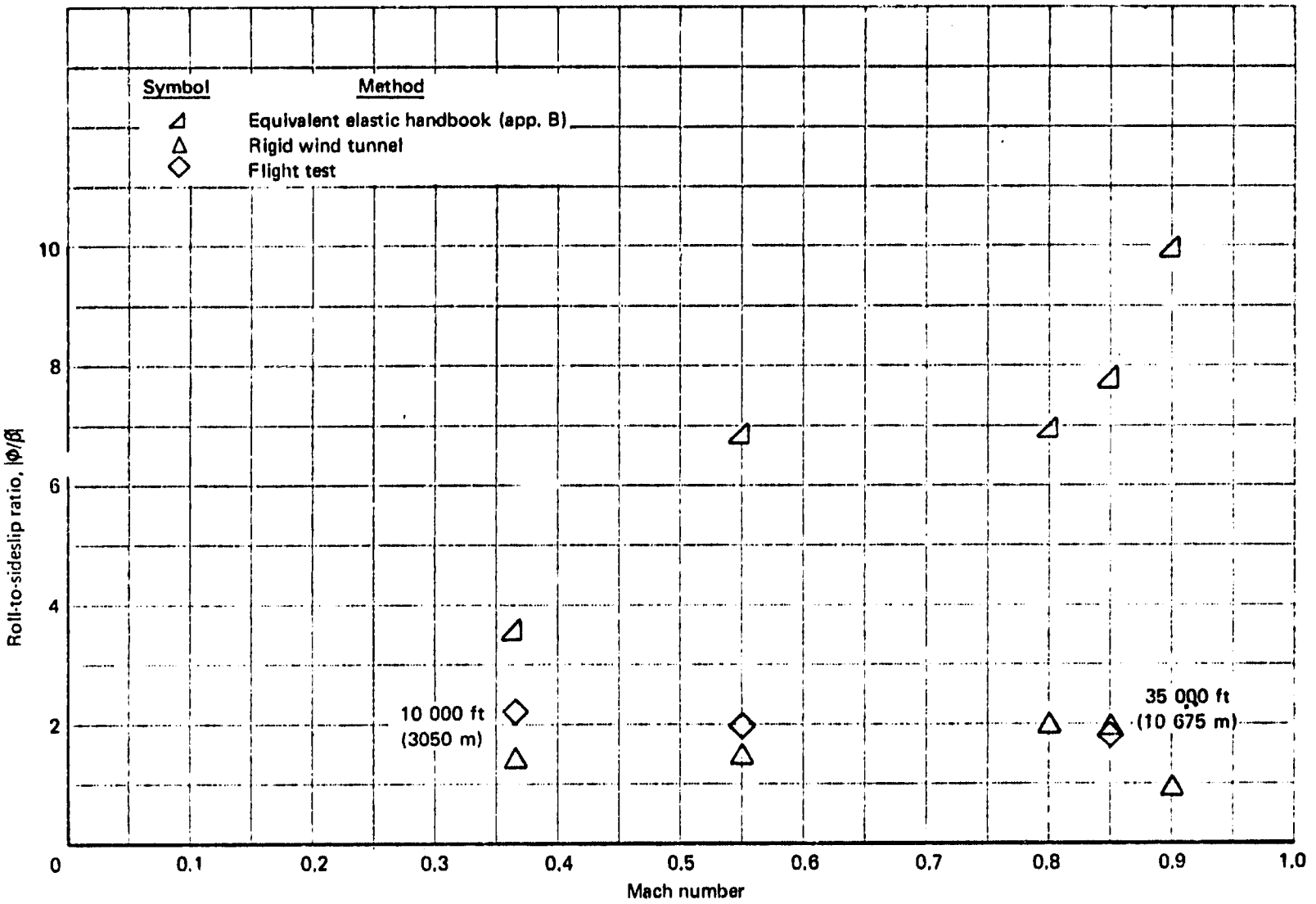

FIGURE 35. DUTCH ROLL |Φ/β| – 707-320B

characteristics. The Dutch roll period and damping are relatively insensitive to the number of elastic modes included.

The variation of the frequency and damping for the lateral-directional modes for the two flight conditions which were analyzed in detail is shown in figs. 36 and 37. The analysis predicts a lateral-phugoid mode (in addition to the usual Dutch roll mode) at a Mach number = 0.85 which disappears when no elastic modes are included and when more than 10 elastic modes are included. The equivalent elastic analysis predicts a rolling convergence and spiral mode in addition to the Dutch roll for all cases (par. 8.5). A detailed discussion of this unstable lateral-phugoid mode and its variation with the number of elastic modes included would be useful mainly for academic purposes. The period of this mode and the time to double amplitude are so long (200 to 300 sec) as to make this motion of relatively minor importance. The completely elastic analysis was based on the rigid wind tunnel derivatives except that the $\dot{\beta}$ derivatives were not used. These rigid derivatives, along with the values calculated for use with the static elastic mathematical model, are listed in table 10 for M = 0.85. The inertia values used in the completely elastic analysis are presented also in table 10. These values are slightly different than those used for the rigid and equivalent elastic models. This difference appears in the plots of frequency and damping for the Dutch roll. The three rigid wind tunnel modes would give results identical to those of the three truncated, completely elastic modes if the inertia were the same, except for the effect of the $\dot{\beta}$ derivatives not appearing in the latter mathematical model. The parametric study of Sec. 7 discusses the significance of the $\dot{\beta}$ derivatives. Only $C_{n_{\dot{\beta}}}$ has any effect, and that is on the damping only. Therefore, the plot of Dutch roll frequency illustrates the difference due to the different values of I_{zz} used in the two mathematical models. The most important results illustrated in figs. 36 and 37 are as follows.

(1) The Dutch roll frequency is relatively insensitive to elastic effects. For stability and control purposes an elastic modal analysis is not necessary to predict the frequency for this type of configuration. At most, all that would be needed is a good static-elastic analysis.

(2) The damping of the Dutch roll mode decreases with the addition of the first two elastic modes, but then remains relatively insensitive to any additional number of modes.

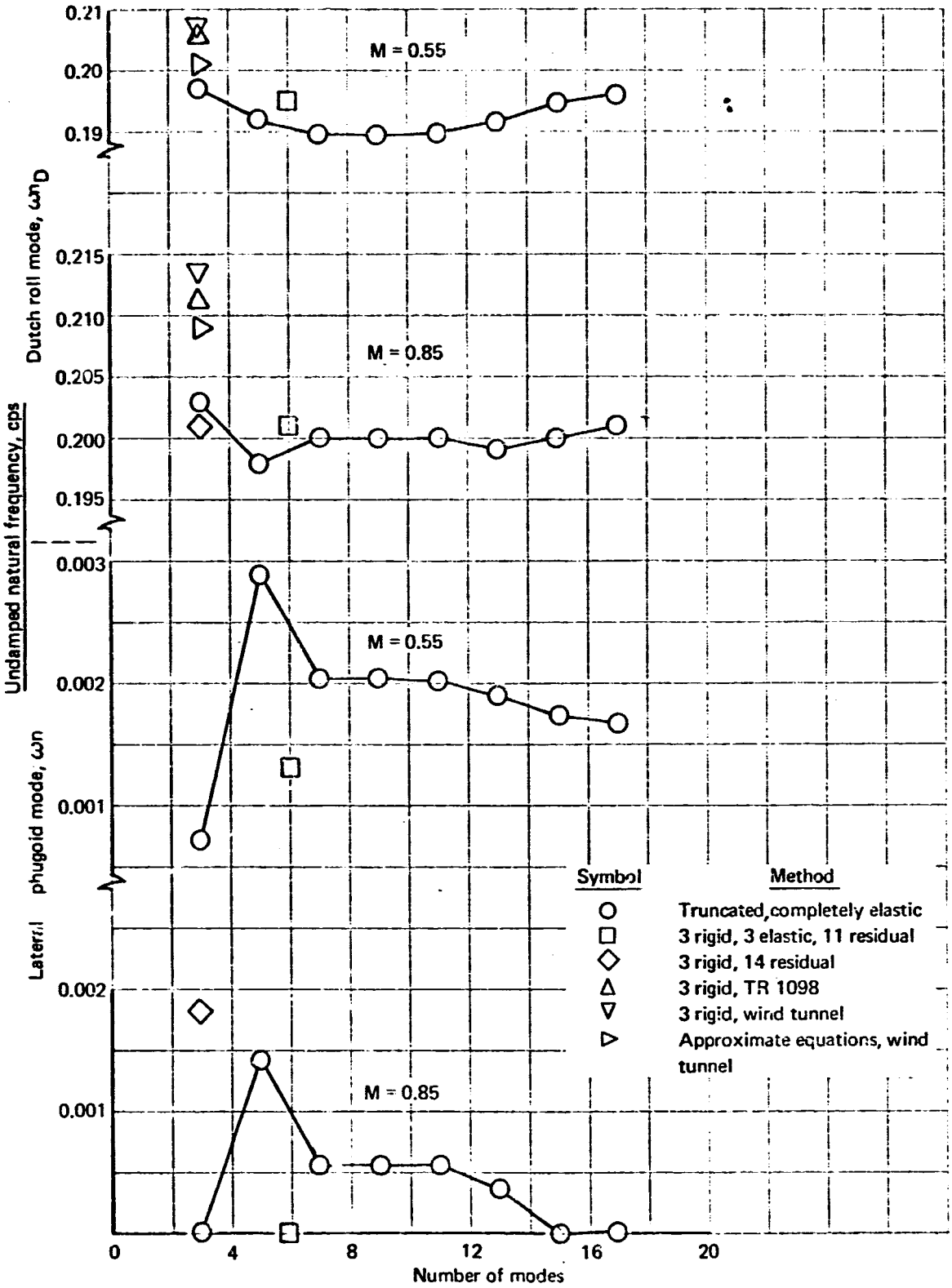

FIGURE 36. DUTCH ROLL AND LATERAL PHUGOID FREQUENCY - 707-320B

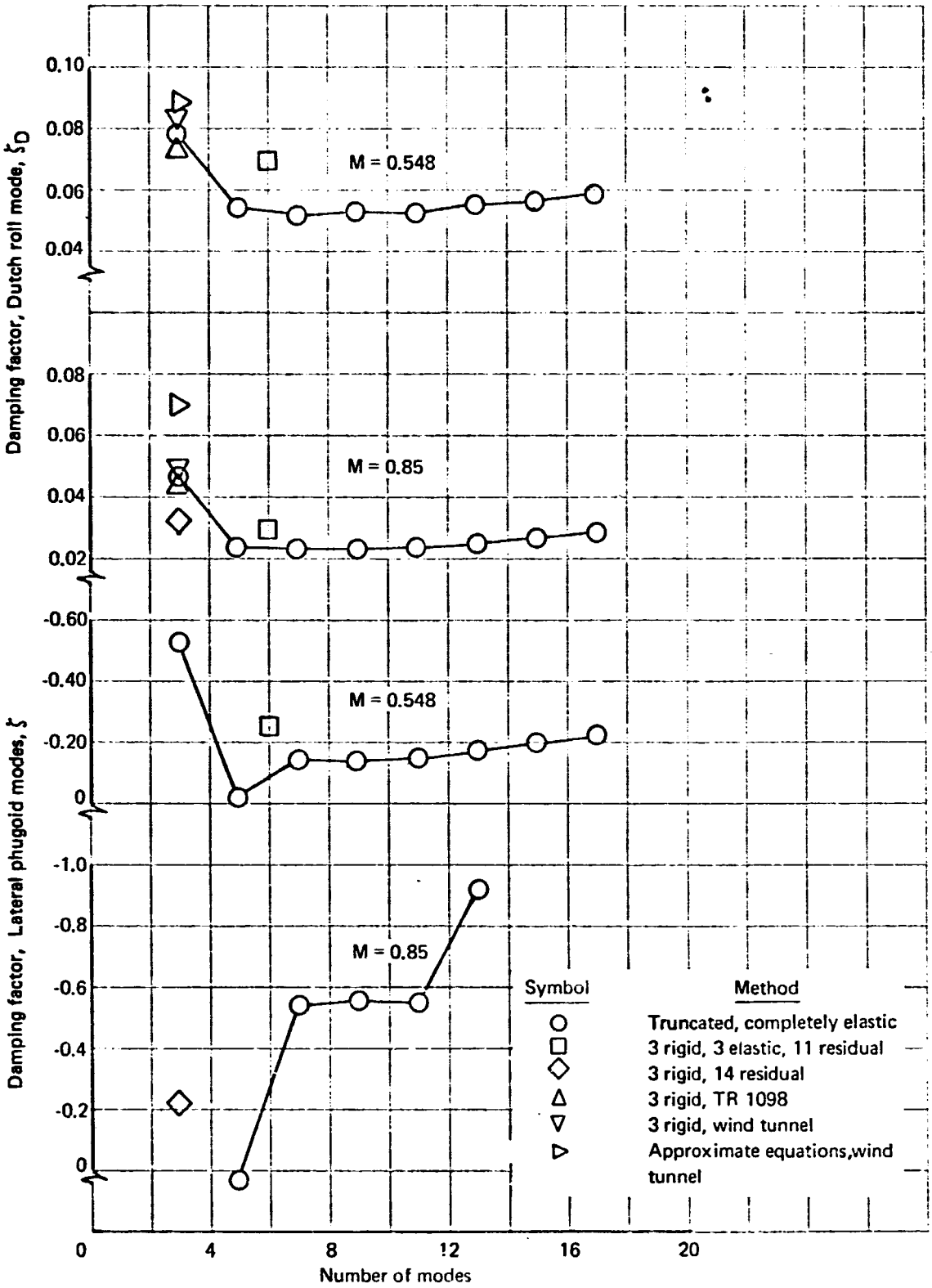

FIGURE 37. DUTCH ROLL AND LATERAL PHUGOID DAMPING – 707-320B

TABLE 10. – LATERAL-DIRECTIONAL DERIVATIVES USED IN ANALYSES OF COMPLETELY ELASTIC 707-320B

Derivative*	Rigid value	Static elastic value
Cy_β	-0.547	-0.54
C_{ℓ_β}	-0.215	-0.229
Cn_β	0.165	0.162
$Cy_{\hat{p}}$	-0.1118	-0.114
$C_{\ell_{\hat{p}}}$	-0.688	-0.54
$Cn_{\hat{p}}$	-0.0187	-0.0176
$Cy_{\hat{r}}$	0.354	0.34
$C_{\ell_{\hat{r}}}$	0.21	0.22
$Cn_{\hat{r}}$	-0.2032	-0.198

Inertial characteristics		
I_{XX} = 4.8		Slug-ft^2 x 10^{-6},
I_{ZZ} = 11.0		Stability axes
I_{XZ} = -0.12		

*All derivatives are for angles measured in radians. Static elastic values are based on normal modes. M = 0.85, 35 000 ft (10 675 m)

There was no lateral-directional analysis of the completely elastic SST. The detailed results of the rigid and equivalent elastic analysis appear in par. 8.5. The important conclusions of that study are as follows.

(1) There is no significant difference in Dutch roll period between rigid and equivalent elastic airplanes. Elasticity generally decreases the damping of this mode.

(2) The rolling convergence mode is highly damped for both rigid and equivalent elastic mathematical models. Only a very negligible difference exists between the time to damp to half amplitude for the two models.

(3) Elasticity generally has a destabilizing effect on the spiral mode for the subsonic cases. However, for the supersonic flight conditions a small stabilizing effect due to elasticity is generally noted for this mode.

Figures 38 and 39 are examples of the results of the rigid and equivalent elastic lateral-directional SST analysis supporting the conclusions stated above.

Lift growth (Wagner effect) has the same effect on the lateral modes as for the longitudinal short period discussed in the last section. The period of the Dutch roll mode remains unchanged, but the damping decreases with the addition of lift growth. Table 11 lists the value of the roots with lift growth calculated for two different values of aspect ratio and for a basic case without the lift growth function. For a particular Mach number the lift growth functions are sensitive to only planform details. Therefore, the sensitivity of the Dutch roll characteristics to aspect ratio is shown in the latter table.

6.3.2 Lateral-directional time histories. — This section presents some typical Dutch roll time histories for the Boeing 707-320B. Figures 40 and 41 show time histories of the Dutch roll motion for the 707-320B for the rigid and equivalent elastic airplane at M = 0.85 following a rudder pulse. A stable motion is shown for the rigid airplane; however, an unstable Dutch roll is predicted for the equivalent elastic airplane with the period increasing from 6 seconds for the rigid airplane to 8 seconds for the equivalent elastic airplane. Paragraph 8.2 lists the input data used to produce these motions. The unstable motion predicted in figs. 33, 40, and 41 does not reflect the true characteristics of the

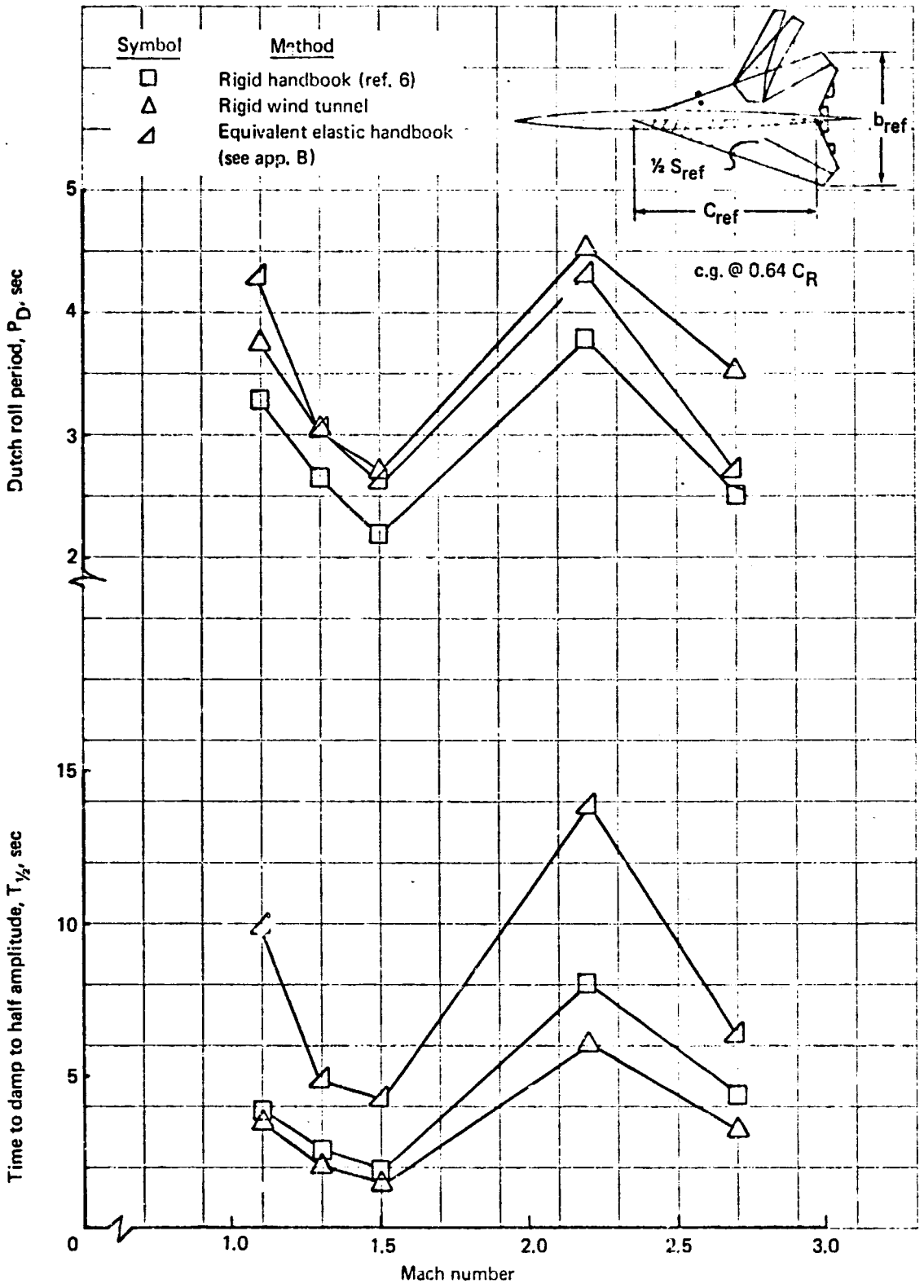

FIGURE 38. DUTCH ROLL PERIOD AND DAMPING, RIGID AND EQUIVALENT ELASTIC AIRPLANES -- 72° SST

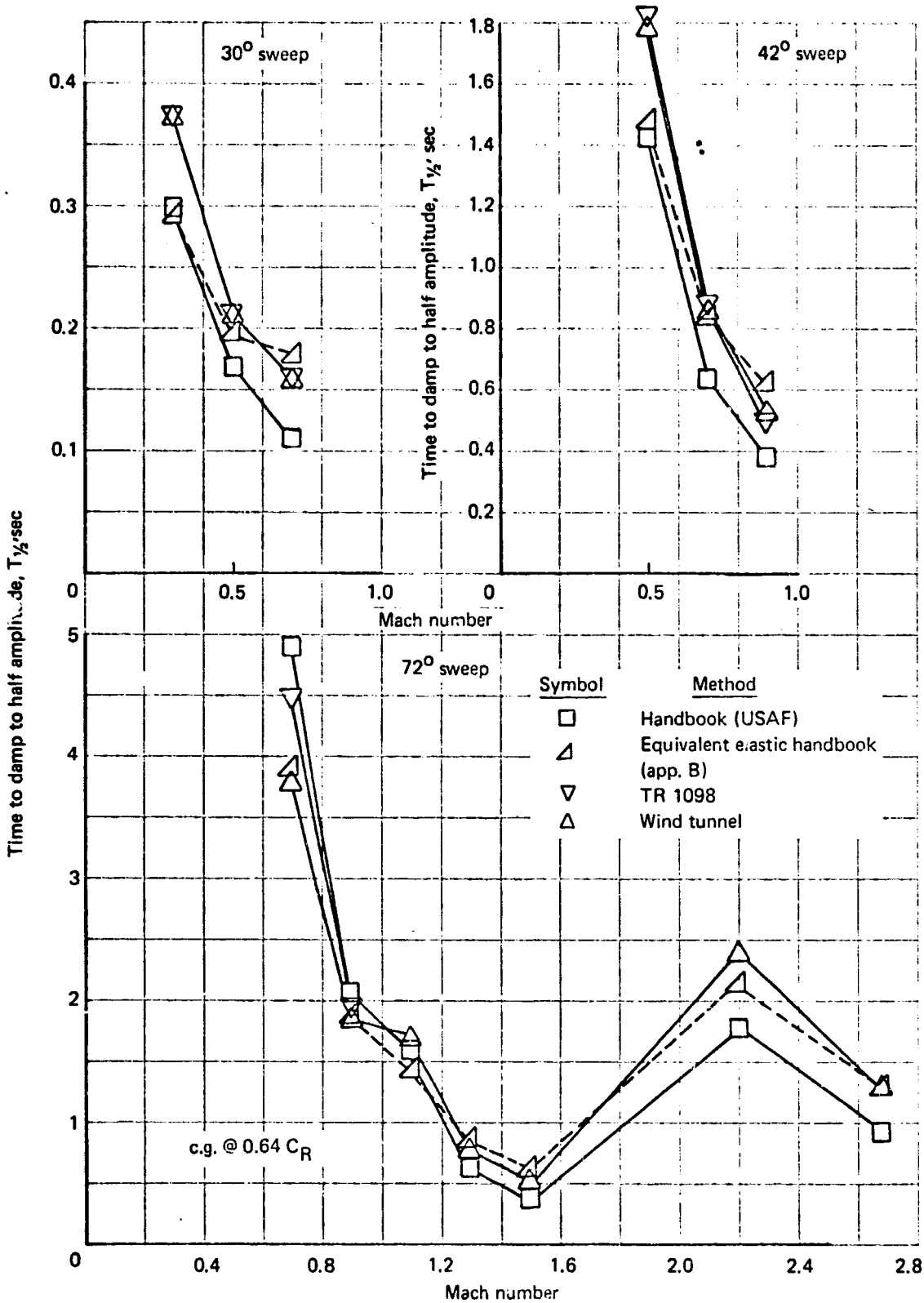

FIGURE 39. ROLLING CONVERGENCE MODE RIGID AND EQUIVALENT ELASTIC AIRPLANES – SST

TABLE 11. – DUTCH ROLL CHARACTERISTICS WITH LIFT GROWTH FOR TRUNCATED, COMPLETELY ELASTIC AIRPLANE, 17 MODES (14 ELASTIC MODES) – 707-320B

	Basic case without lift growth	Aspect ratio	
		3	6
σ_D	-0.0355	-0.031	-0.0281
ω_D rad/sec	1.26	1.26	1.264
ζ_D	0.028	0.025	0.022
ω_{n_D} rad/sec	0.201	0.201	0.201

M = 0.85, 35 000 ft (10 675 m)

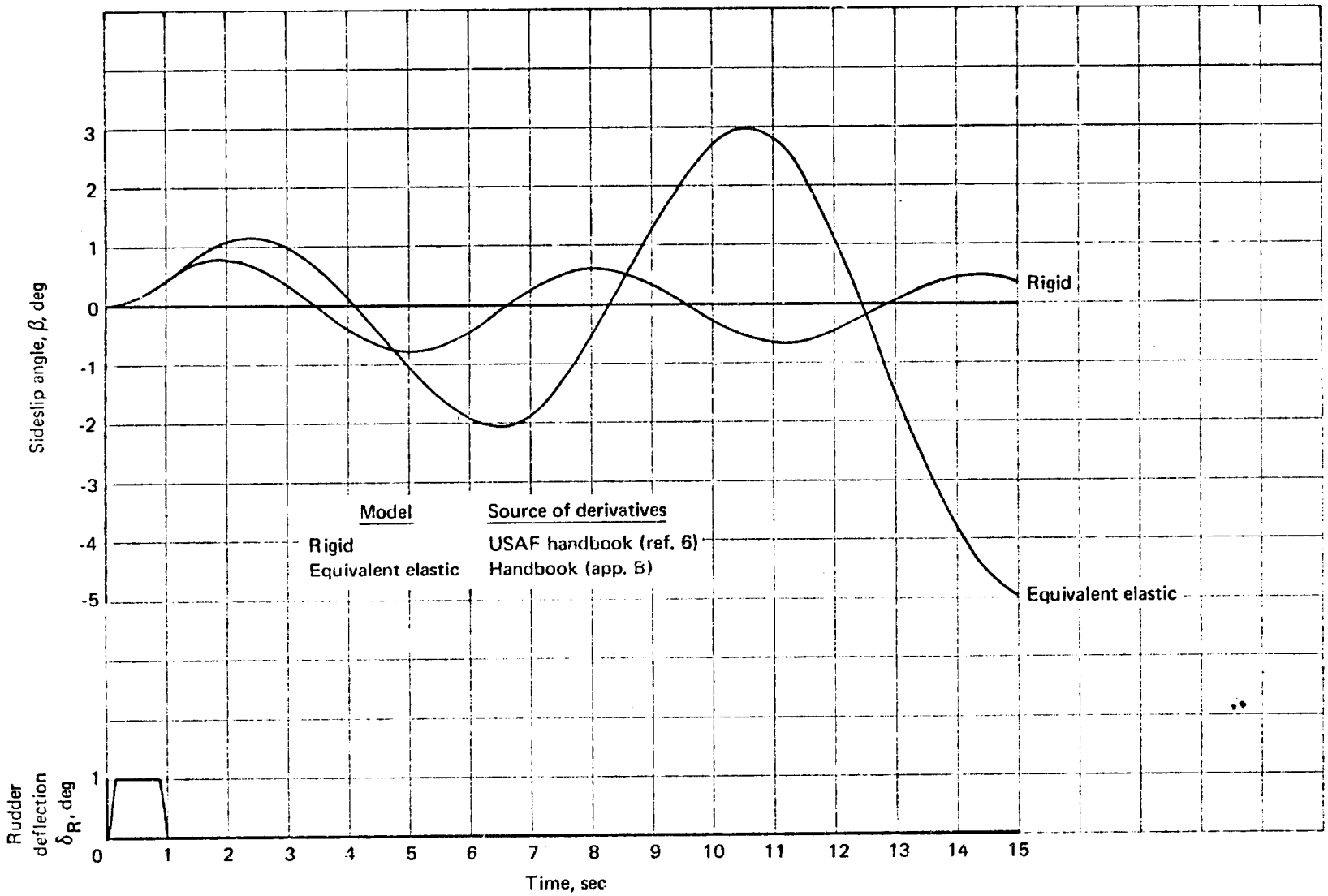

FIGURE 40. DUTCH ROLL MOTION, SIDE SLIP ANGLE RIGID AND EQUIVALENT ELASTIC AIRPLANES – 707-320B

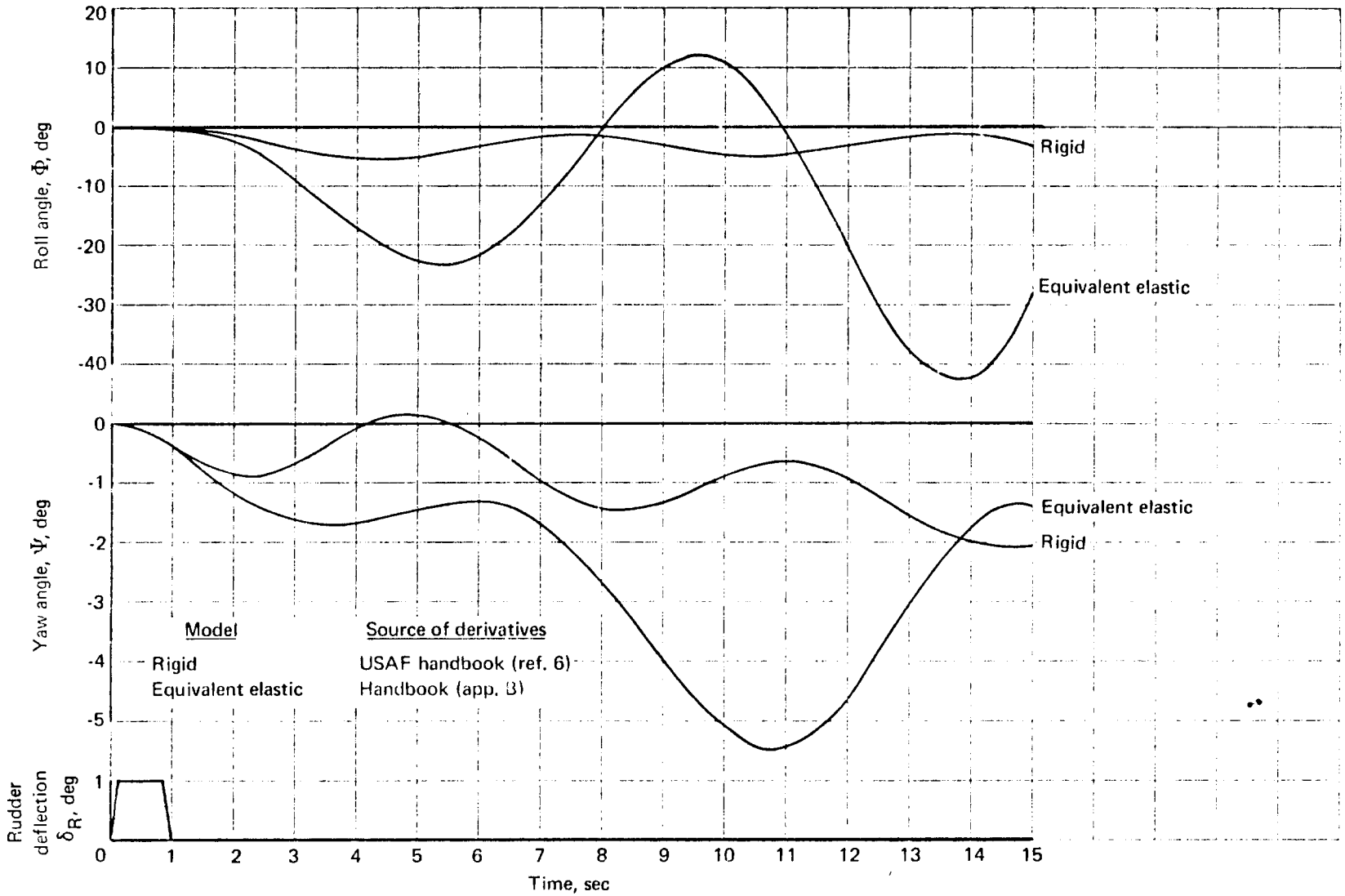

FIGURE 41. DUTCH ROLL MOTION, YAW AND ROLL ANGLES RIGID AND EQUIVALENT ELASTIC AIRPLANES – 707-320B

Boeing 707-320B, as can be seen by referring to par. 6.3.1. An analysis of flight test data as presented in fig. 33 shows the 707-320B to have a damping ratio of 2.0 percent of critical damping at M = 0.85 and at 35 000 ft (10 675m) (versus approximately 15 percent unstable damping predicted). The reasons for the poor correlation of the equivalent elastic airplane Dutch roll motion with flight test results were given in par. 6.3.1. Appendix B also discusses the method of calculating the equivalent elastic stability derivatives that were used.

Time histories of Ψ and Φ are shown in fig. 42 for the completely elastic analysis of the 707-320B. The results are not directly comparable to those of figs. 40 and 41 because wind tunnel values were used for the basic rigid stability derivatives in fig. 42 instead of the USAF Handbook values used in figs. 40 and 41. Figure 42 does, however, serve to illustrate the differences between three different mathematical models, one of which includes some elastic mode participation. All three cases predict a stable motion even though the equivalent elastic analysis, as illustrated by figs. 40 and 41, shows an unstable motion. The structural dynamic analysis then predicts essentially the same motion for the elastic airplane as for the rigid -- approximately the same frequencies and only slightly larger amplitudes. It appears as if a static elastic analysis would be sufficient for stability and control purposes for this case because the elastic mode participation in the Dutch roll motion is negligible. Figures 36 and 37 present the change of frequency and damping factor with the number of elastic modes included in the analysis.

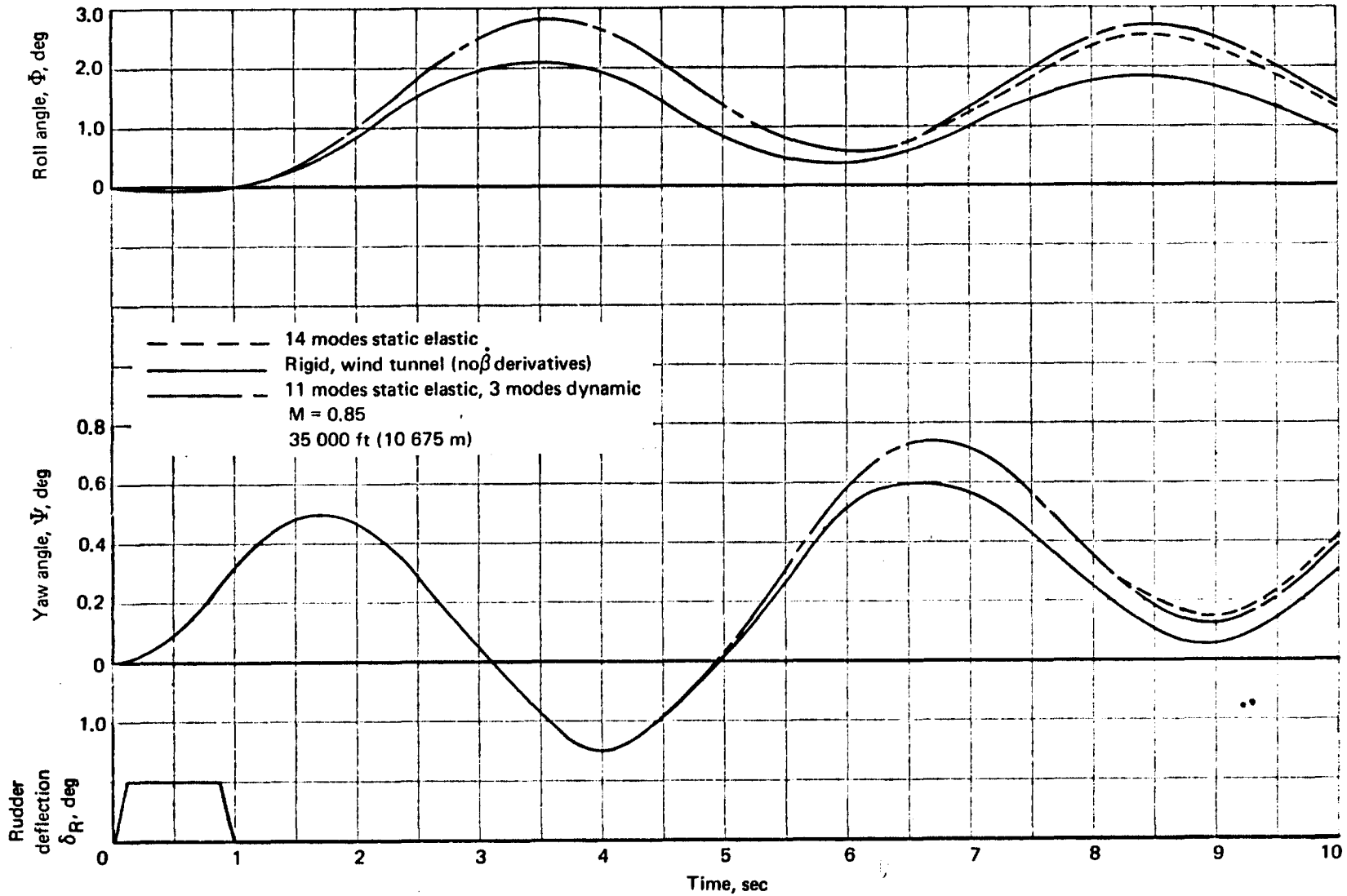

FIGURE 42. DUTCH ROLL MOTION, STRUCTURAL DYNAMIC ANALYSIS – 707-320B

7. PARAMETRIC STUDIES

7.1 Relative Importance of Rigid and Equivalent Elastic Derivatives

It is reasonable to observe the equivalent elastic mathematical model as a set of rigid airplane equations of motion with some rather sophisticated "derivatives" that account for static aeroelasticity. Similarity between the rigid and equivalent elastic equations of motion, therefore, allows the discussion of their significant terms to be considered together. In the discussion to follow the airplane may be considered to be either case with inertial elastic effects implicit in the derivatives for the equivalent elastic airplane.

It is necessary to vary derivatives and coefficients one at a time in the equations of motion to assess their influence on the resulting characteristics. However, it is obvious that this presents an isolated case in which all but one derivative (or coefficient) is fixed and the results are relative only to a given airplane and flight condition. The end results thus obtained are, therefore, configuration and mission oriented. However, it is possible to gain some insight into the significance of the derivatives in this manner. Some work has been done along those lines.

Etkin (ref. 4) has covered some of these aspects in his textbook. For example, he has shown stability boundaries based on relative values of C_{m_q} and C_{m_α} longitudinally, as well as C_{n_β} and C_{ℓ_β} in the lateral-directional case. Some other isolated special cases are also treated.

A much more extensive treatment has been presented in ref. 36. In addition to the discussion of the approximate transfer functions and root expressions already mentioned in par. 5.2, ref. 36 contains a study showing the changes in longitudinal and lateral-directional characteristics due to variations in the derivatives. The derivatives considered are:

Longitudinal derivatives and coefficient:

$$C_{D_u},\ C_{L_u},\ C_{m_u},\ C_{D_\alpha},\ C_{L_\alpha},\ C_{m_\alpha},\ C_{L_{\dot\alpha}},\ C_{m_q},\ C_{L_q},\ C_{D_q}$$

Lateral-directional derivatives:

$$C_{Y_\beta},\ C_{l_\beta},\ C_{n_\beta},\ C_{Y_p},\ C_{l_p},\ C_{n_p},\ C_{Y_r},\ C_{l_r},\ C_{n_r}$$

Variations in frequency and damping for complex roots and root values for real roots are presented in detail. Also, there are discussions concerning the affecting phenomena and the physical significance of the derivatives in relation to airplane motions. Derivatives missing from the lists are $C_{D_{\dot{q}}}$, $C_{D_{\dot{\alpha}}}$, $C_{L_{\dot{\alpha}}}$, $C_{m_{\dot{\alpha}}}$, $C_{y_{\dot{\beta}}}$, $C_{\ell_{\dot{\beta}}}$, and $C_{n_{\dot{\beta}}}$. All of these except $C_{D_{\dot{q}}}$ and $C_{D_{\dot{\alpha}}}$ are treated parametrically as part of this study. Basic sets of data for the study airplanes were modified to reflect zero, basic, and double the individual derivative values. This was not done for $C_{D_{\dot{q}}}$ because there is no provision for it in the current small perturbation program. The six-degree-of-freedom rigid airplane time history program could have been used, but it would have proven costly in computer and engineering time considering the level of confidence in the values. There is no known technique for generating $C_{D_{\dot{\alpha}}}$.

The detailed data for changes in the stability characteristics due to variations in the $\dot{\alpha}$ and $\dot{\beta}$ derivatives are presented in par. 8.6. The general results are tabulated qualitatively in tables 12 and 13.

The 707-320B study airplane appears to be quite sensitive in the short period mode to $C_{m_{\dot{\alpha}}}$, as illustrated in fig. 43. It is observed that the values of $C_{m_{\dot{\alpha}}}$ as tabulated in par. 8.2 are much higher than what would seem realistic. However, this does not negate the sensitivity of the configuration to the derivative. The phugoid mode was not significantly affected. For the SST, only the damping of the 72° wing sweep configuration was affected. This is illustrated in figs. 44 and 45, where the damping for the three sweep conditions is shown.

Special cases for comparison with the completely elastic airplane were generated at other than $0.25\bar{c}$ and $0.64\ C_R$ moment reference points for the 707-320B and SST. These can be utilized to illustrate the effects of c.g. location on the stability characteristics. The detailed data are presented in par. 8.6. Changes in frequency and damping due to moment reference point c.g. variation for the 707-320B study airplane are shown in fig. 46. The damping shows no change, but the frequency changes considerably. This is due to the long coupled tail (damping), the small c.g. shift, and the significance of the wing in contributing to C_{m_α}, thus changing the frequency. The SST (figs. 47 and 48) has a short coupled tail and large c.g. shift, and the 30° and 42° sweep data reflect this in the large change in damping and not-so-large

TABLE 12. – QUALITATIVE ASSESSMENT OF $\dot{\alpha}$ DERIVATIVES ON LONGITUDINAL DYNAMICS

Derivative effects		$C_{D_{\dot{\alpha}}}$	$C_{L_{\dot{\alpha}}}$	$C_{m_{\dot{\alpha}}}$		
707-320B (lifting surface derivatives)						
Short period:	frequency	No data available	Very small effect	Significant effect		
	damping		Very small effect	Significant effect		
Phugoid:	frequency		No effect	No effect		
	damping		No effect	Very small effect		
SST (lifting surface derivatives)						
				Sweep		
				30°	42°	72°
Short period:	frequency	No data available	No effect	Small effect	Small effect	Small effect
	damping			Very small effect	Very small effect	Significant effect
Phugoid:	frequency			Small effect[a]	Small effect[a]	No effect supersonic
	damping			Small effect[a]	Small effect[a]	No effect supersonic

a. Real roots

TABLE 13. – QUALITATIVE ASSESSMENT OF $\dot{\beta}$ DERIVATIVES ON LATERAL-DIRECTIONAL DYNAMICS

Derivative effects		$C_{y_{\dot{\beta}}}$	$C_{\ell_{\dot{\beta}}}$	$C_{n_{\dot{\beta}}}$	
707-320B (TR 1098 derivatives)					
Dutch roll:	frequency	No effect	No effect	No effect	
	damping	↓	↓	Small effect	
Rolling convergence $1/T_r$				No effect	
Spiral mode $1/T_s$				No effect	
SST (TR 1098 derivatives)					
				Sweep	
				30°	42°
Dutch roll:	frequency	No effect	No effect	No effect	No effect
	damping	↓	↓	Small effect	Very small effect
Rolling convergence $1/T_r$				No effect	No effect
Spiral mode $1/T_s$				No effect	No effect

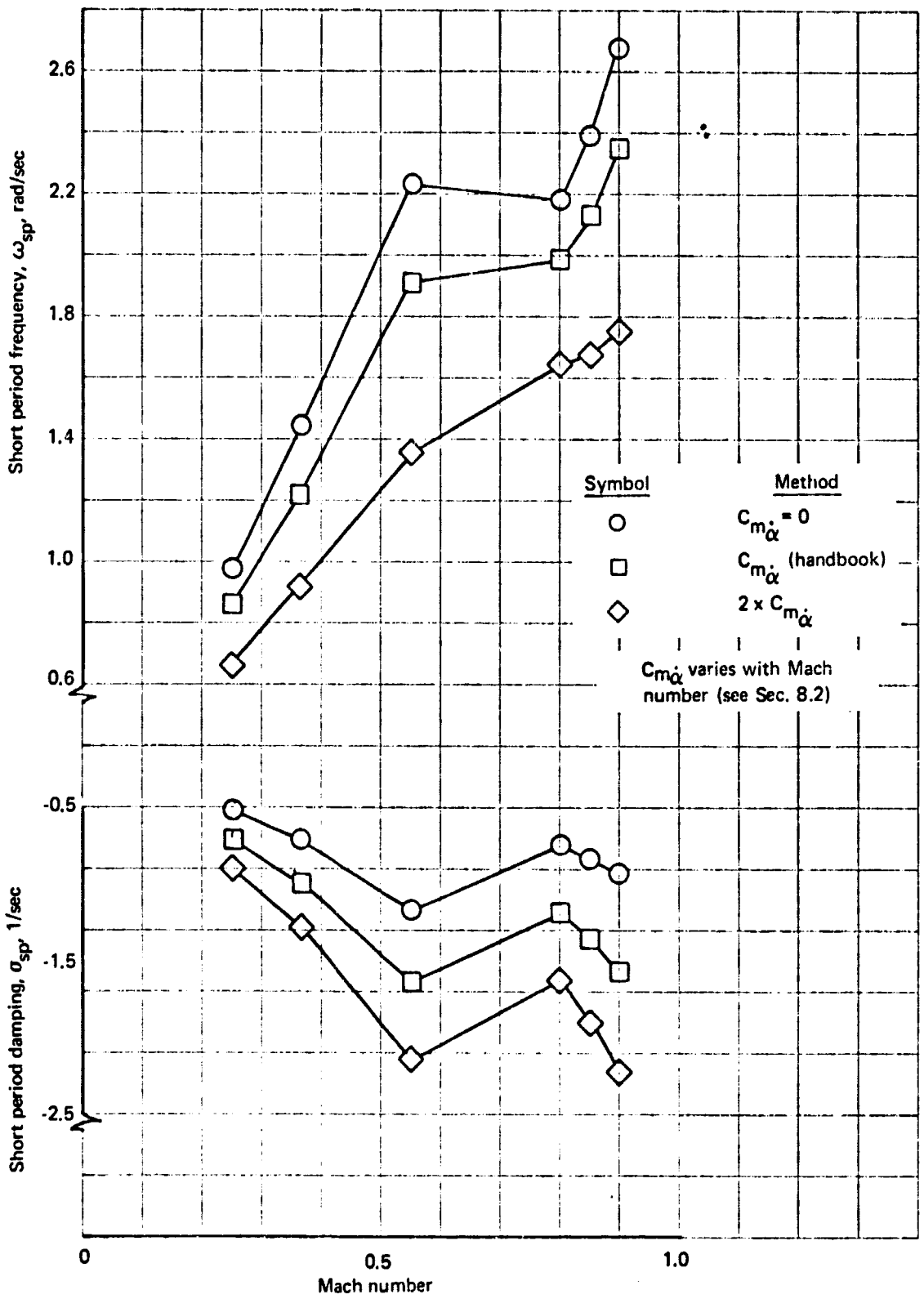

FIGURE 43. CHANGES IN SHORT PERIOD MODE CHARACTERISTICS DUE TO VARIATION IN $C_{m_{\dot{\alpha}}}$ – 707-320B

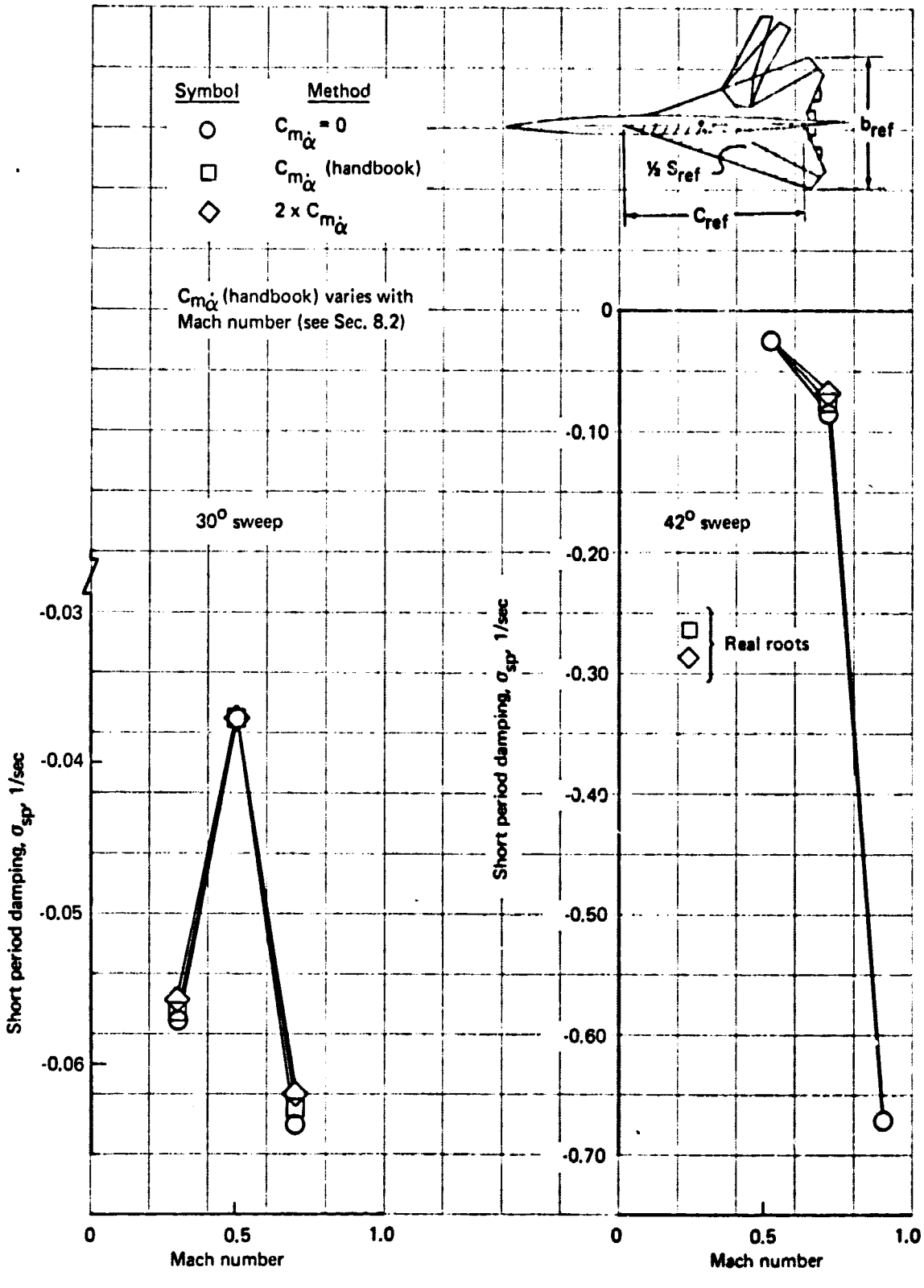

FIGURE 44. CHANGES IN SHORT PERIOD DAMPING DUE TO VARIATIONS IN $C_{m_{\dot{\alpha}}}$ - 30° AND 42° SST

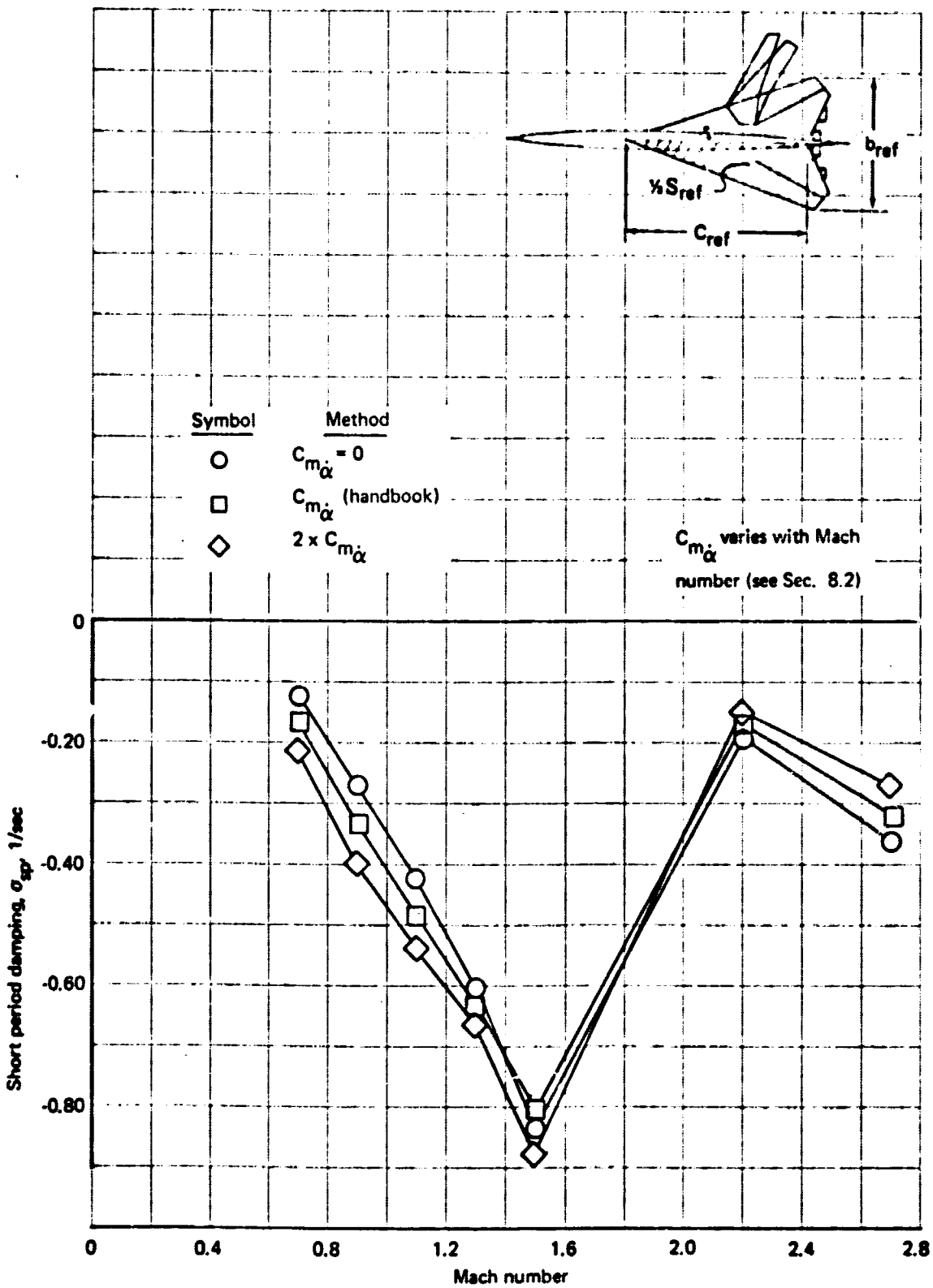

FIGURE 45. CHANGES IN SHORT PERIOD DAMPING DUE TO VARIATIONS IN $C_{m_{\dot{\alpha}}}$ – 72° SST

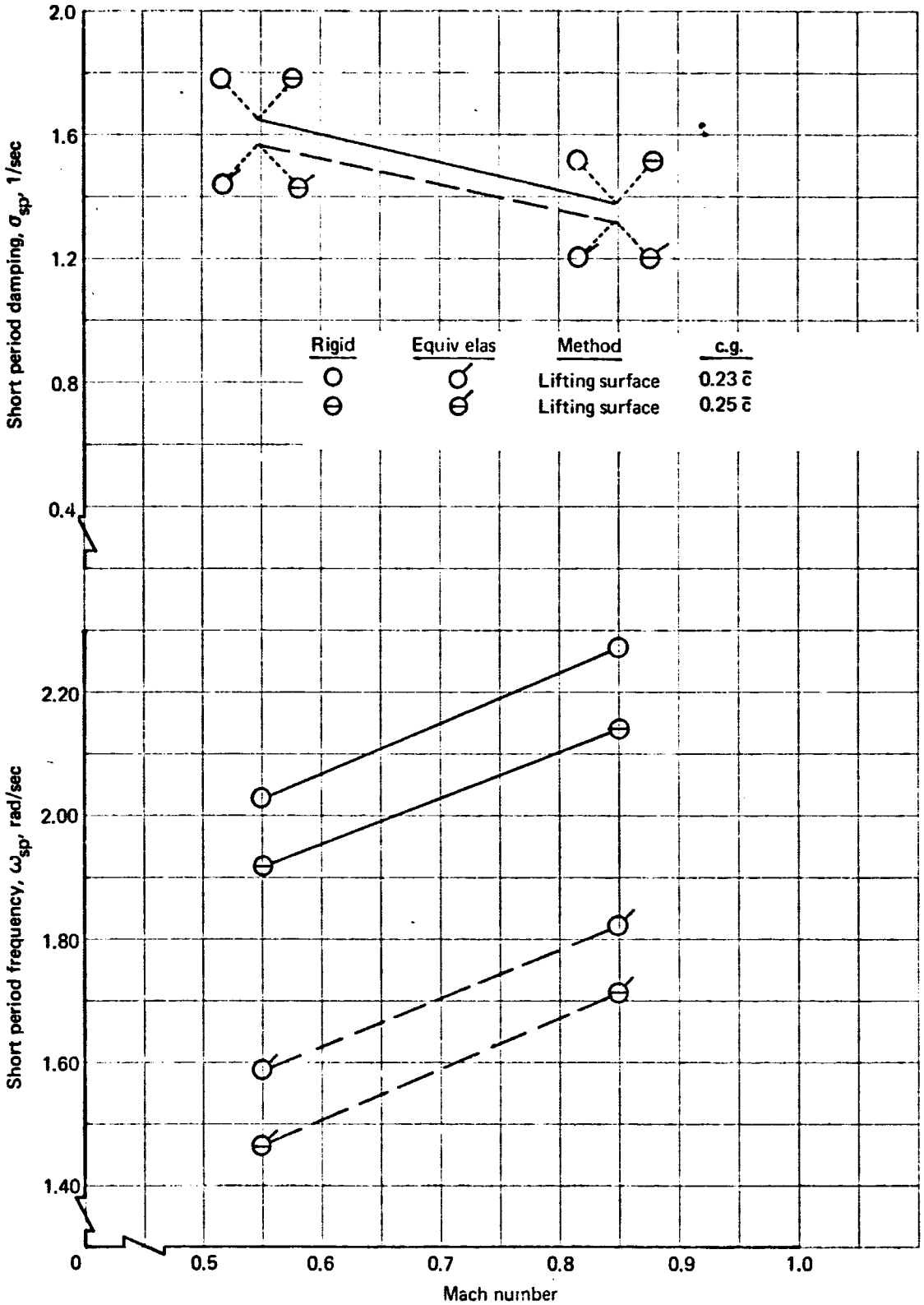

FIGURE 46. CHANGES IN SHORT PERIOD MODE DUE TO CENTER-OF-GRAVITY SHIFTS – 707-320B

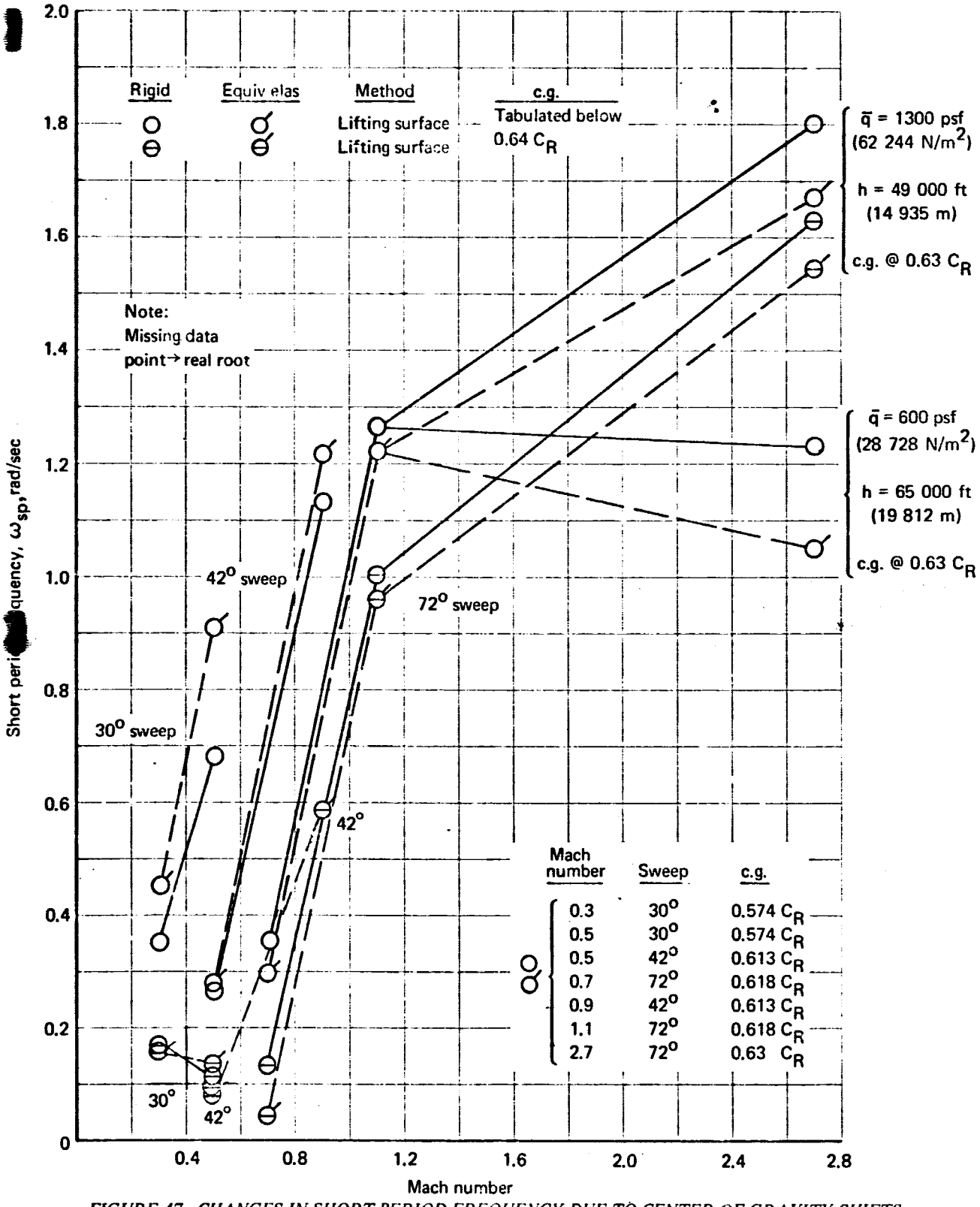

FIGURE 47. CHANGES IN SHORT PERIOD FREQUENCY DUE TO CENTER-OF-GRAVITY SHIFTS AND DYNAMIC PRESSURE – SST

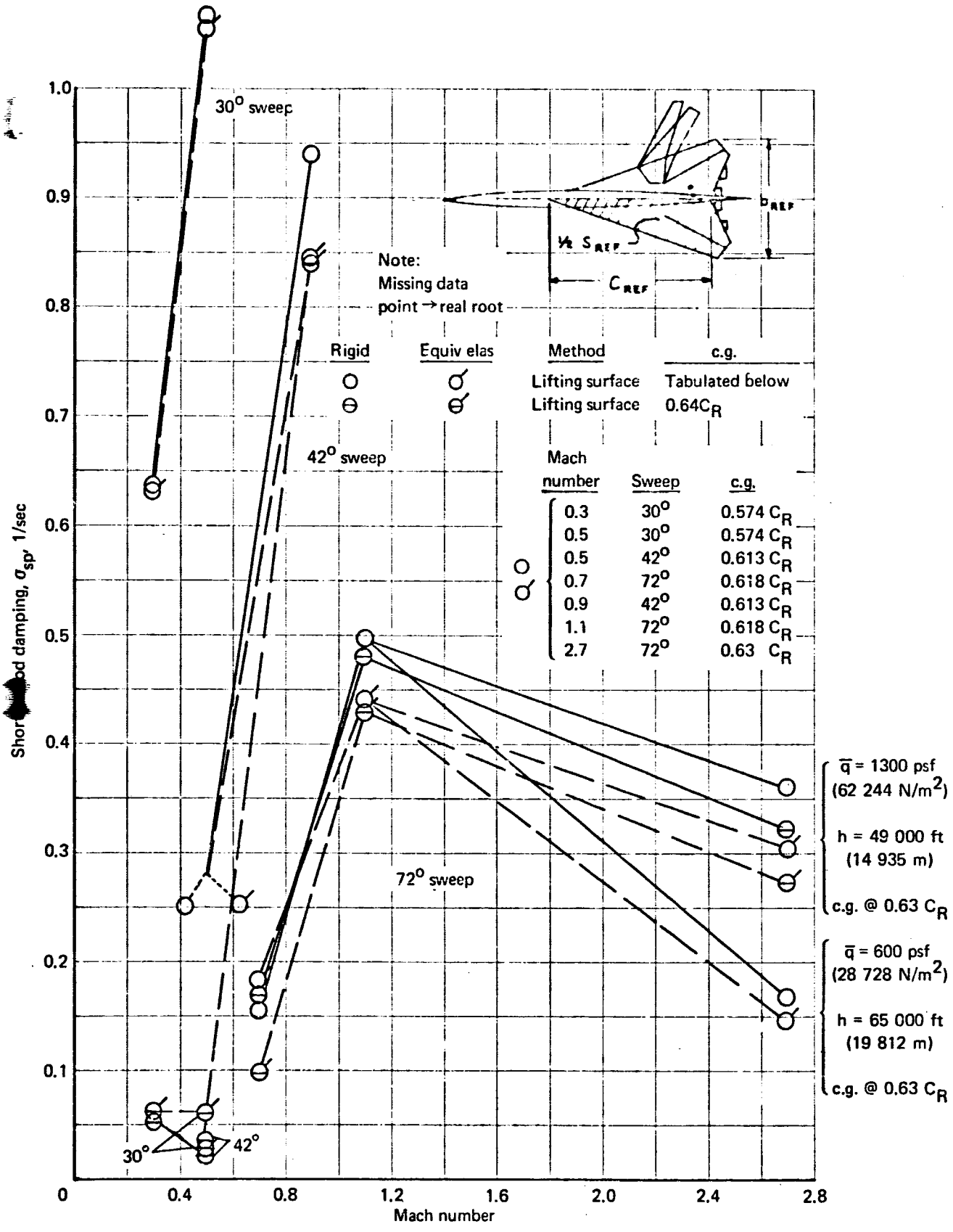

FIGURE 48. – CHANGES IN SHORT PERIOD DAMPING DUE TO CENTER-OF-GRAVITY SHIFTS AND DYNAMIC PRESSURE–SST

(in percentage) change in frequency. For the 72° sweep data none of the changes are so pronounced. Note in figs. 46, 47, and 48 that the incremental changes due to elastic considerations are relatively insensitive to changes in c.g. location for these cases.

It should be evident that the data presented here point toward uniqueness affected by configuration with regard to the influence of various parameters on stability characteristics. In this respect, general statements regarding similar configurations may be made. Extrapolating or interpolating to treat new configurations could generate misleading results.

7.2 Importance of Various Elastic Effects for Completely Elastic Airplane Mathematical Models

Some of the effects of adding elastic degrees of freedom have been illustrated in the data presented in Sec. 6. The changes in longitudinal frequency and damping due to adding elastic degrees of freedom were shown in figs. 17 through 20, 23, and 24. As was mentioned in Sec. 6, for the type of analysis used on the 707-320B it is much easier to attach physical significance to the elastic effects that change the stability characteristics. This is not true for the analysis done on the SST. Differences in these techniques are discussed in detail in Sec. 9.

A detailed analysis of approximate transfer functions and characteristics of completely elastic airplane longitudinal mathematical models has been accomplished in the literature. The reader is directed to ref. 39 for a detailed discussion of approximate transfer functions for elastic airplanes. However, the reader is also cautioned against using similar simplifications for too few elastic modes. It should be recalled that in par. 6.2 the trend for both the 707-320B and SST at all three sweeps was toward pronounced changes when the first few low-frequency elastic modes were added and then an apparent convergence on some value as more and more elastic modes were included. These "few mode" trends could be misleading in approximate techniques. Considerations of the influence of the number of elastic modes with and without residual flexibility were also discussed in ref. 5. Some of the conclusions drawn in the study are quoted below:

"2. An accurate approximation for the aeroelastic behavior of a structure may be made in terms of its normal coordinates by including some of its modes explicitly and the 'residual flexibility' approximation to all higher modes. The modes explicitly included should be all those in the frequency range from zero to the maximum frequency of interest plus the next higher mode.

3. The inclusion of the residual flexibility in the representation suggested in "2" is very important. Although the magnitude of the 'residual flexibility' decreases as the number of modes explicitly included in the representation increases, it is inadvisable to attempt to supplant the 'residual flexibility' by additional modes. In the examples considered here better accuracy was obtained at frequencies below the first elastic mode by including one mode explicitly plus residual flexibility than was obtained by including five modes explicitly and no residual flexibility.

4. An except to the rule of "2" occurs in the case of 'mode interaction', which may be defined as a condition of potential or incipient aeroelastic instability involving one elastic mode and one rigid body mode. This condition, as observed in the example of configuration 4 of this report, will require further investigation before conclusive statements can be made concerning adequate structural representation.

5. All configurations studied showed that aeroelasticity can have very large effects on the response of a system even at frequencies well below the first elastic mode."

Also in ref. 5 is a treatment of variations in levels of flexibility. Variations are shown for the transfer function response levels for values of 0.7, 0.5, 0.3, 0.2, 0.1, and 0 (rigid airplane) times the basic flexibility. For the delta wing configuration treated therein, the effects were significant. The difference between rigid and rigid-with-many-elastic-modes for the airplanes in this study (shown in the previous section) indicates the elastic effects are not so large.

The studies contained in refs. 5 and 39 should be viewed as guides to how to approach analyses. Most airplanes will present unique problems and answers with regard to the effects of elasticity, i.e., the completely elastic airplane mathematical model does not lend itself to generalized statements regarding individual effects or handbook-type methods.

Similar studies have not been accomplished for lateral-directional cases.

8.0 SUPPORTING DATA AND RELATED MATERIAL

8.1 Introduction

This section presents detailed input and output data and other supporting material. Some of the static and dynamic characteristics presented and discussed in the other sections are included here also. All the data for the rigid and equivalent elastic airplanes appear in this section, although there is no discussion of the results.

8.2 Rigid and Equivalent Elastic Stability Derivatives, Coefficients, and Inertial Properties

8.2.1 General considerations. — Paragraph 8.2 presents tables of the data (derivatives, coefficients, etc.) used to calculate the static and dynamic stability characteristics presented in Secs. 4 and 6. These data are separated into two groups. Paragraph 8.2.2 presents the data used in the general comparisons of rigid and equivalent elastic airplane characteristics. They represent an accumulation of the data presented in app. B. Paragraph 8.2.3 presents those data used in the special comparisons which included the completely elastic airplane mathematical model.

All the input data of pars. 8.2.2 and 8.2.3 are tabulated in the English system (lb feet sec). The conversion factors for the data into the metric system are:

1 foot = 0.305 meters

1 lb = 4.448 newtons

1 psf = 47.880 newtons/meter^2

1 slug ft^2 = 1.357 kg meter^2

1 slug = 14.594 kg

8.2.2 Data tabulations - rigid and equivalent elastic derivatives and coefficients - general comparison data. — The data presented in this section have been extracted from those used to generate the derivative comparisons in app. B. They are presented as a set of tables (16 through 19), preceded by a list (table 14) of the various conditions and the number of the table in which they are located. Table 15 is an example data table.

TABLE 14. – LIST OF TABLES OF DERIVATIVES AND COEFFICIENTS USED IN GENERAL COMPARISONS

Altitude, ft	Dynamic pressure, $\bar{q}$, psf	Mach number	Weight, lb	Table number	Wing leading edge sweep
a. Longitudinal data 707-320B					
10 000	66.7	0.255	268 000	16a	
↓	136.0	0.365	↓	16b	
	306.0	0.548		16c	
35 000	223.0	0.800		16d	
↓	251.0	0.850		16e	
	283.0	0.900		16f	
SST					
8 500	98	0.300	370 000	17a	30°
9 500	260	0.500	↓	17b	↓
11 000	470	0.700		17c	
32 500	98	0.500	675 000	17d	42°
26 000	260	0.700	↓	17e	↓
23 500	470	0.900		17f	
47 500	98	0.700	668 000	17g	72°
37 000	260	0.900	↓	17h	↓
33 000	470	1.100		17i	
30 000	750	1.300	520 000	17j	
24 000	1300	1.500	↓	17k	
60 500	500	2.200		17l	
49 000	1300	2.700		17m	
b. Lateral directional data 707-320B					
10 000	66.7	0.255	268 000	18a	
↓	136.0	0.365	↓	18b	
	306.0	0.548		18c	
35 000	223.0	0.800		18d	
↓	251.0	0.850		18e	
	283.0	0.900		18f	

TABLE 14. – LIST OF TABLES OF DERIVATIVES AND COEFFICIENTS USED IN GENERAL COMPARISONS (CONCLUDED)

b. Lateral directional data (Continued)
SST

Altitude, ft	Dynamic pressure, $\bar{q}$, psf	Mach number	Weight, lb	Table number	Wing leading edge sweep
8 500	98	0.300	370 000	19a	30°
9 500	260	0.500	↓	19b	↓
11 000	470	0.700	↓	19c	↓
32 500	98	0.500	675 000	19d	42°
26 000	260	0.700	↓	19e	↓
23 500	470	0.900	↓	19f	↓
47 500	98	0.700	668 000	19g	72°
37 000	260	0.900	↓	19h	↓
33 000	470	1.100	↓	19i	↓
30 000	750	1.300	520 000	19j	↓
24 000	1300	1.500	↓	19k	↓
60 500	500	2.200	↓	19l	↓
49 000	1300	2.700	↓	19m	↓

TABLE 15. – EXAMPLE DATA TABLE

Altitude, h, ft	00 000	Velocity, V_{c_1}, ft/sec ...	000.00
Gross weight, W, lb	000 000	Drag, C_{D_1}	0.0000
Mach number, M	0.0	Lift, C_{L_1}	0.0000
Dynamic pressure, $\bar{q}$, psf	000	Iyy, rigid, slug-ft^2	00.0x00^0
Density ratio .. 0.00000	C.G. 0.00C_R	Iyy, equiv elas, slug-ft^2	00.000x00^0

Derivatives	Methods				
	Rigid			Equivalent elastic [a]	
	Lifting surface ○ (TA-67A)	Handbook methods □	Wind tunnel ◇ data	Lifting surface △ (TA-67A)	Handbook methods ▽
C_{L_O}	0.00000			0.00000	Not Available
C_{m_o}	0.0000			0.0000	
C_{L_α}, deg^{-1}	0.0000	0.0000	0.0000	0.0000	
C_{m_α}, deg^{-1}	-0.00000	-0.0000	-0.0000	-0.00000	
C_{D_α}, deg^{-1}	0.0000	0.0000	0.0000	0.00000	
$C_{L_{\dot\alpha}}$, rad^{-1}	□	-0.00	□	□	
$C_{m_{\dot\alpha}}$, rad^{-1}	□	-0.00	□	□	
$C_{D_{\dot\alpha}}$, rad^{-1}					
C_{L_q}, rad^{-1}	0.00	0.000	○	0.000	
C_{m_q}, rad^{-1}	-0.00	-0.000	○		
C_{D_q}, rad^{-1}					
C_{L_u}, rad^{-1}					
C_{m_u}, rad^{-1}					

Not available

Indicates $C_{L_{\dot\alpha}}$ and $C_{m_{\dot\alpha}}$ not calculated using lifting surface method; data from handbook methods used, i.e. $C_{L_{\dot\alpha}(\text{lifting surface})} = C_{L_{\dot\alpha}(\text{handbook})}$.

TABLE 16a. – 707-320B LONGITUDINAL DERIVATIVES AND COEFFICIENTS USED IN GENERAL COMPARISONS

Altitude, h, ft	10 000	Velocity, V_{c_1}, ft/sec ...	274.74
Gross weight, W, lb	268 000	Drag, C_{D_1}	0.111
Mach number, M	0.255	Lift, C_{L_1}	1.3895
Dynamic pressure, $\bar{q}$, psf	66.7	Iyy, rigid, slug-ft^2	5.025×10^6
Density ratio	0.73859 c.g.@ 0.25$\bar{c}$	Iyy, equiv elas, slug-ft^2	4.887×10^6

Derivatives	Methods				
	Rigid			Equivalent elastic [a]	
	Lifting surface ○ (TA 37A)	Handbook methods [c] □	Wind tunnel ◇ data	Lifting surface △ (TA 67A)	Handbook methods ▽
C_{L_O}	0.2085	○	○	0.1914	△
C_{m_o}	-0.083	○	○	-0.0116	△
C_{L_α}, deg^{-1}	0.089	0.088	0.0865	0.0861	0.084
C_{m_α}, deg^{-1}	-0.0208	-0.0312	-0.0188	-0.0189	-0.0188
C_{D_α}, deg^{-1}	0.0475	0.01175 [b]	○	0.0425	△
$C_{L_{\dot\alpha}}$, rad^{-1}	□	4.15	□	□	□
$C_{m_{\dot\alpha}}$, rad^{-1}	□	-10.95	□	□	□
$C_{D_{\dot\alpha}}$, rad^{-1}					
C_{L_q}, rad^{-1}	9.85	8.53	○	9.10	4.89
C_{m_q}, rad^{-1}	-16.5	-16.2	○	-15.66	-12.2
C_{D_q}, rad^{-1}	0.135	○	○	○	○
C_{L_u}, rad^{-1}	0.058	0.094	○	0.04781	△
C_{m_u}, rad^{-1}	-0.071	○	○	-0.01530	△
C_{D_u}, rad^{-1}	0.00169	○	○	○	○
$C_{L_{\ddot\theta_I}}$, (rad/sec^2)$^{-1}$				-0.0369	△
$C_{m_{\ddot\theta_I}}$, (rad/sec^2)$^{-1}$				0.0316	△
$C_{L_{\delta_E}}$, deg^{-1}	0.0070	0.0065	○	0.0065	△
$C_{m_{\delta_E}}$, deg^{-1}	-0.0195	-0.0191	○	-0.0181	△
$C_{L_{i_H}}$, deg^{-1}	□	0.0133	□	▽	0.00836
$C_{m_{i_H}}$, deg^{-1}	□	-0.0388	□	▽	-0.0243

a. Formulation II b. Reference 4 c. Reference 6

TABLE 16b. – 707-320B LONGITUDINAL DERIVATIVES AND COEFFICIENTS USED IN GENERAL COMPARISONS (CONTINUED)

Altitude, h, ft	10 000	Velocity, V_{c_1}, ft/sec ...	393.25
Gross weight, W, lb	268 000	Drag, C_{D_1}	0.0352
Mach number, M	0.365	Lift, C_{L_1}	0.6815
Dynamic pressure, $\bar{q}$, psf	136	Iyy, rigid, slug-ft^2	5.025×10^6
Density ratio	0.73859 c.g.@ 0.25 $\bar{c}$	Iyy, equiv elas, slug-ft^2	4.762×10^6

Derivatives	Methods				
	Rigid			Equivalent elastic [a]	
	Lifting surface ○ (TA 67A)	Handbook methods [c] □	Wind tunnel ◇ data	Lifting surface △ (TA 67A)	Handbook methods ▽
C_{L_O}	0.2118	○	○	0.1767	△
C_{m_o}	-0.085	○	○	-0.0092	△
C_{L_α}, deg^{-1}	0.090	0.094	0.087	0.0832	0.0825
C_{m_α}, deg^{-1}	-0.0212	-0.0313	-0.0191	-0.0174	-0.0179
C_{D_α}, deg^{-1}	0.0211	0.0058 [b]	○	0.0165	△
$C_{L_{\dot{\alpha}}}$, rad^{-1}	□	3.99	□	□	□
$C_{m_{\dot{\alpha}}}$, rad^{-1}	□	-11.49	□	□	□
$C_{D_{\dot{\alpha}}}$, rad^{-1}					
C_{L_q}, rad^{-1}	9.7	7.2	○	8.61	4.51
C_{m_q}, rad^{-1}	-16.8	-16.45		-15.10	-11.50
C_{D_q}, rad^{-1}	0.137	○	○	○	○
C_{L_u}, rad^{-1}	0.068	0.1055 [b]	○	0.04836	△
C_{m_u}, rad^{-1}	-0.055	○	○	-0.01658	△
C_{D_u}, rad^{-1}	0.00065	○	○	○	○
$C_{L_{\ddot{\theta}_I}}$, (rad/sec^2)$^{-1}$				-0.0338	△
$C_{m_{\ddot{\theta}_I}}$, (rad/sec^2)$^{-1}$				0.0295	△
$C_{L_{\delta_E}}$, deg^{-1}	0.0071	0.0065	○	0.00623	△
$C_{m_{\delta_E}}$, deg^{-1}	-0.0199	-0.0191	○	-0.0172	△
$C_{L_{i_H}}$, deg^{-1}	□	0.0135	□	▽	0.00823
$C_{m_{i_H}}$, deg^{-1}	□	-0.0393	□	▽	-0.0239

a. Formulation II b. Reference 4 c. Reference 6

TABLE 16c. – 707-320B LONGITUDINAL DERIVATIVES AND COEFFICIENTS USED IN GENERAL COMPARISONS (CONTINUED)

Altitude, h, ft 10 000		Velocity, V_{c_1}, ft/sec ... 590.42	
Gross weight, W, lb 268 000		Drag, C_{D_1} 0.0145	
Mach number, M 0.548		Lift, C_{L_1} 0.3028	
Dynamic pressure, $\bar{q}$, psf 306		Iyy, rigid, slug-ft^2	5.025×10^6
Density ratio ..... 0.73859 c.g.@ $0.25\bar{c}$		Iyy, equiv elas, slug-ft^2	4.497×10^6

Derivatives	Methods				
	Rigid			Equivalent elastic [a]	
	Lifting surface ○ (TA 67A)	Handbook methods [c] □	Wind tunnel ◇ data	Lifting surface △ (TA 67A)	Handbook methods ▽
C_{L_O}	0.2275	○	○	0.1548	△
C_{m_o}	-0.091	○	○	-0.0029	△
C_{L_α}, deg^{-1}	0.096	0.098	0.0875	0.08063	0.0806
C_{m_α}, deg^{-1}	-0.02325	-0.0325	-0.0205	-0.0145	-0.0163
C_{D_α}, deg^{-1}	0.005	0.0049[b]	0.0035	0.0042	△
$C_{L_{\dot{\alpha}}}$, rad^{-1}	□	2.99	□	□	□
$C_{m_{\dot{\alpha}}}$, rad^{-1}	□	-13.24	□	□	□
$C_{D_{\dot{\alpha}}}$, rad^{-1}					
C_{L_q}, rad^{-1}	11.1	7.9	○	7.64	4.35
C_{m_q}, rad^{-1}	-17.7	-16.95	○	-14.05	-10.4
C_{D_q}, rad^{-1}	0.144	○	○	○	○
C_{L_u}, rad^{-1}	0.109	0.130[b]	0.100	0.04658	△
C_{m_u}, rad^{-1}	-0.071	◇	-0.061	-0.01644	△
C_{D_u}, rad^{-1}	0.000375	◇	0.00025	◇	◇
$C_{L_{\ddot{\theta}_I}}$, (rad/sec^2)$^{-1}$				-0.0281	△
$C_{m_{\ddot{\theta}_I}}$, (rad/sec^2)$^{-1}$				0.0263	△
$C_{L_{\delta_E}}$, deg^{-1}	0.00745	0.0068	○	0.0055	△
$C_{m_{\delta_E}}$, deg^{-1}	-0.02125	-0.01998	○	-0.0151	△
$C_{L_{i_H}}$, deg^{-1}	□	0.0140	□	▽	0.00789
$C_{m_{i_H}}$, deg^{-1}	□	-0.0407	□	▽	-0.0228

a. Formulation II b. Reference 4 c. Reference 6

TABLE 16d. – 707-320B LONGITUDINAL DERIVATIVES AND COEFFICIENTS USED IN GENERAL COMPARISONS (CONTINUED)

Altitude, h, ft	35 000	Velocity, V_{c_1}, ft/sec ...	778.51
Gross weight, W, lb	268 000	Drag, C_{D_1}	0.0210
Mach number, M	0.8	Lift, C_{L_1}	0.4164
Dynamic pressure, $\bar{q}$, psf	223	Iyy, rigid, slug-ft^2	5.025×10^6
Density ratio	0.31058 c.g.@ $0.25\bar{c}$	Iyy, equiv elas, slug-ft^2	4.549×10^6

Derivatives	Methods				
	Rigid			Equivalent elastic [a]	
	Lifting surface ○ (TA 67A)	Handbook methods [c] □	Wind tunnel ◇ data	Lifting surface △ (TA 67A)	Handbook methods ▽
C_{L_O}	0.2677	○	○	0.1884	△
C_{m_o}	-0.100	○	○	-0.0222	△
C_{L_α}, deg^{-1}	0.110	0.1065	0.105	0.09327	0.0933
C_{m_α}, deg^{-1}	-0.0291	-0.0361	-0.0243	-0.01967	-0.0203
C_{D_α}, deg^{-1}	0.009	0.00425 [b]	0.00975	0.0065	△
$C_{L_{\dot{\alpha}}}$, rad^{-1}	□	-1.35	□	□	□
$C_{m_{\dot{\alpha}}}$, rad^{-1}	□	-21.00	□	□	□
$C_{D_{\dot{\alpha}}}$, rad^{-1}					
C_{L_q}, rad^{-1}	13.9	10.3	○	9.96	5.12
C_{m_q}, rad^{-1}	-20.1	-17.8		-16.52	-12.25
C_{D_q}, rad^{-1}	0.162	○	○	○	○
C_{L_u}, rad^{-1}	0.239	◇	0.241	0.208	△
C_{m_u}, rad^{-1}	-0.196	◇	-0.208	-0.0780	△
C_{D_u}, rad^{-1}	0.0020	◇	0.0026	◇	◇
$C_{L_{\ddot{\theta}_I}}$, (rad/sec^2)$^{-1}$				-0.0340	△
$C_{m_{\ddot{\theta}_I}}$, (rad/sec^2)$^{-1}$				0.0326	△
$C_{L_{\delta_E}}$, deg^{-1}	0.00844	0.00698	○	0.00645	△
$C_{m_{\delta_E}}$, deg^{-1}	-0.0251	-0.0204	○	-0.0186	△
$C_{L_{i_H}}$, deg^{-1}	□	0.0144	□	▽	0.00907
$C_{m_{i_H}}$, deg^{-1}	□	-0.0419	□	▽	-0.0263

a. Formulation II b. Reference 4 c. Reference 6

TABLE 16c. – 707-320B LONGITUDINAL DERIVATIVES AND COEFFICIENTS USED IN GENERAL COMPARISONS (CONTINUED)

Altitude, h, ft	35 000	Velocity, V_{c_1}, ft/sec ...	827.17
Gross weight, W, lb	268 000	Drag, C_{D_1}	0.02305
Mach number, M	0.85	Lift, C_{L_1}	0.3691
Dynamic pressure, $\bar{q}$, psf	251	Iyy, rigid, slug-ft^2	5.025×10^6
Density ratio	0.31058 c.g. @ $0.25\bar{c}$	Iyy, equiv elas, slug-ft^2	4.488×10^6

Derivatives	Methods				
	Rigid			Equivalent elastic [a]	
	Lifting surface ○ (TA 67A)	Handbook methods [c] □	Wind tunnel ◇ data	Lifting surface △ (TA 67A)	Handbook methods ▽
C_{L_O}	0.2825	○	○	0.1885	△
C_{m_o}	-0.104	○	○	-0.0257	△
C_{L_α}, deg^{-1}	0.115	0.111	0.1095	0.09505	0.0950
C_{m_α}, deg^{-1}	-0.0309	-0.0376	-0.02675	-0.01992	-0.0212
C_{D_α}, deg^{-1}	0.0074	0.0070 [b]	0.0085	0.0045	△
$C_{L_{\dot{\alpha}}}$, rad^{-1}	□	-3.86	□	□	□
$C_{m_{\dot{\alpha}}}$, rad^{-1}	□	-24.20	□	□	□
$C_{D_{\dot{\alpha}}}$, rad^{-1}					
C_{L_q}, rad^{-1}	14.9	11.45	○	8.92	5.85
C_{m_q}, rad^{-1}	-20.95	-18.1	○	-16.69	-12.3
C_{D_q}, rad^{-1}	0.166	○	○	○	○
C_{L_u}, rad^{-1}	0.2705	◇	0.280	0.2295	△
C_{m_u}, rad^{-1}	-0.238	◇	-0.204	-0.08712	△
C_{D_u}, rad^{-1}	0.00191	◇	0.00356	◇	◇
$C_{L_{\ddot{\theta}_I}}$, (rad/sec^2)$^{-1}$				-0.0334	
$C_{m_{\ddot{\theta}_I}}$, (rad/sec^2)$^{-1}$				0.0327	△
$C_{L_{\delta_E}}$, deg^{-1}	0.00872	0.0073	○	0.00630	△
$C_{m_{\delta_E}}$, deg^{-1}	-0.0265	-0.0213	○	-0.0185	△
$C_{L_{i_H}}$, deg^{-1}	□	0.0146	□	▽	0.00918
$C_{m_{i_H}}$, deg^{-1}	□	-0.0425	□	▽	-0.0267

a. Formulation II b. Reference 4 c. Reference 6

TABLE 16f. – 707-320B LONGITUDINAL DERIVATIVES AND COEFFICIENTS USED IN GENERAL COMPARISONS (CONCLUDED)

Altitude, h, ft	35 000	Velocity, V_{c_1}, ft/sec ...	875.83
Gross weight, W, lb	268 000	Drag, C_{D_1}	0.0378
Mach number, M	0.9	Lift, C_{L_1}	0.3274
Dynamic pressure, $\bar{q}$, psf	283	Iyy, rigid, slug-ft^2	5.025×10^6
Density ratio	0.31058 c.g.@ 0.25$\bar{c}$	Iyy, equiv elas, slug-ft^2	4.414×10^6

Derivatives	Methods				
	Rigid			Equivalent elastic [a]	
	Lifting surface ○ (TA 67A)	Handbook methods [c] □	Wind tunnel ◇ data	Lifting surface △ (TA 67A)	Handbook methods ▽
C_{L_O}	0.3011	○	○	0.1891	△
C_{m_o}	-0.113	○	○	-0.0421	△
C_{L_α}, deg^{-1}	0.121	0.0755	0.095	0.09733	0.0973
C_{m_α}, deg^{-1}	-0.034	-0.020	-0.0267	-0.02089	-0.0221
C_{D_α}, deg^{-1}	0.0050	0.00975 [b]	0.0090	0.0037	△
$C_{L_{\dot\alpha}}$, rad^{-1}	□	-13.74	□	□	□
$C_{m_{\dot\alpha}}$, rad^{-1}	□	-27.10	□	□	□
$C_{D_{\dot\alpha}}$, rad^{-1}					
C_{L_q}, rad^{-1}	16.1	8.55	○	8.73	5.62
C_{m_q}, rad^{-1}	-22.2	-18.0	○	-17.01	-12.5
C_{D_q}, rad^{-1}	0.173	○	○	○	○
C_{L_u}, rad^{-1}	0.315	◇	0.307	0.26325	△
C_{m_u}, rad^{-1}	-0.305	◇	-0.198	-0.10125	△
C_{D_u}, rad^{-1}	0.00185	◇	0.00306	◇	◇
$C_{L_{\ddot\theta_I}}$, (rad/sec^2)$^{-1}$				-0.0325	△
$C_{m_{\ddot\theta_I}}$, (rad/sec^2)$^{-1}$				0.0329	△
$C_{L_{\delta_E}}$, deg^{-1}	0.00919	0.0070	○	0.00618	△
$C_{m_{\delta_E}}$, deg^{-1}	-0.0287	-0.0204	○	-0.0184	△
$C_{L_{i_H}}$, deg^{-1}	□	0.0145	□	▽	0.00939
$C_{m_{i_H}}$, deg^{-1}	□	-0.0422	□	▽	-0.0273

a. Formulation II b. Reference 4 c. Reference 6

TABLE 17a. – SST LONGITUDINAL DERIVATIVES AND COEFFICIENTS USED IN GENERAL COMPARISONS

Leading edge sweep = 30°

Altitude, h, ft	8 500	Velocity, V_{c_1}, ft/sec	325.01
Gross weight, W, lb	370 000	Drag, C_{D_1}	0.098
Mach number, M	0.3	Lift, C_{L_1}	0.4198
Dynamic pressure, $\bar{q}$, psf	98	Iyy, rigid, slug-ft^2	40.2×10^6
Density ratio	0.77408 cg @ 0.64C_R	Iyy, equiv elas, slug-ft^2	39.88×10^6

Derivatives	Methods				
	Rigid			Equivalent elastic [a]	
	Lifting surface ○ (TA 37A)	Handbook methods [c] □	Wind tunnel ◇ data	Lifting surface △ (TA 37A)	Handbook methods ▽
C_{L_0}	0.15761	○	○	0.21240	△
C_{m_0}	0.0105	○	○	0.0088	△
C_{L_α}, deg^{-1}	0.0564	0.0638	0.0532	0.0559	0.0526
C_{m_α}, deg^{-1}	0.00238	-0.00135	0.0003	0.00192	0.00129
C_{D_α}, deg^{-1}	0.0098	◇	0.0058	0.01107	△
$C_{L_{\dot\alpha}}$, rad^{-1}	□	0.203	□	□	□
$C_{m_{\dot\alpha}}$, rad^{-1}	□	-0.0898	□	□	□
$C_{D_{\dot\alpha}}$, rad^{-1}					
C_{L_q}, rad^{-1}	1.275	0.748	○	1.218	0.988
C_{m_q}, rad^{-1}	-0.280	-0.167	○	-0.276	-0.195
C_{D_q}, rad^{-1}					△
C_{L_u}, rad^{-1}	0.0288	0.0426 [b]	0.038	0.0193	△
C_{m_u}, rad^{-1}	0.00166	◇	-0.001	0.0009	△
C_{D_u}, rad^{-1}	0.0033	◇	0.0033	◇	◇
$C_{L_{\ddot\theta_I}}$, (rad/sec^2)$^{-1}$				-0.0657	△
$C_{m_{\ddot\theta_I}}$, (rad/sec^2)$^{-1}$				0.0023	△
$C_{L_{\delta_E}}$, deg^{-1}	0.00705	○	○	○	○
$C_{m_{\delta_E}}$, deg^{-1}	-0.00148	○	○	○	○
$C_{L_{i_H}}$, deg^{-1}	□	0.02205	□	▽	0.0159
$C_{m_{i_H}}$, deg^{-1}	□	-0.0191	□	▽	-0.00492

a. Formulation I b. Reference 4 c. Reference 6

TABLE 17b. – SST LONGITUDINAL DERIVATIVES AND COEFFICIENTS USED IN GENERAL COMPARISONS (CONTINUED)

Leading edge sweep = 30°

Altitude, h, ft	9 500	Velocity, V_{c_1}, ft/sec ...	539.69
Gross weight, W, lb	370 000	Drag, C_{D_1}	0.032
Mach number, M	0.5	Lift, C_{L_1}	0.1581
Dynamic pressure, $\bar{q}$, psf	260	Iyy, rigid, slug-ft^2	40.2×10^6
Density ratio	0.75032 cg @ 0.64C_R	Iyy, equiv elas, slug-ft^2	39.201×10^6

Derivatives	Methods				
	Rigid			Equivalent elastic [a]	
	Lifting surface ○ (TA 67A)	Handbook methods [c] □	Wind tunnel ◇ data	Lifting surface △ (TA 67A)	Handbook methods ▽
C_{L_O}	0.16888	○	○	0.20396	△
C_{m_o}	0.0120	○	○	0.0074	△
C_{L_α}, deg^{-1}	0.0587	0.0646	0.0582	0.0570	0.0526
C_{m_α}, deg^{-1}	0.00206	-0.00145	-0.00165	0.00133	0.00057
C_{D_α}, deg^{-1}	0.0102	◇	0.00645	0.00204	△
$C_{L_{\dot\alpha}}$, rad^{-1}	□	0.150	□	□	□
$C_{m_{\dot\alpha}}$, rad^{-1}	□	-0.160	□	□	□
$C_{D_{\dot\alpha}}$, rad^{-1}					
C_{L_q}, rad^{-1}	1.340	0.805	○	1.151	0.949
C_{m_q}, rad^{-1}	-0.290	-0.169	○	-0.287	-0.209
C_{D_q}, rad^{-1}					
C_{L_u}, rad^{-1}	0.0315	0.054 [b]	0.049	0.0233	△
C_{m_u}, rad^{-1}	0.0001	◇	-0.0047	-0.00285	△
C_{D_u}, rad^{-1}	0.0047	◇	0.00715	◇	◇
$C_{L_{\ddot\theta_I}}$, (rad/sec^2)$^{-1}$				-0.0592	△
$C_{m_{\ddot\theta_I}}$, (rad/sec^2)$^{-1}$				0.0017	△
$C_{L_{\delta_E}}$, deg^{-1}	0.0073	○	○	○	○
$C_{m_{\delta_E}}$, deg^{-1}	-0.00161	○	○	○	○
$C_{L_{i_H}}$, deg^{-1}	□	0.0228	□	▽	0.01635
$C_{m_{i_H}}$, deg^{-1}	□	-0.01978	□	▽	-0.00583

a. Formulation I b. Reference 4 c. Reference 6

TABLE 17c. – SST LONGITUDINAL DERIVATIVES AND COEFFICIENTS USED IN GENERAL COMPARISONS (CONTINUED)

Leading edge sweep = 30°

Altitude, h, ft	11 000	Velocity, V_{c_1}, ft/sec ...	751.39
Gross weight, W, lb	370 000	Drag, C_{D_1}	0.018
Mach number, M	0.7	Lift, C_{L_1}	0.0375
Dynamic pressure, $\bar{q}$, psf	470	Iyy, rigid, slug-ft^2	40.2×10^6
Density ratio	0.71568 cg @ 0.64C_R	Iyy, equiv elas, slug-ft^2	39.331×10^6

Derivatives	Methods				
	Rigid			Equivalent elastic [a]	
	Lifting surface ○ (TA 67A)	Handbook methods [c] □	Wind tunnel ◇ data	Lifting surface △ (TA 67A)	Handbook methods ▽
C_{L_O}	0.18239	○	○	0.19414	△
C_{m_o}	0.0135	○	○	0.0039	△
C_{L_α}, deg^{-1}	0.0632	0.0652	0.0632	0.0587	0.0536
C_{m_α}, deg^{-1}	0.00158	-0.00198	-0.00375	0.00040	-0.00039
C_{D_α}, deg^{-1}	0.0110	◇	0.00715	-0.00028	△
$C_{L_{\dot\alpha}}$, rad^{-1}	□	-0.214	□	□	□
$C_{m_{\dot\alpha}}$, rad^{-1}	□	-0.262	□	□	□
$C_{D_{\dot\alpha}}$, rad^{-1}					
C_{L_q}, rad^{-1}	1.440	0.897	○	1.062	0.912
C_{m_q}, rad^{-1}	-0.31	-0.172	○	-0.306	-0.224
C_{D_q}, rad^{-1}					
C_{L_u}, rad^{-1}	0.0392	0.0856 [b]	0.063	0.0246	△
C_{m_u}, rad^{-1}	-0.0037	◇	-0.0098	-0.00399	△
C_{D_u}, rad^{-1}	0.0118	◇	0.0118	◇	◇
$C_{L_{\ddot\theta_I}}$, (rad/sec^2)$^{-1}$				-0.0523	△
$C_{m_{\ddot\theta_I}}$, (rad/sec^2)$^{-1}$				0.0013	△
$C_{L_{\delta_E}}$, deg^{-1}	0.0078	○	○	○	○
$C_{m_{\delta_E}}$, deg^{-1}	-0.00185	○	○	○	○
$C_{L_{i_H}}$, deg^{-1}	□	0.0237	□	▽	0.01704
$C_{m_{i_H}}$, deg^{-1}	□	-0.02055	□	▽	-0.00687

a. Formulation I b. Reference 4 c. Reference 6

TABLE 17d. – SST LONGITUDINAL DERIVATIVES AND COEFFICIENTS USED IN GENERAL COMPARISONS (CONTINUED)

Leading edge sweep = 42°

Altitude, h, ft	32 500	Velocity, V_{c_1}, ft/sec ...	492.02
Gross weight, W, lb	675 000	Drag, C_{D_1}	0.057
Mach number, M	0.5	Lift, C_{L_1}	0.7659
Dynamic pressure, $\bar{q}$, psf	98	Iyy, rigid, slug-ft^2	47.2×10^6
Density ratio	0.35455 cg @ 0.64C_R	Iyy, equiv elas, slug-ft^2	47.437×10^6

Derivatives	Methods				
	Rigid			Equivalent elastic [a]	
	Lifting surface ○ (TA 67A)	Handbook methods [c] □	Wind tunnel ◇ data	Lifting surface △ (TA 67A)	Handbook methods ▽
C_{L_O}	0.11181	○	○	0.12110	△
C_{m_o}	0.0109	○	○	0.0100	△
C_{L_α}, deg^{-1}	0.0511	0.056	0.0500	0.0498	0.0470
C_{m_α}, deg^{-1}	0.00082	-0.00258	-0.00005	0.00071	0.00036
C_{D_α}, deg^{-1}	0.0089	0.0191	0.00859	0.0237	△
$C_{L_{\dot\alpha}}$, rad^{-1}	□	0.155	□	□	□
$C_{m_{\dot\alpha}}$, rad^{-1}	□	-0.1084	□	□	□
$C_{D_{\dot\alpha}}$, rad^{-1}					
C_{L_q}, rad^{-1}	1.37	0.932	○	1.267	1.021
C_{m_q}, rad^{-1}	-0.32	-0.236	○	-0.309	-0.204
C_{D_q}, rad^{-1}					
C_{L_u}, rad^{-1}	0.0748	0.254 [b]	0.03525	0.0738	△
C_{m_u}, rad^{-1}	-0.0015	◇	-0.00215	-0.002	△
C_{D_u}, rad^{-1}	0.011	◇	0.005	◇	◇
$C_{L_{\ddot\Theta_I}}$, (rad/sec^2)$^{-1}$				-0.0433	△
$C_{m_{\ddot\Theta_I}}$, (rad/sec^2)$^{-1}$				-0.0017	△
$C_{L_{\delta_E}}$, deg^{-1}	0.0072	◇	0.0064	◇	◇
$C_{m_{\delta_E}}$, deg^{-1}	-0.00165	◇	-0.00180	◇	◇
$C_{L_{i_H}}$, deg^{-1}	□	0.0218	□	▽	0.01647
$C_{m_{i_H}}$, deg^{-1}	□	-0.01845	□	▽	-0.00491

a. Formulation I b. Reference 4 c. Reference 6

TABLE 17e. – SST LONGITUDINAL DERIVATIVES AND COEFFICIENTS USED IN GENERAL COMPARISONS (CONTINUED)

Leading edge sweep = 42°

Altitude, h, ft	26 000	Velocity, V_{c_1}, ft/sec ...	708.32
Gross weight, W, lb	675 000	Drag, C_{D_1}	0.0186
Mach number, M	0.7	Lift, C_{L_1}	0.2884
Dynamic pressure, $\bar{q}$, psf	260	Iyy, rigid, slug-ft^2	47.2×10^6
Density ratio .....0.43300 cg @ 0.64C_R		Iyy, equiv elas, slug-ft^2	47.792×10^6

Derivatives	Methods				
	Rigid			Equivalent elastic [a]	
	Lifting surface ○ (TA 67A)	Handbook methods [c] □	Wind tunnel ◇ data	Lifting surface △ (TA 67A)	Handbook methods ▽
C_{L_O}	0.12010	○	○	0.11833	△
C_{m_o}	0.0124	○	○	0.0101	△
C_{L_α}, deg^{-1}	0.0541	0.0572	0.0527	0.0501	0.0475
C_{m_α}, deg^{-1}	0.00033	-0.00340	-0.00022	0.00014	-0.00013
C_{D_α}, deg^{-1}	0.0094	0.0035	0.0146	0.00719	△
$C_{L_{\dot\alpha}}$, rad^{-1}	□	0.0	□	□	□
$C_{m_{\dot\alpha}}$, rad^{-1}	□	-0.200	□	□	□
$C_{D_{\dot\alpha}}$, rad^{-1}					
C_{L_q}, rad^{-1}	1.46	1.040	○	1.187	1.001
C_{m_q}, rad^{-1}	-0.35	-0.245	○	-0.331	-0.230
C_{D_q}, rad^{-1}					
C_{L_u}, rad^{-1}	0.0904	0.274 [b]	0.083	0.0557	△
C_{m_u}, rad^{-1}	-0.0091	◇	-0.0087	-0.0082	△
C_{D_u}, rad^{-1}	0.0111	◇	0.0071	◇	◇
$C_{L_{\ddot\Theta_I}}$, (rad/sec^2)$^{-1}$				-0.0392	△
$C_{m_{\ddot\Theta_I}}$, (rad/sec^2)$^{-1}$				-0.0016	△
$C_{L_{\delta_E}}$, deg^{-1}	0.0077	◇	0.00685	◇	◇
$C_{m_{\delta_E}}$, deg^{-1}	-0.00190	◇	-0.00204	◇	◇
$C_{L_{i_H}}$, deg^{-1}	□	0.02245	□	▽	0.01736
$C_{m_{i_H}}$, deg^{-1}	□	-0.0190	□	▽	-0.00573

a. Formulation I b. Reference 4 c. Reference 6

TABLE 17f. – SST LONGITUDINAL DERIVATIVES AND COEFFICIENTS USED IN GENERAL COMPARISONS (CONTINUED)

Leading edge sweep = 42°

Altitude, h, ft 23 500	Velocity, V_{c_1}, ft/sec ... 920.15
Gross weight, W, lb 675 000	Drag, C_{D_1} 0.014
Mach number, M 0.9	Lift, C_{L_1} 0.1596
Dynamic pressure, $\bar{q}$, psf 470	Iyy, rigid, slug-ft^2 ..... 47.2×10^6
Density ratio .....0.47285 cg @ 0.64C_R	Iyy, equiv elas, slug-ft^2 48.136×10^6

Derivatives	Methods				
	Rigid			Equivalent elastic [a]	
	Lifting surface ○ (TA 67A)	Handbook methods [c] □	Wind tunnel ◇ data	Lifting surface △ (TA 67A)	Handbook methods ▽
C_{L_O}	0.13745	○	○	0.11635	△
C_{m_o}	0.0139	○	○	0.0097	△
C_{L_α}, deg^{-1}	0.0602	0.0581	0.0579	0.0506	0.0495
C_{m_α}, deg^{-1}	-0.0005	-0.00435	-0.00098	-0.00093	-0.00096
C_{D_α}, deg^{-1}	0.0105	0.0065	0.0147	0.00276	△
$C_{L_{\dot\alpha}}$, rad^{-1}	□	-0.771	□	□	□
$C_{m_{\dot\alpha}}$, rad^{-1}	□	-0.480	□	□	□
$C_{D_{\dot\alpha}}$, rad^{-1}					
C_{L_q}, rad^{-1}	1.61	1.174	○	1.074	1.002
C_{m_q}, rad^{-1}	-0.42	-0.258	○	-0.366	-0.250
C_{D_q}, rad^{-1}					
C_{L_u}, rad^{-1}	0.1187	0.669 [b]	0.148	0.0538	△
C_{m_u}, rad^{-1}	-0.0178	◇	-0.0167	-0.0162	△
C_{D_u}, rad^{-1}	0.0117	◇	0.0117	◇	◇
$C_{L_{\ddot\theta_I}}$, (rad/sec^2)$^{-1}$				-0.0351	△
$C_{m_{\ddot\theta_I}}$, (rad/sec^2)$^{-1}$				-0.0014	△
$C_{L_{\delta_E}}$, deg^{-1}	0.00875	◇	0.0068	◇	◇
$C_{m_{\delta_E}}$, deg^{-1}	-0.00251	◇	-0.00222	◇	◇
$C_{L_{i_H}}$, deg^{-1}	□	0.0203	□	▽	0.01868
$C_{m_{i_H}}$, deg^{-1}	□	-0.0195	□	▽	-0.00679

a. Formulation I b. Reference 4 c. Reference 6

TABLE 17g. – SST LONGITUDINAL DERIVATIVES AND COEFFICIENTS USED IN GENERAL COMPARISONS (CONTINUED)

Leading edge sweep = 72°

Altitude, h, ft 47 500	Velocity, V_{c_1}, ft/sec ... 677.66
Gross weight, W, lb 668 000	Drag, C_{D_1} 0.11
Mach number, M 0.7	Lift, C_{L_1} 0.7580
Dynamic pressure, $\bar{q}$, psf 98	Iyy, rigid, slug-ft^2 ..... 48.3×10^6
Density ratio .....0.17261 eg @ 0.64C_R	Iyy, equiv elas, slug-ft^2 48.398×10^6

Derivatives	Methods				
	Rigid			Equivalent elastic [a]	
	Lifting surface ○ (TA 67A)	Handbook methods [c] □	Wind tunnel ◇ data	Lifting surface △ (TA 67A)	Handbook methods ▽
C_{L_O}	0.01542	○	○	0.02108	Not Available
C_{m_o}	0.0082	○	○	0.0081	
C_{L_α}, deg^{-1}	0.0306	0.0278	0.0303	0.0306	
C_{m_α}, deg^{-1}	-0.00018	-0.0014	-0.00025	0.00011	
C_{D_α}, deg^{-1}	0.0053	0.0031	0.00975	0.0262	
$C_{L_{\dot\alpha}}$, rad^{-1}	□	-0.32	□	□	
$C_{m_{\dot\alpha}}$, rad^{-1}	□	-0.262	□	□	
$C_{D_{\dot\alpha}}$, rad^{-1}					
C_{L_q}, rad^{-1}	1.17	0.410	○	1.122	
C_{m_q}, rad^{-1}	-0.33	-0.150	○	-0.327	
C_{D_q}, rad^{-1}					
C_{L_u}, rad^{-1}	0.089	0.731 [b]	0.107	0.0934	
C_{m_u}, rad^{-1}	0.0182	◇	0.0129	-0.0248	
C_{D_u}, rad^{-1}	0.0011	○	○	○	
$C_{L_{\ddot\theta_I}}$, (rad/sec^2)$^{-1}$				-0.0319	
$C_{m_{\ddot\theta_I}}$, (rad/sec^2)$^{-1}$				-0.0007	
$C_{L_{\delta_E}}$, deg^{-1}	0.0076	◇	0.00725	◇	
$C_{m_{\delta_E}}$, deg^{-1}	-0.0021	◇	-0.00258	◇	
$C_{L_{i_H}}$, deg^{-1}					
$C_{m_{i_H}}$, deg^{-1}					Not Available

a. Formulation I b. Reference 4 c. Reference 6

TABLE 17h. -- SST LONGITUDINAL DERIVATIVES AND COEFFICIENTS USED IN GENERAL COMPARISONS (CONTINUED)

Leading edge sweep = 72°

Altitude, h, ft	37 000	Velocity, V_{c_1}, ft/sec	871.27
Gross weight, W, lb	668 000	Drag, C_{D_1}	0.0404
Mach number, M	0.9	Lift, C_{L_1}	0.2854
Dynamic pressure, $\bar{q}$, psf	260	Iyy, rigid, slug-ft^2	48.3×10^6
Density ratio	0.28525 cg @ $0.64C_R$	Iyy, equiv elas, slug-ft^2	48.448×10^6

Derivatives	Methods				
	Rigid			Equivalent elastic [a]	
	Lifting surface ○ (TA 67A)	Handbook methods [c] □	Wind tunnel ◇ data	Lifting surface △ (TA 67A)	Handbook methods ▽
C_{L_O}	0.01335	○	○	0.02242	Not Available
C_{m_o}	0.0090	○	○	0.0086	
C_{L_α}, deg^{-1}	0.0324	0.0298	0.0322	0.0320	
C_{m_α}, deg^{-1}	-0.00035	-0.0019	-0.0014	-0.00044	
C_{D_α}, deg^{-1}	0.0055	0.0033	0.0100	0.00959	
$C_{L_{\dot\alpha}}$, rad^{-1}	□	-0.25	□	□	
$C_{m_{\dot\alpha}}$, rad^{-1}	□	-0.18	□	□	
$C_{D_{\dot\alpha}}$, rad^{-1}					
C_{L_q}, rad^{-1}	1.37	0.570	○	1.150	
C_{m_q}, rad^{-1}	-0.44	-0.340	○	-0.362	
C_{D_q}, rad^{-1}					
C_{L_u}, rad^{-1}	0.120	1.21 [b]	0.128	0.0731	
C_{m_u}, rad^{-1}	0.0136	◇	0.01152	-0.0254	
C_{D_u}, rad^{-1}	0.0204	◇	0.0217	◇	
$C_{L_{\ddot\theta_I}}$, (rad/sec^2)$^{-1}$				-0.0321	
$C_{m_{\ddot\theta_I}}$, (rad/sec^2)$^{-1}$				-0.0004	
$C_{L_{\delta_E}}$, deg^{-1}	0.0092	◇	0.0080	◇	
$C_{m_{\delta_E}}$, deg^{-1}	-0.00261	◇	-0.0031	◇	
$C_{L_{i_H}}$, deg^{-1}					
$C_{m_{i_H}}$, deg^{-1}					Not Available

a. Formulation I b. Reference 4 c. Reference 6

TABLE 17i. – SST LONGITUDINAL DERIVATIVES AND COEFFICIENTS USED IN GENERAL COMPARISONS (CONTINUED)

Leading edge sweep = 72°

Altitude, h, ft 33 000	Velocity, V_{c_1}, ft/sec ... 1080.07
Gross weight, W, lb 668 000	Drag, C_{D_1} 0.0232
Mach number, M 1.1	Lift, C_{L_1} 0.1579
Dynamic pressure, $\bar{q}$, psf 470	Iyy, rigid, slug-ft^2 ..... 48.3×10^6
Density ratio .....0.33513 cg @ 0.64C_R	Iyy, equiv elas, slug-ft^2 47.832×10^6

Derivatives	Methods				
	Rigid			Equivalent elastic [a]	
	Lifting surface ○ (TA 67A)	Handbook methods [c] □	Wind tunnel ◇ data	Lifting surface △ (TA 67A)	Handbook methods ▽
C_{L_O}	0.01176	○	○	0.02966	Not Available
C_{m_o}	0.0110	○	○	0.0110	
C_{L_α}, deg^{-1}	0.0345	0.0325	0.0345	0.0323	
C_{m_α}, deg^{-1}	-0.00136	-0.00226	-0.0016	-0.00122	
C_{D_α}, deg^{-1}	0.0061	0.0032	0.0097	0.00503	
$C_{L_{\dot\alpha}}$, rad^{-1}	□	-0.17	□	□	
$C_{m_{\dot\alpha}}$, rad^{-1}	□	-0.11	□	□	
$C_{D_{\dot\alpha}}$, rad^{-1}					
C_{L_q}, rad^{-1}	1.43	0.756	○	0.979	
C_{m_q}, rad^{-1}	-0.48	-0.310	○	-0.383	
C_{D_q}, rad^{-1}					
C_{L_u}, rad^{-1}	0.0364	-0.902 [b]	0.037	0.0311	
C_{m_u}, rad^{-1}	0.0071	◇	0.0077	-0.0102	
C_{D_u}, rad^{-1}	0.0088	◇	0.0165	◇	
$C_{L_{\ddot\theta_I}}$, (rad/sec^2)$^{-1}$				-0.0295	
$C_{m_{\ddot\theta_I}}$, (rad/sec^2)$^{-1}$				0.0007	
$C_{L_{\delta_E}}$, deg^{-1}	0.0094	◇	0.0055	◇	
$C_{m_{\delta_E}}$, deg^{-1}	-0.00323	◇	-0.00222	◇	
$C_{L_{i_H}}$, deg^{-1}					
$C_{m_{i_H}}$, deg^{-1}					Not Available

a. Formulation I b. Reference 4 c. Reference 6

TABLE 17j. – SST LONGITUDINAL DERIVATIVES AND COEFFICIENTS USED IN GENERAL COMPARISONS (CONTINUED)

Leading edge sweep = 72°

Altitude, h, ft	30 000	Velocity, V_{c_1}, ft/sec ...	1293.31
Gross weight, W, lb	520 000	Drag, C_{D_1}	0.0133
Mach number, M	1.3	Lift, C_{L_1}	0.0770
Dynamic pressure, $\bar{q}$, psf	750	Iyy, rigid, slug-ft^2	47.6×10^6
Density ratio	0.37473 cg @ 0.64 C_R	Iyy, equiv elas, slug-ft^2	49.627×10^6

Derivatives	Methods				
	Rigid			Equivalent elastic [a]	
	Lifting surface ○ (TA 67A)	Handbook methods [c] □	Wind tunnel ◇ data	Lifting surface △ (TA 67A)	Handbook methods ▽
C_{L_O}	0.02429	○	○	0.04192	Not Available
C_{m_o}	0.0097	○	○	0.0066	
C_{L_α}, deg^{-1}	0.0336	0.0344	0.0323	0.0317	
C_{m_α}, deg^{-1}	-0.00151	-0.00232	-0.0019	-0.00160	
C_{D_α}, deg^{-1}	0.0059	0.0021	0.0092	0.00215	
$C_{L_{\dot\alpha}}$, rad^{-1}	□	-0.16	□	□	
$C_{m_{\dot\alpha}}$, rad^{-1}	□	-0.04	□	□	
$C_{D_{\dot\alpha}}$, rad^{-1}					
C_{L_q}, rad^{-1}	1.21	0.800	○	0.746	
C_{m_q}, rad^{-1}	-0.43	-0.205	○	-0.358	
C_{D_q}, rad^{-1}					
C_{L_u}, rad^{-1}	-0.0013	-0.191 [b]	0.	0.0182	
C_{m_u}, rad^{-1}	-0.0013	◇	-0.00217	-0.0111	
C_{D_u}, rad^{-1}	0.0039	◇	-0.0015	◇	
$C_{L_{\ddot\theta_I}}$, (rad/sec^2)$^{-1}$				-0.0215	
$C_{m_{\ddot\theta_I}}$, (rad/sec^2)$^{-1}$				-0.0019	
$C_{L_{\delta_E}}$, deg^{-1}	0.0053	◇	0.0037	◇	
$C_{m_{\delta_E}}$, deg^{-1}	-0.0020	◇	-0.00161	◇	
$C_{L_{i_H}}$, deg^{-1}					
$C_{m_{i_H}}$, deg^{-1}					Not Available

a. Formulation I b. Reference 4 c. Reference 6

TABLE 17k. – SST LONGITUDINAL DERIVATIVES AND COEFFICIENTS USED IN GENERAL COMPARISONS (CONTINUED)

Leading edge sweep = 72°

Altitude, h, ft 24 000	Velocity, V_{c_1}, ft/sec ... 1530.45
Gross weight, W, lb ..... [illegible]	Drag, C_{D_1} 0.0092
Mach number, M 1.5	Lift, C_{L_1} 0.0444
Dynamic pressure, $\bar{q}$, psf 1300	Iyy, rigid, slug-ft^2 ..... 47.6×10^6
Density ratio .....0.46462 cg @ 0.64C_R	Iyy, equiv elas, slug-ft^2 56.295×10^6

Derivatives	Methods				
	Rigid			Equivalent elastic [a]	
	Lifting surface ○ (TA 67A)	Handbook methods [c] □	Wind tunnel ◇ data	Lifting surface △ (TA 67A)	Handbook methods ▽
C_{L_O}	0.03166	○	○	0.04792	Not Available
C_{m_o}	0.0089	○	○	0.0041	
C_{L_α}, deg^{-1}	0.0325	0.0329	0.0313	0.0296	
C_{m_α}, deg^{-1}	-0.00158	-0.00221	-0.00145	-0.00173	
C_{D_α}, deg^{-1}	0.0056	0.0010	0.0087	0.0010	
$C_{L_{\dot\alpha}}$, rad^{-1}	□	-0.114	□	□	
$C_{m_{\dot\alpha}}$, rad^{-1}	□	0.024	□	□	
$C_{D_{\dot\alpha}}$, rad^{-1}					
C_{L_q}, rad^{-1}	1.04	0.595	○	0.502	
C_{m_q}, rad^{-1}	-0.385	-0.230	○	-0.341	
C_{D_q}, rad^{-1}					
C_{L_u}, rad^{-1}	-0.0048	-0.08 [b]	-0.0101	0.0019	
C_{m_u}, rad^{-1}	-0.0039	◇	-0.003	-0.0067	
C_{D_u}, rad^{-1}	0.0007	◇	-0.001	◇	
$C_{L_{\ddot\theta_I}}$, (rad/sec^2)$^{-1}$			-0.0164		
$C_{m_{\ddot\theta_I}}$, (rad/sec^2)$^{-1}$			-0.0047		
$C_{L_{\delta_E}}$, deg^{-1}	0.0041	◇	0.003	◇	
$C_{m_{\delta_E}}$, deg^{-1}	-0.00158	◇	-0.00126	◇	
$C_{L_{i_H}}$, deg^{-1}					
$C_{m_{i_H}}$, deg^{-1}					Not Available

a. Formulation I b. Reference 4 c. Reference 6

TABLE 17l. – SST LONGITUDINAL DERIVATIVES AND COEFFICIENTS USED IN GENERAL COMPARISONS (CONTINUED)

Leading edge sweep = 72°

Altitude, h, ft	60 500	Velocity, V_{c_1}, ft/sec ...	2129.78
Gross weight, W, lb	520 000	Drag, C_{D_1}	0.0098
Mach number, M	2.2	Lift, C_{L_1}	0.0770
Dynamic pressure, $\bar{q}$, psf	500	Iyy, rigid, slug-ft^2	47.6×10^6
Density ratio .....0.092704 cg @ 0.64C_R		Iyy, equiv elas, slug-ft^2	52.082×10^6

Derivatives	Methods				
	Rigid			Equivalent elastic [a]	
	Lifting surface ○ (TA 67A)	Handbook methods [c] □	Wind tunnel ◇ data	Lifting surface △ (TA 67A)	Handbook methods ▽
C_{L_O}	0.03618	○	○	0.04230	Not Available
C_{m_o}	0.0079	○	○	0.0056	
C_{L_α}, deg^{-1}	0.0283	0.0289	0.0271	0.0265	
C_{m_α}, deg^{-1}	-0.00143	-0.00183	-0.00107	-0.00144	
C_{D_α}, deg^{-1}	0.0048	0.0010	0.0065	0.00206	
$C_{L_{\dot\alpha}}$, rad^{-1}	□	-0.104	□	□	
$C_{m_{\dot\alpha}}$, rad^{-1}	□	0.06	□	□	
$C_{D_{\dot\alpha}}$, rad^{-1}					
C_{L_q}, rad^{-1}	0.575	0.310	○	0.331	
C_{m_q}, rad^{-1}	-0.300	-0.225	○	-0.293	
C_{D_q}, rad^{-1}					
C_{L_u}, rad^{-1}	-0.0198	-0.092 [b]	-0.017	-0.0402	
C_{m_u}, rad^{-1}	-0.00154	◇	-0.0003	-0.0028	
C_{D_u}, rad^{-1}	-0.0012	◇	-0.0006	◇	
$C_{L_{\ddot\theta_I}}$, (rad/sec^2)$^{-1}$				-0.0193	
$C_{m_{\ddot\theta_I}}$, (rad/sec^2)$^{-1}$				-0.0042	
$C_{L_{\delta_E}}$, deg^{-1}	0.0024	◇	0.0020	◇	
$C_{m_{\delta_E}}$, deg^{-1}	-0.00093	◇	-0.00069	◇	
$C_{L_{i_H}}$, deg^{-1}					
$C_{m_{i_H}}$, deg^{-1}					Not Available

a. Formulation I b. Reference 4 c. Reference 6

TABLE 17m. – SST LONGITUDINAL DERIVATIVES AND COEFFICIENTS USED IN GENERAL COMPARISONS (CONCLUDED)

Leading edge sweep = 72°

Altitude, h, ft	49 000	Velocity, V_{c_1}, ft/sec	2613.82
Gross weight, W, lb	520 000	Drag, C_{D_1}	0.007
Mach number, M	2.7	Lift, C_{L_1}	0.0444
Dynamic pressure, $\bar{q}$, psf	1300	Iyy, rigid, slug-ft^2	47.6×10^6
Density ratio	0.16061 cg @ 0.64C_R	Iyy, equiv elas, slug-ft^2	60.180×10^6

Derivatives	Methods				
	Rigid			Equivalent elastic [a]	
	Lifting surface ○ (TA 67A)	Handbook methods [c] □	Wind tunnel ◇ data	Lifting surface △ (TA 67A)	Handbook methods ▽
C_{L_O}	0.03141	○	○	0.03723	Not Available
C_{m_o}	0.0077	○	○	0.0041	
C_{L_α}, deg^{-1}	0.0255	0.0257	0.0238	0.0229	
C_{m_α}, deg^{-1}	-0.00118	-0.00142	-0.00095	-0.00133	
C_{D_α}, deg^{-1}	0.0045	0.0013	0.0050	0.00106	
$C_{L_{\dot{\alpha}}}$, rad^{-1}	□	-0.101	□	□	
$C_{m_{\dot{\alpha}}}$, rad^{-1}	□	0.077	□	□	
$C_{D_{\dot{\alpha}}}$, rad^{-1}					
C_{L_q}, rad^{-1}	0.370	0.205	○	0.089	
C_{m_q}, rad^{-1}	-0.273	-0.161	○	-0.271	
C_{D_q}, rad^{-1}					
C_{L_u}, rad^{-1}	-0.0375	-0.0516 [b]	-0.0193	-0.070	
C_{m_u}, rad^{-1}	-0.00162	◇	-0.00068	0.0072	
C_{D_u}, rad^{-1}	-0.0014	◇	-0.001	◇	
$C_{L_{\ddot{\theta}_I}}$, (rad/sec^2)$^{-1}$				-0.0223	
$C_{m_{\ddot{\theta}_I}}$, (rad/sec^2)$^{-1}$				-0.0068	
$C_{L_{\delta_E}}$, deg^{-1}	0.0020	◇	0.0016	◇	
$C_{m_{\delta_E}}$, deg^{-1}	-0.00079	◇	-0.00058	◇	
$C_{L_{i_H}}$, deg^{-1}					
$C_{m_{i_H}}$, deg^{-1}					Not Available

a. Formulation I b. Reference 4 c. Reference 6

TABLE 18a. – 707-320B LATERAL-DIRECTIONAL DERIVATIVES USED IN GENERAL COMPARISONS

Altitude, h, ft	10 000	Ixx_b, rigid, slug-ft^2	4.925×10^6
Gross weight, W, lb	268 000	Izz_b, rigid, slug-ft^2	9.900×10^6
Mach number, M	0.255	Ixz_b, rigid, slug-ft^2	0.210×10^6
Dynamic pressure, $\bar{q}$, psf	66.7	Mass, M, rigid, slugs	8335
Density ratio	0.73859	I_{xxb}, equiv elas slug-ft^2	4.922×10^6
Velocity, V_{c_1}, ft/sec	274.74	I_{zzb}, equiv elas slug-ft^2	9.876×10^6
Lift, C_{L_1}	1.3895	I_{xzb}, equiv elas slug-ft^2	0.202×10^6
c.g.@ 0.25 $\bar{c}$		Mass, M, equiv elas slug	8316

Derivatives	Methods			
	Rigid			Equivalent elastic[a]
	Handbook methods		◇	
	TR1098 (ref. 72) ○	USAF (ref. 6) □	Wind tunnel	Handbook method ▽
C_{l_β}, deg^{-1}	-0.00603[b]	-0.00425	-0.00275	-0.00706
C_{n_β}, deg^{-1}	◇	0.00268	0.00198	0.00243
C_{y_β}, deg^{-1}	◇	-0.00808	-0.0088	-0.00750
$C_{l_{\dot\beta}}$, rad^{-1}	□	0.00044[c]	□	□
$C_{n_{\dot\beta}}$, rad^{-1}	□	-0.0098[c]	□	□
$C_{y_{\dot\beta}}$, rad^{-1}	□	+0.0229[c]	□	□
C_{l_p}, rad^{-1}	-0.440	-0.384	-0.522[d]	-0.455[d] / -0.379
C_{n_p}, rad^{-1}	-0.1495	-0.2230	□	-0.1499
C_{y_p}, rad^{-1}	0.1066	0.301	□	0.1077
C_{l_r}, rad^{-1}	0.2817	0.535	□	0.281
C_{n_r}, rad^{-1}	-0.2015	○	○	-0.192
C_{y_r}, rad^{-1}	0.318	○	○	0.294

Inertial derivatives	Handbook method	Inertial derivatives	Handbook method
$C_{l_{\dot p_I}}$, sec^2/rad	7.4×10^{-6}	$C_{y_{\dot r_I}}$, sec^2/rad	-0.00234
$C_{n_{\dot p_I}}$, sec^2/rad	-1.63×10^{-4}	$C_{l_{\ddot y_I}}$, sec^2/ft	8.94×10^{-7}
$C_{y_{\dot p_I}}$, sec^2/rad	3.82×10^{-4}	$C_{n_{\ddot y_I}}$, sec^2/ft	-1.98×10^{-5}
$C_{l_{\dot r_I}}$, sec^2/rad	-4.52×10^{-5}	$C_{y_{\ddot y_I}}$, sec^2/ft	4.63×10^{-5}
$C_{n_{\dot r_I}}$, sec^2/rad	9.99×10^{-4}		

a. Formulation I b. (ref. 73) c. V. T. Only d. TA 67A

TABLE 18b. – 707-320B LATERAL-DIRECTIONAL DERIVATIVES USED IN GENERAL COMPARISONS (CONTINUED)

Altitude, h, ft 10 000	Ixx_b, rigid, slug-ft^2 .....4.925×10^6
Gross weight, W, lb 268 000	Izz_b, rigid, slug-ft^2 .....9.900×10^6
Mach number, M 0.365	Ixz_b, rigid, slug-ft^2 .....0.210×10^6
Dynamic pressure, $\bar{q}$, psf. 136	Mass, M, rigid, slugs 8335
Density ratio 0.73859	I_{xxb}, equiv elas slug-ft^2 .....4.923×10^6
Velocity, V_{c_1}, ft/sec 393.25	I_{zzb}, equiv elas slug-ft^2 .....9.851×10^6
Lift, C_{L_1} 0.6815	I_{xzb}, equiv elas slug-ft .....0.199×10^6
c.g. @ 0.25 $\bar{c}$	Mass, M, equiv elas slug 8308

Derivatives	Methods			
	Rigid			Equivalent elastic[a]
	Handbook methods		◇	
	TR1098 (ref. 72) ○	USAF (ref. 6) □	Wind tunnel	Handbook method ▽
C_{l_β}, deg^{-1}	-0.00418	-0.00300	-0.00264	-0.00515[b]
C_{n_β}, deg^{-1}	◇	0.00154	0.00203	0.00108
C_{y_β}, deg^{-1}	◇	-0.00805	-0.00892	-0.00698
$C_{l_{\dot\beta}}$, rad^{-1}	□	0.00165[c]	□	□
$C_{n_{\dot\beta}}$, rad^{-1}	□	-0.0097[c]	□	□
$C_{y_{\dot\beta}}$, rad^{-1}	□	0.0228[c]	□	□
C_{l_p}, rad^{-1}	-0.414	-0.389	-0.533	-0.413[d] / -0.320
C_{n_p}, rad^{-1}	-0.0531	-0.0938	□	-0.0568
C_{y_p}, rad^{-1}	-0.0122	0.0308	□	-0.0037
C_{l_r}, rad^{-1}	0.2183	0.280	□	0.215
C_{n_r}, rad^{-1}	-0.1513	○	○	-0.130
C_{y_r}, rad^{-1}	0.318	○	○	0.268

Inertial derivatives	Handbook method	Inertial derivatives	Handbook method
$C_{l_{\dot p_I}}$, sec^2/rad	7.3×10^{-6}	$C_{y_{\dot r_I}}$, sec^2/rad	-0.00213
$C_{n_{\dot p_I}}$, sec^2/rad	-4.31×10^{-5}	$C_{l_{\ddot y_I}}$, sec^2/ft	3.05×10^{-6}
$C_{y_{\dot p_I}}$, sec^2/rad	1.01×10^{-4}	$C_{n_{\ddot y_I}}$, sec^2/ft	-1.80×10^{-5}
$C_{l_{\dot r_I}}$, sec^2/rad	-1.545×10^{-4}	$C_{y_{\ddot y_I}}$, sec^2/ft	4.21×10^{-5}
$C_{n_{\dot r_I}}$, sec^2/rad	9.09×10^{-4}		

a. Formulation I b. (ref. 73) c. V. T. Only d. TA 67A

TABLE 18c. – 707-320B LATERAL-DIRECTIONAL DERIVATIVES USED IN GENERAL COMPARISONS (CONTINUED)

Altitude, h, ft 10 000	I_{xx_b}, rigid, slug-ft^2 ..... 4.925×10^6
Gross weight, W, lb 268 000	I_{zz_b}, rigid, slug-ft^2 ..... 9.900×10^6
Mach number, M 0.548	I_{xz_b}, rigid, slug-ft^2 ..... 0.210×10^6
Dynamic pressure, $\bar{q}$, psf 306	Mass, M, rigid, slugs 8335
Density ratio 0.73859	I_{xxb}, equiv elas slug-ft^2 ..... 4.873×10^6
Velocity, V_{c_1}, ft/sec 590.42	I_{zzb}, equiv elas slug-ft^2 ..... 9.800×10^6
Lift, C_{L_1} 0.3028	I_{xzb}, equiv elas slug-ft^2 ..... 0.195×10^6
c.g. @ 0.25 $\bar{c}$	Mass, M, equiv elas slug 8292

Derivatives	Methods			
	Rigid			Equivalent elastic[a]
	Handbook methods		◇	
	TR1098 (ref. 72) ○	USAF (ref. 6) □	Wind tunnel	Handbook method ▽
C_{l_β}, deg^{-1}	-0.00329[b]	-0.00258	-0.00268	-0.00410[b]
C_{n_β}, deg^{-1}	◇	0.00136	0.00219	0.00044
C_{y_β}, deg^{-1}	◇	-0.00829	-0.00919	-0.00613
$C_{l_{\dot\beta}}$, rad^{-1}	□	0.00254[c]	□	□
$C_{n_{\dot\beta}}$, rad^{-1}	□	-0.0100[c]	□	□
$C_{y_{\dot\beta}}$, rad^{-1}	□	0.0235[c]	□	□
C_{l_p}, rad^{-1}	-0.412	-0.408	-0.562[d]	-0.339[d] / -0.248
C_{n_p}, rad^{-1}	0.0015	-0.0131	□	-0.0091
C_{y_p}, rad^{-1}	-0.1431	-0.1235	□	-0.1183
C_{l_r}, rad^{-1}	0.1947	0.148	□	0.184
C_{n_r}, rad^{-1}	-0.1465	○	○	-0.105
C_{y_r}, rad^{-1}	0.329	○	○	0.231

Inertial derivatives	Handbook method	Inertial derivatives	Handbook method
$C_{l_{\dot p_I}}$, sec^2/rad	5.4×10^{-6}	$C_{y_{\dot r_I}}$, sec^2/rad	-0.00187
$C_{n_{\dot p_I}}$, sec^2/rad	2.13×10^{-5}	$C_{l_{\ddot y_I}}$, sec^2/ft	3.98×10^{-6}
$C_{y_{\dot p_I}}$, sec^2/rad	-5.0×10^{-5}	$C_{n_{\ddot y_I}}$, sec^2/ft	-1.57×10^{-5}
$C_{l_{\dot r_I}}$, sec^2/rad	-2.025×10^{-4}	$C_{y_{\ddot y_I}}$, sec^2/ft	3.68×10^{-5}
$C_{n_{\dot r_I}}$, sec^2/rad	7.98×10^{-4}		

a. Formulation I b. (ref. 73) c. V. T. Only d. TA 67A

TABLE 18d. – 707-320B LATERAL-DIRECTIONAL DERIVATIVES USED IN GENERAL COMPARISONS (CONTINUED)

Altitude, h, ft 35 000	Ixx_b, rigid, slug-ft^2 ..... 4.925×10^6
Gross weight, W, lb 268 000	Izz_b, rigid, slug-ft^2 ..... 9.900×10^6
Mach number, M 0.8	Ixz_b, rigid, slug-ft^2 ..... 0.210×10^6
Dynamic pressure, $\bar{q}$, psf 223	Mass, M, rigid, slugs 8335
Density ratio 0.31058	I_{xxb}, equiv elas slug-ft^2 .... 4.924×10^6
Velocity, V_{c_1}, ft/sec 778.51	I_{zzb}, equiv elas slug-ft^2 .... 9.826×10^6
Lift, C_{L_1} 0.4164	I_{xzb}, equiv elas slug-ft^2 ..... 0.199×10^6
c.g.@ 0.25 $\bar{c}$	Mass, M, equiv elas slug 8300

Derivatives	Methods			
	Rigid			Equivalent elastic[a]
	Handbook methods		◇	
	TR1098 (ref. 72) ○	USAF (ref. 6) □	Wind tunnel	Handbook method ▽
C_{l_β}, deg^{-1}	-0.00407	-0.00305	-0.00350	-0.00488[b]
C_{n_β}, deg^{-1}	◇	0.00162	0.00260	0.00076
C_{y_β}, deg^{-1}	◇	-0.00876	-0.00965	-0.00677
$C_{l_{\dot\beta}}$, rad^{-1}	□	0.00244[c]	□	□
$C_{n_{\dot\beta}}$, rad^{-1}	□	-0.0107[c]	□	□
$C_{y_{\dot\beta}}$, rad^{-1}	□	0.0250[c]	□	□
C_{l_p}, rad^{-1}	-0.412	-0.437	-0.658[d]	-0.411[d] / -0.243
C_{n_p}, rad^{-1}	-0.0123	-0.0290	□	-0.0211
C_{y_p}, rad^{-1}	-0.1150	-0.0850	□	-0.0943
C_{l_r}, rad^{-1}	0.2446	0.222	□	0.231
C_{n_r}, rad^{-1}	-0.1995	○	○	-0.119
C_{y_r}, rad^{-1}	0.349	○	○	0.259

Inertial derivatives	Handbook method	Inertial derivatives	Handbook method
$C_{l_{\dot p_I}}$, sec^2/rad	4.5×10^{-6}	$C_{y_{\dot r_I}}$, sec^2/rad	-0.00192
$C_{n_{\dot p_I}}$, sec^2/rad	1.96×10^{-5}	$C_{l_{\ddot y_I}}$, sec^2/ft	3.76×10^{-6}
$C_{y_{\dot p_I}}$, sec^2/rad	-4.6×10^{-5}	$C_{n_{\ddot y_I}}$, sec^2/ft	-1.64×10^{-5}
$C_{l_{\dot r_I}}$, sec^2/rad	-1.876×10^{-4}	$C_{y_{\ddot y_I}}$, sec^2/ft	3.85×10^{-5}
$C_{n_{\dot r_I}}$, sec^2/rad	8.20×10^{-4}		

a. Formulation I b. (ref. 73) c. V.T. Only d. TA 67A

TABLE 18e. – 707-320B LATERAL-DIRECTIONAL DERIVATIVES USED IN GENERAL COMPARISONS (CONTINUED)

Altitude, h, ft 35 000	Ixx_b, rigid, slug-ft^2 ..... 4.925×10^6
Gross weight, W, lb 268 000	Izz_b, rigid, slug-ft^2 ..... 9.900×10^6
Mach number, M 0.85	Ixz_b, rigid, slug-ft^2 ..... 0.210×10^6
Dynamic pressure, $\bar{q}$, psf 251	Mass, M, rigid, slugs 8335
Density ratio 0.31058	I_{xxb}, equiv elas slug-ft^2 .... 4.925×10^6
Velocity, Vc_1, ft/sec 827.17	I_{zzb}, equiv elas slug-ft^2 .... 9.819×10^6
Lift, C_{L_1} 0.3691	I_{xzb}, equiv elas slug-ft^2 ..... 0.199×10^6
c.g. @ 0.25 $\bar{c}$	Mass, M, equiv elas slug 8298

Derivatives	Methods			
	Rigid			Equivalent elastic[a]
	Handbook methods		◇	
	TR1098 (ref. 72) ○	USAF (ref. 6) □	Wind tunnel	Handbook method ▽
C_{l_β}, deg^{-1}	-0.00405[b]	-0.00314	-0.00375	-0.00486[b]
C_{n_β}, deg^{-1}	◇	0.00162	0.00288	0.00068
C_{y_β}, deg^{-1}	◇	-0.00883	-0.00955	-0.00663
$C_{l_{\dot\beta}}$, rad^{-1}	□	0.00260[c]	□	□
$C_{n_{\dot\beta}}$, rad^{-1}	□	-0.0108[c]	□	□
$C_{y_{\dot\beta}}$, rad^{-1}	□	0.0254[c]	□	□
C_{l_p}, rad^{-1}	-0.413	-0.451	-0.688[d]	-0.402[d] / -0.245
C_{n_p}, rad^{-1}	-0.0050	-0.0187	□	-0.0155
C_{y_p}, rad^{-1}	-0.1321	-0.1118	□	-0.1078
C_{l_r}, rad^{-1}	0.2554	0.210	□	0.245
C_{n_r}, rad^{-1}	-0.2032	○	○	-0.118
C_{y_r}, rad^{-1}	0.354	○	○	0.253

Inertial derivatives	Handbook method	Inertial derivatives	Handbook method
$C_{l_{\dot p_I}}$, sec^2/rad	-7.7×10^{-6}	$C_{y_{\dot r_I}}$, sec^2/rad	-0.00185
$C_{n_{\dot p_I}}$, sec^2/rad	3.20×10^{-5}	$C_{l_{\dot y_I}}$, sec^2/ft	3.80×10^{-6}
$C_{y_{\dot p_I}}$, sec^2/rad	-7.5×10^{-5}	$C_{n_{\dot y_I}}$, sec^2/ft	-1.58×10^{-5}
$C_{l_{\dot r_I}}$, sec^2/rad	-1.894×10^{-4}	$C_{y_{\dot y_I}}$, sec^2/ft	3.71×10^{-5}
$C_{n_{\dot r_I}}$, sec^2/rad	7.90×10^{-4}		

a. Formulation I b. (ref. 73) c. V. T. Only d. TA 67A

TABLE 18f. – 707-320B LATERAL-DIRECTIONAL DERIVATIVES USED IN GENERAL COMPARISONS (CONCLUDED)

Altitude, h, ft 35 000	Ixx_b, rigid, slug-ft^2 ..... 4.925×10^6
Gross weight, W, lb 268 000	Izz_b, rigid, slug-ft^2 ..... 9.900×10^6
Mach number, M 0.9	Ixz_b, rigid, slug-ft^2 ..... 0.210×10^6
Dynamic pressure, $\bar{q}$, psf 283	Mass, M, rigid, slugs 8335
Density ratio 0.31058	I_{xxb}, equiv elas slug-ft^2 .... 4.926×10^6
Velocity, V_{c_1}, ft/sec 875.83	I_{zzb}, equiv elas slug-ft^2 .... 9.834×10^6
Lift, C_{L_1} 0.3274	I_{xzb}, equiv elas slug-ft^2 ..... 0.203×10^6
c.g. @ 0.25 $\bar{c}$	Mass, M, equiv elas slug 8302

Derivatives	Methods			
	Rigid			Equivalent elastic[a]
	Handbook methods		◇	
	TR1098 (ref. 72) ○	USAF (ref. 6) □	Wind tunnel	Handbook method ▽
C_{l_β}, deg^{-1}	-0.00394[b]	-0.00308	-0.00213	-0.00472
C_{n_β}, deg^{-1}	◇	0.00128	0.00360	0.00036
C_{y_β}, deg^{-1}	◇	-0.00808	-0.0099	-0.00593
$C_{l_{\dot\beta}}$, rad^{-1}	□	0.00275[c]	□	□
$C_{n_{\dot\beta}}$, rad^{-1}	□	-0.0111[c]	□	□
$C_{y_{\dot\beta}}$, rad^{-1}	□	0.0229[c]	□	□
C_{l_p}, rad^{-1}	-0.415	-0.459	-0.722[d]	-0.392[d] / -0.230
C_{n_p}, rad^{-1}	-0.0028	-0.0141	□	-0.0131
C_{y_p}, rad^{-1}	-0.1383	-0.1167	□	-0.1141
C_{l_r}, rad^{-1}	0.1600	0.176	□	0.150
C_{n_r}, rad^{-1}	-0.1542	○	○	-0.114
C_{y_r}, rad^{-1}	0.318	○	○	0.222

Inertial derivatives	Handbook method	Inertial derivatives	Handbook method
$C_{l_{\dot p_I}}$, sec^2/rad	-1.56×10^{-5}	$C_{y_{\dot r_I}}$, sec^2/rad	-0.00134
$C_{n_{\dot p_I}}$, sec^2/rad	6.28×10^{-5}	$C_{l_{\ddot y_I}}$, sec^2/ft	2.94×10^{-6}
$C_{y_{\dot p_I}}$, sec^2/rad	-1.47×10^{-4}	$C_{n_{\ddot y_I}}$, sec^2/ft	-1.19×10^{-5}
$C_{l_{\dot r_I}}$, sec^2/rad	-1.419×10^{-4}	$C_{y_{\ddot y_I}}$, sec^2/ft	2.78×10^{-5}
$C_{n_{\dot r_I}}$, sec^2/rad	5.72×10^{-4}		

a. Formulation I b. (ref. 73) c. V. T. Only d. TA 67A

TABLE 19a.–SST LATERAL-DIRECTIONAL DERIVATIVES USED IN GENERAL COMPARISONS

Leading edge sweep = 30°

Altitude, h, ft	8 500	Ixx_b, rigid, slug-ft^2	4.2×10^6
Gross weight, W, lb	370 000	Izz_b, rigid, slug-ft^2	46.11×10^6
Mach number, M	0.3	Ixz_b, rigid, slug-ft^2	0.242×10^6
Dynamic pressure, $\bar{q}$, psf	98	Mass, M, rigid, slugs	11 491
Density ratio	0.73859	I_{xxb}, equiv elas slug-ft^2	4.209×10^6
Velocity, V_{c_1}, ft/sec	274.74	I_{zzb}, equiv elas slug-ft^2	46.062×10^6
Lift, C_{L_1}	0.4198	I_{xzb}, equiv elas slug-ft^2	0.252×10^6
c.g. @0.64 C_R		Mass, M, equiv elas slug	11 475

Derivatives	Methods			
	Rigid			Equivalent elastic[a]
	Handbook methods		◇	
	TR1098 (ref. 72) ○	USAF (ref. 6) □	Wind tunnel	Handbook method ▽
C_{l_β}, deg^{-1}	□	-0.00214	□	-0.00213
C_{n_β}, deg^{-1}	□	0.00208	□	0.00208
C_{y_β}, deg^{-1}	◇	-0.00382	-0.00363	-0.00382
$C_{l_{\dot\beta}}$, rad^{-1}	□	0.00242[c]	□	□
$C_{n_{\dot\beta}}$, rad^{-1}	□	-0.0138[c]	□	□
$C_{y_{\dot\beta}}$, rad^{-1}	□	0.0232[c]	□	□
C_{l_p}, rad^{-1}	◇	-0.68	-0.543[d]	-0.512[d] / -0.6836
C_{n_p}, rad^{-1}	-0.0574	○	○	-0.0615
C_{y_p}, rad^{-1}	0.228	0.183	□	□
C_{l_r}, rad^{-1}	0.1113	0.1090	○	0.1090
C_{n_r}, rad^{-1}	-0.1495	○	○	-0.1338
C_{y_r}, rad^{-1}	0.226	○	○	0.2136

Inertial derivatives	Handbook method	Inertial derivatives	Handbook method
$C_{l_{\dot p_I}}$, sec^2/rad	-61.67×10^{-6}	$C_{y_{r_I}}$, sec^2/rad	-761.6×10^{-6}
$C_{n_{\dot p_I}}$, sec^2/rad	382.1×10^{-6}	$C_{l_{\ddot y_I}}$, sec^2/ft	1.241×10^{-6}
$C_{y_{\dot p_I}}$, sec^2/rad	638.9×10^{-6}	$C_{n_{\ddot y_I}}$, sec^2/ft	-11.12×10^{-6}
$C_{l_{\dot r_I}}$, sec^2/rad	-44.07×10^{-6}	$C_{y_{\ddot y_I}}$, sec^2/ft	17.93×10^{-6}
$C_{n_{\dot r_I}}$, sec^2/rad	479.6×10^{-6}		

a. Formulation I b. (ref. 73) c. V. T. Only d. TA 67A

TABLE 19b.–SST LATERAL-DIRECTIONAL DERIVATIVES USED IN GENERAL COMPARISONS (CONTINUED)

Leading edge sweep = 30°

Altitude, h, ft	9 500	Ixx_b, rigid, slug-ft^2	4.2×10^6
Gross weight, W, lb	370 000	Izz_b, rigid, slug-ft^2	46.11×10^6
Mach number, M	0.5	Ixz_b, rigid, slug-ft^2	0.242×10^6
Dynamic pressure, $\bar{q}$, psf	260	Mass, M, rigid, slugs	11 491
Density ratio	0.75032	I_{xxb}, equiv elas slug-ft^2	4.229×10^6
Velocity, V_{c_1}, ft/sec	539.69	I_{zzb}, equiv elas slug-ft^2	45.988×10^6
Lift, C_{L_1}	0.1581	I_{xzb}, equiv elas slug-ft^2	0.276×10^6
c.g. @ 0.64 C_R		Mass, M, equiv elas slug	11 450

Derivatives	Methods			
	Rigid			Equivalent elastic[a]
	Handbook methods		◇	
	TR1098 (ref. 72) ○	USAF (ref. 6) □	Wind tunnel	Handbook method ▽
C_{l_β}, deg^{-1}	□	-0.00132	□	-0.00131
C_{n_β}, deg^{-1}	□	0.00209	□	0.00203
C_{y_β}, deg^{-1}	◇	-0.00387	-0.0033	-0.00373
$C_{l_{\dot\beta}}$, rad^{-1}	□	0.00382[c]	□	□
$C_{n_{\dot\beta}}$, rad^{-1}	□	-0.0138[c]	□	□
$C_{y_{\dot\beta}}$, rad^{-1}	□	0.0233[c]	□	□
C_{l_p}, rad^{-1}	◇	-0.713	-0.571[d]	-0.491[d] / -0.6196
C_{n_p}, rad^{-1}	0.0013	○	○	-0.0034
C_{y_p}, rad^{-1}	0.0631	0.042	□	0.052
C_{l_r}, rad^{-1}	0.0668	0.0650	○	0.0611
C_{n_r}, rad^{-1}	-0.1453	○	○	-0.1214
C_{y_r}, rad^{-1}	0.229	○	○	0.2063

Inertial derivatives	Handbook method	Inertial derivatives	Handbook method
$C_{l_{\dot p_I}}$, sec^2/rad	-103.23×10^{-6}	$C_{y_{\dot r_I}}$, sec^2/rad	-760.1×10^{-6}
$C_{n_{\dot p_I}}$, sec^2/rad	418.2×10^{-6}	$C_{l_{\ddot y_I}}$, sec^2/ft	2.112×10^{-6}
$C_{y_{\dot p_I}}$, sec^2/rad	699.5×10^{-6}	$C_{n_{\ddot y_I}}$, sec^2/ft	-10.98×10^{-6}
$C_{l_{\dot r_I}}$, sec^2/rad	-82.42×10^{-6}	$C_{y_{\ddot y_I}}$, sec^2/ft	17.68×10^{-6}
$C_{n_{\dot r_I}}$, sec^2/rad	478.6×10^{-6}		

a. Formulation I b. (ref. 73) c. V. T. Only d. TA 67A

TABLE 19c.- SST LATERAL-DIRECTIONAL DERIVATIVES USED IN GENERAL COMPARISONS (CONTINUED)

Leading edge sweep = 30°

Altitude, h, ft 11 000	Ixx_b, rigid, slug-ft^2 ..... 4.2×10^6
Gross weight, W, lb 370 000	Izz_b, rigid, slug-ft^2 ..... 46.11×10^6
Mach number, M 0.7	Ixz_b, rigid, slug-ft^2 ..... 0.242×10^6
Dynamic pressure, $\bar{q}$, psf 470	Mass, M, rigid, slugs 11 491
Density ratio 0.71568	I_{xxb}, equiv elas slug-ft^2 ... 4.251×10^6
Velocity, V_{c_1}, ft/sec 751.39	I_{zzb}, equiv elas slug-ft^2 ... 45.892×10^6
Lift, C_{L_1} 0.0875	I_{xzb}, equiv elas slug-ft^2 .... 0.311×10^6
c.g.@ 0.64 C_R	Mass, M, equiv elas slug ... 11 416

Derivatives	Methods			
	Rigid			Equivalent elastic[a]
	Handbook methods		◇	
	TR1098 (ref. 72) ○	USAF (ref. 6) □	Wind tunnel	Handbook method ▽
C_{l_β}, deg^{-1}	□	-0.00110	□	-0.00106
C_{n_β}, deg^{-1}	□	0.00213	□	0.00197
C_{y_β}, deg^{-1}	◇	-0.00390	-0.0031	-0.00364
$C_{l_{\dot\beta}}$, rad^{-1}	□	0.00394[c]	□	□
$C_{n_{\dot\beta}}$, rad^{-1}	□	-0.0140[c]	□	□
$C_{y_{\dot\beta}}$, rad^{-1}	□	0.0236[c]	□	□
C_{l_p}, rad^{-1}	◇	-0.820	-0.625[d]	-0.467[d] / -0.5571
C_{n_p}, rad^{-1}	0.0173	○	○	0.0121
C_{y_p}, rad^{-1}	0.0166	-0.013	□	0.0067
C_{l_r}, rad^{-1}	0.05200	0.514	○	0.0475
C_{n_r}, rad^{-1}	-0.1411	○	○	-0.1251
C_{y_r}, rad^{-1}	0.231	○	○	0.2031

Inertial derivatives	Handbook method	Inertial derivatives	Handbook method
$C_{l_{\dot p_I}}$, sec^2/rad	-111.0×10^{-6}	$C_{y_{\dot r_I}}$, sec^2/rad	-770.4×10^{-6}
$C_{n_{\dot p_I}}$, sec^2/rad	416.8×10^{-6}	$C_{l_{\ddot y_I}}$, sec^2/ft	1.685×10^{-6}
$C_{y_{\dot p_I}}$, sec^2/rad	696.9×10^{-6}	$C_{n_{\ddot y_I}}$, sec^2/ft	-10.94×10^{-6}
$C_{l_{\dot r_I}}$, sec^2/rad	-93.13×10^{-6}	$C_{y_{\ddot y_I}}$, sec^2/ft	17.63×10^{-6}
$C_{n_{\dot r_I}}$, sec^2/rad	484.6×10^{-6}		

a. Formulation I b. (ref. 73) c. V. T. Only d. TA 67A

TABLE 19d.–SST LATERAL-DIRECTIONAL DERIVATIVES USED IN GENERAL COMPARISONS (CONTINUED)

Leading edge sweep = 42°

Altitude, h, ft 32 500	Ixz_b, rigid, slug-ft^2 ..... 9.6×10^6
Gross weight, W, lb 675 000	Izz_b, rigid, slug-ft^2 ..... 67.3×10^6
Mach number, M 0.5	Ixz_b, rigid, slug-ft^2 ..... 0.763×10^6
Dynamic pressure, $\bar{q}$, psf 98	Mass, M, rigid, slugs 20 963
Density ratio 0.35455	I_{xxb}, equiv elas slug-ft^2 .... 9.598×10^6
Velocity, V_{c_1}, ft/sec 492.02	I_{zzb}, equiv elas slug-ft^2 .... 67.182×10^6
Lift, C_{L_1} 0.7659	I_{xzb}, equiv elas slug-ft^2 ..... 0.743×10^6
c.g. @ 0.64 CR	Mass, M, equiv elas slug 20 928

Derivatives	Methods			
	Rigid			Equivalent elastic[a]
	Handbook methods		◇	
	TR1098 (ref. 72) ○	USAF (ref. 6) □	Wind tunnel	Handbook method ▽
C_{l_β}, deg^{-1}	◇	-0.00134	-0.00324	-0.00126
C_{n_β}, deg^{-1}	◇	0.00212	0.00205	0.00210
C_{y_β}, deg^{-1}	◇	-0.00387	-0.00543	-0.00384
$C_{l_{\dot\beta}}$, rad^{-1}	□	0.00004[c]	□	□
$C_{n_{\dot\beta}}$, rad^{-1}	□	-0.0148[c]	□	□
$C_{y_{\dot\beta}}$, rad^{-1}	□	0.0249[c]	□	□
C_{l_p}, rad^{-1}	◇	-0.575	-0.425[d]	-0.338[d] / -0.5294
C_{n_p}, rad^{-1}	-0.1706	○	○	-0.1763
C_{y_p}, rad^{-1}	0.699	0.866	□	0.698
C_{l_r}, rad^{-1}	0.1806	0.1686	○	0.1748
C_{n_r}, rad^{-1}	-0.1595	○	○	-0.1422
C_{y_r}, rad^{-1}	0.0288	○	○	0.2143

Inertial derivatives	Handbook method	Inertial derivatives	Handbook method
$C_{l_{\dot p_I}}$, sec^2/rad	-2.406×10^{-6}	$C_{y_{\dot r_I}}$, sec^2/rad	-2087.8×10^{-6}
$C_{n_{\dot p_I}}$, sec^2/rad	259.0×10^{-6}	$C_{l_{\ddot y_I}}$, sec^2/ft	4.3×10^{-6}
$C_{y_{\dot p_I}}$, sec^2/rad	431.9×10^{-6}	$C_{n_{\ddot y_I}}$, sec^2/ft	-24.73×10^{-6}
$C_{l_{\dot r_I}}$, sec^2/rad	36.54×10^{-6}	$C_{y_{\ddot y_I}}$, sec^2/ft	40.25×10^{-6}
$C_{n_{\dot r_I}}$, sec^2/rad	1288.3×10^{-6}		

a. Formulation I b. (ref. 73) c. V. T. Only d. TA-67A

TABLE 19e.–SST LATERAL-DIRECTIONAL DERIVATIVES USED IN GENERAL COMPARISONS (CONTINUED)

Leading edge sweep = 42°

Altitude, h, ft	26 000	Ixx_b, rigid, slug-ft^2	9.6×10^6
Gross weight, W, lb	675 000	Izz_b, rigid, slug-ft^2	67.3×10^6
Mach number, M	0.7	Ixz_b, rigid, slug-ft^2	0.763×10^6
Dynamic pressure, $\bar{q}$, psf	260	Mass, M, rigid, slugs	20 963
Density ratio	0.43300	I_{xxb}, equiv elas slug-ft^2	9.617×10^6
Velocity, V_{c_1}, ft/sec	708.32	I_{zzb}, equiv elas slug-ft^2	66.980×10^6
Lift, C_{L_1}	0.2884	I_{xzb}, equiv elas slug-ft^2	0.751×10^6
c.g. @	0.64 C_R	Mass, M, equiv elas slug	20 869

Derivatives	Methods			
	Rigid			Equivalent elastic[a]
	Handbook methods		◇	
	TR1098 (ref. 72) ○	USAF (ref. 6) □	Wind tunnel	Handbook method ▽
C_{l_β}, deg^{-1}	◇	-0.00114	-0.00198	-0.00106
C_{n_β}, deg^{-1}	◇	0.00215	0.00203	0.00206
C_{y_β}, deg^{-1}	◇	-0.00393	-0.00558	-0.00378
$C_{l_{\dot\beta}}$, rad^{-1}	□	0.00274[c]	□	□
$C_{n_{\dot\beta}}$, rad^{-1}	□	-0.0150[c]	□	□
$C_{y_{\dot\beta}}$, rad^{-1}	□	0.0252[c]	□	□
C_{l_p}, rad^{-1}	◇	-0.600	-0.456[d]	-0.360[d] / -0.4719
C_{n_p}, rad^{-1}	-0.0417	○	○	-0.0467
C_{y_p}, rad^{-1}	0.234	0.298	□	0.230
C_{l_r}, rad^{-1}	0.0869	0.0819	○	0.0852
C_{n_r}, rad^{-1}	-0.1485	○	○	-0.1290
C_{y_r}, rad^{-1}	0.231	○	○	0.2123

Inertial derivatives	Handbook method	Inertial derivatives	Handbook method
$C_{l_{\dot p_I}}$, sec^2/rad	63.541×10^{-6}	$C_{y_{r_I}}$, sec^2/rad	-2082.1×10^{-6}
$C_{n_{\dot p_I}}$, sec^2/rad	378.1×10^{-6}	$C_{l_{\ddot y_I}}$, sec^2/ft	3.21×10^{-6}
$C_{y_{\dot p_I}}$, sec^2/rad	632.3×10^{-6}	$C_{n_{\ddot y_I}}$, sec^2/ft	-24.58×10^{-6}
$C_{l_{\dot r_I}}$, sec^2/rad	-160.72×10^{-6}	$C_{y_{\ddot y_I}}$, sec^2/ft	40.0×10^{-6}
$C_{n_{\dot r_I}}$, sec^2/rad	1284.8×10^{-6}		

a. Formulation I b. (ref. 73) c. V. T. Only d. TA 67A

TABLE 19f.–SST LATERAL-DIRECTIONAL DERIVATIVES USED IN GENERAL COMPARISONS (CONTINUED)

Leading edge sweep = 42°

Altitude, h, ft	23 500
Gross weight, W, lb	675 000
Mach number, M	0.9
Dynamic pressure, $\bar{q}$, psf	470
Density ratio	0.47285
Velocity, V_{c_1}, ft/sec	920.15
Lift, C_{L_1}	0.1596
	c.g.@ 0.64 C_R

Ixx_b, rigid, slug-ft^2	9.6×10^6
Izz_b, rigid, slug-ft^2	67.3×10^6
Ixz_b, rigid, slug-ft^2	0.763×10^6
Mass, M, rigid, slugs	20 963
I_{xxb}, equiv elas slug-ft^2	9.642×10^6
I_{zzb}, equiv elas slug-ft^2	66.736×10^6
I_{xzb}, equiv elas slug-ft^2	0.760×10^6
Mass, M, equiv elas slug	20 798

Derivatives	Methods			
	Rigid			Equivalent elastic[a]
	Handbook methods		◇	
	TR1098 (ref. 72) ○	USAF (ref. 6) □	Wind tunnel	Handbook method ▽
C_{l_β}, deg^{-1}	◇	-0.00104	-0.00139	-0.00101
C_{n_β}, deg^{-1}	◇	0.00219	0.00201	0.00202
C_{y_β}, deg^{-1}	◇	-0.00396	-0.00575	-0.00370
$C_{l_{\dot\beta}}$, rad^{-1}	□	0.00350[c]	□	□
$C_{n_{\dot\beta}}$, rad^{-1}	□	-0.0150[c]	□	□
$C_{y_{\dot\beta}}$, rad^{-1}	□	0.0255[c]	□	□
C_{l_p}, rad^{-1}	◇	-0.675	-0.518[d]	-0.337[d] / -0.4227
C_{n_p}, rad^{-1}	-0.0147	○	○	-0.0131
C_{y_p}, rad^{-1}	0.112	0.123	□	0.106
C_{l_r}, rad^{-1}	0.0636	0.0602	○	0.0604
C_{n_r}, rad^{-1}	-0.1425	○	○	-0.1278
C_{y_r}, rad^{-1}	0.233	○	○	0.2071

Inertial derivatives	Handbook method	Inertial derivatives	Handbook method
$C_{l_{\dot p_I}}$, sec^2/rad	-86.921×10^{-6}	$C_{y_{r_I}}$, sec^2/rad	-2030.8×10^{-6}
$C_{n_{\dot p_I}}$, sec^2/rad	401.4×10^{-6}	$C_{l_{\ddot y_I}}$, sec^2/ft	4.232×10^{-6}
$C_{y_{\dot p_I}}$, sec^2/rad	671.2×10^{-6}	$C_{n_{\ddot y_I}}$, sec^2/ft	-24.0×10^{-6}
$C_{l_{\dot r_I}}$, sec^2/rad	-213.8×10^{-6}	$C_{y_{\ddot y_I}}$, sec^2/ft	39.01×10^{-6}
$C_{n_{\dot r_I}}$, sec^2/rad	1254.3×10^{-6}		

a. Formulation I b. (ref. 73) c. V. T. Only d. TA 67A

TABLE 19g.–SST LATERAL-DIRECTIONAL DERIVATIVES USED IN GENERAL COMPARISONS (CONTINUED)

Leading edge sweep = 72°

Altitude, h, ft 47 500	Ixx_b, rigid, slug-ft^2 ..... 6.27×10^6
Gross weight, W, lb 668 000	Izz_b, rigid, slug-ft^2 ..... 54.68×10^6
Mach number, M 0.7	Ixz_b, rigid, slug-ft^2 ..... 0.684×10^6
Dynamic pressure, $\bar{q}$, psf 98	Mass, M, rigid, slugs 20 745
Density ratio 0.17261	I_{xxb}, equiv elas slug-ft^2 .... 6.261×10^6
Velocity, V_{c1}, ft/sec 677.66	I_{zzb}, equiv elas slug-ft^2 .... 54.569×10^6
Lift, C_{L_1} 0.7580	I_{xzb}, equiv elas slug-ft^2 ..... 0.650×10^6
c.g. @ 0.64 C_R	Mass, M, equiv elas slug 20 710

Derivatives	Methods			
	Rigid			Equivalent elastic[a]
	Handbook methods		◇	
	TR1098 (ref. 72) ○	USAF (ref. 6) □	Wind tunnel	Handbook method ▽
C_{l_β}, deg^{-1}	◇	-0.00172	-0.00225	-0.00116
C_{n_β}, deg^{-1}	◇	0.00312	0.00225	◇
C_{y_β}, deg^{-1}	◇	-0.00605	-0.0066	-0.00388
$C_{l_{\dot\beta}}$, rad^{-1}				
$C_{n_{\dot\beta}}$, rad^{-1}				
$C_{y_{\dot\beta}}$, rad^{-1}				
C_{l_p}, rad^{-1}	◇	-0.150	-0.164[d]	-0.1621
C_{n_p}, rad^{-1}	-0.401	○	○	-0.4488
C_{y_p}, rad^{-1}	1.59	○	○	1.36
C_{l_r}, rad^{-1}	0.1810	0.1713	○	0.1502
C_{n_r}, rad^{-1}	-0.1392	○	○	-0.1155
C_{y_r}, rad^{-1}	0.225	○	○	0.2169

Inertial derivatives	Handbook method	Inertial derivatives	Handbook method
$C_{l_{\dot p_I}}$, sec^2/rad	24.502×10^{-6}	$C_{y_{r_I}}$, sec^2/rad	-2040.9×10^{-6}
$C_{n_{\dot p_I}}$, sec^2/rad	128.3×10^{-6}	$C_{l_{\ddot y_I}}$, sec^2/ft	-5.218×10^{-6}
$C_{y_{\dot p_I}}$, sec^2/rad	212.5×10^{-6}	$C_{n_{\ddot y_I}}$, sec^2/ft	-24.7×10^{-6}
$C_{l_{\dot r_I}}$, sec^2/rad	327.96×10^{-6}	$C_{y_{\ddot y_I}}$, sec^2/ft	40.19×10^{-6}
$C_{n_{\dot r_I}}$, sec^2/rad	1260.0×10^{-6}		

a. Formulation I b. (ref. 73) c. V. T. Only d. TA 67A

TABLE 19h.–SST LATERAL-DIRECTIONAL DERIVATIVES USED IN GENERAL COMPARISONS (CONTINUED)

Leading edge sweep = 72°

Altitude, h, ft 37 000	I_{xx_b}, rigid, slug-ft^2 ..... 6.27×10^6
Gross weight, W, lb 668 000	I_{zz_b}, rigid, slug-ft^2 ..... 54.68×10^6
Mach number, M 0.9	I_{xz_b}, rigid, slug-ft^2 ..... 0.684×10^6
Dynamic pressure, $\bar{q}$, psf 260	Mass, M, rigid, slugs 20 745
Density ratio 0.28525	I_{xxb}, equiv elas slug-ft^2 ..... 6.28×10^6
Velocity, V_{c_1}, ft/sec 871.27	I_{zzb}, equiv elas slug-ft^2 ..... 54.38×10^6
Lift, C_{L_1} 0.2854	I_{xzb}, equiv elas slug-ft^2 ..... 0.648×10^6
c.g. @ 0.64 C_R	Mass, M, equiv elas slug 20 653

Derivatives	Methods			
	Rigid			Equivalent elastic[a]
	Handbook methods		◇	
	TR1098 (ref. 72) ○	USAF (ref. 6) □	Wind tunnel	Handbook method ▽
C_{l_β}, deg^{-1}	◇	-0.00228	-0.00265	-0.00119
C_{n_β}, deg^{-1}	◇	0.00362	0.00245	◇
C_{y_β}, deg^{-1}	◇	-0.00712	-0.0075	-0.00382
$C_{l_{\dot\beta}}$, rad^{-1}				
$C_{n_{\dot\beta}}$, rad^{-1}				
$C_{y_{\dot\beta}}$, rad^{-1}				
C_{l_p}, rad^{-1}	◇	-0.161	-0.175[d]	-0.1578
C_{n_p}, rad^{-1}	-0.1466	○	○	-0.1515
C_{y_p}, rad^{-1}	0.492	0.500	□	0.488
C_{l_r}, rad^{-1}	0.0840	0.0690	○	0.0637
C_{n_r}, rad^{-1}	-0.1442	○	○	-0.1281
C_{y_r}, rad^{-1}	0.233	○	○	0.2129

Inertial derivatives	Handbook method	Inertial derivatives	Handbook method
$C_{l_{\dot p_I}}$, sec^2/rad	-24.64×10^{-6}	$C_{y_{\dot r_I}}$, sec^2/rad	$-1993. \times 10^{-6}$
$C_{n_{\dot p_I}}$, sec^2/rad	318.7×10^{-6}	$C_{l_{\ddot y_I}}$, sec^2/ft	1.029×10^{-6}
$C_{y_{\dot p_I}}$, sec^2/rad	532.3×10^{-6}	$C_{n_{\ddot y_I}}$, sec^2/ft	-24.19×10^{-6}
$C_{l_{\dot r_I}}$, sec^2/rad	-44.82×10^{-6}	$C_{y_{\ddot y_I}}$, sec^2/ft	39.34×10^{-6}
$C_{n_{\dot r_I}}$, sec^2/rad	1231.5×10^{-6}		

a. Formulation I b. (ref. 73) c. V. T. Only d. TA 67A

TABLE 19i.–SST LATERAL-DIRECTIONAL DERIVATIVES USED IN GENERAL COMPARISONS (CONTINUED)

Leading edge sweep = 72°

Altitude, h, ft 33 000	Ixx_b, rigid, slug-ft^2 .....6.27×10^6
Gross weight, W, lb 668 000	Izz_b, rigid, slug-ft^2 .....54.68×10^6
Mach number, M 1.1	Ixz_b, rigid, slug-ft^2 .....0.684×10^6
Dynamic pressure, $\bar{q}$, psf 470	Mass, M, rigid, slugs 20 745
Density ratio 0.33513	I_{xxb}, equiv elas slug-ft^2 .....6.298×10^6
Velocity, V_{c_1}, ft/sec 1080.07	I_{zzb}, equiv elas slug-ft^2 .....53.788×10^6
Lift, C_{L_1} 0.1579	I_{xzb}, equiv elas slug-ft^2 .....0.640×10^6
c.g. @ 0.64 C_R	Mass, M, equiv elas slug 20 496

Derivatives	Methods			
	Rigid			Equivalent elastic[a]
	Handbook methods		◇	
	TR1098 (ref. 72) ○	USAF (ref. 6) □	Wind tunnel	Handbook method ▽
C_{l_β}, deg^{-1}		-0.00280	-0.00304	-0.00158
C_{n_β}, deg^{-1}		0.00420	0.00275	◇
C_{y_β}, deg^{-1}		-0.00789	-0.008	-0.0071
$C_{l_{\dot\beta}}$, rad^{-1}				
$C_{n_{\dot\beta}}$, rad^{-1}				
$C_{y_{\dot\beta}}$, rad^{-1}				
C_{l_p}, rad^{-1}		-0.181	-0.181[d]	-0.1475
C_{n_p}, rad^{-1}		-0.0045	□	-0.0750
C_{y_p}, rad^{-1}		0.145	□	□
C_{l_r}, rad^{-1}		0.0400	○	0.0360
C_{n_r}, rad^{-1}	-0.240[c]	○	○	-0.168
C_{y_r}, rad^{-1}	0.306[c]	○	○	0.320

Inertial derivatives	Handbook method	Inertial derivatives	Handbook method
$C_{l_{\dot p_I}}$, sec^2/rad	-55.37×10^{-6}	$C_{y_{\dot r_I}}$, sec^2/rad	-3072×10^{-6}
$C_{n_{\dot p_I}}$, sec^2/rad	435.9×10^{-6}	$C_{l_{\ddot y_I}}$, sec^2/ft	2.275×10^{-6}
$C_{y_{\dot p_I}}$, sec^2/rad	714.7×10^{-6}	$C_{n_{\ddot y_I}}$, sec^2/ft	-37.68×10^{-6}
$C_{l_{\dot r_I}}$, sec^2/rad	-102.2×10^{-6}	$C_{y_{\ddot y_I}}$, sec^2/ft	58.75×10^{-6}
$C_{n_{\dot r_I}}$, sec^2/rad	1984×10^{-6}		

a. Formulation I b. (ref. 73) c. V. T. Only d. TA 67A

TABLE 19j.- SST LATERAL-DIRECTIONAL DERIVATIVES USED IN GENERAL COMPARISONS (CONTINUED)

Leading edge sweep = 72°

Altitude, h, ft 30 000	Ixx_b, rigid, slug-ft^2 .....3.92x10^6
Gross weight, W, lb 520 000	Izz_b, rigid, slug-ft^2 .....49.84x10^6
Mach number, M 1.3	Ixz_b, rigid, slug-ft^2 .....0.564x10^6
Dynamic pressure, $\bar{q}$, psf 750	Mass, M, rigid, slugs 16 149
Density ratio 0.37473	I_{xxb}, equiv elas slug-ft^2 .....4.087x10^6
Velocity, V_{c_1}, ft/sec 1293.31	I_{zzb}, equiv elas slug-ft^2 .....48.751x10^6
Lift, C_{L_1} 0.0770	I_{xzb}, equiv elas slug-ft^2 .....0.814x10^6
c.g. @ 0.64C_R	Mass, M, equiv elas slug 15 799

Derivatives	Methods			
	Rigid			Equivalent elastic[a]
	Handbook methods		◇	
	TR1098 (ref. 72) ○	USAF (ref. 6) □	Wind tunnel	Handbook method ▽
C_{l_β}, deg^{-1}		-0.00178	-0.00239	-0.00139
C_{n_β}, deg^{-1}		0.00496	0.00302	0.00399
C_{y_β}, deg^{-1}		-0.00839	-0.00905	-0.00651
$C_{l_{\dot\beta}}$, rad^{-1}				
$C_{n_{\dot\beta}}$, rad^{-1}				
$C_{y_{\dot\beta}}$, rad^{-1}				
C_{l_p}, rad^{-1}		-0.182	-0.174[d]	-0.123
C_{n_p}, rad^{-1}		-0.011	□	-0.273
C_{y_p}, rad^{-1}		0.0165	□	0.0152
C_{l_r}, rad^{-1}		0.0317	○	0.0139
C_{n_r}, rad^{-1}	-0.232[c]	○	○	-0.1925
C_{y_r}, rad^{-1}	0.341[c]	○	○	0.2928

Inertial derivatives	Handbook method	Inertial derivatives	Handbook method
$C_{l_{\dot p_I}}$, sec^2/rad	-168.3 x 10^{-6}	$C_{y_{\dot r_I}}$, sec^2/rad	-2202 x 10^{-6}
$C_{n_{\dot p_I}}$, sec^2/rad	1068 x 10^{-6}	$C_{l_{\ddot y_I}}$, sec^2/ft	2.569 x 10^{-6}
$C_{y_{\dot p_I}}$, sec^2/rad	1721 x 10^{-6}	$C_{n_{\ddot y_I}}$, sec^2/ft	-34.24 x 10^{-6}
$C_{l_{\dot r_I}}$, sec^2/rad	-99.91 x 10^{-6}	$C_{y_{\ddot y_I}}$, sec^2/ft	51.90 x 10^{-6}
$C_{n_{\dot r_I}}$, sec^2/rad	1460 x 10^{-6}		

a. Formulation I b. (ref. 73) c. V. T. Only d. TA 67A

TABLE 19k.–SST LATERAL-DIRECTIONAL DERIVATIVES USED IN GENERAL COMPARISONS (CONTINUED)

Leading edge sweep = 72°

Altitude, h, ft 24 000	Ixx_b, rigid, slug-ft^2 .....3.92×10^6
Gross weight, W, lb 520 000	Izz_b, rigid, slug-ft^2 .....49.84×10^6
Mach number, M 1.5	Ixz_b, rigid, slug-ft^2 .....0.564×10^6
Dynamic pressure, $\bar{q}$, psf 1300	Mass, M, rigid, slugs 16 149
Density ratio 0.46462	I_{xxb}, equiv elas slug-ft^2 .....4.165×10^6
Velocity, V_{c_1}, ft/sec 1530.45	I_{zzb}, equiv elas slug-ft^2 .....48.063×10^6
Lift, C_{L_1} 0.0444	I_{xzb}, equiv elas slug-ft^2 .....0.989×10^6
c.g. @ 0.64 C_R	Mass, M, equiv elas slug 15 581

Derivatives	Methods			
	Rigid			Equivalent elastic[a]
	Handbook methods		◇	
	TR1098 (ref. 72) ○	USAF (ref. 6) □	Wind tunnel	Handbook method ▽
C_{l_β}, deg^{-1}		-0.00130	-0.00219	-0.00078
C_{n_β}, deg^{-1}		0.00502	0.00263	0.00362
C_{y_β}, deg^{-1}		-0.00851	-0.00845	-0.00594
$C_{l_{\dot\beta}}$, rad^{-1}				
$C_{n_{\dot\beta}}$, rad^{-1}				
$C_{y_{\dot\beta}}$, rad^{-1}				
C_{l_p}, rad^{-1}		-0.182	-0.165[d]	-0.1095
C_{n_p}, rad^{-1}		-0.0070	□	-0.0081
C_{y_p}, rad^{-1}		0.0029	□	0.0003
C_{l_r}, rad^{-1}		0.0374	○	0.0150
C_{n_r}, rad^{-1}	-0.225[c]	○	○	-0.1712
C_{y_r}, rad^{-1}	0.331[c]	○	○	0.2585

Inertial derivatives	Handbook method	Inertial derivatives	Handbook method
$C_{l_{\dot p_I}}$, sec^2/rad	-167.2×10^{-6}	$C_{y_{\dot r_I}}$, sec^2/rad	-2121×10^{-6}
$C_{n_{\dot p_I}}$, sec^2/rad	950.1×10^{-6}	$C_{l_{\ddot y_I}}$, sec^2/ft	3.577×10^{-6}
$C_{y_{\dot p_I}}$, sec^2/rad	1523×10^{-6}	$C_{n_{\ddot y_I}}$, sec^2/ft	-32.09×10^{-6}
$C_{l_{\dot r_I}}$, sec^2/rad	-131.1×10^{-6}	$C_{y_{\ddot y_I}}$, sec^2/ft	48.54×10^{-6}
$C_{n_{\dot r_I}}$, sec^2/rad	1405×10^{-6}		

a. Formulation I b. (ref. 73) c. V.T. Only d. TA 67A

TABLE 191.–SST LATERAL-DIRECTIONAL DERIVATIVES USED IN GENERAL COMPARISONS (CONTINUED)

Leading edge sweep = 72°

Altitude, h, ft 60 500	Ixx_b, rigid, slug-ft^2 ..... 3.92×10^6
Gross weight, W, lb 520 000	Izz_b, rigid, slug-ft^2 ..... 49.84×10^6
Mach number, M 2.2	Ixz_b, rigid, slug-ft^2 ..... 0.564×10^6
Dynamic pressure, $\bar{q}$, psf 500	Mass, M, rigid, slugs 16 149
Density ratio 0.092704	I_{xxb}, equiv elas slug-ft^2 ..... 4.077×10^6
Velocity, V_{c_1}, ft/sec 2129.78	I_{zzb}, equiv elas slug-ft^2 ..... 48.802×10^6
Lift, C_{L_1} 0.0770	I_{xzb}, equiv elas slug-ft^2 ..... 0.788×10^6
c.g. @ 0.64 C_R	Mass, M, equiv elas slug 15 817

Derivatives	Methods			
	Rigid			Equivalent elastic[a]
	Handbook methods		◇	
	TR1098 (ref. 72) ○	USAF (ref. 6) □	Wind tunnel	Handbook method ▽
C_{l_β}, deg^{-1}		-0.00092	-0.00175	-0.00074
C_{n_β}, deg^{-1}		0.00383	0.00177	0.00312
C_{y_β}, deg^{-1}		-0.00705	-0.00632	-0.00617
$C_{l_{\dot\beta}}$, rad^{-1}				
$C_{n_{\dot\beta}}$, rad^{-1}				
$C_{y_{\dot\beta}}$, rad^{-1}				
C_{l_p}, rad^{-1}		-0.150	-0.140[d]	-0.1170
C_{n_p}, rad^{-1}		-0.0082	□	-0.0246
C_{y_p}, rad^{-1}		-0.0040	□	0.0011
C_{l_r}, rad^{-1}		0.0350	○	0.0188
C_{n_r}, rad^{-1}	-0.20[c]	○	○	-0.1722
C_{y_r}, rad^{-1}	0.296[c]	○	○	0.2656

Inertial derivatives	Handbook method	Inertial derivatives	Handbook method
$C_{l_{\dot p_I}}$, sec^2/rad	-167.2×10^{-6}	$C_{y_{r_I}}$, sec^2/rad	-2162×10^{-6}
$C_{n_{\dot p_I}}$, sec^2/rad	991.5×10^{-6}	$C_{l_{\ddot y_I}}$, sec^2/ft	3.115×10^{-6}
$C_{y_{\dot p_I}}$, sec^2/rad	1611×10^{-6}	$C_{n_{\ddot y_I}}$, sec^2/ft	-31.84×10^{-6}
$C_{l_{\dot r_I}}$, sec^2/rad	-135.3×10^{-6}	$C_{y_{\ddot y_I}}$, sec^2/ft	49.15×10^{-6}
$C_{n_{\dot r_I}}$, sec^2/rad	1402×10^{-6}		

a. Formulation I b. (ref. 73) c. V. T. Only d. TA 67A

TABLE 19m.–SST LATERAL-DIRECTIONAL DERIVATIVES USED IN GENERAL COMPARISONS (CONCLUDED)

Leading edge sweep = 72°

Altitude, h, ft 49 000	Ixx_b, rigid, slug-ft^2 ..... 3.92×10^6
Gross weight, W, lb 520 000	Izz_b, rigid, slug-ft^2 ..... 49.84×10^6
Mach number, M 2.7	Ixz_b, rigid, slug-ft^2 ..... 0.564×10^6
Dynamic pressure, $\bar{q}$, psf 1300	Mass, M, rigid, slugs 16 149
Density ratio 0.16061	I_{xxb}, equiv elas slug-ft^2 ..... 4.179×10^6
Velocity, V_{c_1}, ft/sec 2613.82	I_{zzb}, equiv elas slug-ft^2 ..... 48.180×10^6
Lift, C_{L_1} 0.0444	I_{xzb}, equiv elas slug-ft^2 ..... 0.891×10^6
c.g. @ 0.64 C_R	Mass, M, equiv elas slug 15 623

Derivatives	Methods			
	Rigid			Equivalent elastic[a]
	Handbook methods		◇	
	TR1098 (ref. 72) ○	USAF (ref. 6) □	Wind tunnel	Handbook method ▽
C_{l_β}, deg^{-1}		-0.00084	-0.00115	-0.00071
C_{n_β}, deg^{-1}		0.00359	0.00140	0.00306
C_{y_β}, deg^{-1}		-0.00573	-0.00479	-0.00568
$C_{l_{\dot\beta}}$, rad^{-1}				
$C_{n_{\dot\beta}}$, rad^{-1}				
$C_{y_{\dot\beta}}$, rad^{-1}				
C_{l_p}, rad^{-1}		-0.136	-0.124[d]	-0.0966
C_{n_p}, rad^{-1}		0.0125	□	-0.0060
C_{y_p}, rad^{-1}		-0.0004	□	-0.0009
C_{l_r}, rad^{-1}		0.0342	○	0.0194
C_{n_r}, rad^{-1}	-0.181[c]	○	○	-0.1520
C_{y_r}, rad^{-1}	0.270[c]	○	○	0.2353

Inertial derivatives	Handbook method	Inertial derivatives	Handbook method
$C_{l_{\dot p_I}}$, sec^2/rad	-168.2×10^{-6}	$C_{y_{\dot r_I}}$, sec^2/rad	-2021×10^{-6}
$C_{n_{\dot p_I}}$, sec^2/rad	891.1×10^{-6}	$C_{l_{\ddot y_I}}$, sec^2/ft	3.584×10^{-6}
$C_{y_{\dot p_I}}$, sec^2/rad	1450×10^{-6}	$C_{n_{\ddot y_I}}$, sec^2/ft	-28.95×10^{-6}
$C_{l_{\dot r_I}}$, sec^2/rad	-162.4×10^{-6}	$C_{y_{\ddot y_I}}$, sec^2/ft	44.95×10^{-6}
$C_{n_{\dot r_I}}$, sec^2/rad	1301×10^{-6}		

a. Formulation I b. (ref. 73) c. V. T. Only d. TA-67A

8.2.3 Data tabulation - rigid and equivalent elastic derivatives and coefficients - special comparisons. — The data presented in this section are those used for the special comparisons with the completely elastic airplane mathematical model. The stability derivatives differed because the c.g. positions were something other than $0.25\bar{c}$ for the Boeing 707-320B and 0.64 C_R for the SST configurations. Table 20 lists the flight conditions used to investigate the longitudinal motions and the corresponding location of the data. The lateral-directional data were not adjusted for the c.g. changes; instead, the data presented in par. 8.2.2 for the general comparisons were used.

TABLE 20. – LIST OF TABLES OF DERIVATIVES AND COEFFICIENTS USED IN SPECIAL COMPARISONS

Altitude, ft	Dynamic pressure, $\bar{q}$, psf	Mach number	Weight, lb	Table number	Wing leading edge sweep
707-320B					
10 000	306	0.548	268 000	21a	
35 000	251	0.850	↓	21b	
SST					
8 500	98	0.3	370 000	22a	30°
9 500	260	0.5	↓	22b	↓
32 500	98	0.5	675 000	22c	42°
23 500	470	0.9	↓	22d	↓
47 500	98	0.7	668 000	22e	72°
33 000	470	1.1	↓	22f	↓
49 000	1300	2.7	520 000	22g	↓
65 000	600	↓	↓	22h	↓

TABLE 21a. - 707-320B LONGITUDINAL DERIVATIVES AND COEFFICIENTS USED IN SPECIAL COMPARISONS

Altitude, h, ft 10 000	Drag, C_{D_1} 0.0145
Gross weight, W, lb 268 000	
Mach number, M 0.548	Lift, C_{L_1} 0.3028
Dynamic pressure, $\bar{q}$, psf ... 306	Iyy, rigid, slug-ft^2 ..... 5.025×10^6
Density ratio 0.73859	Iyy, equiv elas slug-ft^2 ..... 4.497×10^6
Velocity, V_{c_1}, ft/sec ..... 590.42 cg @ 0.23$\bar{c}$	

Derivatives	Rigid		Equivalent elastic[a]	
		Method		Method
C_{L_o}	0.2275	TA 67A	0.1548	TA 67A
C_{m_o}	-0.091	↓	-0.0029	↓
C_{L_α}, deg^{-1}	0.096	↓	0.08063	↓
C_{m_α}, deg^{-1}	-0.0252	↓	-0.0161	↓
C_{D_α}, deg^{-1}	0.005	↓	0.0042	↓
$C_{L_{\dot\alpha}}$, rad^{-1}	2.99	Ref. 6	2.99	Ref. 6 (Rigid)
$C_{m_{\dot\alpha}}$, rad^{-1}	-13.27	↓	-13.27	↓
$C_{D_{\dot\alpha}}$, rad^{-1}				
C_{L_q}, rad^{-1}	11.1	TA 67A	7.64	TA 67A
C_{m_q}, rad^{-1}	-17.7	↓	-14.05	TA 67A
C_{D_q} rad^{-1}	0.144	↓	0.144	TA 67A (Rigid)
C_{L_u}, rad^{-1}	0.109	↓	0.04658	TA 67A
C_{m_u}, rad^{-1}	-0.071	↓	-0.01644	TA 67A
C_{D_u}, rad^{-1}	0.000375	↓	0.00025	Wind Tunnel
$C_{L_{\ddot\theta_I}}$, (rad/sec^2)$^{-1}$	b	—	-0.0281	TA 67A
$C_{m_{\ddot\theta_I}}$, (rad/sec^2)$^{-1}$	b	—	0.0263	↓
$C_{L_{\delta_E}}$, deg^{-1}	0.00745	TA 67A	0.0055	↓
$C_{m_{\delta_E}}$, deg^{-1}	-0.0214	↓	-0.0152	↓

a. Formulation II

b. Not Applicable

TABLE 21b.–707-320B LONGITUDINAL DERIVATIVES AND COEFFICIENTS USED IN SPECIAL COMPARISONS (CONCLUDED)

Altitude, h, ft 35 000	Drag, C_{D_1} 0.02305
Gross weight, W, lb..... 268 000	
Mach number, M..... 0.85	Lift, C_{L_1} 0.3691
Dynamic pressure, $\bar{q}$, psf... 251	Iyy, rigid, slug-ft^2 ..... 5.025×10^6
Density ratio..... 0.31058	
Velocity, V_{c_1}, ft/sec ..... 827.17 cg @ 0.23$\bar{c}$	Iyy, equiv elas slug-ft^2 ..... 4.488×10^6

Derivatives	Rigid		Equivalent elastic[a]	
		Method		Method
C_{L_o}	0.2825	TA 67A	0.1885	TA 67A
C_{m_o}	-0.104	↓	-0.0257	↓
C_{L_α}, deg^{-1}	0.115	↓	0.09505	↓
C_{m_α}, deg^{-1}	-0.0342	↓	-0.0218	↓
C_{D_α}, deg^{-1}	0.0074	↓	0.0045	↓
$C_{L_{\dot{\alpha}}}$, rad^{-1}	-3.86	Ref. 6	-3.86	Ref. 6 (Rigid)
$C_{m_{\dot{\alpha}}}$, rad^{-1}	-24.20	↓	-24.20	↓
$C_{D_{\dot{\alpha}}}$, rad^{-1}				
C_{L_q}, rad^{-1}	14.9	TA 67A	8.92	TA 67A
C_{m_q}, rad^{-1}	-20.95	↓	-16.69	
C_{D_q}, rad^{-1}	0.166	↓	0.166	TA 67A (Rigid)
C_{L_u}, rad^{-1}	0.2705	↓	0.2295	TA 67A
C_{m_u}, rad^{-1}	-0.238	↓	-0.08712	↓
C_{D_u}, rad^{-1}	0.00191	↓	0.00356	Wind Tunnel
$C_{L_{\ddot{\theta}_I}}$, (rad/sec^2)$^{-1}$	b		-0.0334	TA 67A
$C_{m_{\ddot{\theta}_I}}$, (rad/sec^2)$^{-1}$	b		0.0327	↓
$C_{L_{\delta_E}}$, deg^{-1}	0.00872	TA 67A	0.00630	↓
$C_{m_{\delta_E}}$, deg^{-1}	-0.0267	↓	-0.0186	↓

a. Formulation II

b. Not Applicable

TABLE 22a.–SST LONGITUDINAL DERIVATIVES AND COEFFICIENTS USED IN SPECIAL COMPARISONS

Leading edge sweep = 30°

Altitude, h, ft	8 500	Drag, C_{D_1}	0.098
Gross weight, W, lb	370 000		
Mach number, M	0.3	Lift, C_{L_1}	0.4198
Dynamic pressure, $\bar{q}$, psf	98	Iyy, rigid, slug-ft^2	40.2×10^6
Density ratio	0.77408		
Velocity, V_{c_1}, ft/sec	325.01	Iyy, equiv elas slug-ft^2	39.88×10^6
	@ 0.574 C_R		

Derivatives	Rigid		Equivalent elastic[a]	
		Method		Method
C_{L_o}	0.15761	TA 67A	0.21240	TA 67A
C_{m_o}	0.0105	↓	0.0088	↓
C_{L_α}, deg^{-1}	0.0564	↓	0.0559	↓
C_{m_α}, deg^{-1}	-0.00135	↓	-0.00177	↓
C_{D_α}, deg^{-1}	0.0098	↓	0.01107	↓
$C_{L_{\dot{\alpha}}}$, rad^{-1}	0.462	Ref. 6	0.462	Ref. 6 (Rigid)
$C_{m_{\dot{\alpha}}}$, rad^{-1}	-0.1725	↓	-0.1725	↓
$C_{D_{\dot{\alpha}}}$, rad^{-1}				
C_{L_q}, rad^{-1}	2.06	TA 67A	1.96	TA 67A
C_{m_q}, rad^{-1}	-0.412	↓	-0.406	↓
C_{D_q}, rad^{-1}				
C_{L_u}, rad^{-1}	0.0288	TA 67A	0.0193	TA 67A
C_{m_u}, rad^{-1}	0.00166	↓	0.0009	↓
C_{D_u}, rad^{-1}	0.0033	↓	0.0033	Wind Tunnel
$C_{L_{\ddot{\theta}_I}}$, (rad/sec^2)$^{-1}$	b		-0.0657	TA 67A
$C_{m_{\ddot{\theta}_I}}$, (rad/sec^2)$^{-1}$	b		0.0023	↓
$C_{L_{\delta_E}}$, deg^{-1}	0.00705	TA 67A	0.00705	TA 67A (Rigid)
$C_{m_{\delta_E}}$, deg^{-1}	-0.00195	↓	-0.00195	↓

a. Formulation II

b. Not Applicable

TABLE 22b.–SST LONGITUDINAL DERIVATIVES AND COEFFICIENTS USED IN SPECIAL COMPARISONS (CONTINUED)

Leading edge sweep = 30°

Altitude, h, ft 9 500	Drag, C_{D_1} 0.032
Gross weight, W, lb 370 000	
Mach number, M 0.5	Lift, C_{L_1} 0.1581
Dynamic pressure, $\bar{q}$, psf ... 260	Iyy, rigid, slug-ft^2 ..... 40.2×10^6
Density ratio 0.75032	
Velocity, V_{c_1}, ft/sec ..... 539.69 cg @ $0.574 C_R$	Iyy, equiv elas slug-ft^2 ..... 39.201×10^6

Derivatives	Rigid		Equivalent elastic[a]	
		Method		Method
C_{L_o}	0.16888	TA 67A	0.20396	TA 67A
C_{m_o}	0.0120	↓	0.0074	↓
C_{L_α}, deg^{-1}	0.0587	↓	0.0570	↓
C_{m_α}, deg^{-1}	-0.00181	↓	-0.00243	↓
C_{D_α}, deg^{-1}	0.0102	↓	0.00204	↓
$C_{L_{\dot\alpha}}$, rad^{-1}	0.329	Ref. 6	0.329	Ref. 6 (Rigid)
$C_{m_{\dot\alpha}}$, rad^{-1}	-0.237	↓	-0.237	↓
$C_{D_{\dot\alpha}}$, rad^{-1}				
C_{L_q}, rad^{-1}	2.08	TA 67A	1.79	TA 67A
C_{m_q}, rad^{-1}	-0.420	↓	-0.416	↓
C_{D_q}, rad^{-1}				
C_{L_u}, rad^{-1}	0.0315	TA 67A	0.0233	TA 67A
C_{m_u}, rad^{-1}	0.0001	↓	-0.00285	↓
C_{D_u}, rad^{-1}	0.0047	↓	0.00715	Wind Tunnel
$C_{L_{\ddot\Theta_I}}$, (rad/sec^2)$^{-1}$	b		-0.0592	TA 67A
$C_{m_{\ddot\Theta_I}}$, (rad/sec^2)$^{-1}$	b		0.0017	↓
$C_{L_{\delta_E}}$, deg^{-1}	0.0073	TA 67A	0.0073	TA 67A (Rigid)
$C_{m_{\delta_E}}$, deg^{-1}	-0.00209	↓	-0.00209	↓

a. Formulation II

b. Not Applicable

TABLE 22c.–SST LONGITUDINAL DERIVATIVES AND COEFFICIENTS USED IN SPECIAL COMPARISONS (CONTINUED)

Leading edge sweep = 42°

Altitude, h, ft 32 500	Drag, C_{D_1} 0.057
Gross weight, W, lb.....675 000	
Mach number, M.....0.5	Lift, C_{L_1} 0.7659
Dynamic pressure, $\bar{q}$, psf...98	Iyy, rigid, slug-ft^2 .....47.2x10^6
Density ratio.....0.35455	
Velocity, V_{c_1}, ft/sec .....492.02 cg @ 0.613 C_R	Iyy, equiv elas slug-ft^2.....47.437x10^6

Derivatives	Rigid		Equivalent elastic[a]	
		Method		Method
C_{L_o}	0.11181	TA 67A	0.12110	TA 67A
C_{m_o}	0.0109	↓	0.0100	↓
C_{L_α}, deg^{-1}	0.0511	↓	0.0498	↓
C_{m_α}, deg^{-1}	-0.00056	↓	-0.000635	↓
C_{D_α}, deg^{-1}	-0.0089	↓	0.0237	↓
$C_{L_{\dot\alpha}}$, rad^{-1}	0.364	Ref. 6	0.364	Ref. 6 (Rigid)
$C_{m_{\dot\alpha}}$, rad^{-1}	-0.193	↓	-0.193	↓
$C_{D_{\dot\alpha}}$, rad^{-1}				
C_{L_q}, rad^{-1}	1.62	TA 67A	1.49	TA 67A
C_{m_q}, rad^{-1}	-0.389	↓	-0.376	↓
C_{D_q}, rad^{-1}				
C_{L_u}, rad^{-1}	0.0748	TA 67A	0.0738	TA 67A
C_{m_u}, rad^{-1}	-0.0015	↓	-0.002	↓
C_{D_u}, rad^{-1}	0.011	↓	0.005	Wind Tunnel
$C_{L_{\ddot\theta_I}}$, (rad/sec^2)$^{-1}$	b		-0.0433	TA 67A
$C_{m_{\ddot\theta_I}}$, (rad/sec^2)$^{-1}$	b		-0.0017	↓
$C_{L_{\delta_E}}$, deg^{-1}	0.0072	TA 67A	0.0072	TA 67A (Rigid)
$C_{m_{\delta_E}}$, deg^{-1}	-0.00184	↓	-0.00184	↓

a. Formulation II

b. Not Applicable

TABLE 22d.–SST LONGITUDINAL DERIVATIVES AND COEFFICIENTS USED IN SPECIAL COMPARISONS (CONTINUED)

Leading edge sweep = 42°

Altitude, h, ft 23 500	Drag, C_{D_1} 0.014
Gross weight, W, lb 675 000	Lift, C_{L_1} 0.1596
Mach number, M 0.9	Iyy, rigid, slug-ft^2 ..... 47.2×10^6
Dynamic pressure, $\bar{q}$, psf .. 470	Iyy, equiv elas slug-ft^2 ..... 48.136×10^6
Density ratio 0.47285	
Velocity, V_{c_1}, ft/sec ..... 920.15 @ 0.613 C_R cg	

Derivatives	Rigid		Equivalent elastic[a]	
		Method		Method
C_{L_o}	0.13745	TA 67A	0.11635	TA 67A
C_{m_o}	0.0139	↓	0.0137	↓
C_{L_α}, deg^{-1}	0.0602	↓	0.0506	↓
C_{m_α}, deg^{-1}	-0.002125	↓	-0.00229	↓
C_{D_α}, deg^{-1}	0.0105	↓	0.00276	↓
$C_{L_{\dot{\alpha}}}$, rad^{-1}	-0.544	Ref. 6	-0.554	Ref. 6 (Rigid)
$C_{m_{\dot{\alpha}}}$, rad^{-1}	-0.428	↓	-0.428	↓
$C_{D_{\dot{\alpha}}}$, rad^{-1}				
C_{L_q}, rad^{-1}	1.785	TA 67A	1.19	TA 67A
C_{m_q}, rad^{-1}	-0.492	↓	-0.428	↓
C_{D_q}, rad^{-1}				
C_{L_u}, rad^{-1}	0.1187	TA 67A	0.0538	TA 67A
C_{m_u}, rad^{-1}	-0.0178	↓	-0.0162	↓
C_{D_u}, rad^{-1}	0.0117	↓	0.0117	Wind Tunnel (Rigid)
$C_{L_{\ddot{\theta}_I}}$, (rad/sec^2)$^{-1}$	b		-0.0351	TA 67A
$C_{m_{\ddot{\theta}_I}}$, (rad/sec^2)$^{-1}$	b		-0.0014	↓
$C_{L_{\delta_E}}$, deg^{-1}	0.00875	TA 67A	0.00875	TA 67A (Rigid)
$C_{m_{\delta_E}}$, deg^{-1}	-0.00275	↓	-0.00275	↓

a. Formulation II

b. Not Applicable

TABLE 22e.–SST LONGITUDINAL DERIVATIVES AND COEFFICIENTS USED IN SPECIAL COMPARISONS (CONTINUED)

Leading edge sweep = 72°

Altitude, h, ft	47 500	Drag, C_{D_1}	0.11
Gross weight, W, lb	668 000	Lift, C_{L_1}	0.7580
Mach number, M	0.70	Iyy, rigid, slug-ft^2	48.3×10^6
Dynamic pressure, $\bar{q}$, psf	98	Iyy, equiv elas slug-ft^2	48.398×10^6
Density ratio	0.17261		
Velocity, V_{c_1}, ft/sec	677.66		
	cg @ 0.618 C_R		

Derivatives	Rigid		Equivalent elastic[a]	
		Method		Method
C_{L_o}	0.01542	TA 67A	0.02108	TA 67A
C_{m_o}	0.0082	↓	0.0081	↓
C_{L_α}, deg^{-1}	0.0306	↓	0.0306	↓
C_{m_α}, deg^{-1}	-0.000853	↓	-0.000563	↓
C_{D_α}, deg^{-1}	0.0053	↓	0.0262	↓
$C_{L_{\dot\alpha}}$, rad^{-1}	-0.32	Ref. 6	-0.32	Ref. 6 (Rigid)
$C_{m_{\dot\alpha}}$, rad^{-1}	-0.262	↓	-0.262	↓
$C_{D_{\dot\alpha}}$, rad^{-1}				
C_{L_q}, rad^{-1}	1.20	TA 67A	1.15	TA 67A
C_{m_q}, rad^{-1}	-0.352	↓	-0.348	↓
C_{D_q}, rad^{-1}				
C_{L_u}, rad^{-1}	0.089	TA 67A	0.0934	TA 67A
C_{m_u}, rad^{-1}	0.0182	↓	-0.0248	↓
C_{D_u}, rad^{-1}	0.0011	↓	0.0011	TA 67A (Rigid)
$C_{L_{\ddot\theta_I}}$, (rad/sec^2)$^{-1}$	b		-0.0319	TA 67A
$C_{m_{\ddot\theta_I}}$, (rad/sec^2)$^{-1}$	b		-0.0007	↓
$C_{L_{\delta_E}}$, deg^{-1}	0.0076	TA 67A	0.0076	TA 67A (Rigid)
$C_{m_{\delta_E}}$, deg^{-1}	-0.00227	↓	-0.00227	↓

a. Formulation II

b. Not Applicable

TABLE 22f.–SST LONGITUDINAL DERIVATIVES AND COEFFICIENTS USED IN SPECIAL COMPARISONS (CONTINUED)

Leading edge sweep = 72°

Altitude, h, ft 33 000	Drag, C_{D_1} 0.0232
Gross weight, W, lb.....668 000	
Mach number, M.....1.1	Lift, C_{L_1} 0.1579
Dynamic pressure, $\bar{q}$, psf...470	
Density ratio.....0.33513	Iyy, rigid, slug-ft^2.....48.3x10^6
Velocity, V_{c_1}, ft/sec .....1080.07 @ 0.618 C_R	Iyy, equiv elas slug-ft^2.....47.832x10^6
c_g	

Derivatives	Rigid		Equivalent elastic[a]	
		Method		Method
C_{L_o}	0.01176	TA 67A	0.02966	TA 67A
C_{m_o}	0.0110	↓	0.0110	↓
C_{L_α}, deg^{-1}	0.0345	↓	0.0323	↓
C_{m_α}, deg^{-1}	-0.00212	↓	-0.00193	↓
C_{D_α}, deg^{-1}	-0.0061	↓	0.00503	↓
$C_{L_{\dot\alpha}}$, rad^{-1}	-0.17	Ref. 6	-0.17	Ref. 6 (Rigid)
$C_{m_{\dot\alpha}}$, rad^{-1}	-0.11	↓	-0.11	↓
$C_{D_{\dot\alpha}}$, rad^{-1}				
C_{L_q}, rad^{-1}	1.46	TA 67A	1.00	TA 67A
C_{m_q}, rad^{-1}	-0.511	↓	-0.408	↓
C_{D_q}, rad^{-1}				
C_{L_u}, rad^{-1}	0.0364	TA 67A	0.0311	TA 67A
C_{m_u}, rad^{-1}	0.0071	↓	-0.0102	↓
C_{D_u}, rad^{-1}	0.0088	↓	0.0165	Wind Tunnel
$C_{L_{\ddot\theta_I}}$, (rad/sec^2)$^{-1}$	b		-0.0295	TA 67A
$C_{m_{\ddot\theta_I}}$, (rad/sec^2)$^{-1}$	b		0.0007	↓
$C_{L_{\delta_E}}$, deg^{-1}	0.0094	TA 67A	0.0094	TA 67A (Rigid)
$C_{m_{\delta_E}}$, deg^{-1}	-0.00344	↓	-0.00344	↓

a. Formulation II

b. Not Applicable

TABLE 22g.–SST LONGITUDINAL DERIVATIVES AND COEFFICIENTS USED IN SPECIAL COMPARISONS (CONTINUED)

Leading edge sweep = 72°

Altitude, h, ft 49 000	Drag, C_{D_1} 0.007
Gross weight, W, lb.....520 000	
Mach number, M 2.7	Lift, C_{L_1} 0.0444
Dynamic pressure, $\bar{q}$, psf...1300	Iyy, rigid, slug-ft^2 .....47.6x10^6
Density ratio.....0.16061	
Velocity, V_{c_1}, ft/sec.....2613.82 cg @ 0.63C_R	Iyy, equiv elas slug-ft^2.....60.180x10^6

Derivatives	Rigid		Equivalent elastic[a]	
		Method		Method
C_{L_o}	0.03141	TA 67A	0.03723	TA 67A
C_{m_o}	0.0077	↓	0.0041	↓
C_{L_α}, deg^{-1}	0.0255	↓	0.0229	↓
C_{m_α}, deg^{-1}	-0.00144	↓	-0.00156	↓
C_{D_α}, deg^{-1}	0.0045	↓	0.00106	↓
$C_{L_{\dot\alpha}}$, rad^{-1}	-0.101	Ref. 6	-0.101	Ref. 6
$C_{m_{\dot\alpha}}$, rad^{-1}	0.057	↓	0.057	↓
$C_{D_{\dot\alpha}}$, rad^{-1}				
C_{L_q}, rad^{-1}	0.421	TA 67A	0.101	TA 67A
C_{m_q}, rad^{-1}	-0.319	↓	-0.317	↓
C_{D_q}, rad^{-1}				
C_{L_u}, rad^{-1}	-0.0375	TA 67A	-1.615	TA 67A
C_{m_u}, rad^{-1}	-0.00162	↓	0.0072	↓
C_{D_u}, rad^{-1}	-0.0014	↓	-0.001	Wind Tunnel
$C_{L_{\ddot\theta_I}}$, (rad/sec^2)$^{-1}$	b		-0.0223	TA 67A
$C_{m_{\ddot\theta_I}}$, (rad/sec^2)$^{-1}$	b		-0.0068	↓
$C_{L_{\delta_E}}$, deg^{-1}	0.0020	TA 67A	0.0020	TA 67A (Rigid)
$C_{m_{\delta_E}}$, deg^{-1}	-0.00081	↓	-0.00081	↓

a. Formulation II

b. Not Applicable

TABLE 22h.–SST LONGITUDINAL DERIVATIVES AND COEFFICIENTS USED IN SPECIAL COMPARISONS (CONCLUDED)

Leading edge sweep = 72°

Altitude, h, ft 65 000	Drag, C_{D_1} 0.007
Gross weight, W, lb..... 520 000	
Mach number, M..... 2.7	Lift, C_{L_1} 0.0964
Dynamic pressure, $\bar{q}$, psf... 600	Iyy, rigid, slug-ft^2 ..... 47.6×10^6
Density ratio..... 0.0741	Iyy, equiv elas slug-ft^2 ..... 53.4×10^6
Velocity, V_{c_1}, ft/sec ..... 2613.82 @ 0.63 C_R	

Derivatives	Rigid		Equivalent elastic[a]	
		Method		Method
C_{L_o}	0.03141	TA 67A	0.03517	TA 67A
C_{m_o}	0.0077	↓	0.0041	↓
C_{L_α}, deg^{-1}	0.0255	↓	0.0242	↓
C_{m_α}, deg^{-1}	-0.00144	↓	-0.00132	↓
C_{D_α}, deg^{-1}	0.0045	↓	0.00106	↓
$C_{L_{\dot\alpha}}$, rad^{-1}	-0.101	Ref. 6	-0.101	Ref. 6 (Rigid)
$C_{m_{\dot\alpha}}$, rad^{-1}	0.057	↓	0.057	↓
$C_{D_{\dot\alpha}}$, rad^{-1}				
C_{L_q}, rad^{-1}	0.421	TA 67A	0.178	TA 67A
C_{m_q}, rad^{-1}	-0.319	↓	-0.317	↓
C_{D_q}, rad^{-1}				
C_{L_u}, rad^{-1}	-0.0375	TA 67A	-1.615	TA 67A
C_{m_u}, rad^{-1}	-0.00162	↓	0.0072	↓
C_{D_u}, rad^{-1}	-0.0014	↓	-0.001	Wind Tunnel
$C_{L_{\ddot\theta_I}}$, (rad/sec^2)$^{-1}$	b		-0.0223	TA 67A
$C_{m_{\ddot\theta_I}}$, (rad/sec^2)$^{-1}$	b		-0.0068	↓
$C_{L_{\delta_E}}$, deg^{-1}	0.0020	TA 67A	0.0020	TA 67A (Rigid)
$C_{m_{\delta_E}}$, deg^{-1}	-0.00081	↓	-0.00081	↓

a. Formulation II

b. Not Applicable

8.3 Static Stability Data

This section presents all the substantiating data (figs. 49 through 60) for the static stability data discussed in Section 4. The stability derivatives and coefficients used to calculate the data of this section have been tabulated in par. 8.2.

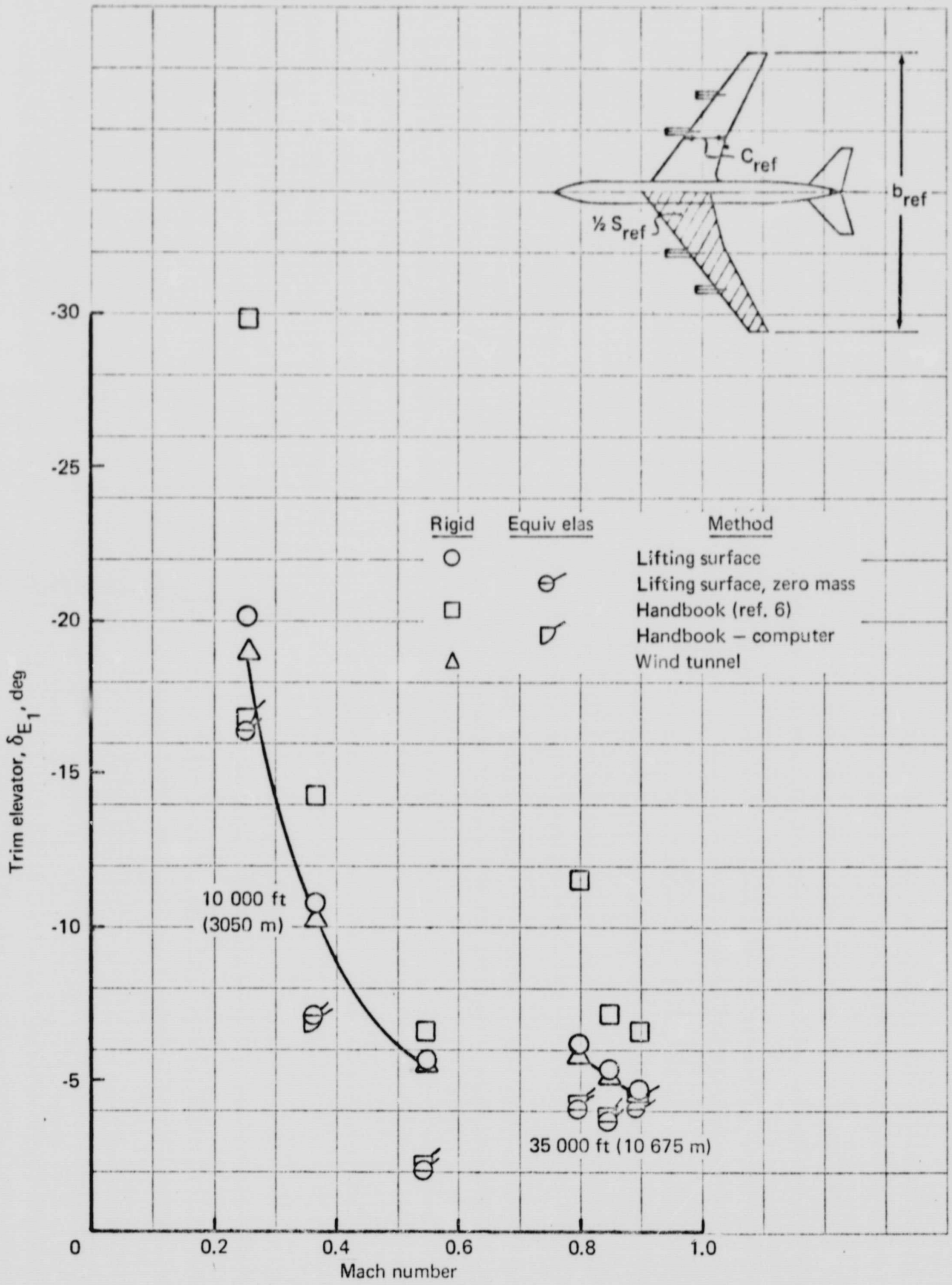

FIGURE 49. COMPARISON OF METHODS FOR TRIM ELEVATOR – 707-320B

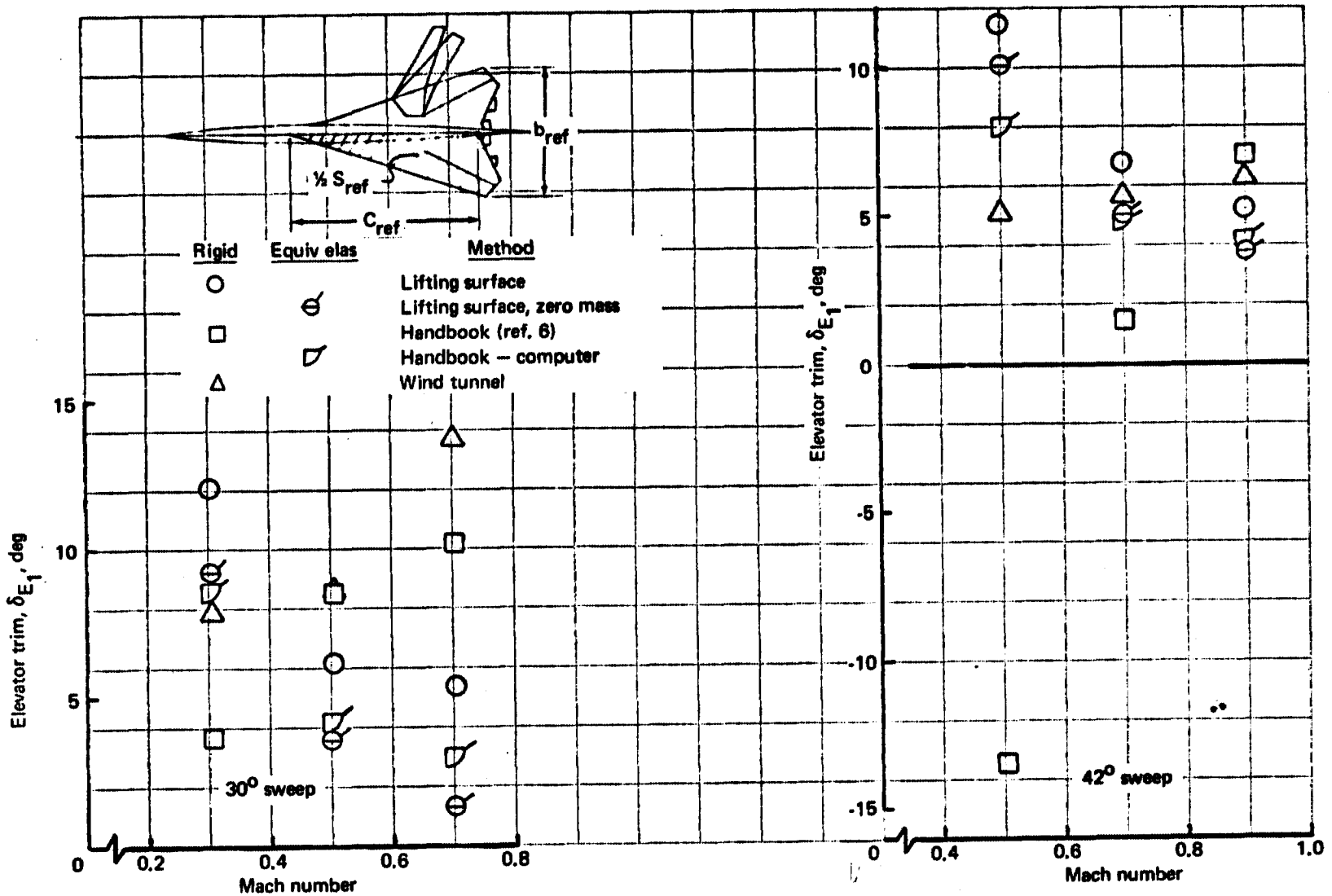

FIGURE 50. COMPARISON OF METHODS FOR TRIM ELEVATOR – 30° AND 42° SST

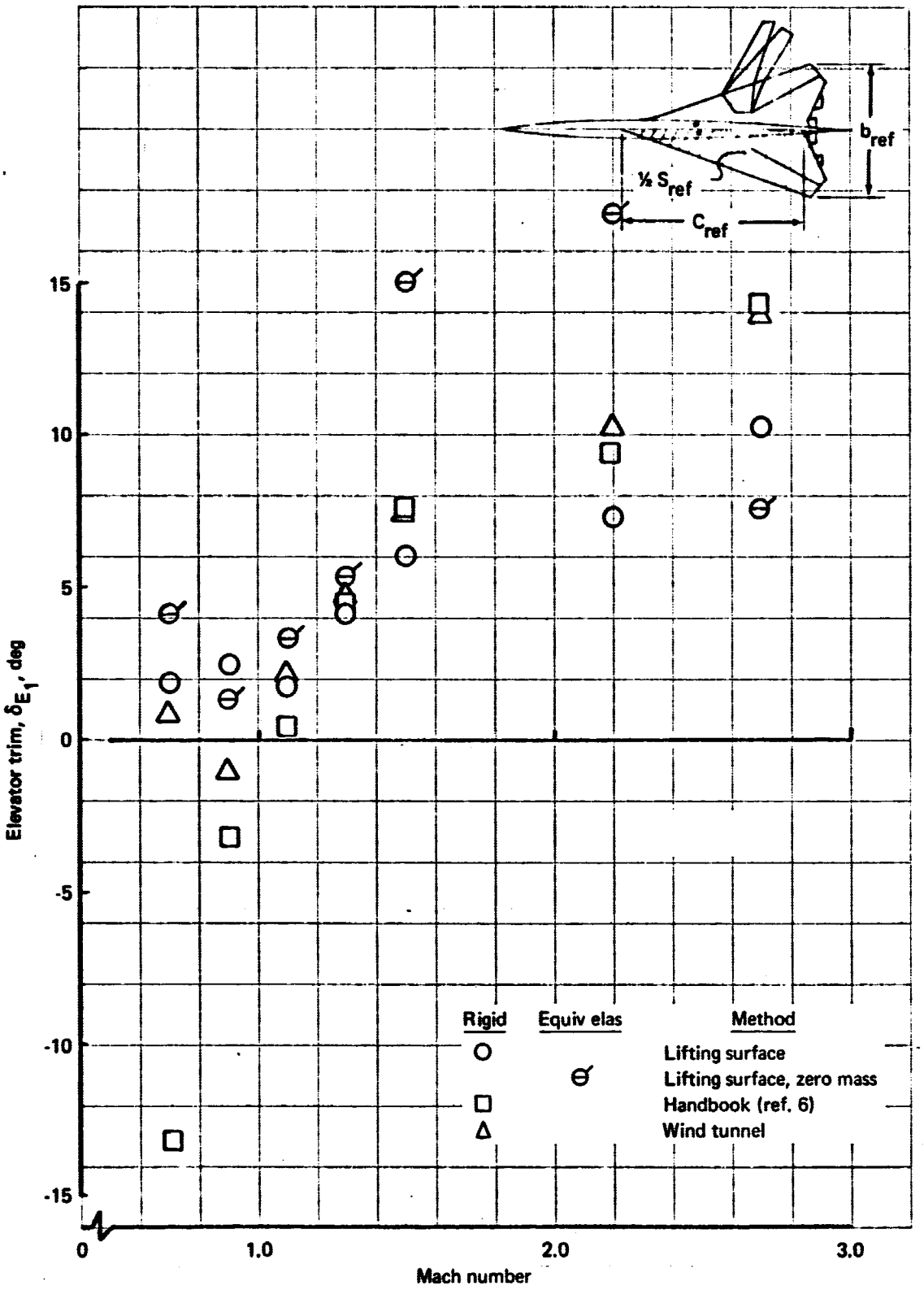

FIGURE 51. COMPARISON OF METHODS FOR TRIM ELEVATOR – 72° SST

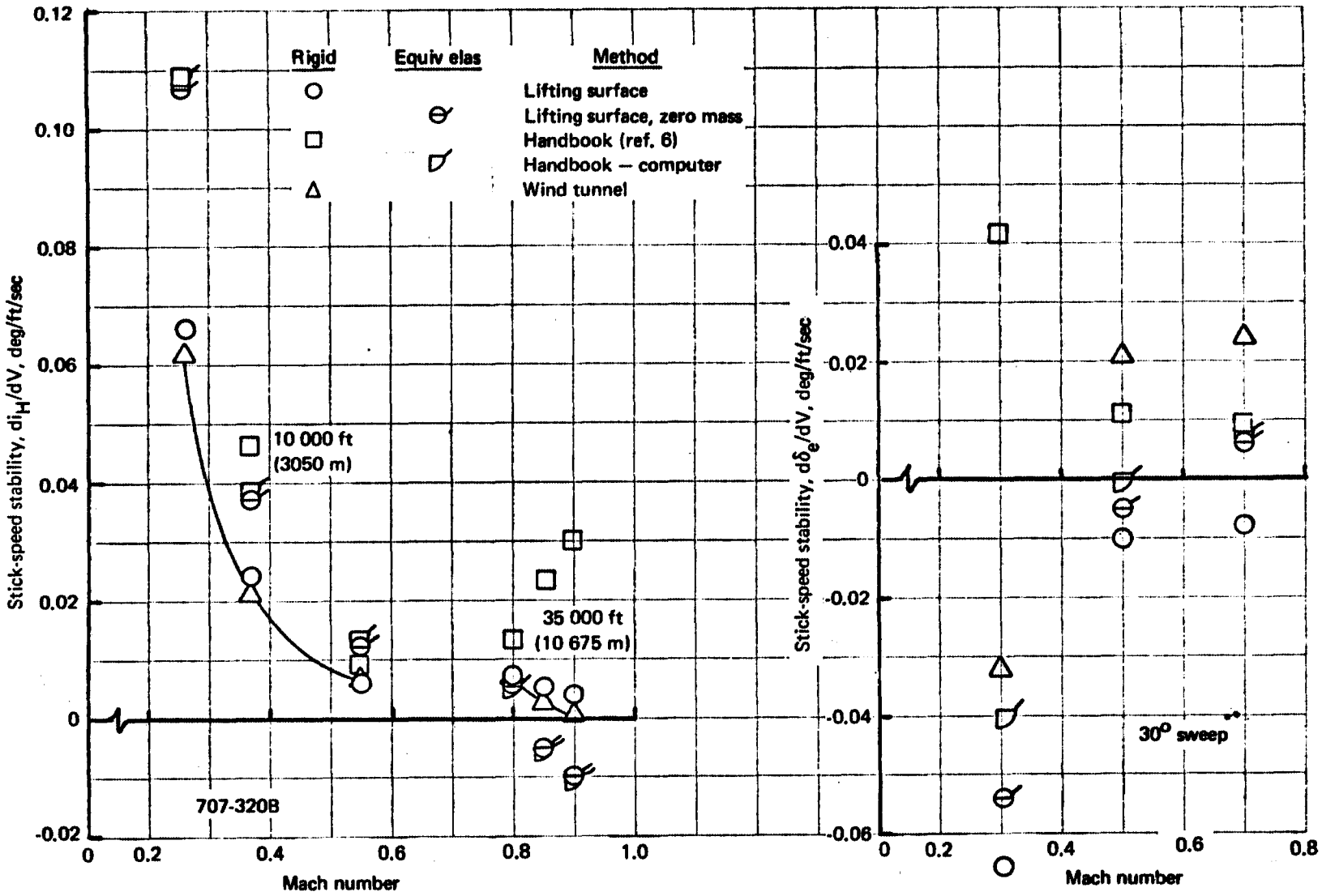

FIGURE 52. COMPARISON OF METHODS FOR STICK-SPEED STABILITY – 707-320B and 30° SST

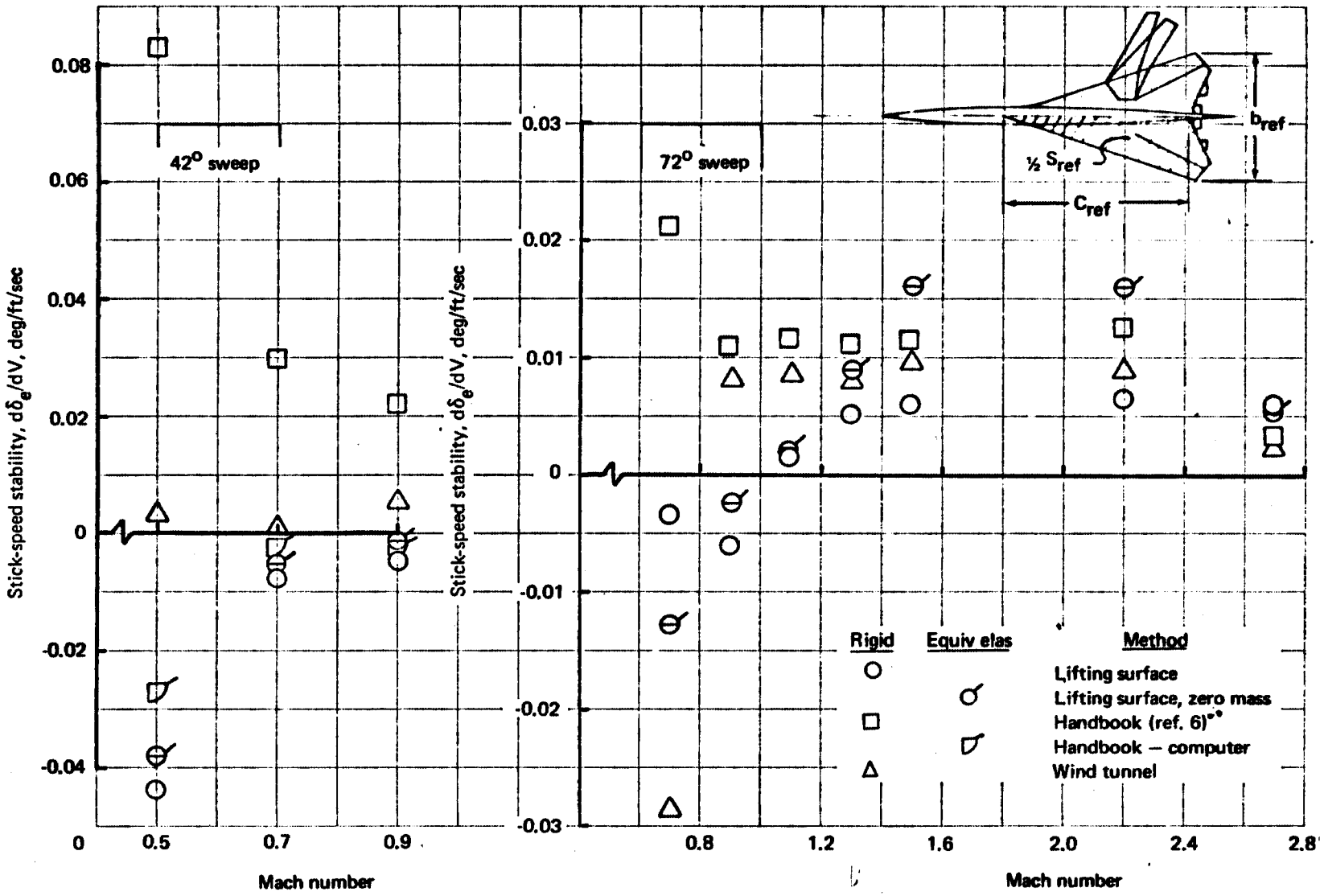

FIGURE 53. COMPARISON OF METHODS FOR STICK-SPEED STABILITY – 42° AND 72° SST

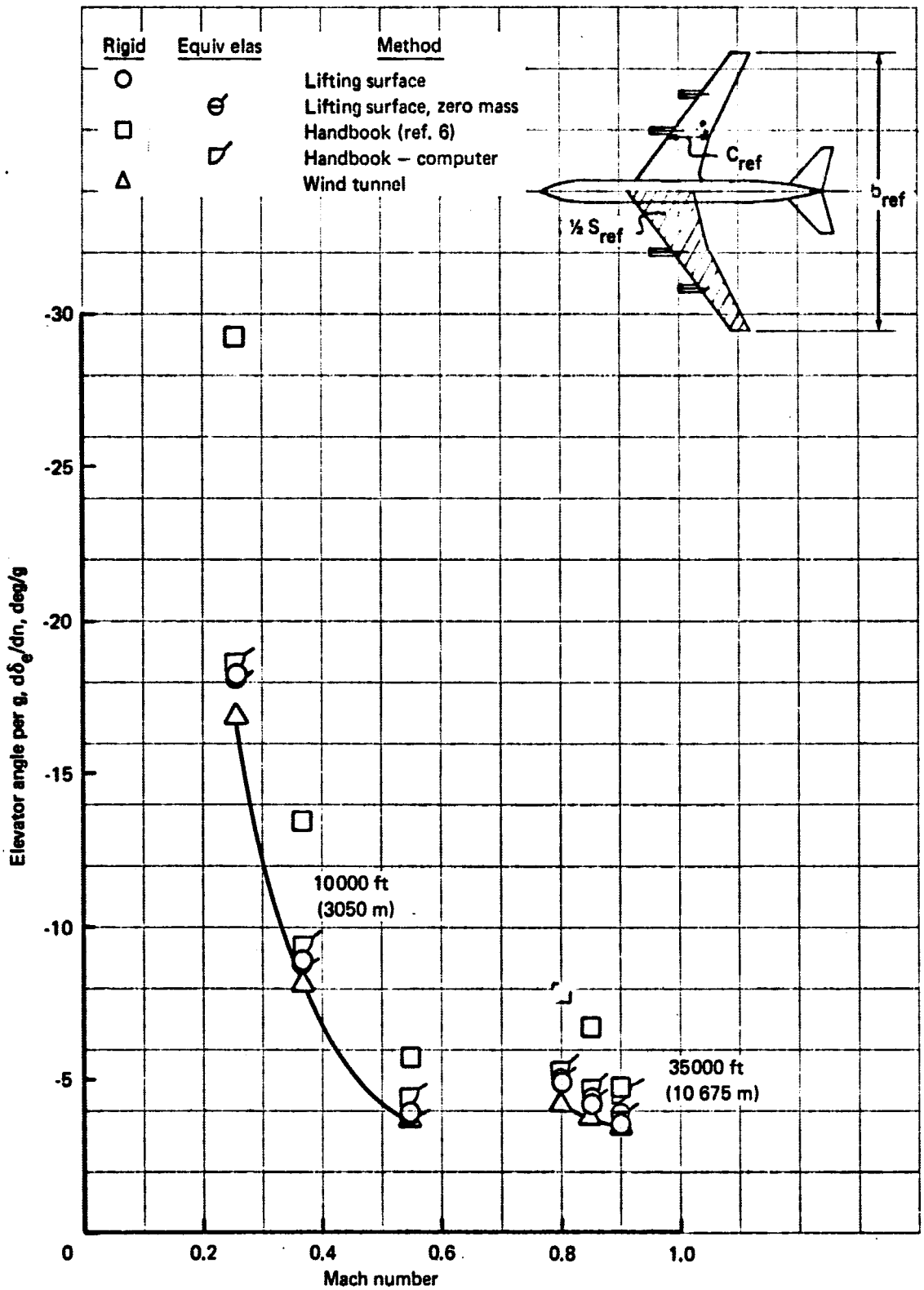

FIGURE 54. COMPARISON OF METHODS FOR ELEVATOR ANGLE PER g – 707-320B

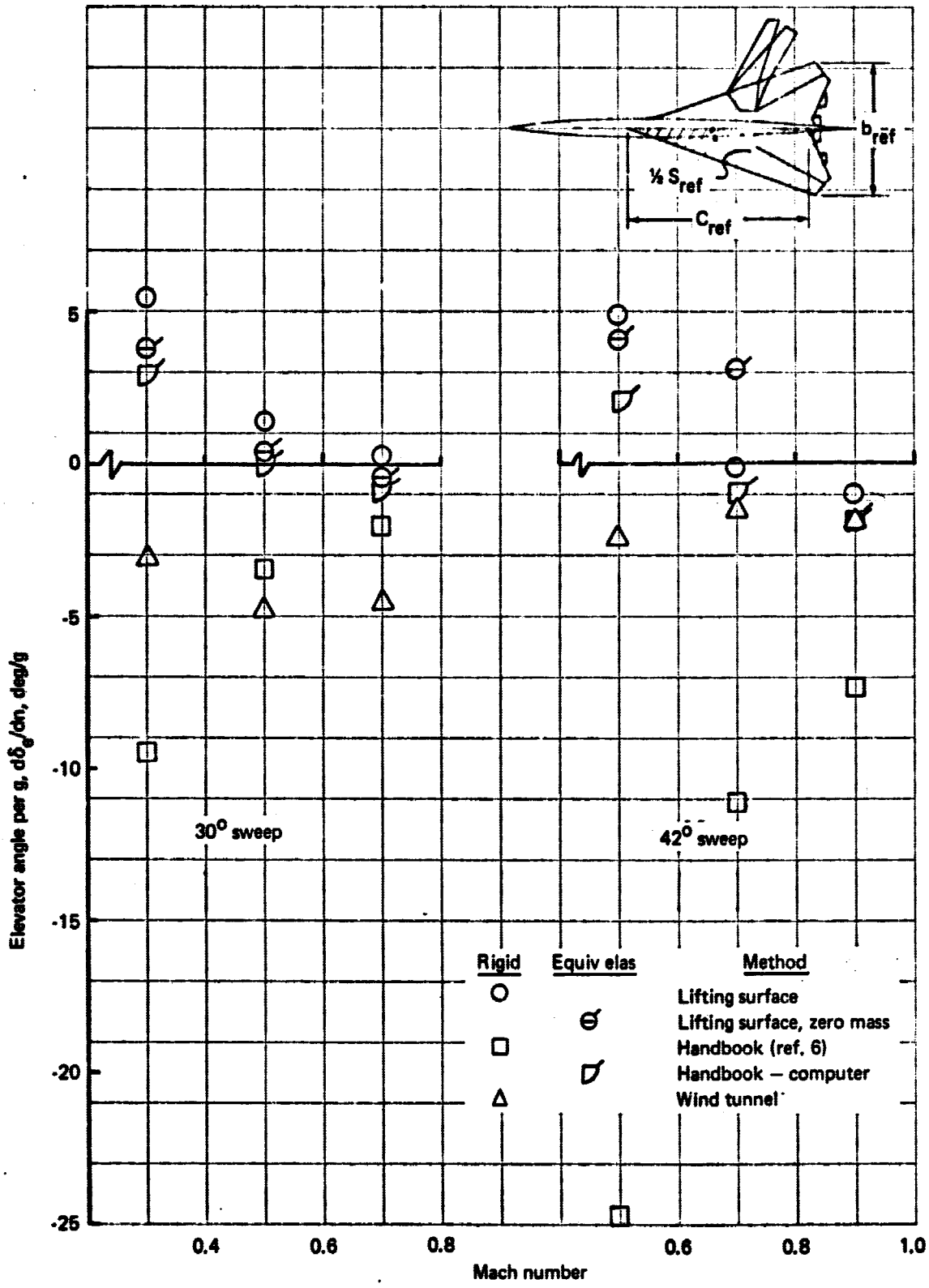

FIGURE 55. COMPARISON OF METHODS FOR ELEVATOR ANGLE PER g – 30° AND 42° SST

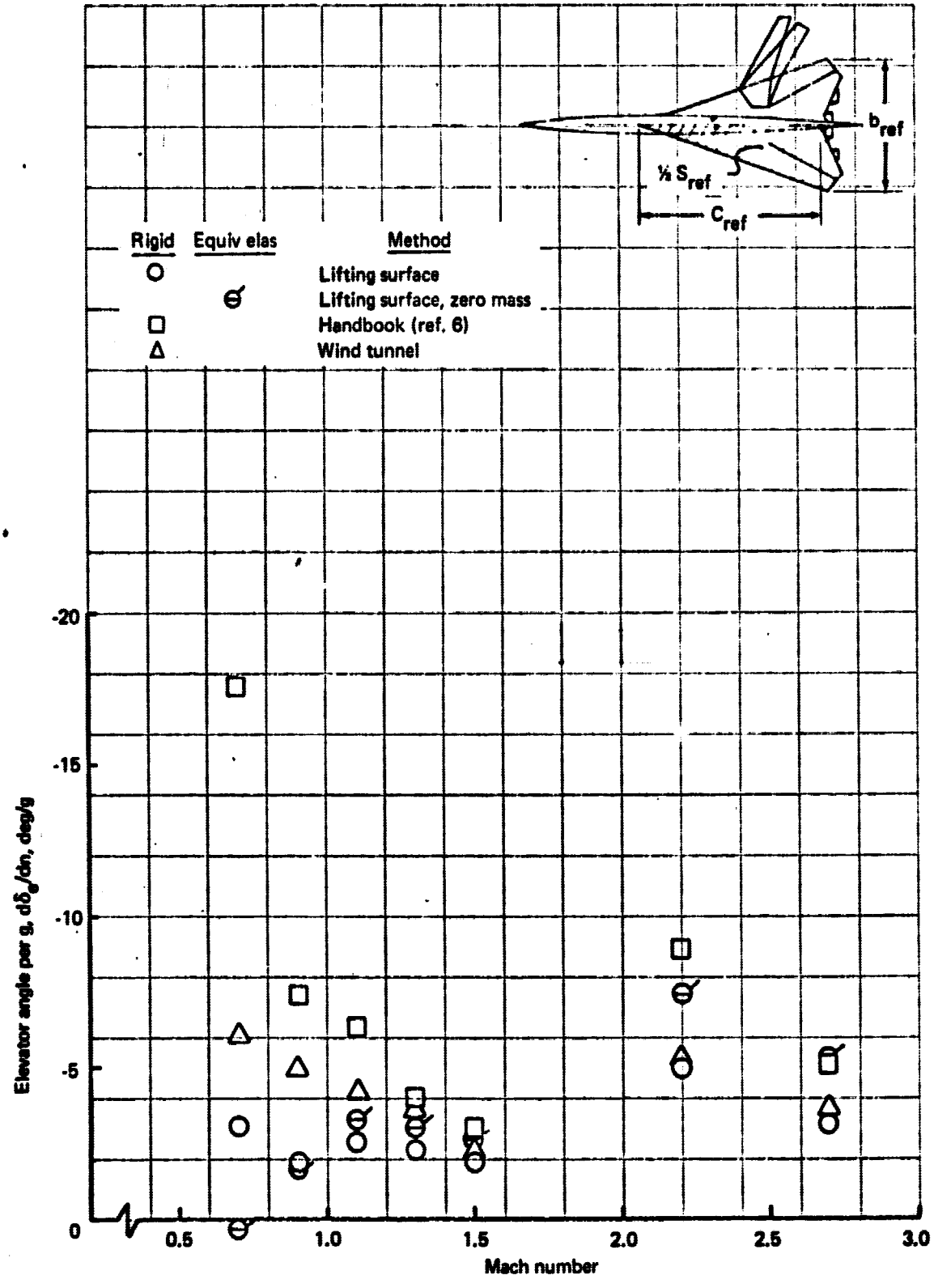

FIGURE 56. COMPARISON OF METHODS FOR ELEVATOR ANGLE PER g – 72° SST

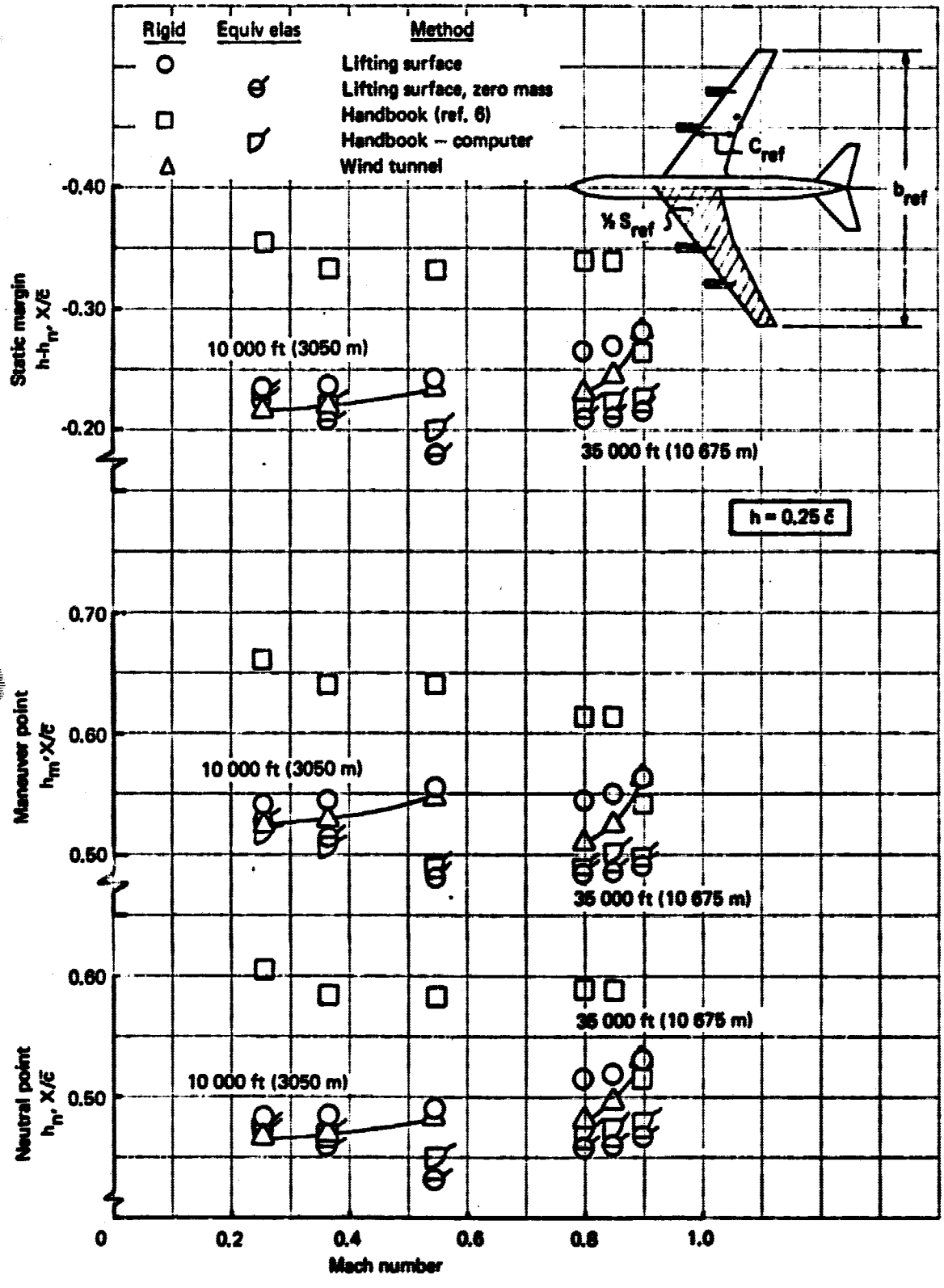

FIGURE 57. COMPARISON OF METHODS FOR NEUTRAL POINT, MANEUVER POINT, AND STATIC MARGIN – 707-320B

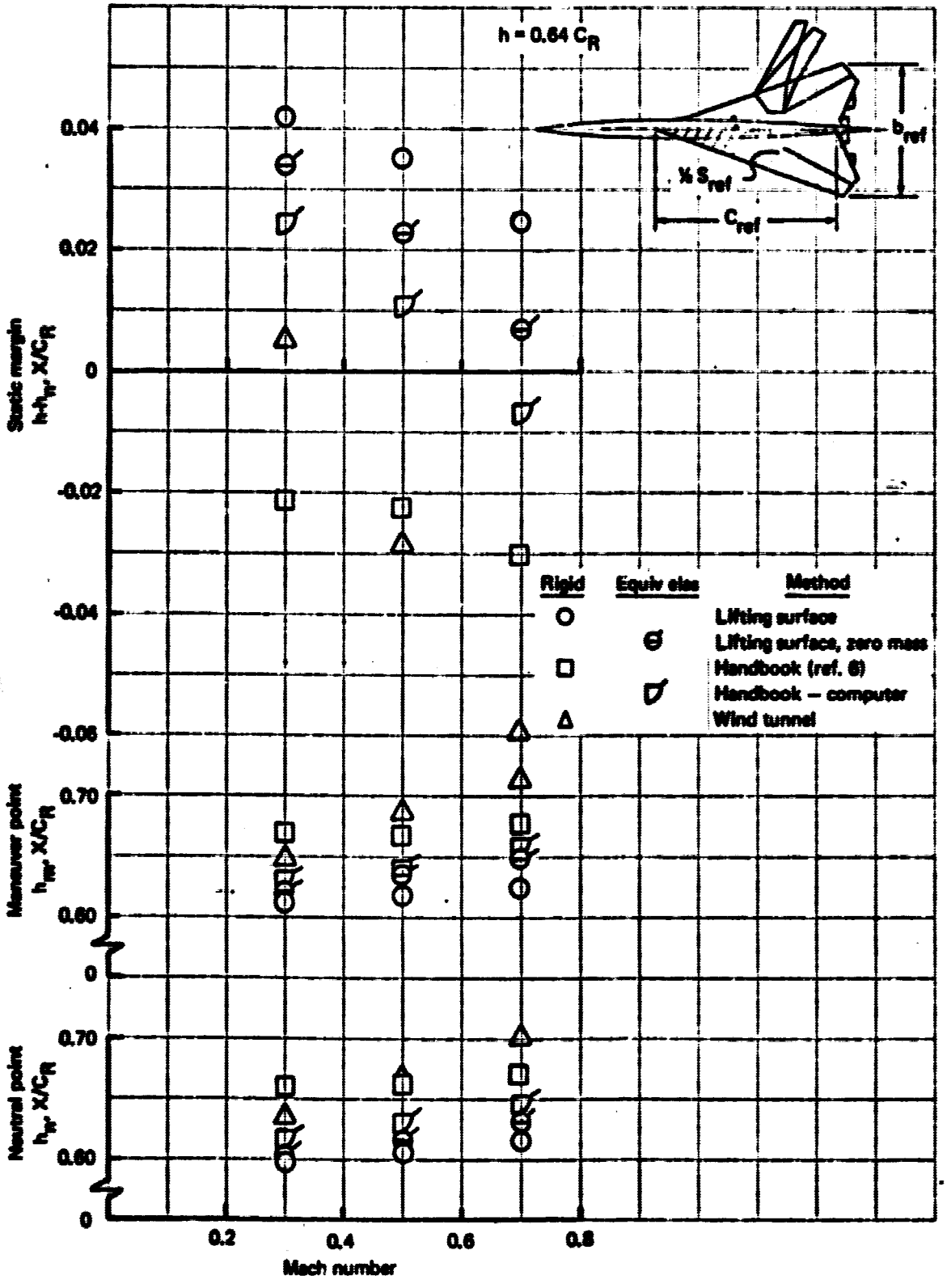

FIGURE 58. COMPARISON OF METHODS FOR NEUTRAL POINT, MANEUVER POINT, AND STATIC MARGIN – 30° SST

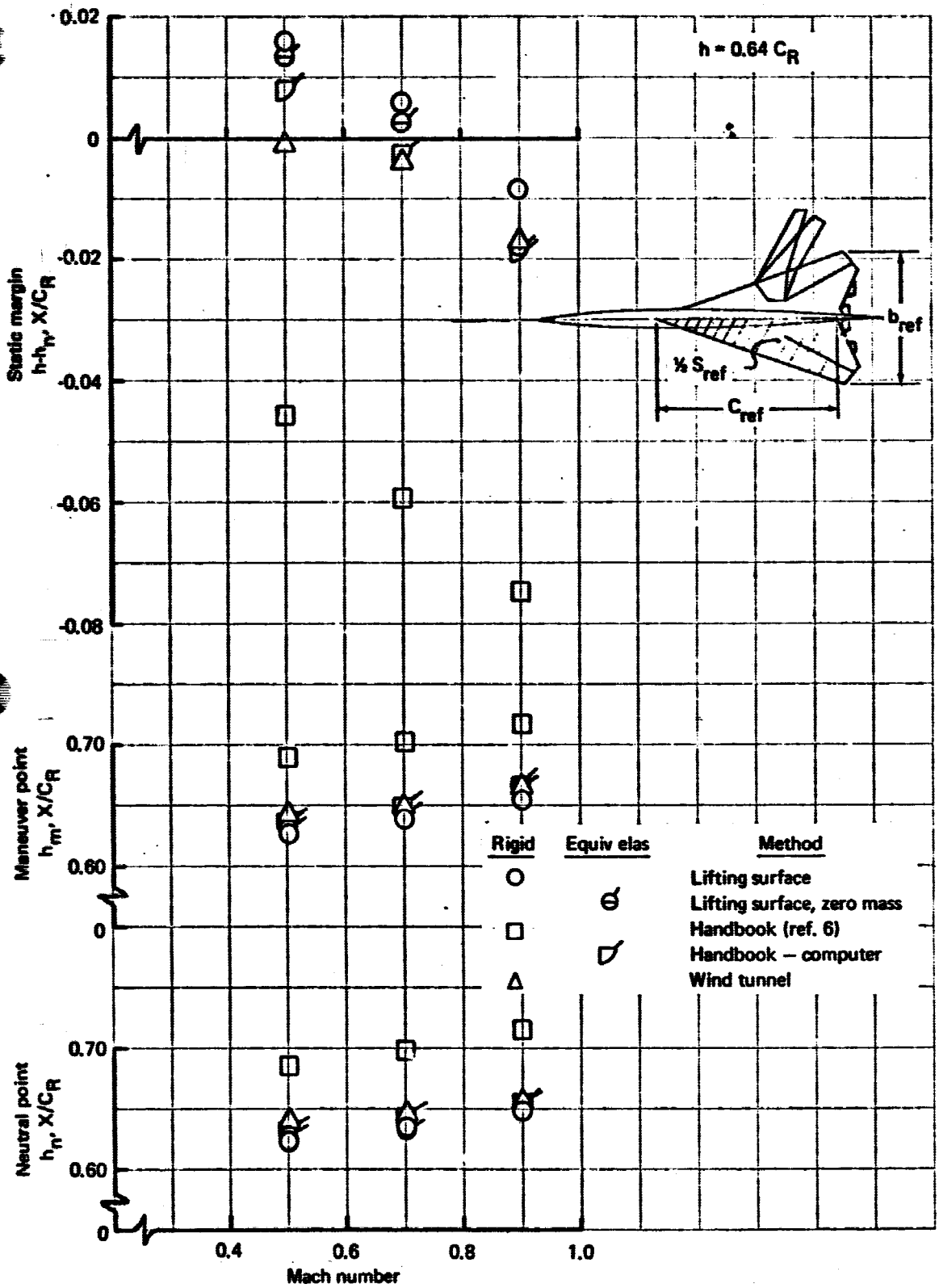

FIGURE 59. COMPARISON OF METHODS FOR NEUTRAL POINT, MANEUVER POINT, AND STATIC MARGIN – 42° SST

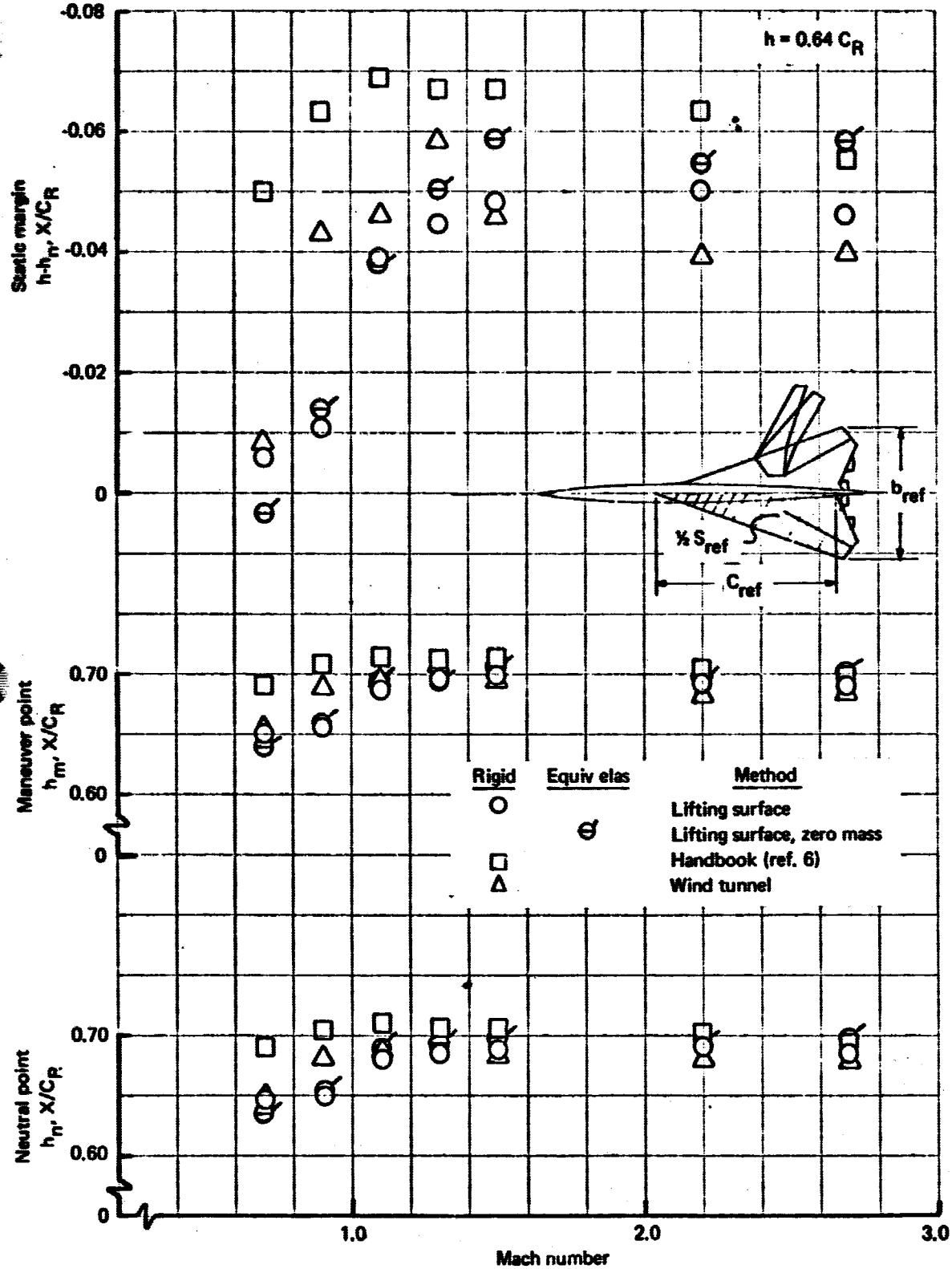

FIGURE 60. COMPARISON OF METHODS FOR NEUTRAL POINT, MANEUVER POINT, AND STATIC MARGIN – 72° SST

8.4 Rigid and Equivalent Elastic Longitudinal Dynamic Stability Data

This section presents the figures that illustrate the results of applying the stability criteria associated with the roots of the longitudinal characteristic equation. This is done for the rigid and equivalent elastic airplane mathematical models. The data presented here supplement those shown and discussed in Sec. 6. The details of the determination of the roots and associated parameters have been discussed in Sec. 5.

The data in figs. 61 through 78 are for the study conditions of table 1 and follow the general order of frequency and damping, period, time to damp to half or double amplitude, and cycles to damp to half or double amplitude for the short period mode; this is followed by data in the same sequence for the phugoid mode. These data illustrate the variations in disturbed motion characteristics as predicted by various rigid and equivalent elastic derivatives. A comparison of rigid and equivalent elastic characteristics using the lifting surface method illustrates the effect of static elasticity. The data of this section and par. 6.2 are used in arriving at the conclusions of Sec. 10.

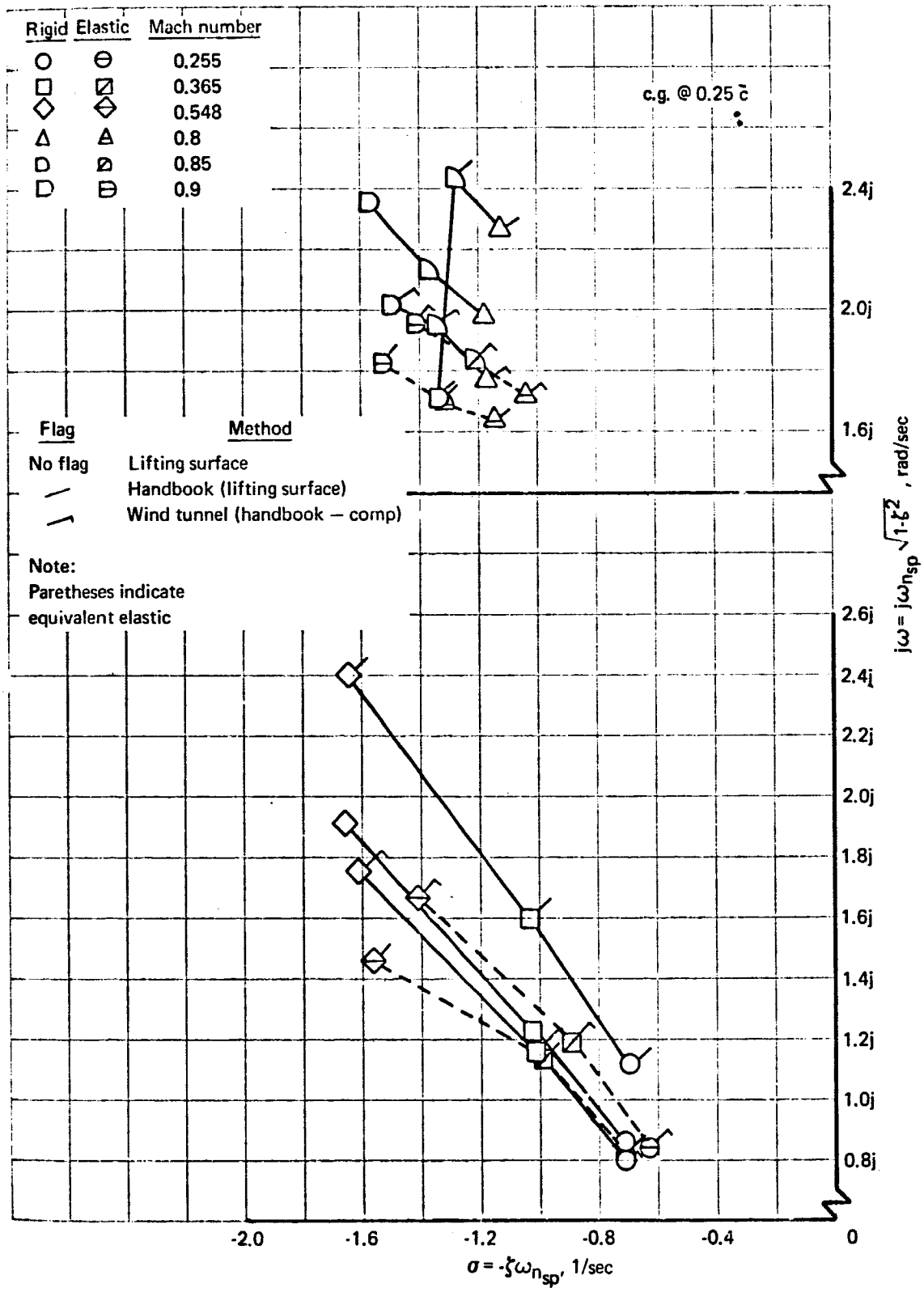

FIGURE 61. LONGITUDINAL SHORT PERIOD, FREQUENCY VERSUS DAMPING – 707-320B

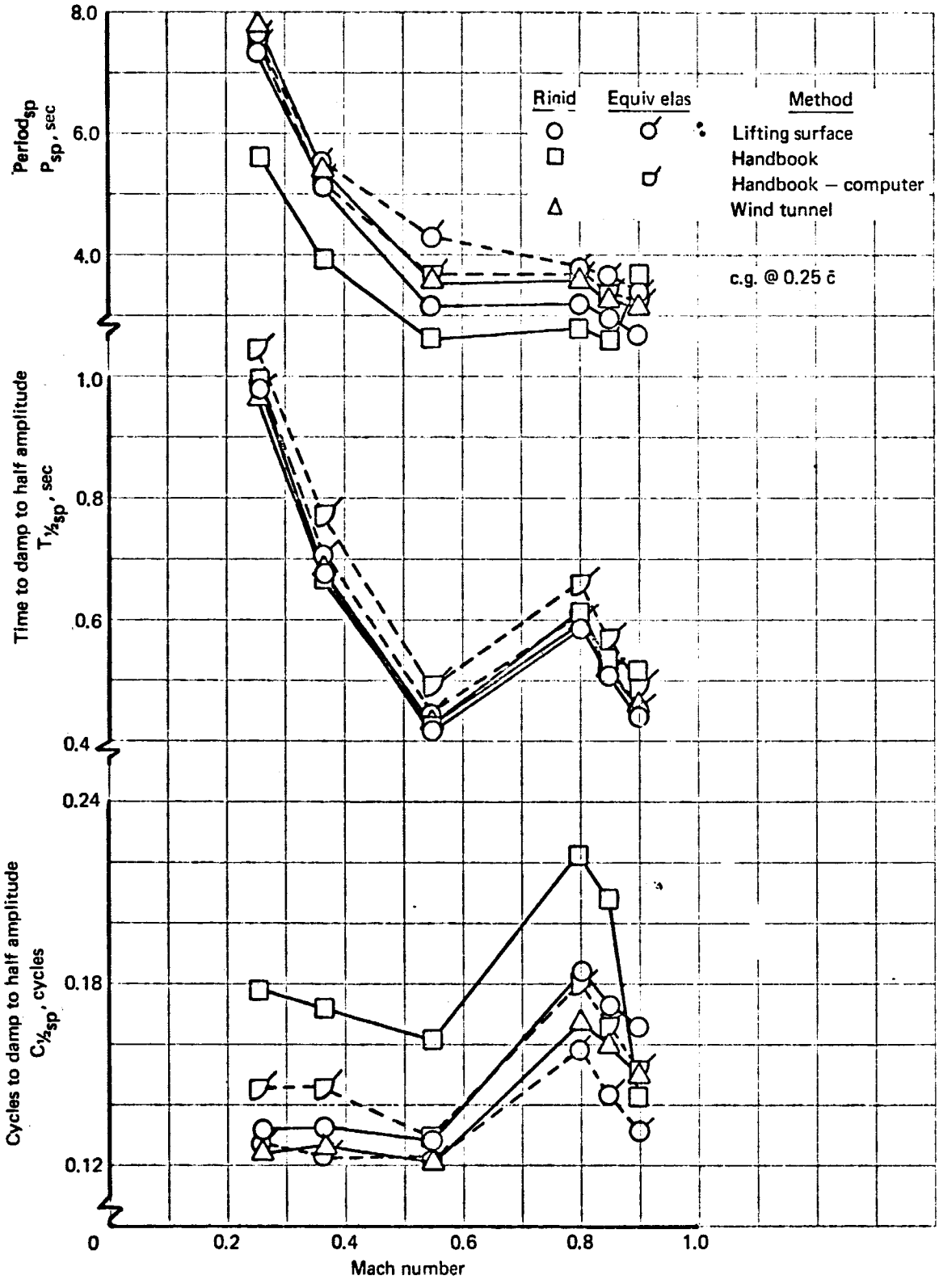

FIGURE 62. LONGITUDINAL SHORT PERIOD P_{sp}, $T_{½}$ AND $C_{½}$ – 707-320B

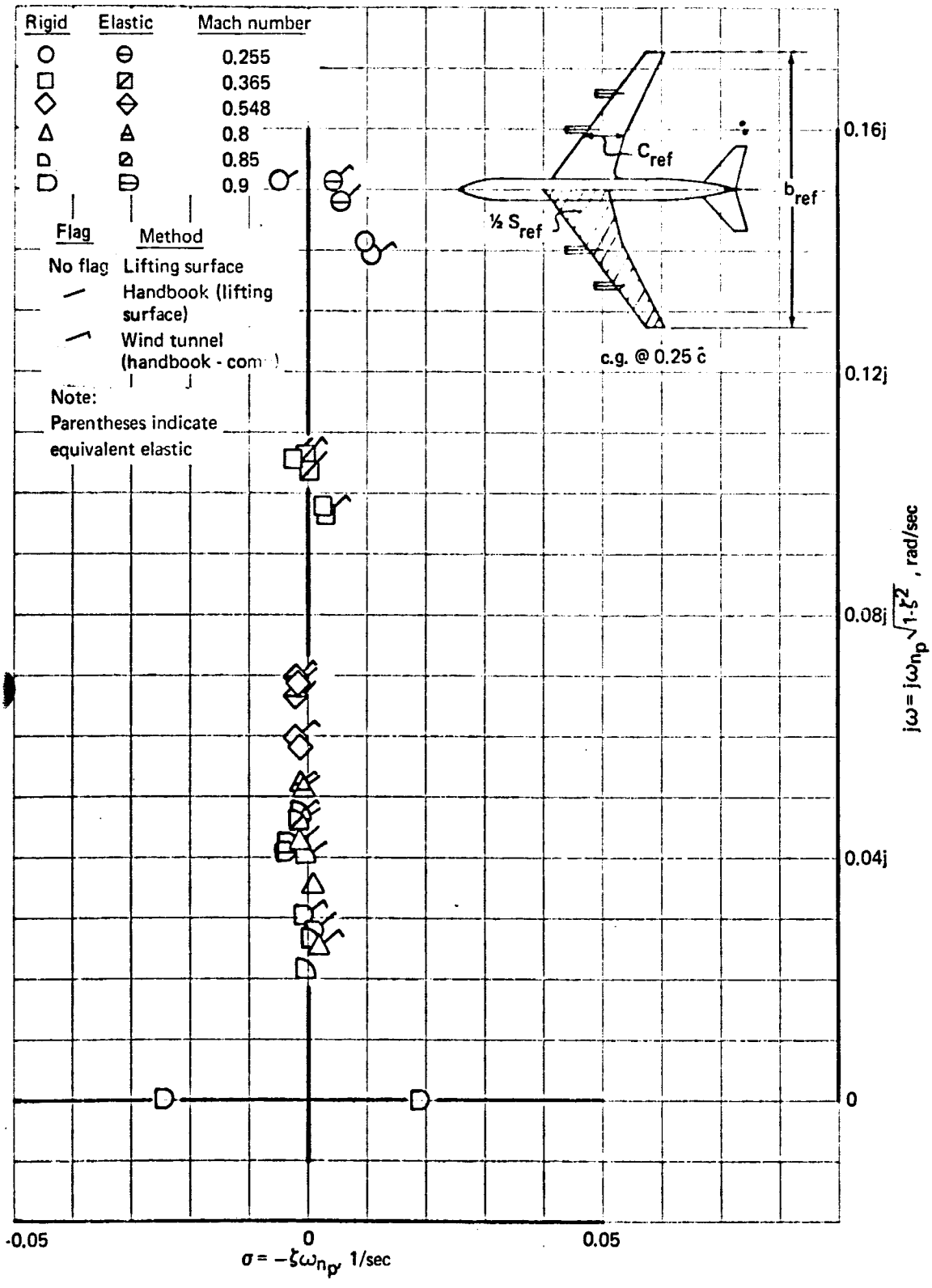

FIGURE 63. LONGITUDINAL PHUGOID FREQUENCY VERSUS DAMPING – 707-320B

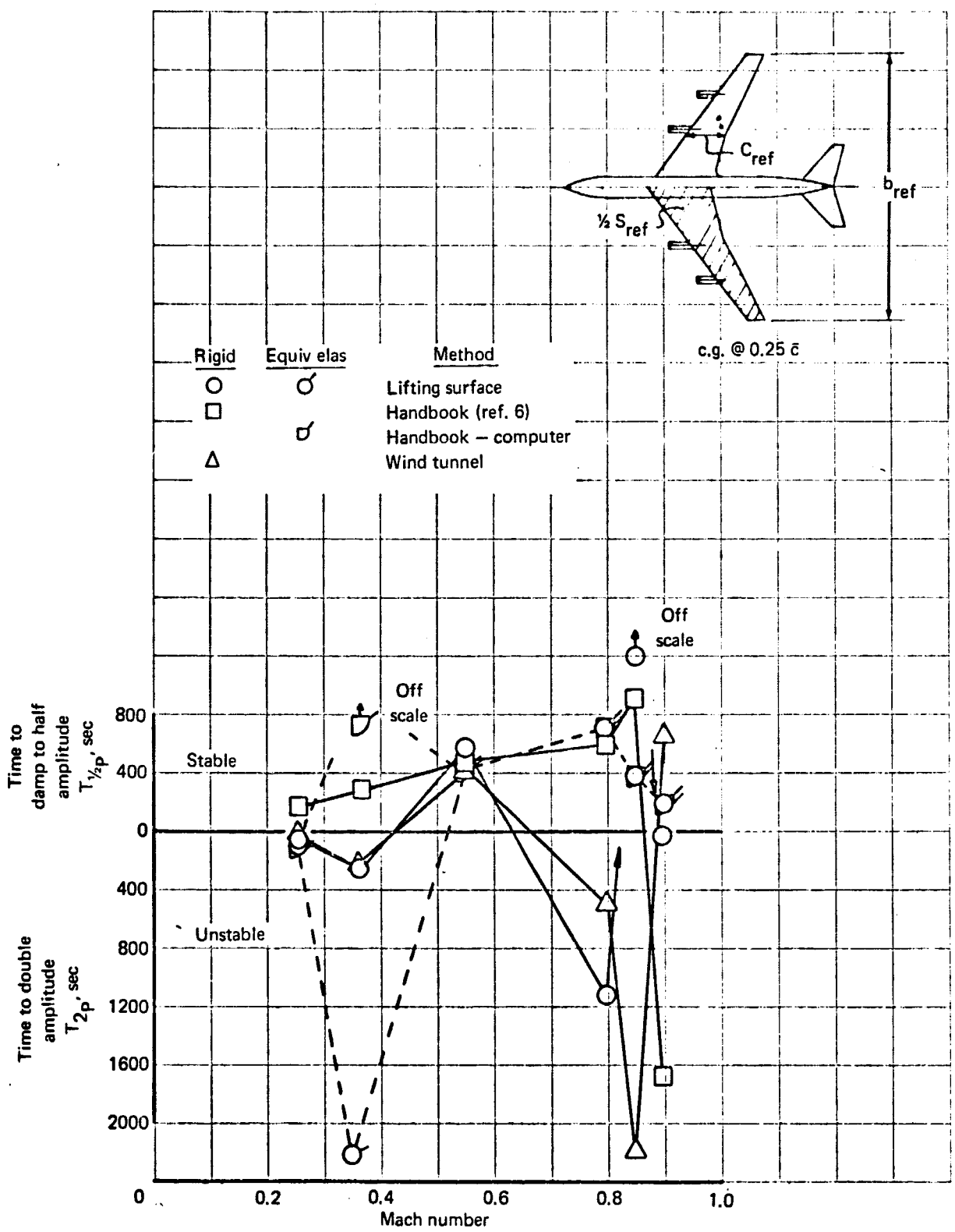

FIGURE 64. LONGITUDINAL PHUGOID $T_{½}$ AND T_2– 707-320B

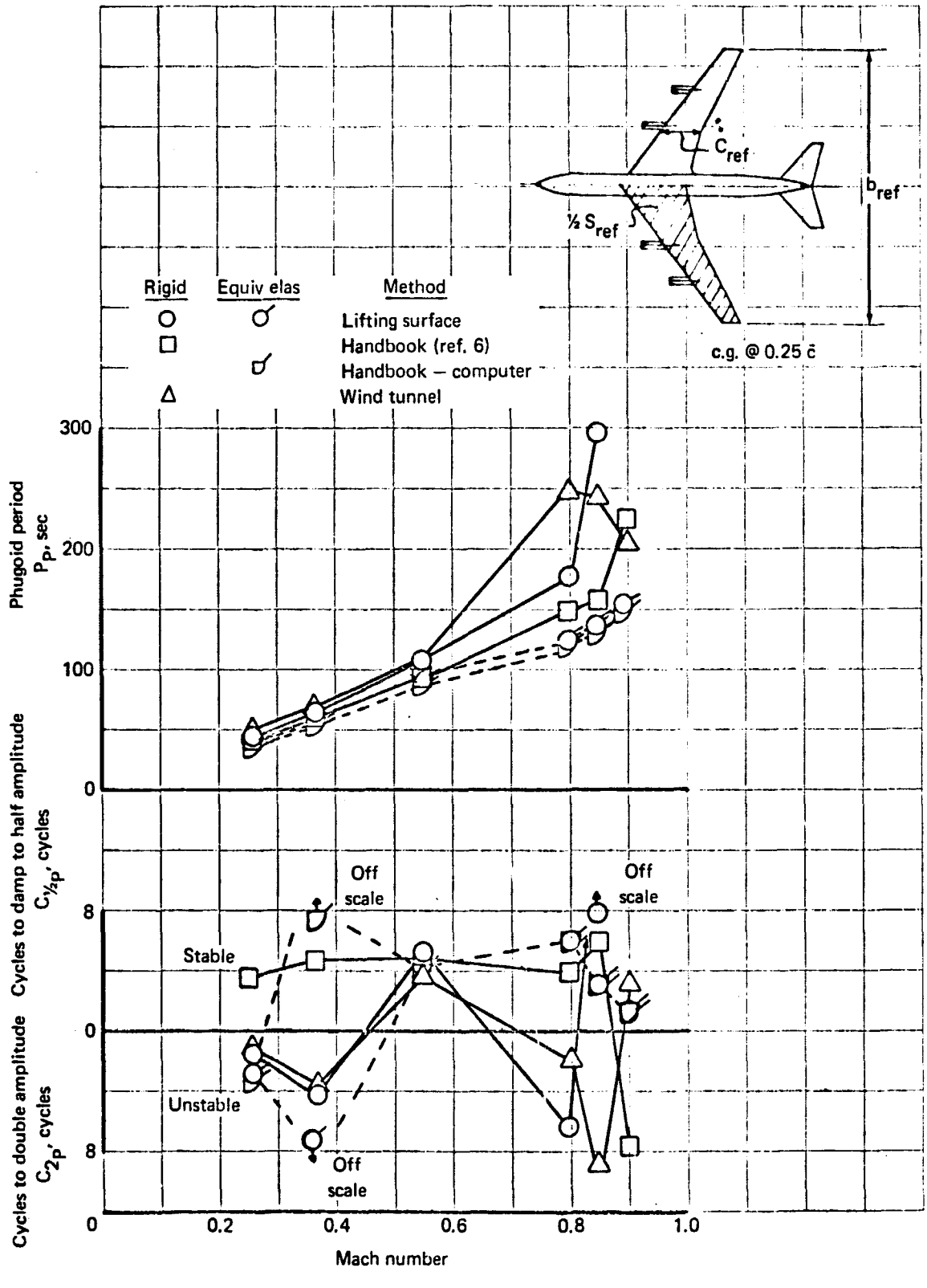

FIGURE 65. LONGITUDINAL PHUGOID P, $C_{½}$, AND C_2--707-320B

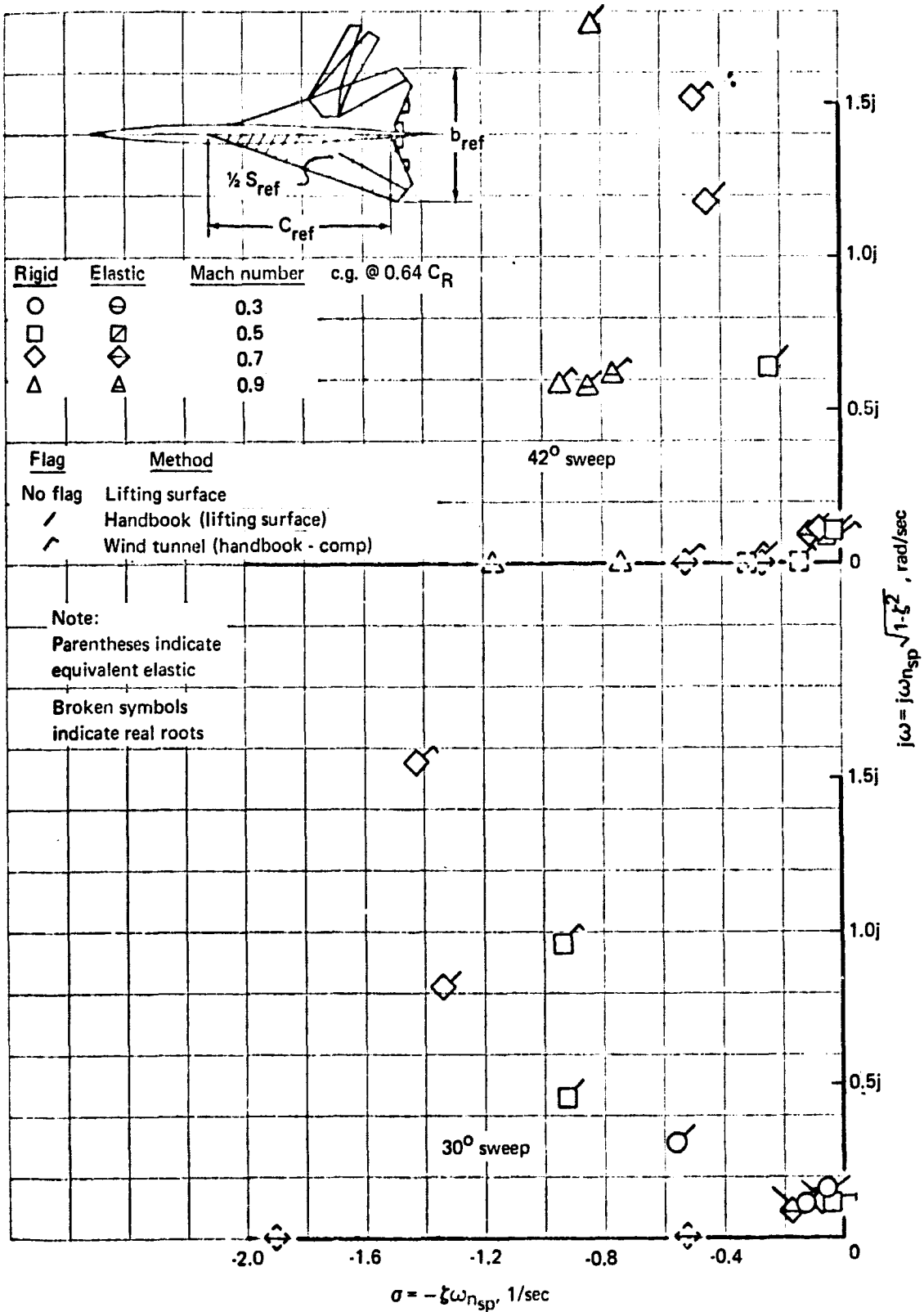

FIGURE 66. LONGITUDINAL SHORT PERIOD FREQUENCY VERSUS DAMPING – 30° AND 42° SST

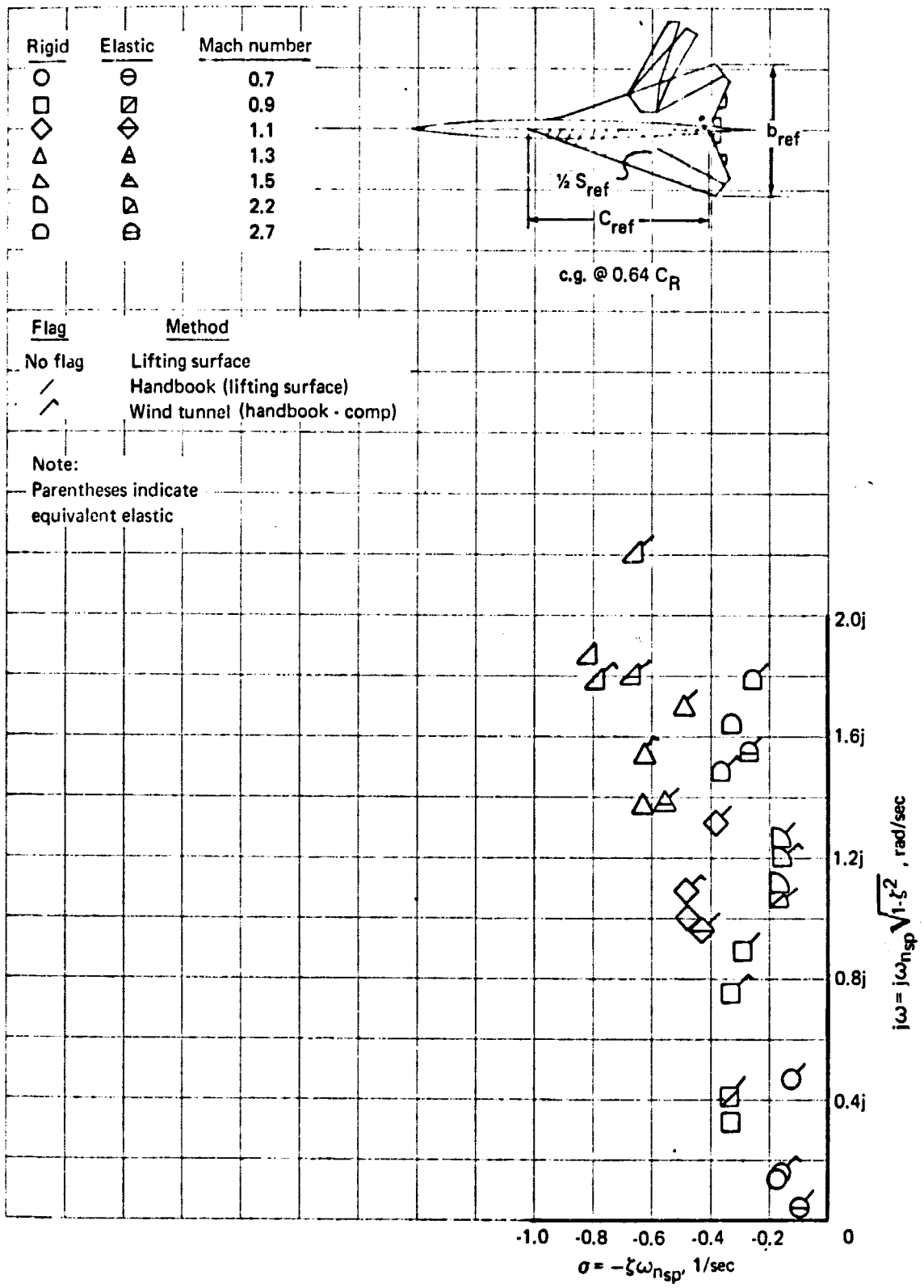

FIGURE 67. LONGITUDINAL SHORT PERIOD FREQUENCY VERSUS DAMPING – 72° SST

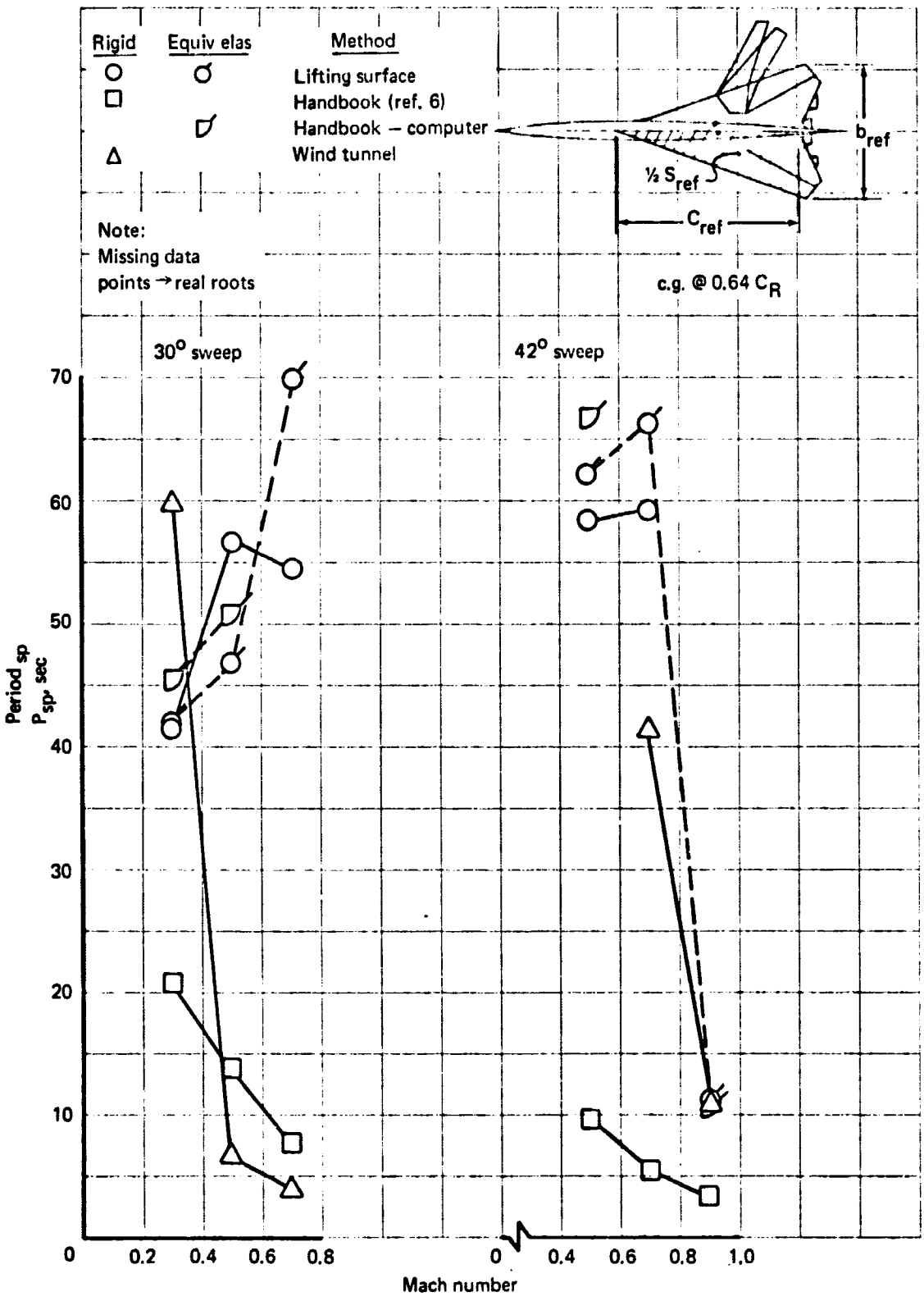

FIGURE 68. LONGITUDINAL SHORT PERIOD, PERIOD – 30° AND 42° SST

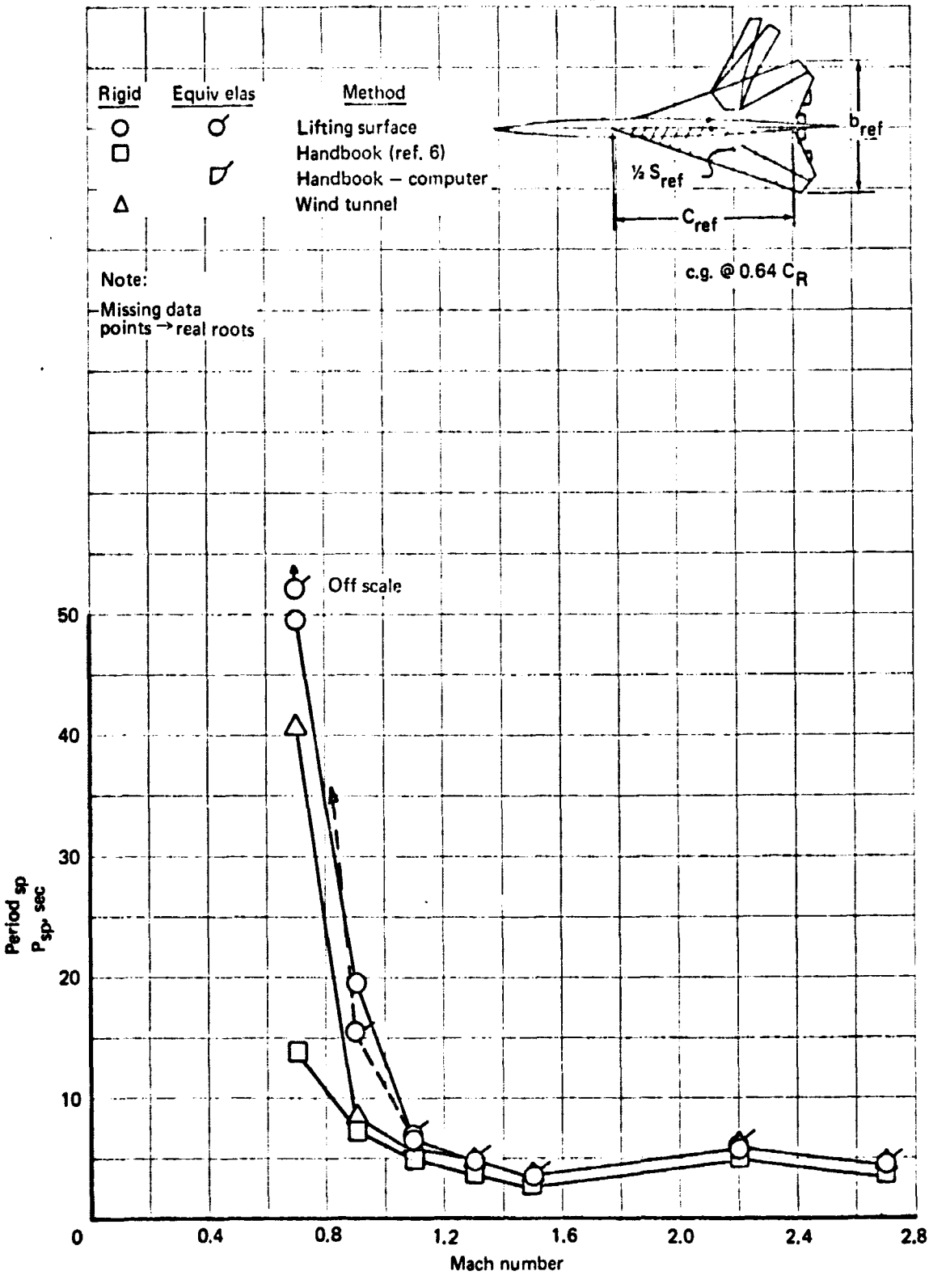

FIGURE 69. LONGITUDINAL SHORT PERIOD, PERIOD–72° SST

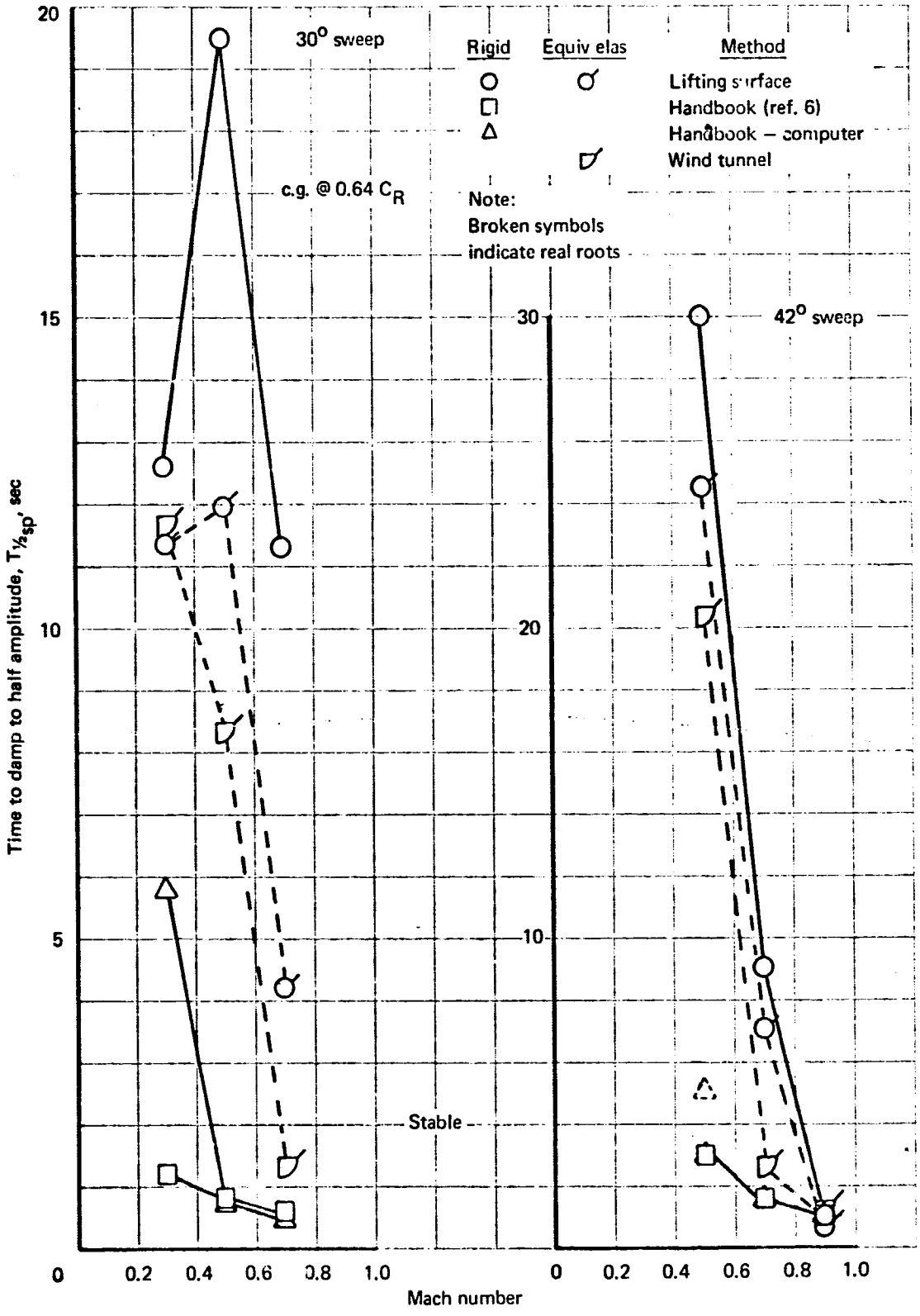

FIGURE 70. LONGITUDINAL SHORT PERIOD, $T_{½}$ – 30° AND 42° SST

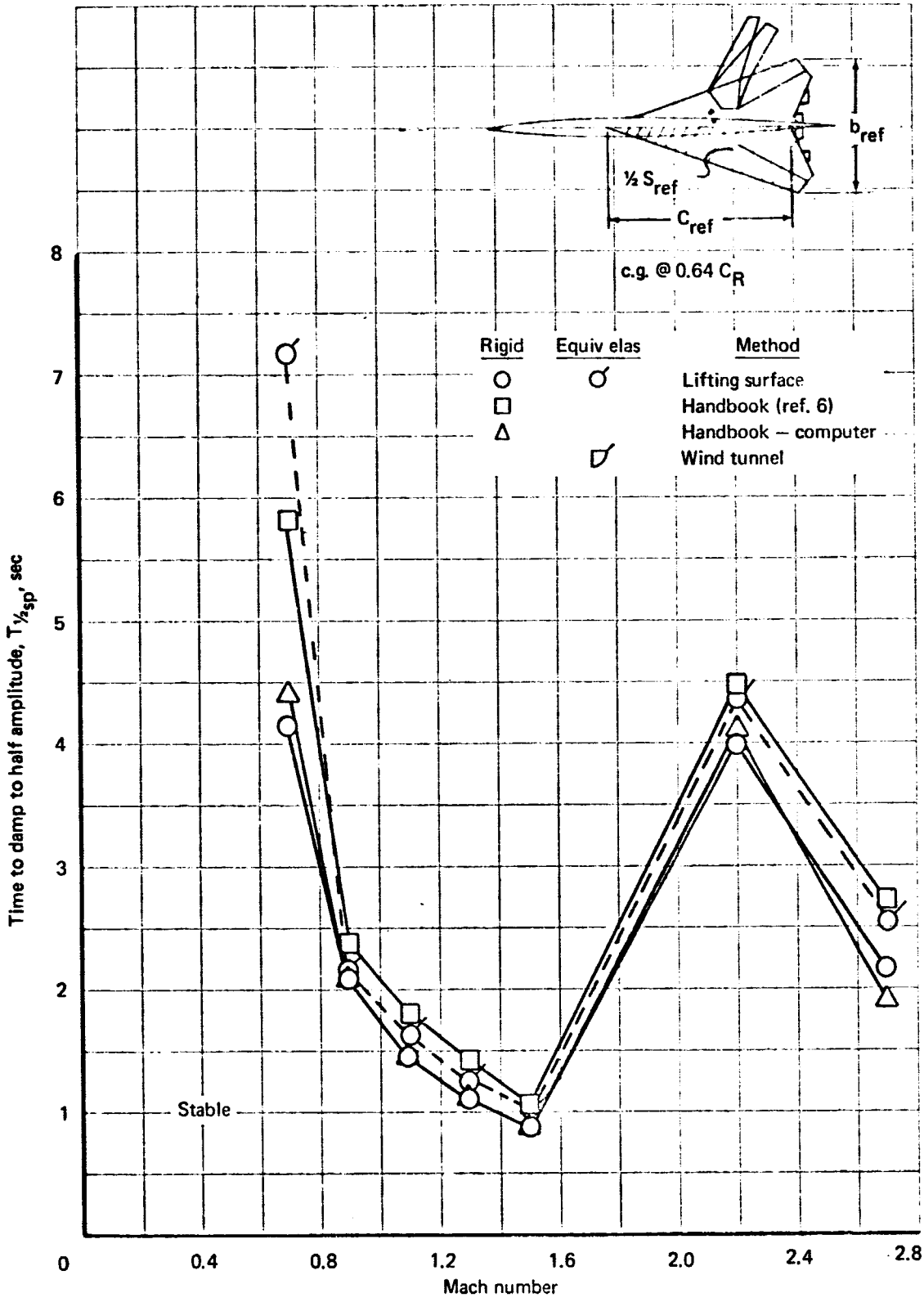

FIGURE 71. LONGITUDINAL SHORT PERIOD, $T_{½}$ – 72° SST

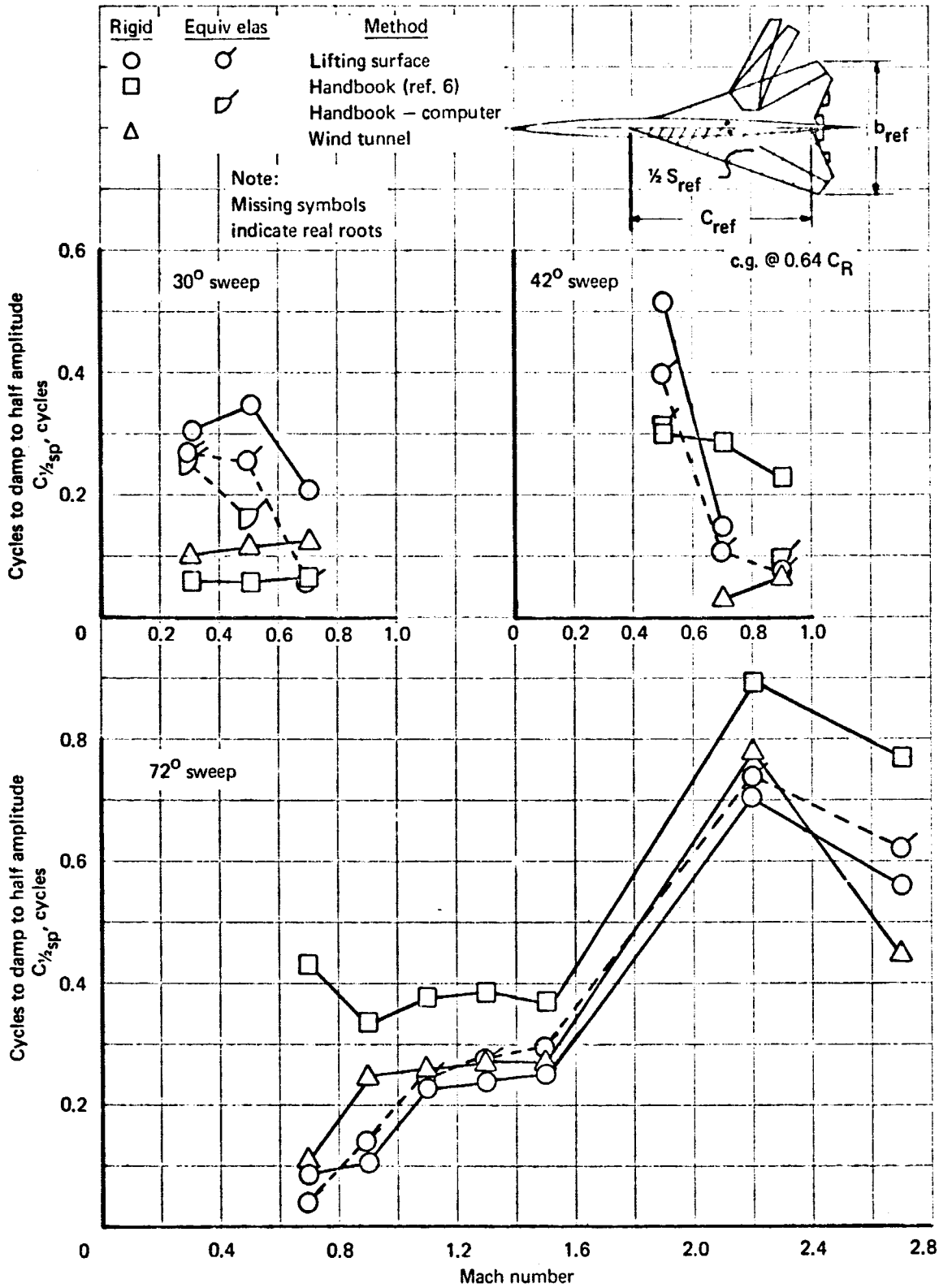

FIGURE 72. LONGITUDINAL SHORT PERIOD, $C_{1/2}$ – 30°, 42° AND 72° SST

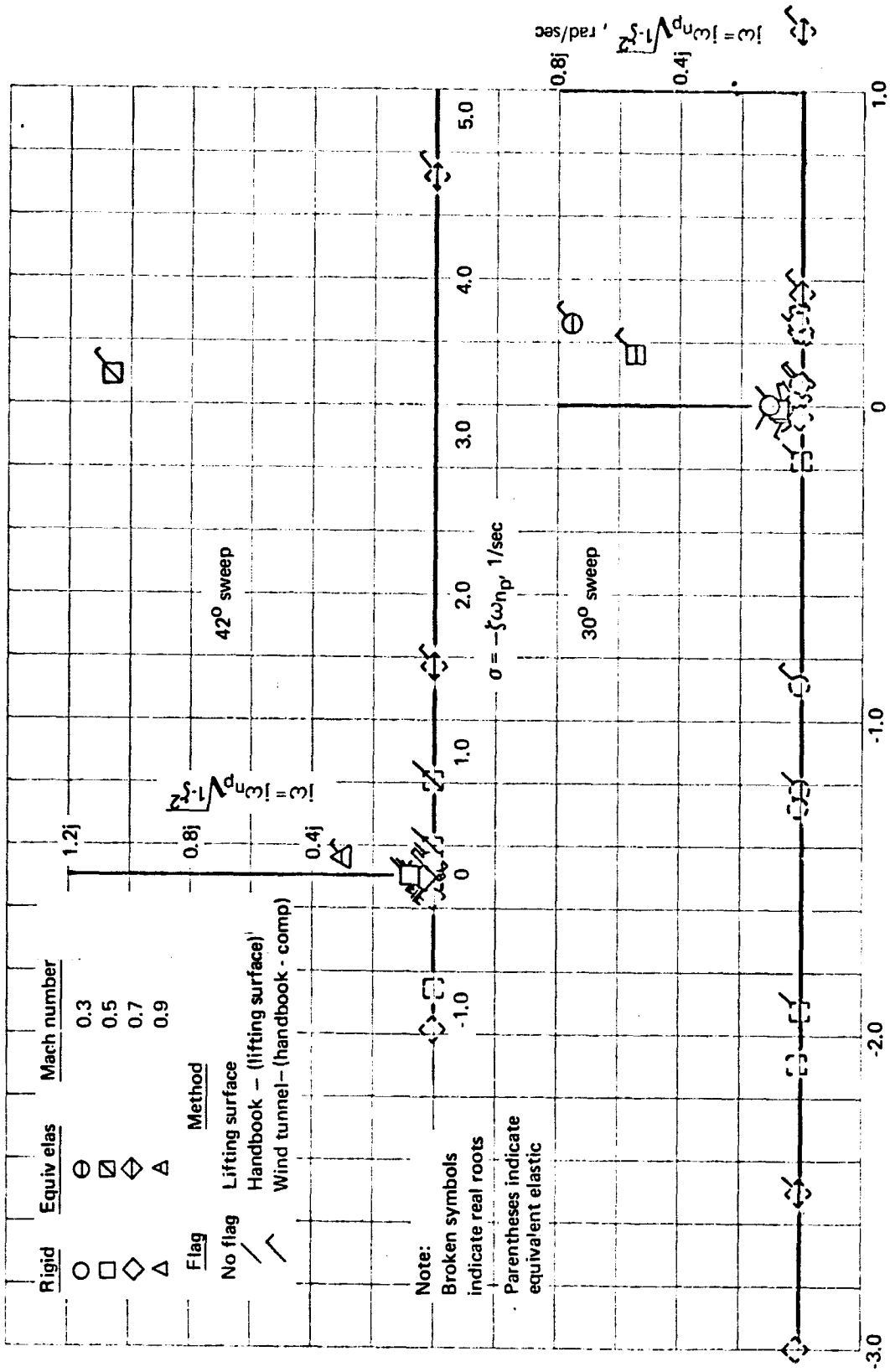

FIGURE 73. LONGITUDINAL PHUGOID FREQUENCY VERSUS DAMPING – 30° AND 42° SST

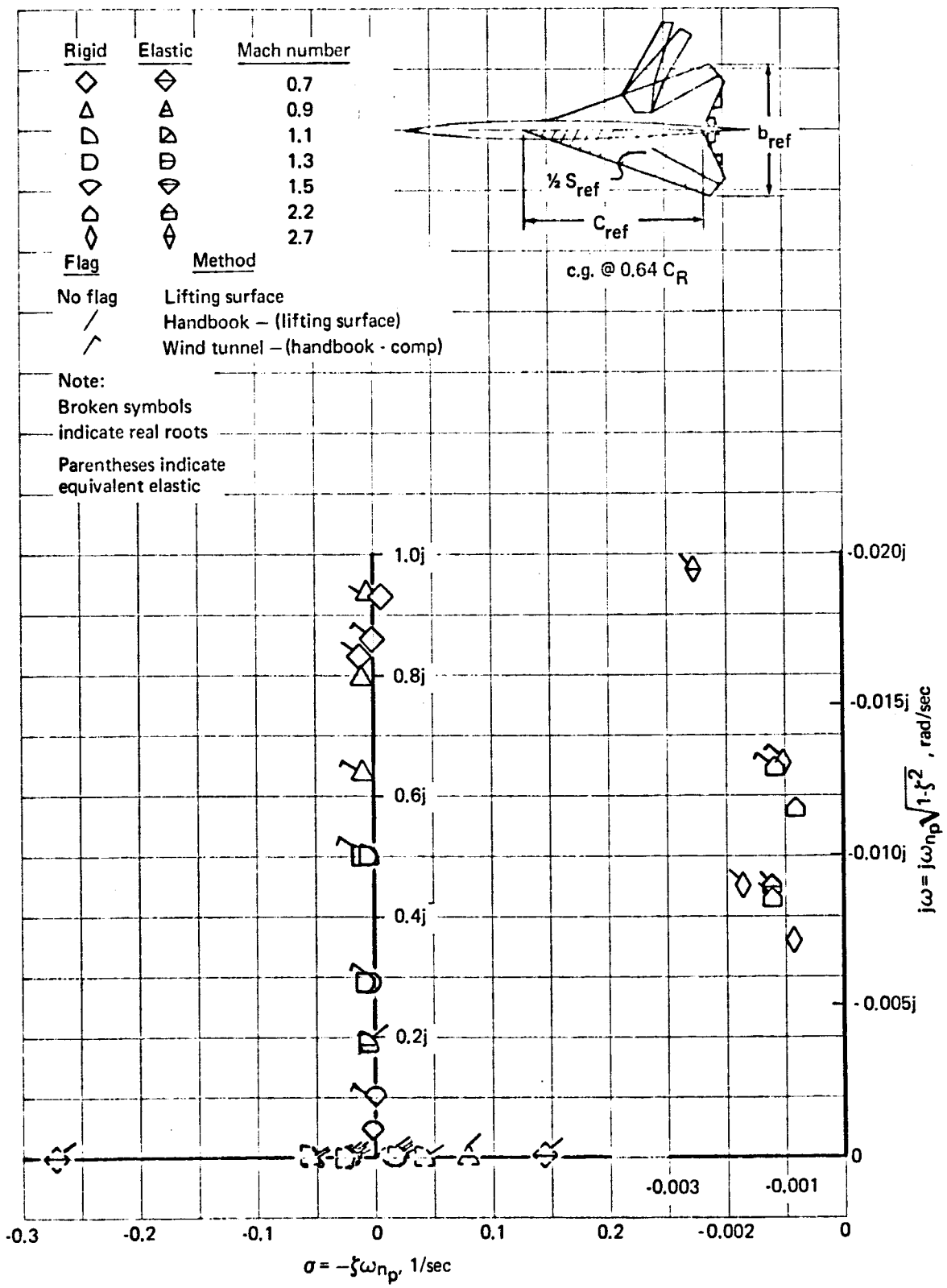

FIGURE 74. LONGITUDINAL PHUGOID FREQUENCY VERSUS DAMPING – 72° SST

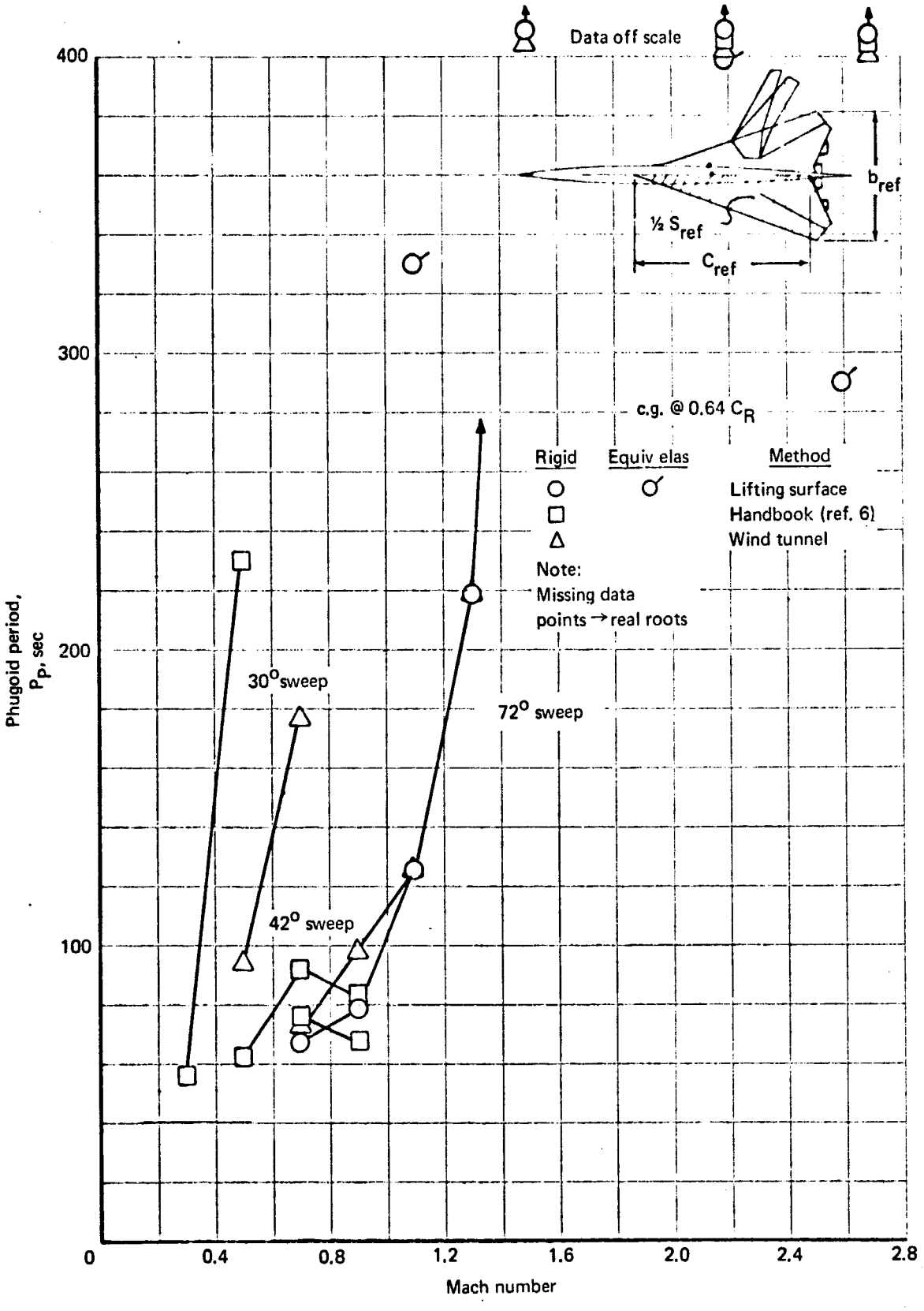

FIGURE 75. LONGITUDINAL PHUGOID, PERIOD 30°, 42° AND 72° SST

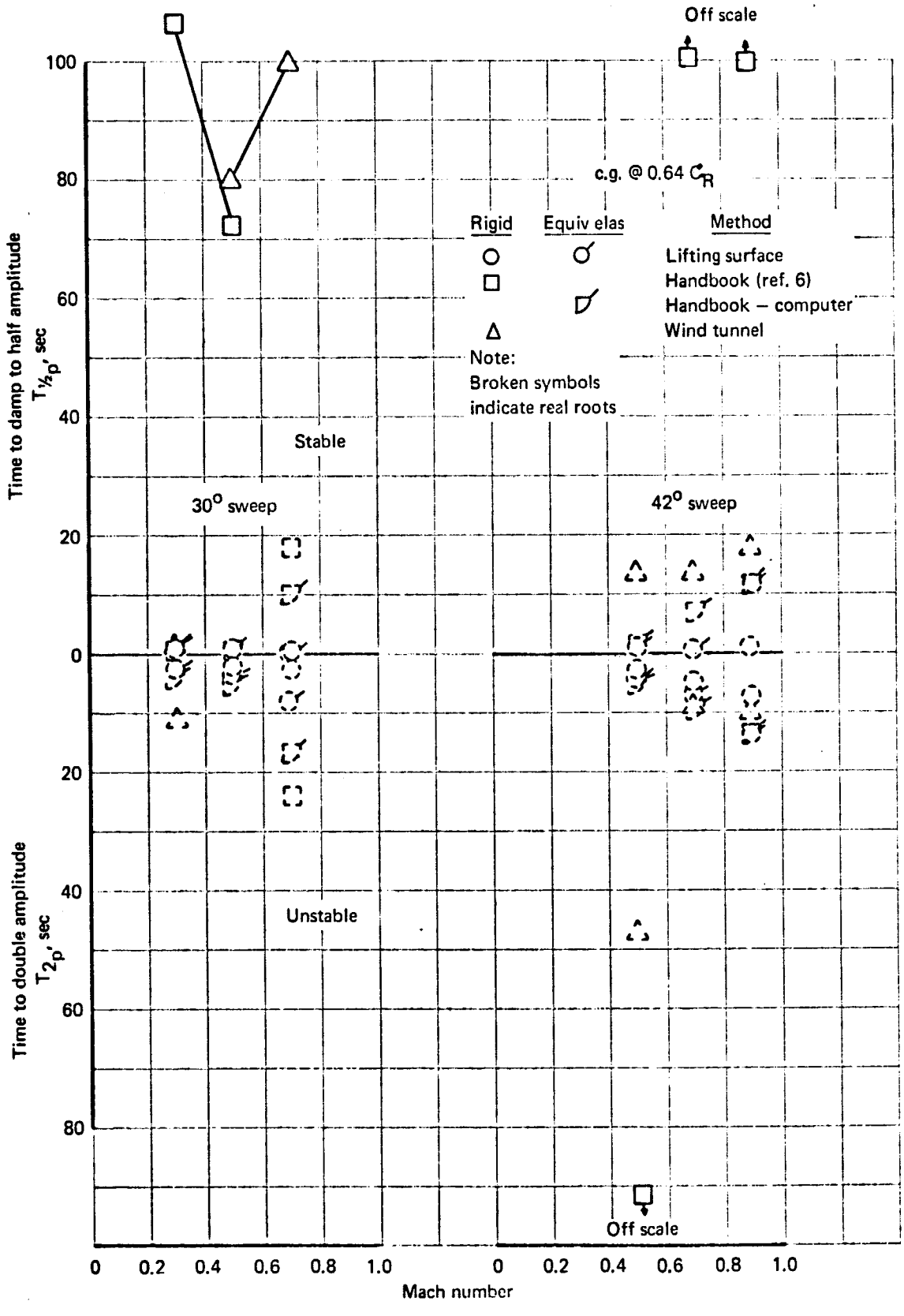

FIGURE 76. LONGITUDINAL PHUGOID $T_{½}$ AND T_2 – 30° AND 42° SST

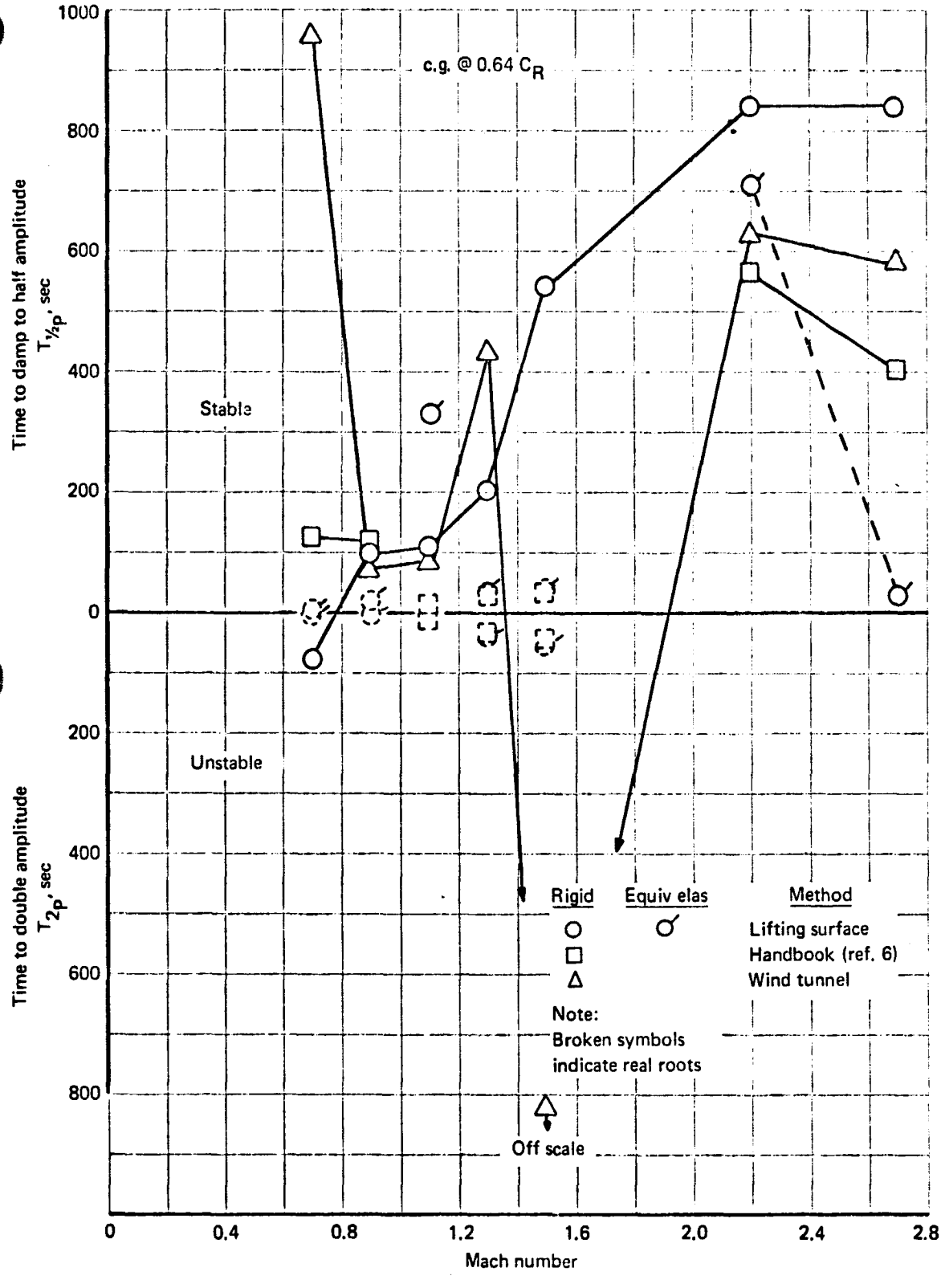

FIGURE 77. LONGITUDINAL PHUGOID $T_{½}$ AND T_2 – 72° SST

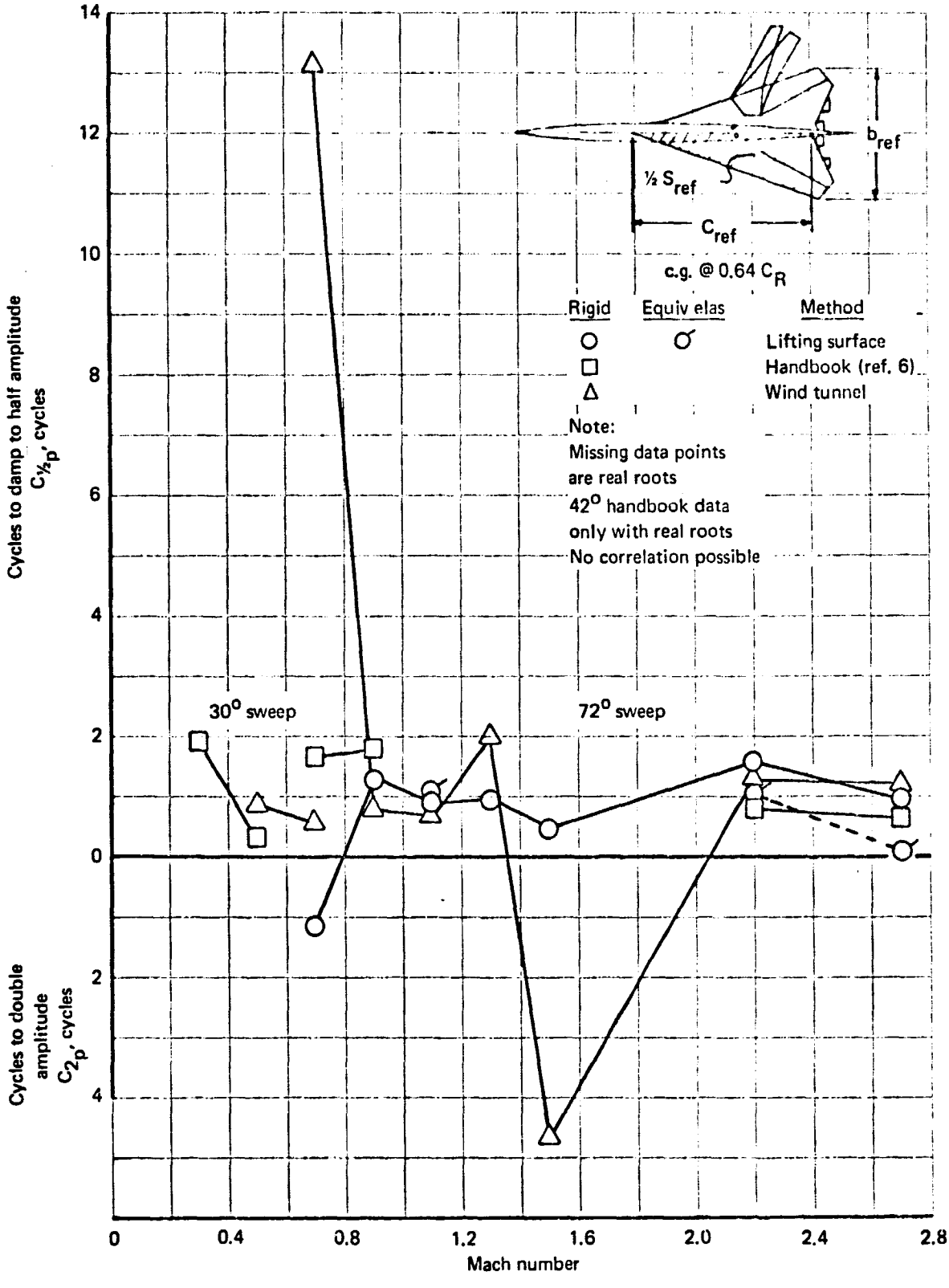

FIGURE 78. LONGITUDINAL PHUGOID $C_{½}$ AND C_2 – 30° AND 72° SST

8.5 Rigid and Equivalent Elastic Lateral-Directional Dynamic Stability Data

This section presents the dynamic stability characteristics obtained in applying dynamic stability criteria to the lateral-directional characteristic equations. The details concerning the methods for obtaining these characteristics were discussed in par. 5.2. Some of the data presented in this section has been discussed in par. 6.3. All the discussion concerning the lateral-directional data is in Sec. 6. The conclusions reached, however, reflect the data of pars. 8.5 and 6.3.

The data in this section (figs 79 through 91) are presented in the general order: (1) Dutch roll frequency and damping, period, time to damp to half or double amplitude, and cycles to damp to half or double amplitude; (2) spiral mode, root, and time to damp to half or double amplitude; and (3) rolling convergence, root, and time to damp to half or double amplitude. These data are shown for the 707-320B and SST at the study flight conditions listed in table 1.

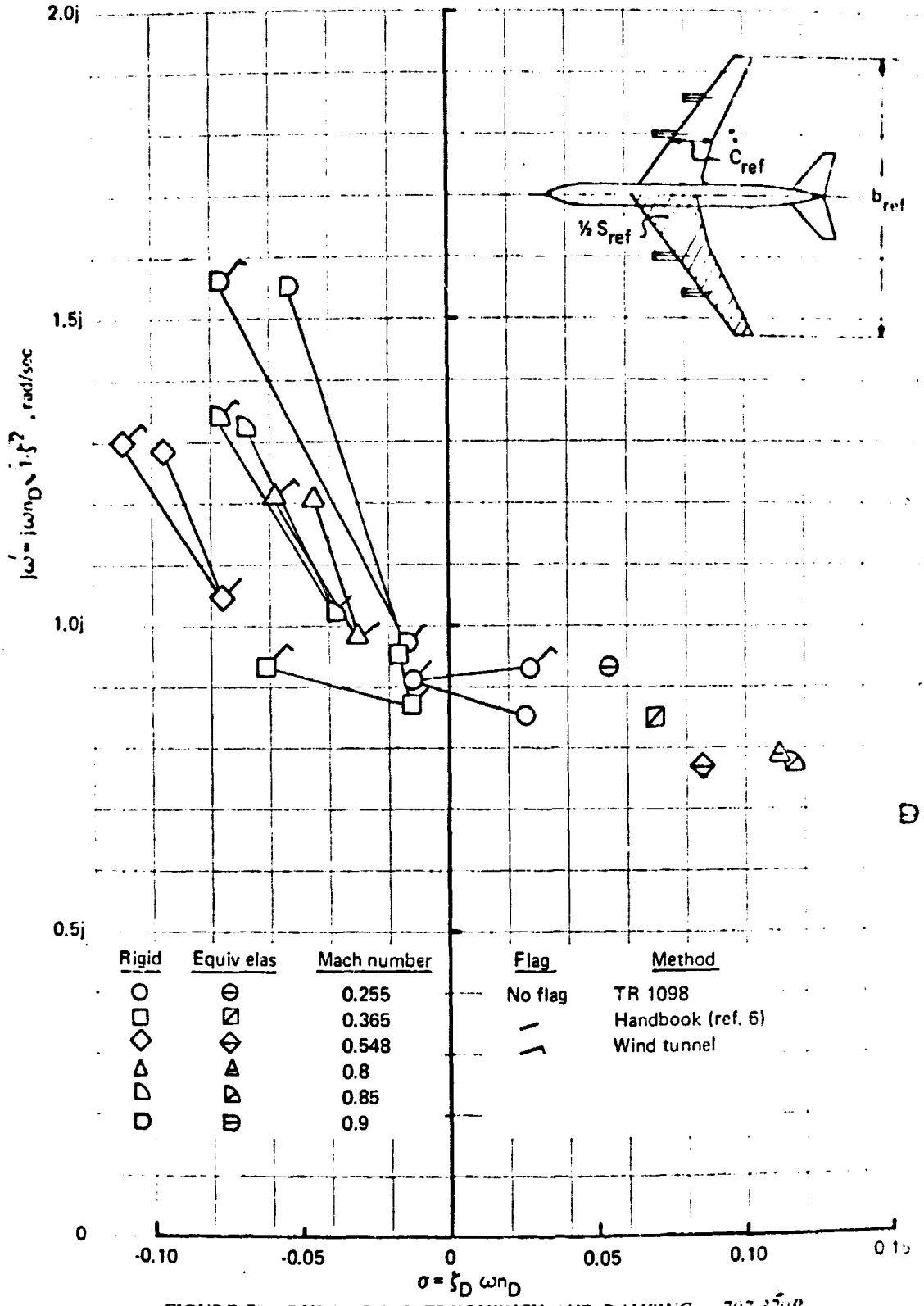

FIGURE 79. DUTCH ROLL FREQUENCY AND DAMPING - 707-320B

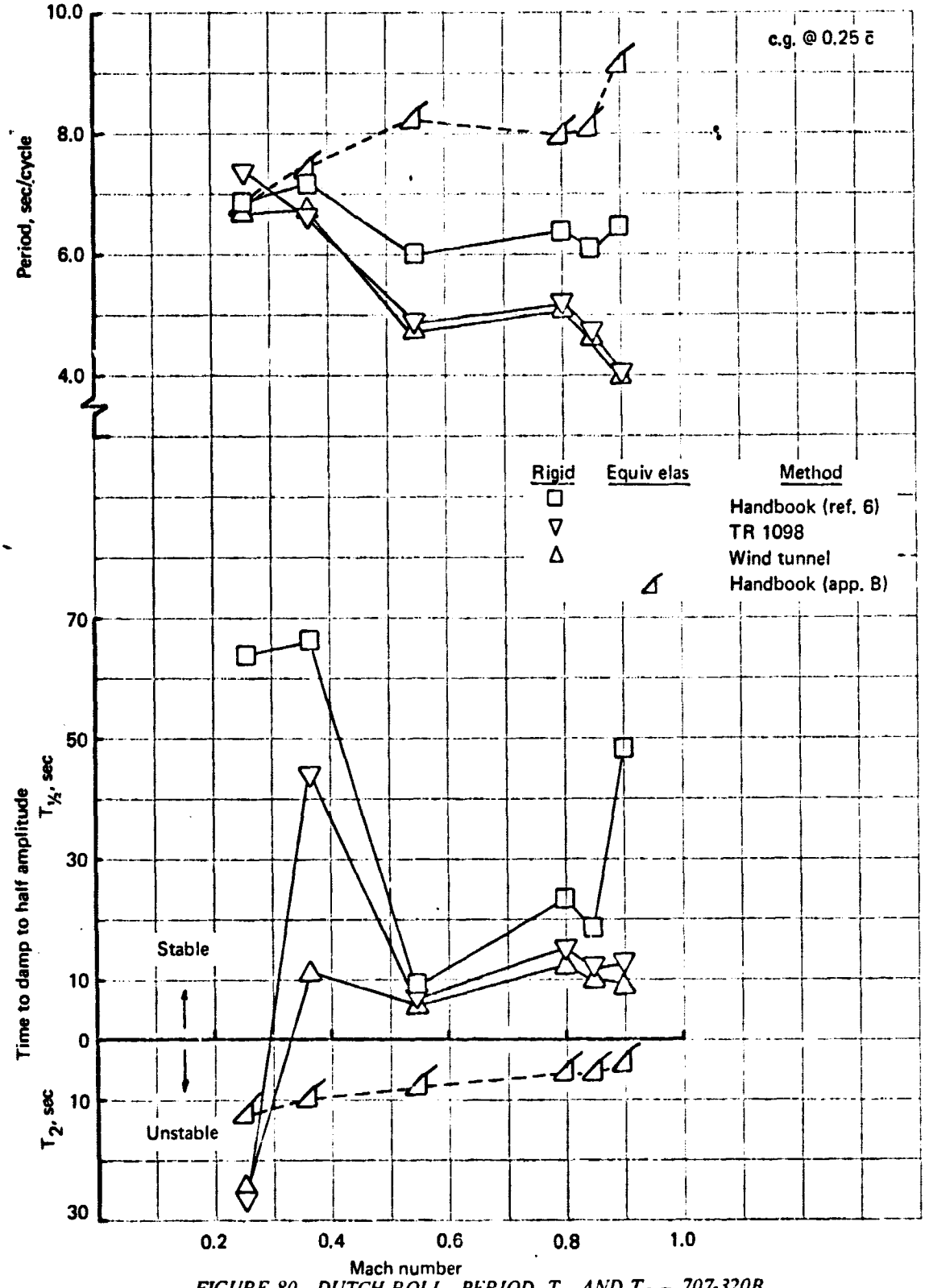

FIGURE 80. DUTCH ROLL PERIOD, $T_{1/2}$ AND T_2 – 707-320B

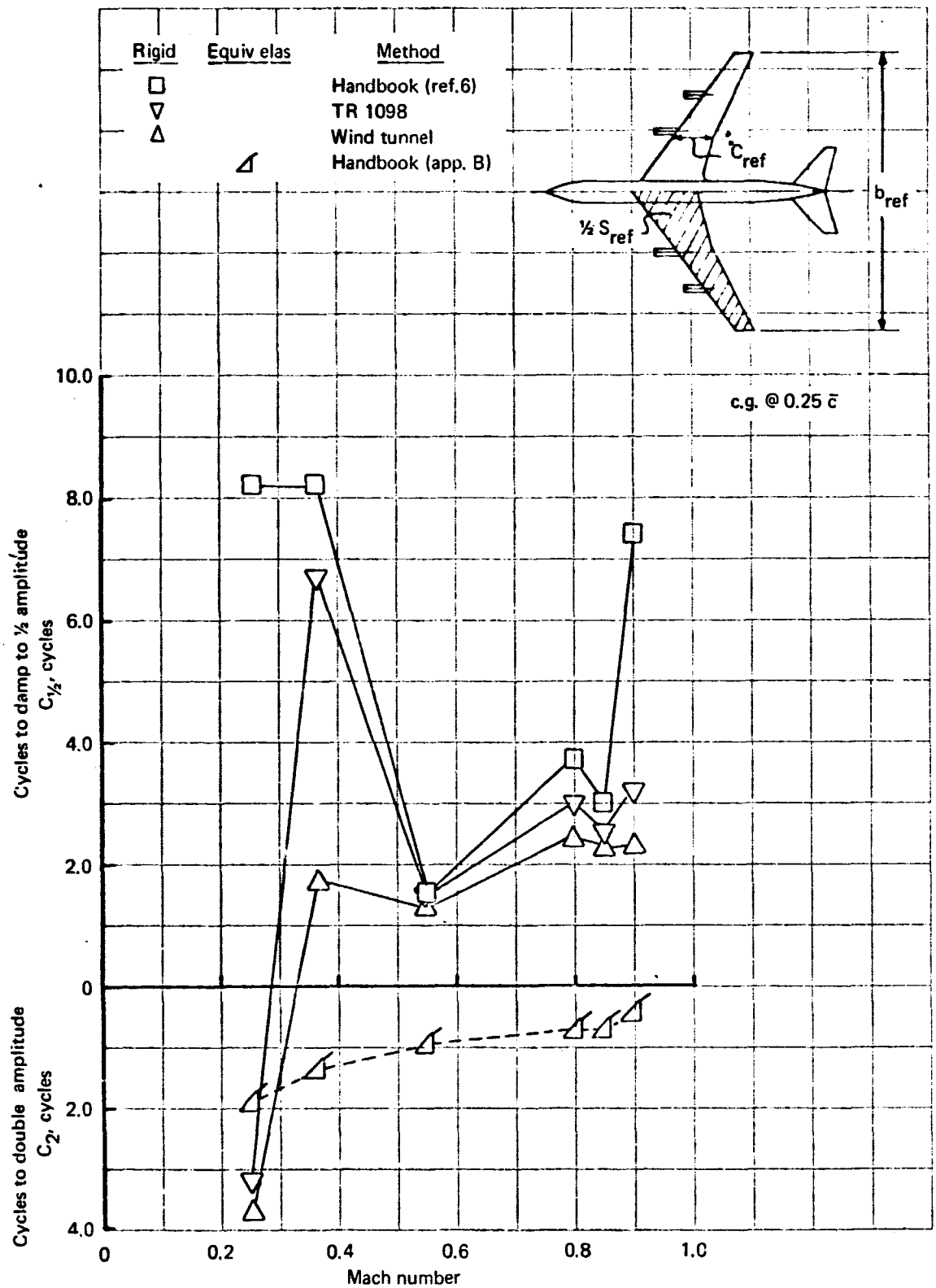

FIGURE 81. DUTCH-ROLL $C_{½}$ AND C_2 – 707-320B

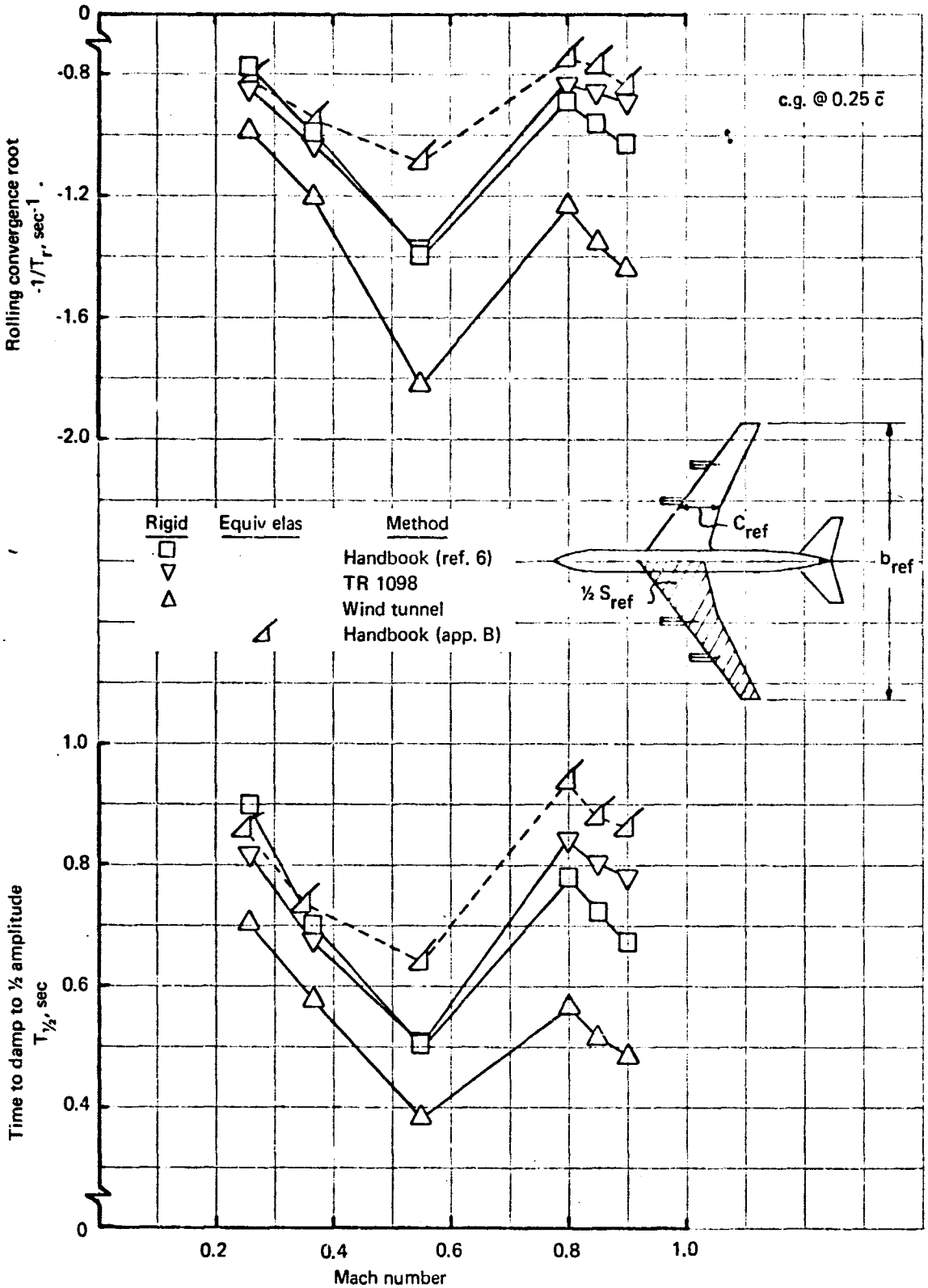

FIGURE 82. ROLLING CONVERGENCE ROOTS AND $T_{½}$ – 707-320B

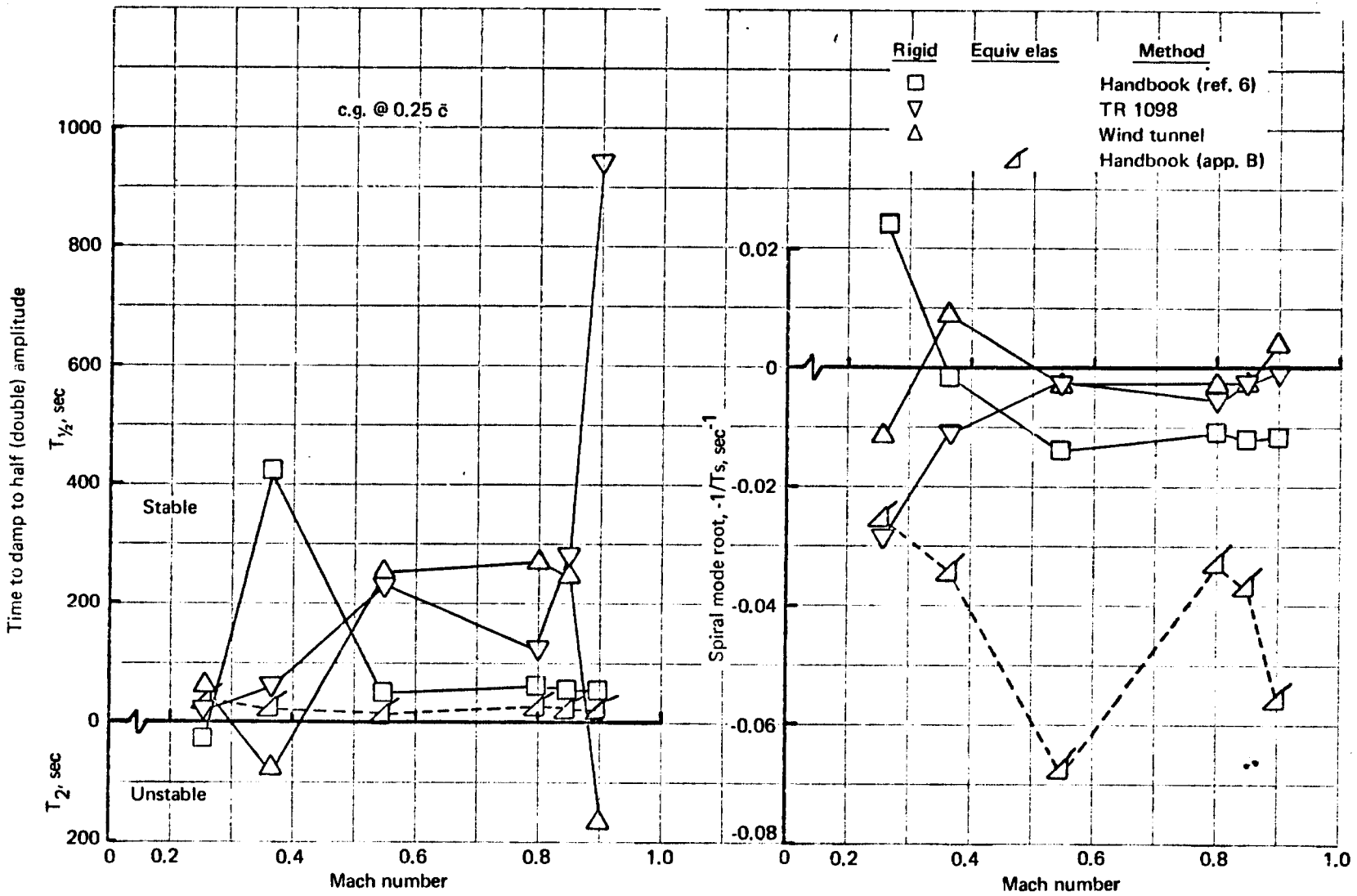

FIGURE 83. SPIRAL MODE ROOTS AND $T_{1/2}$ – 707-320B

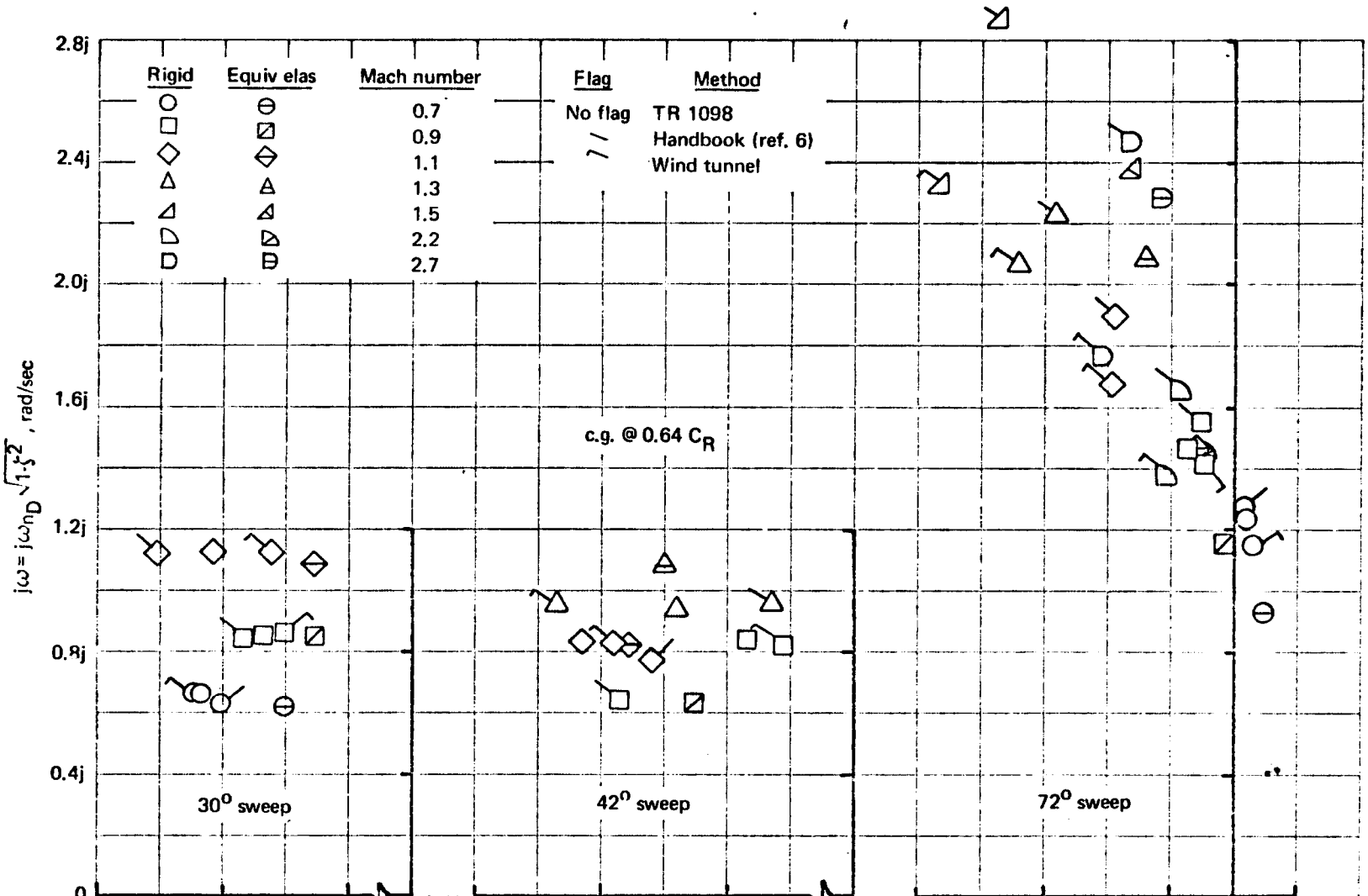

FIGURE 84. DUTCH ROLL FREQUENCY VERSUS DAMPING – SST

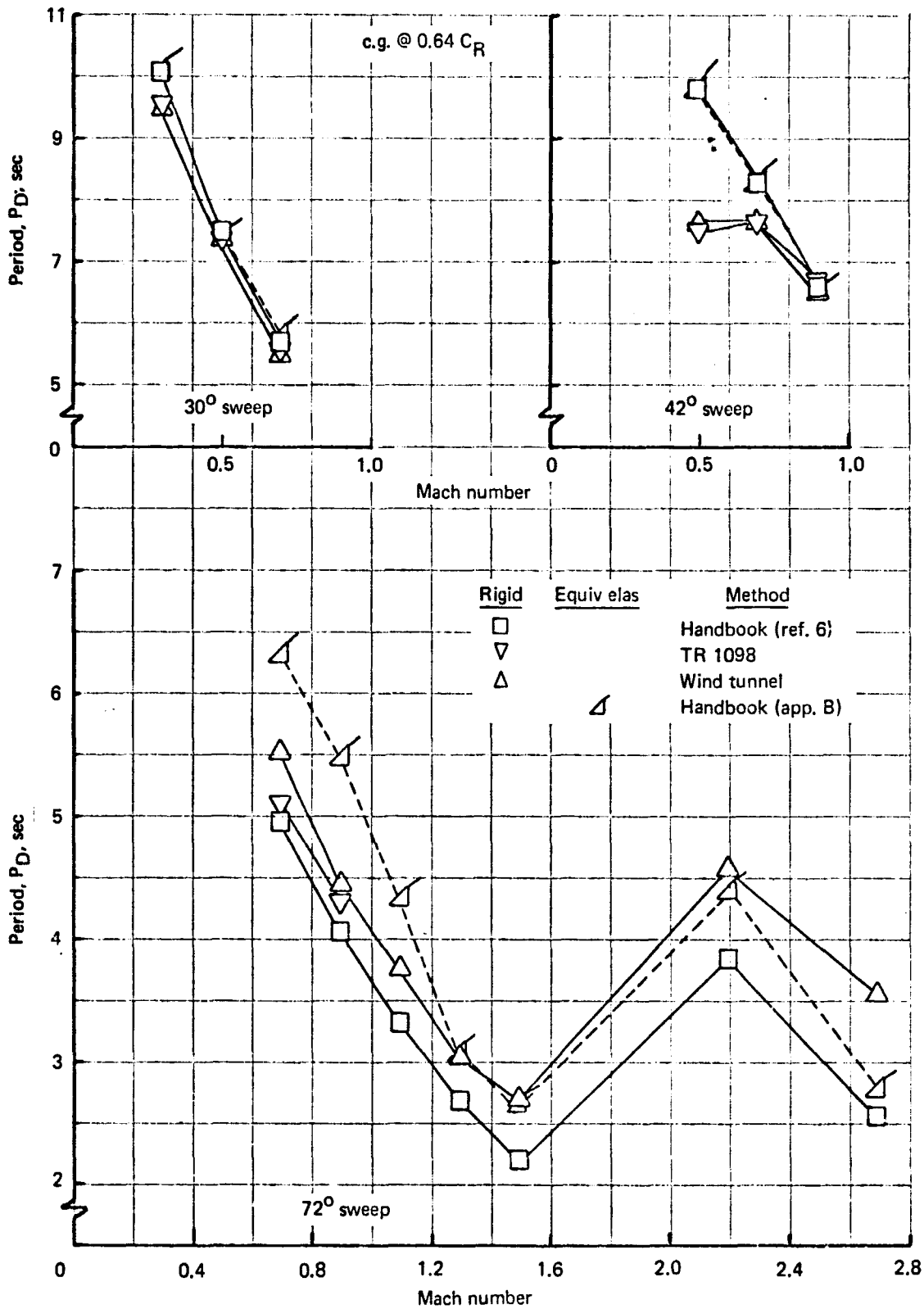

FIGURE 85. DUTCH ROLL PERIOD – SST

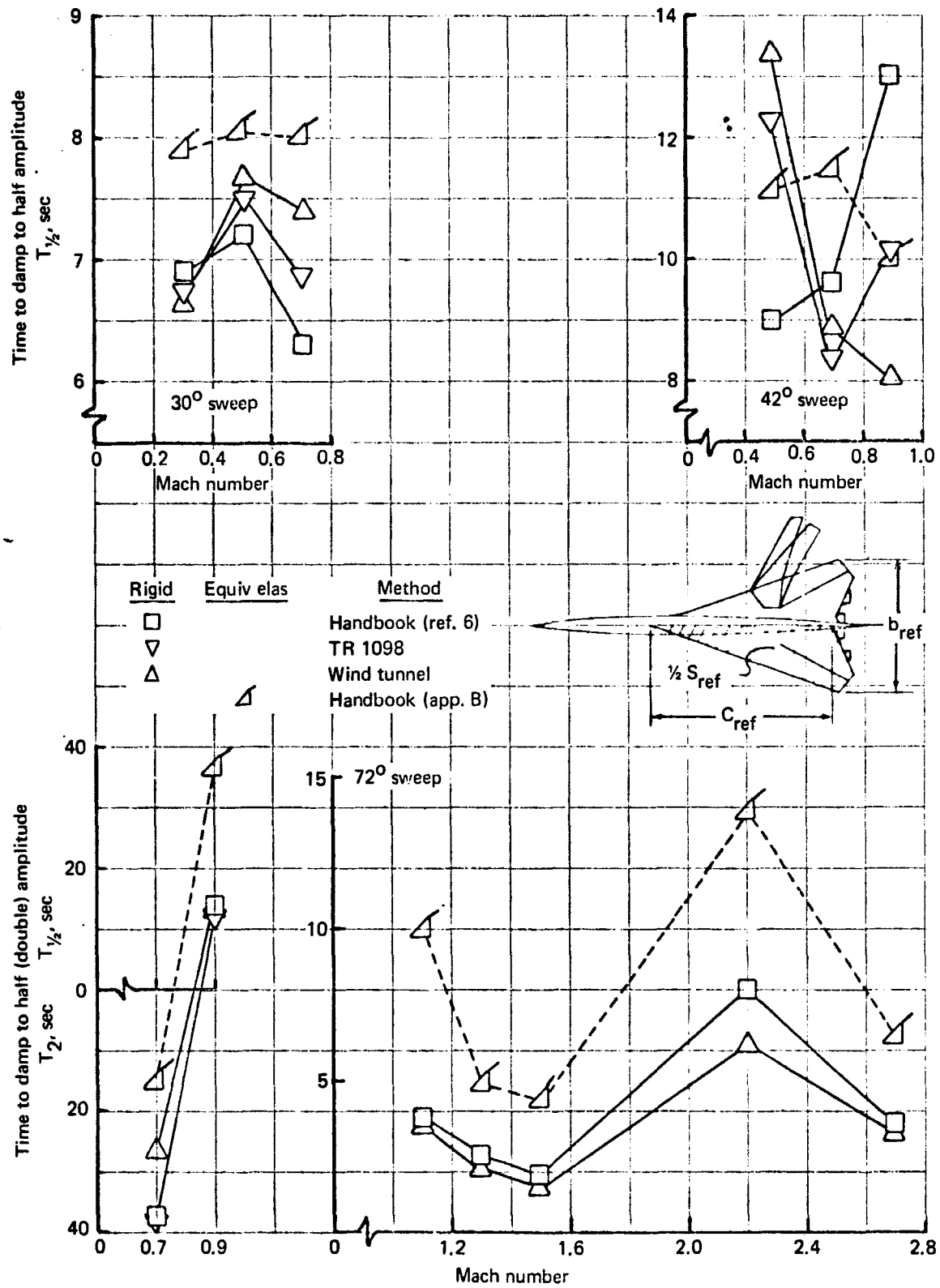

FIGURE 86. DUTCH ROLL $T_{1/2}$ AND T_2 – SST

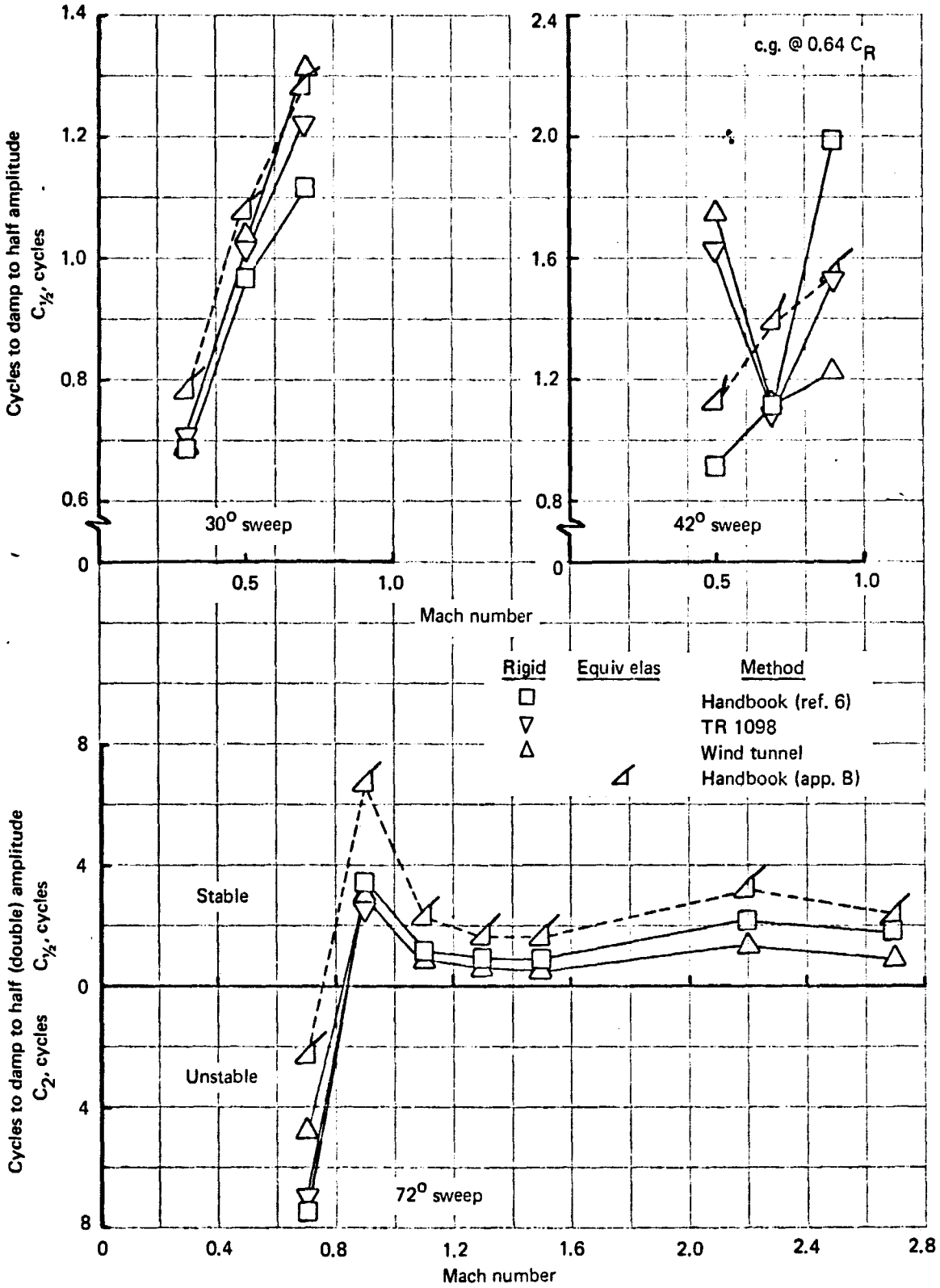

FIGURE 87. DUTCH ROLL $C_{1/2}$ AND C_2 – SST

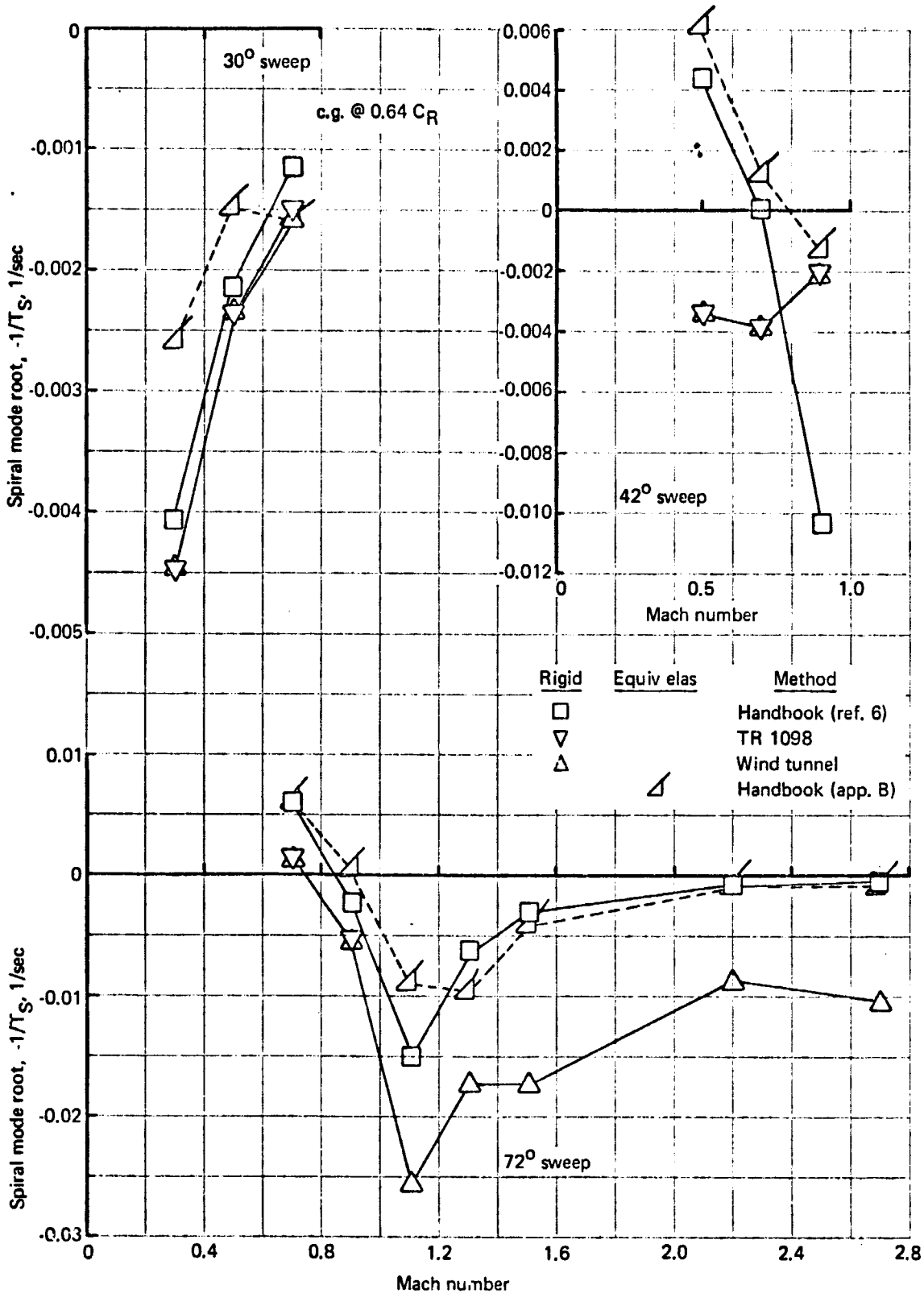

FIGURE 88. SPIRAL MODE ROOTS - SST

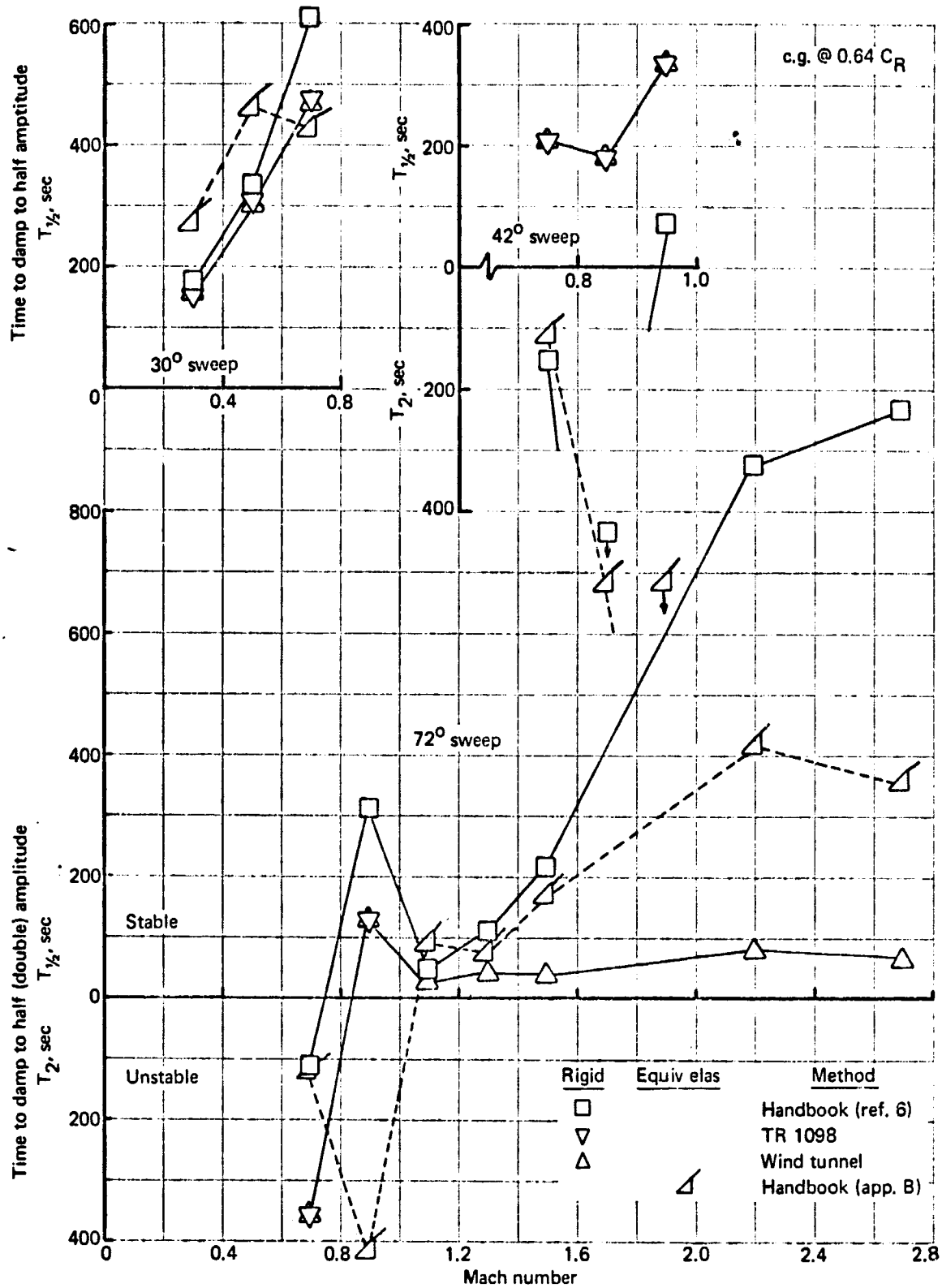

FIGURE 89. SPIRAL MODE $T_{1/2}$ AND T_2 – SST

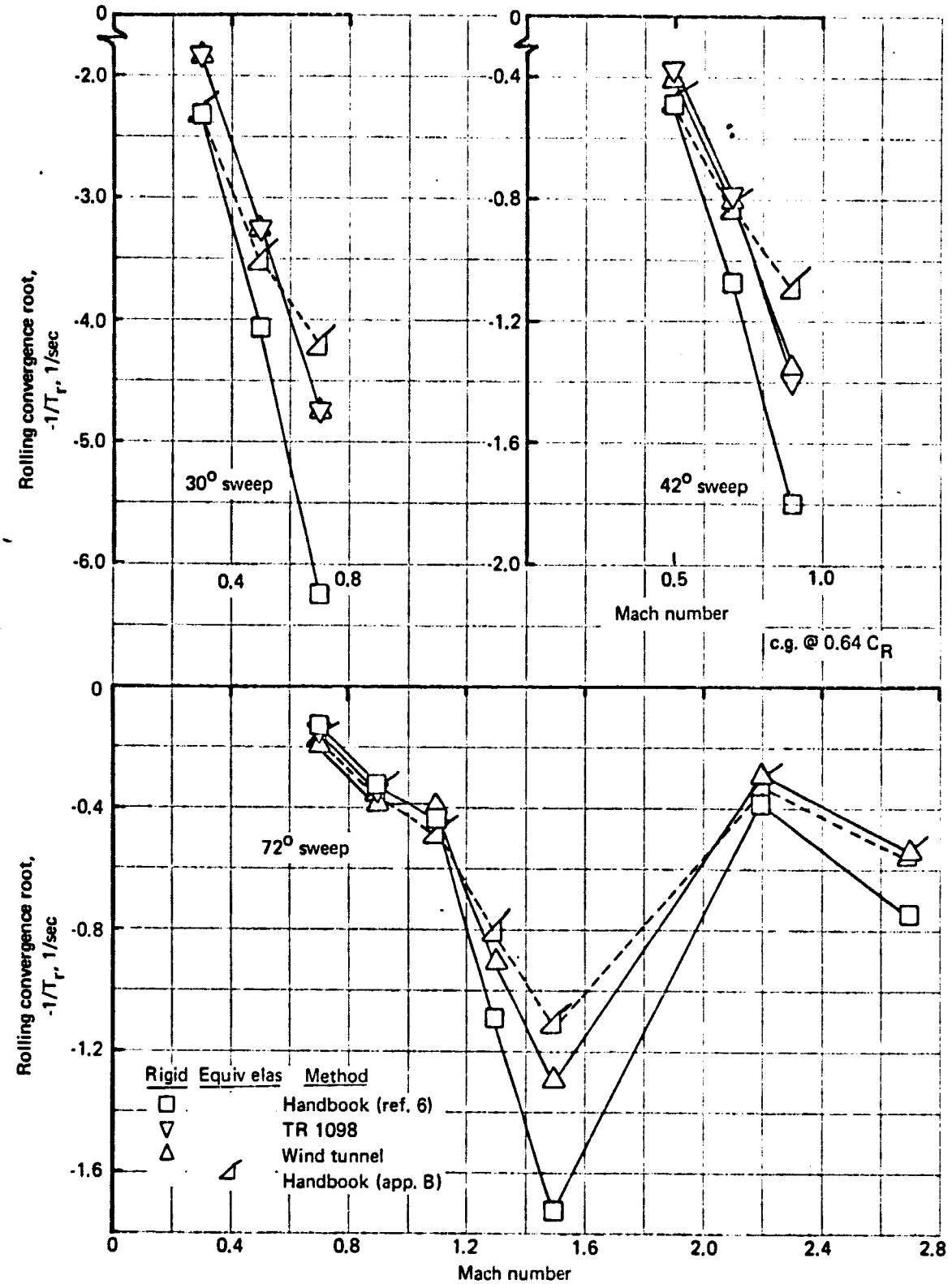

FIGURE 90. ROLLING CONVERGENCE MODE ROOTS – SST

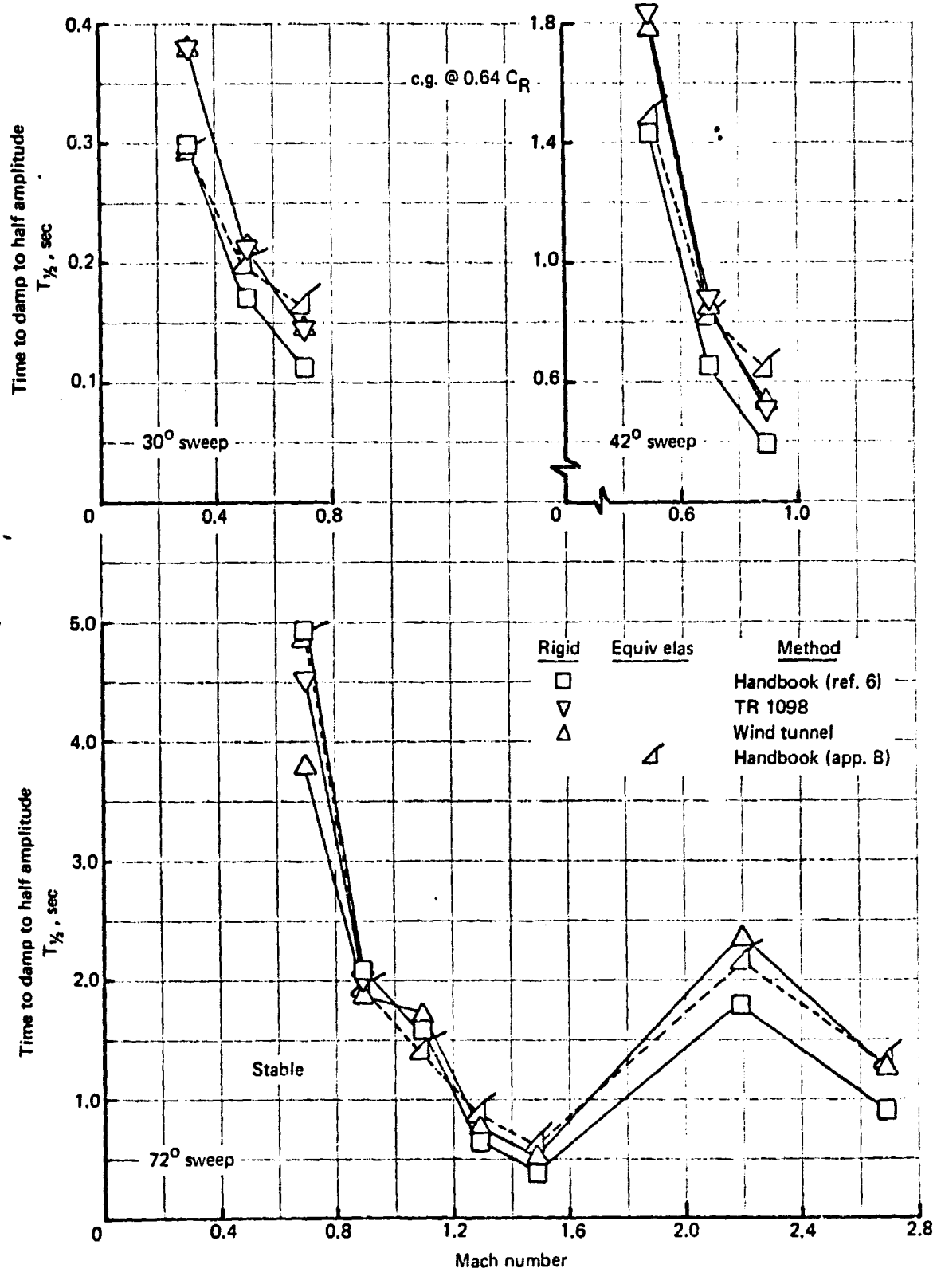

FIGURE 91. ROLLING CONVERGENCE MODE $T_{1/2}$ – SST

8.6 Parametric Study Data

This section presents the complete set of data calculated for the parametric studies. Section 7 contains selected material from and all discussion of the parametric studies. The data in this section show the changes in short period and phugoid frequency and damping due to variations in $C_{L_{\dot{\alpha}}}$ and $C_{m_{\dot{\alpha}}}$ for the study airplane at the study flight conditions. Changes in Dutch roll frequency and damping and the spiral and rolling convergence roots due to variations in $C_{Y_{\dot{\beta}}}$, $C_{\ell_{\dot{\beta}}}$, and $C_{n_{\dot{\beta}}}$ are also shown for the subsonic study flight conditions (except for the SST at 72° leading edge sweep). Figures 92 through 108 and tables 23 through 25 give the parametric study data.

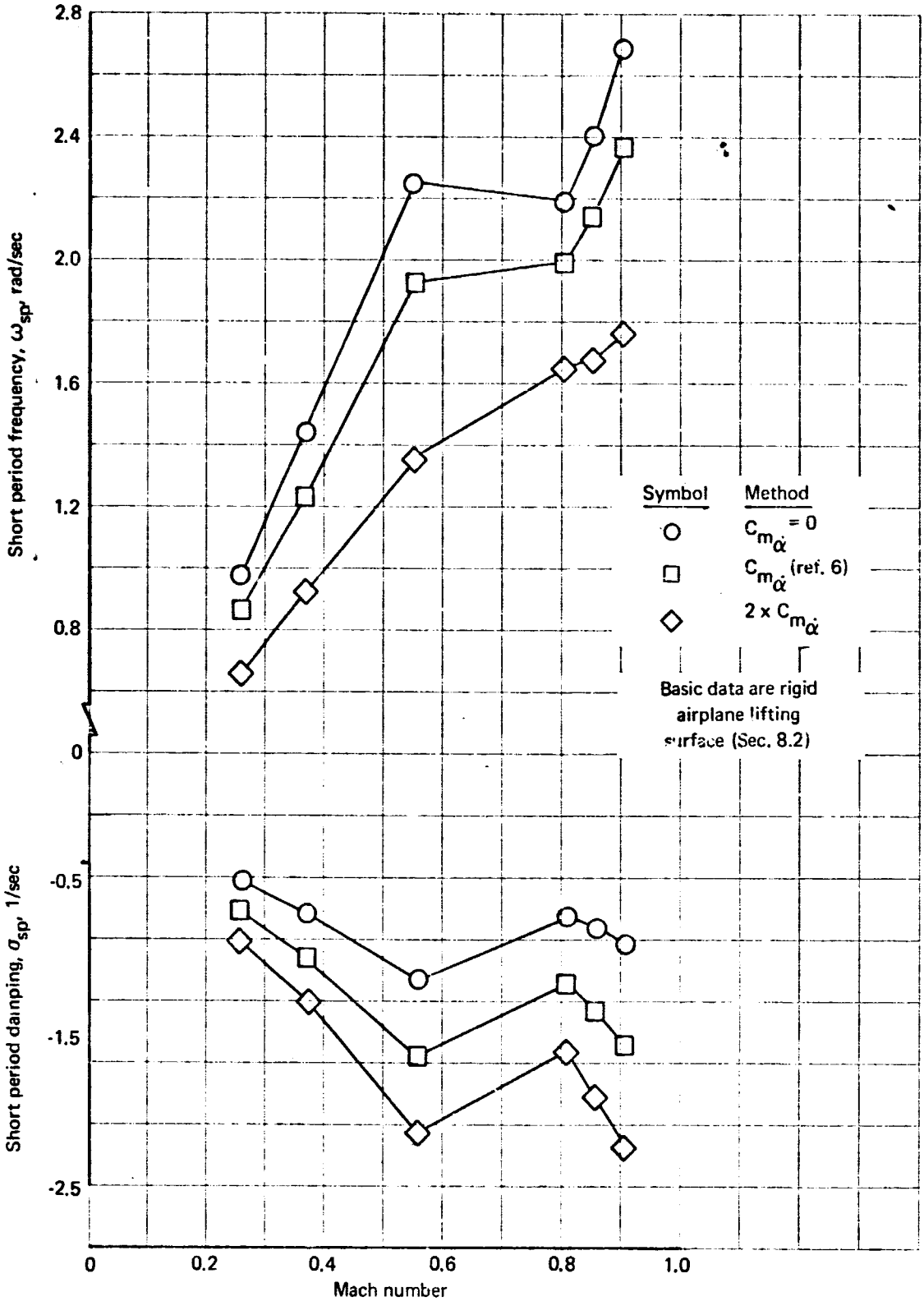

FIGURE 92. CHANGES IN SHORT PERIOD MODE CHARACTERISTICS DUE TO VARIATIONS IN $C_{m_{\dot{\alpha}}}$ – 707-320B

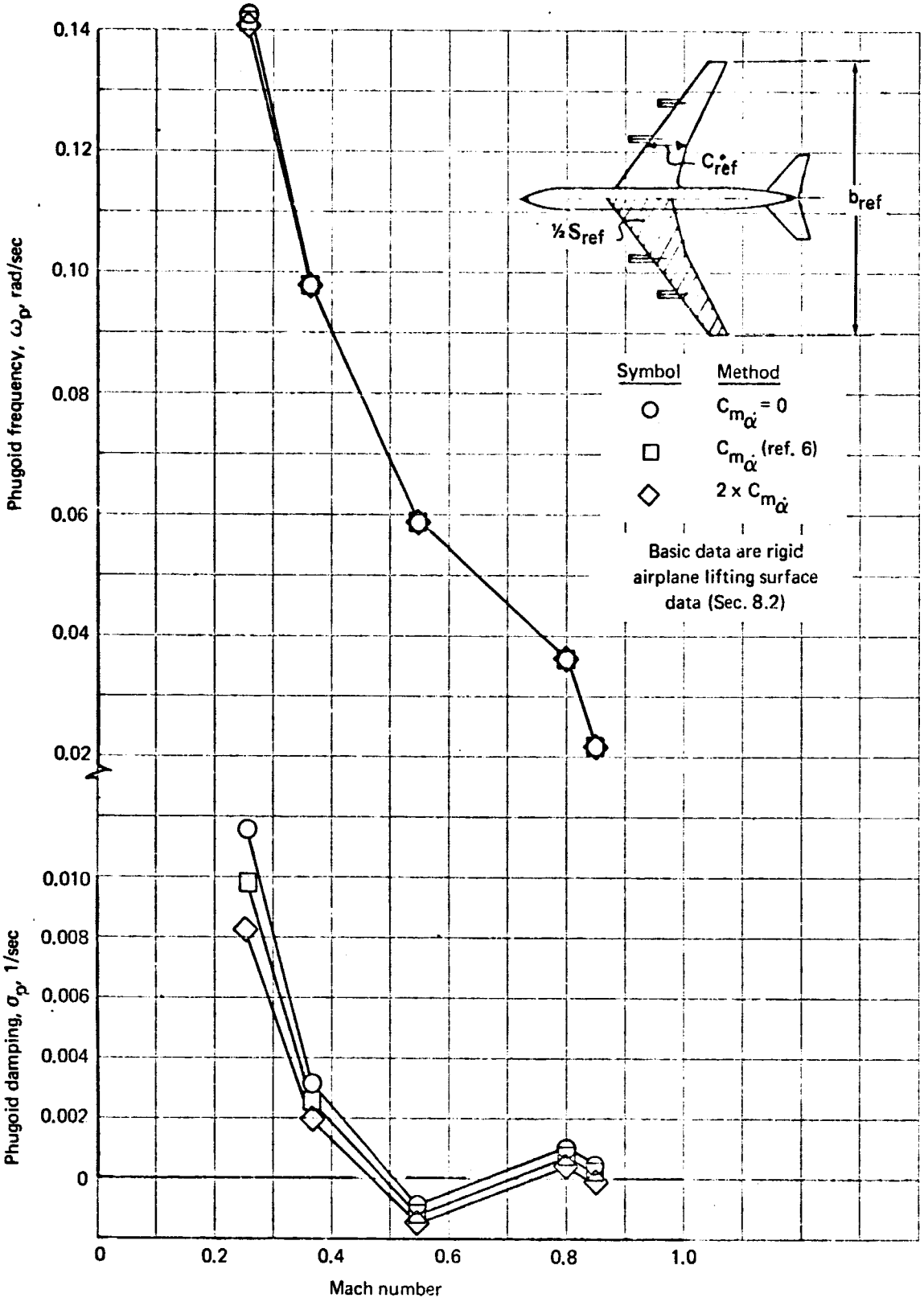

FIGURE 93. CHANGES IN PHUGOID MODE CHARACTERISTICS DUE TO VARIATIONS IN $C_{m_{\dot{\alpha}}}$ – 707-320B

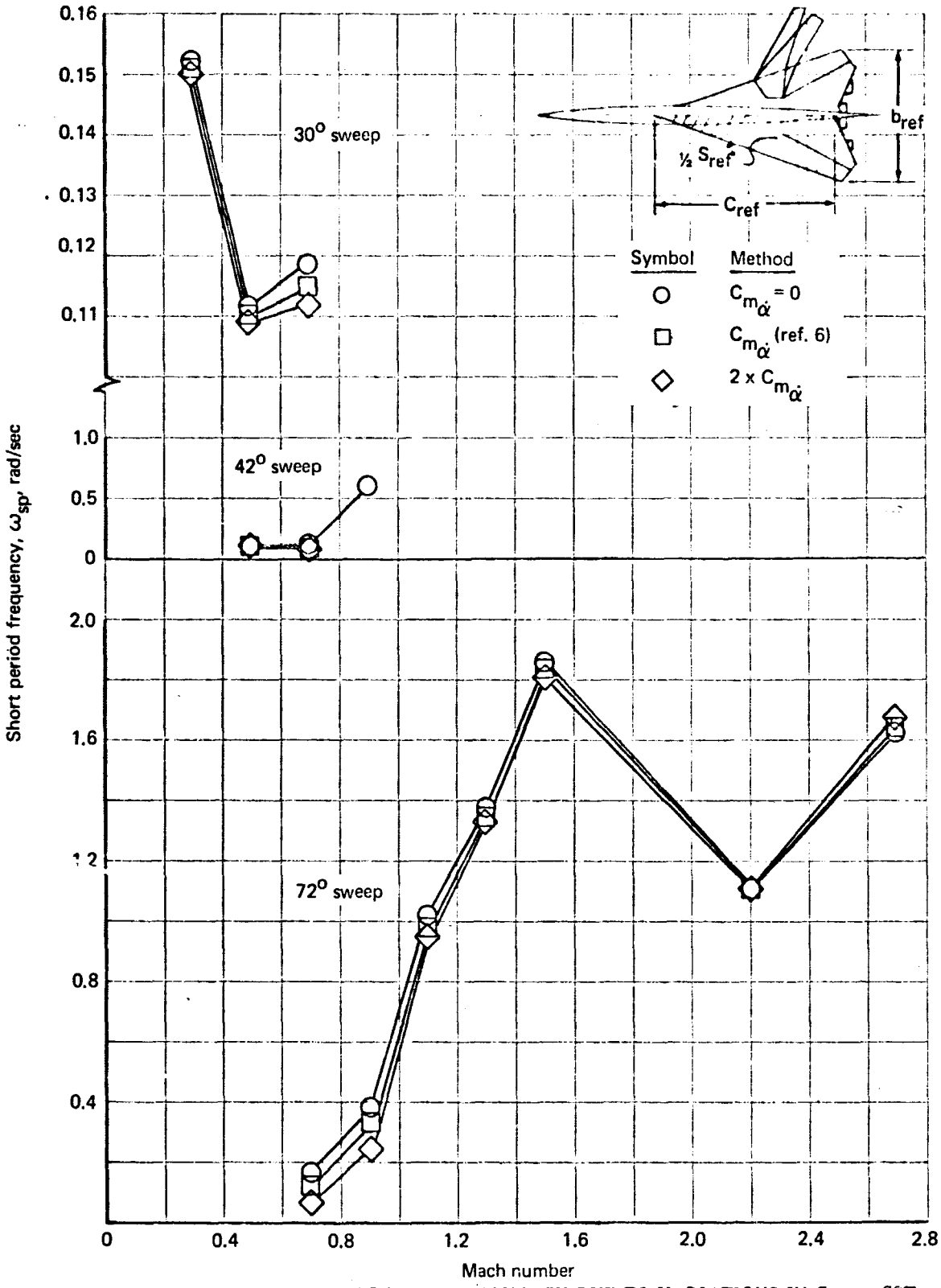

FIGURE 94. CHANGES IN SHORT PERIOD FREQUENCY DUE TO VARIATIONS IN $C_{m_{\dot{\alpha}}}$ – SST

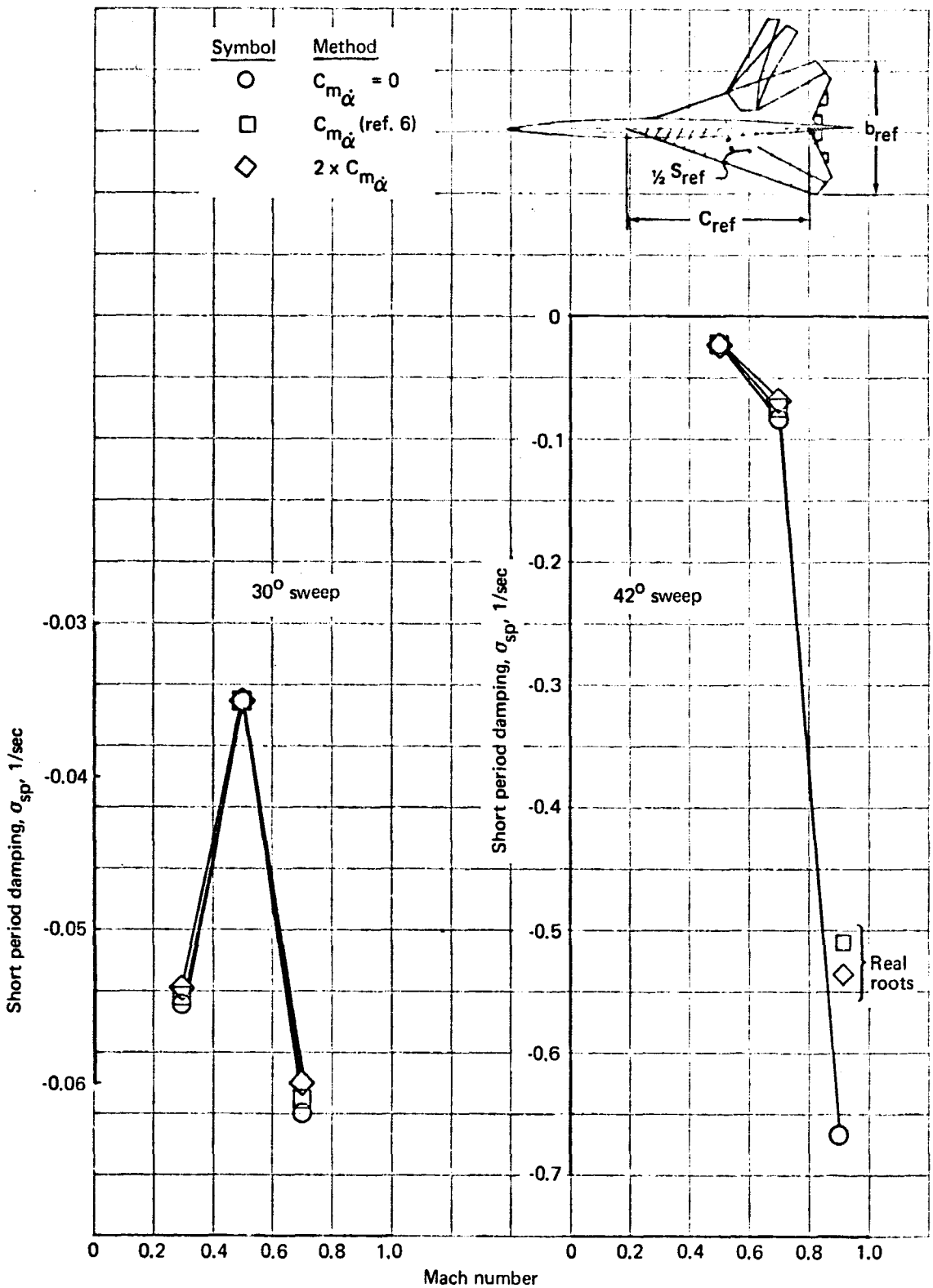

FIGURE 95. CHANGES IN SHORT PERIOD DAMPING DUE TO VARIATIONS IN $C_{m_{\dot{\alpha}}}$ – 30° AND 42° SST

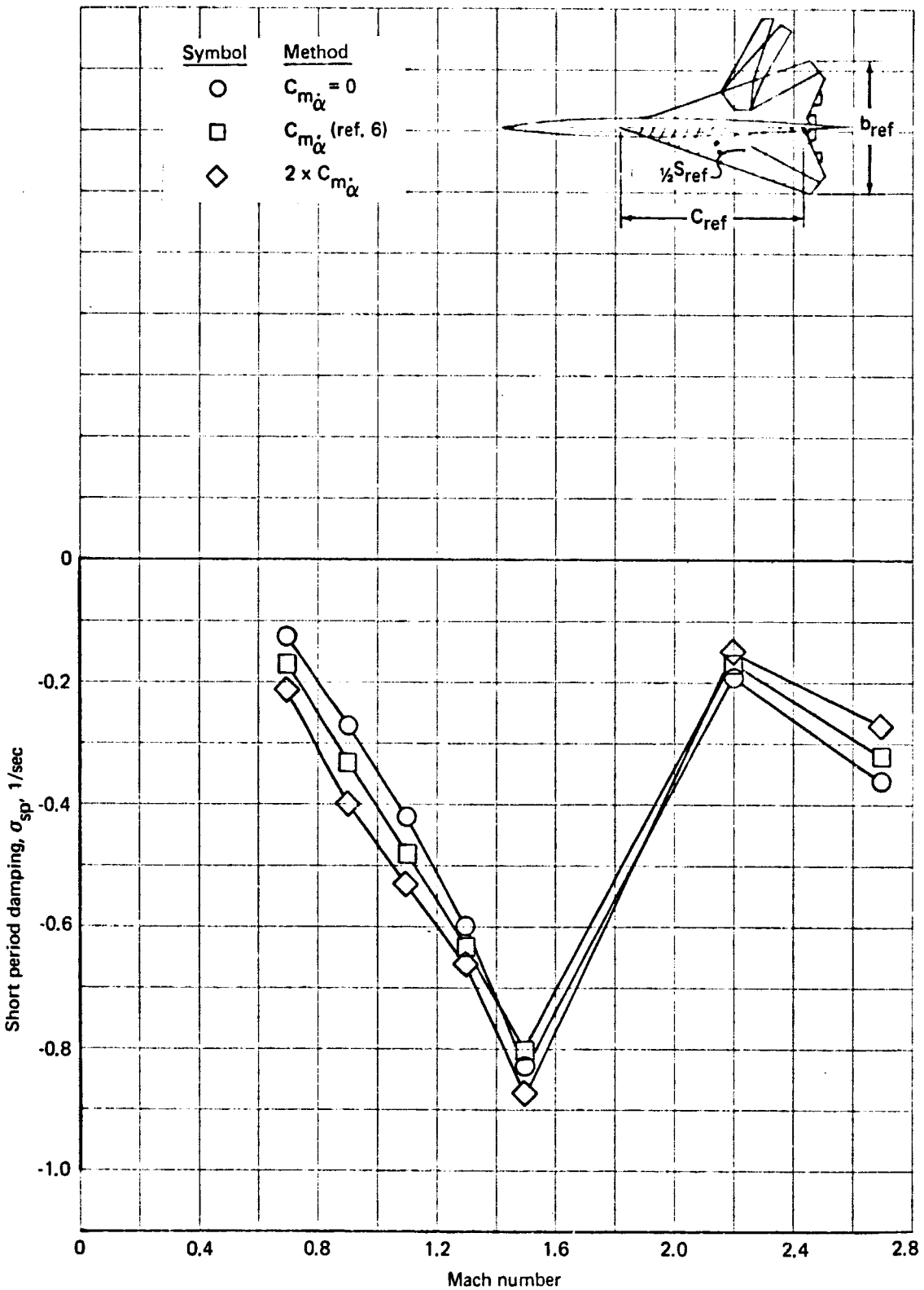

FIGURE 96. CHANGES IN SHORT PERIOD DAMPING DUE TO VARIATIONS IN $C_{m_{\dot{\alpha}}}$ – 72° SST

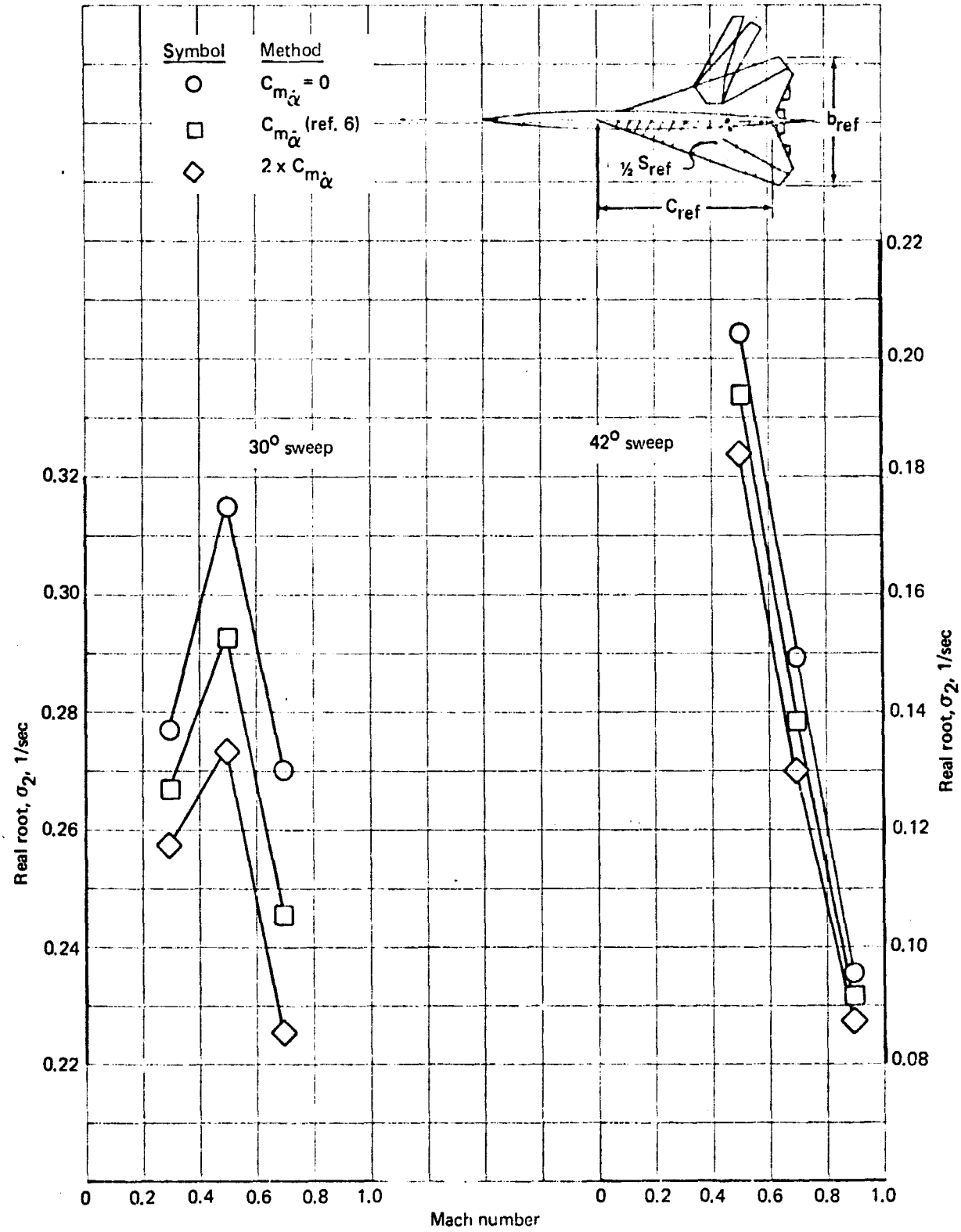

FIGURE 97. CHANGES IN REAL ROOT DUE TO VARIATIONS IN $C_{m_{\dot{\alpha}}}$ – 30° AND 42° SST

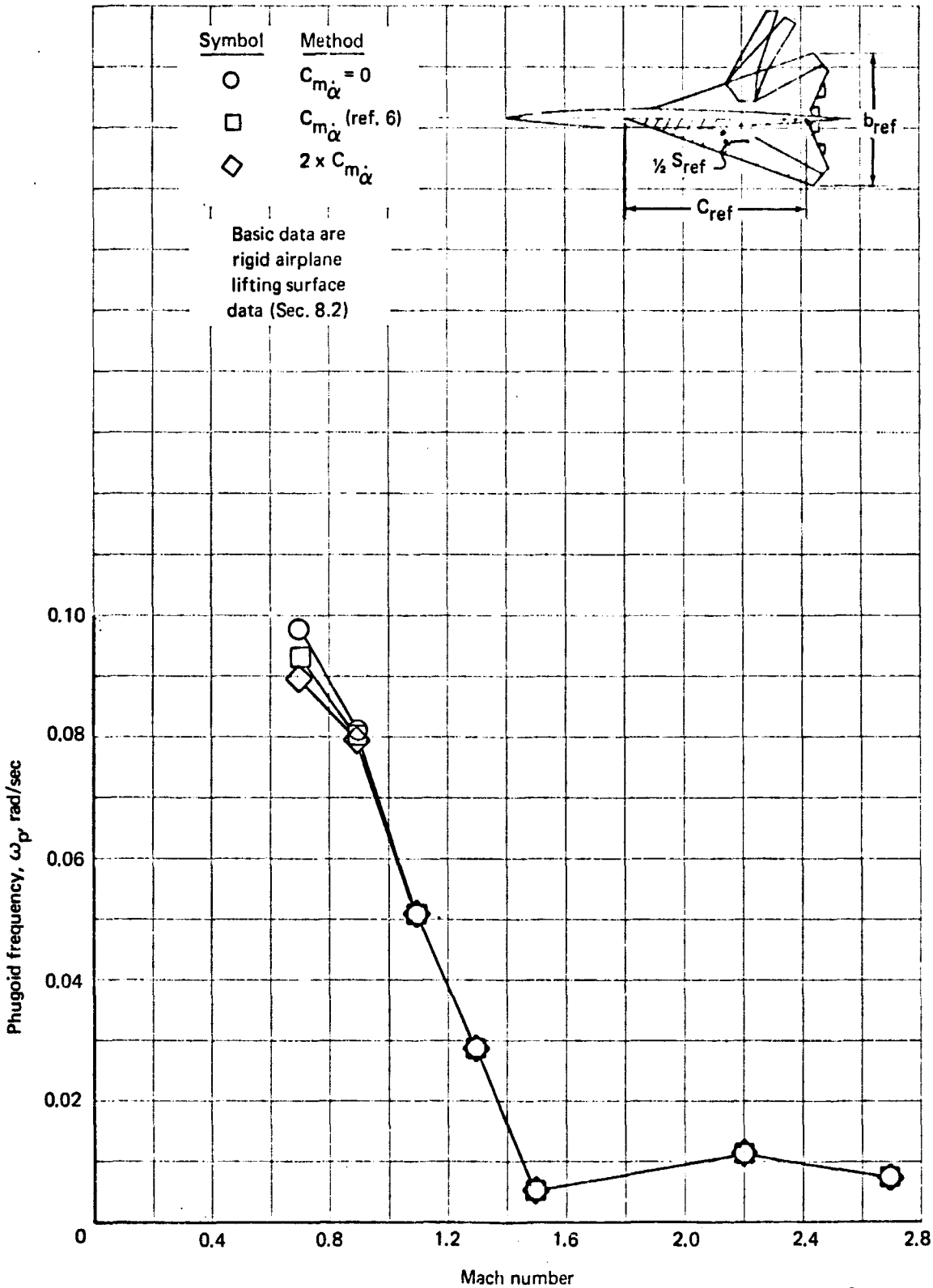

FIGURE 98. CHANGES IN PHUGOID FREQUENCY DUE TO VARIATIONS IN $C_{m_{\dot{\alpha}}}$ – 72° SST

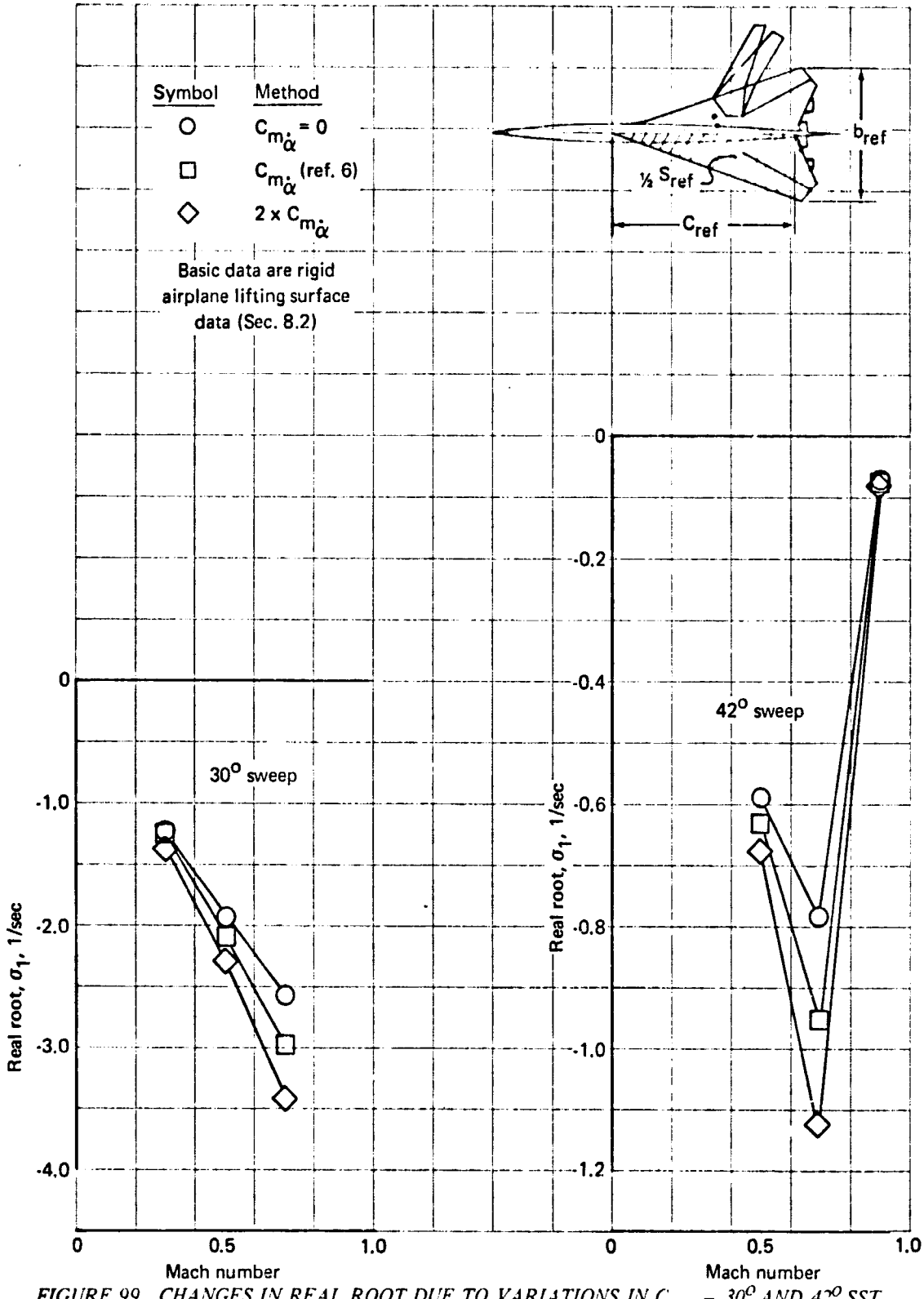

FIGURE 99. CHANGES IN REAL ROOT DUE TO VARIATIONS IN $C_{m_{\dot{\alpha}}}$ – 30° AND 42° SST

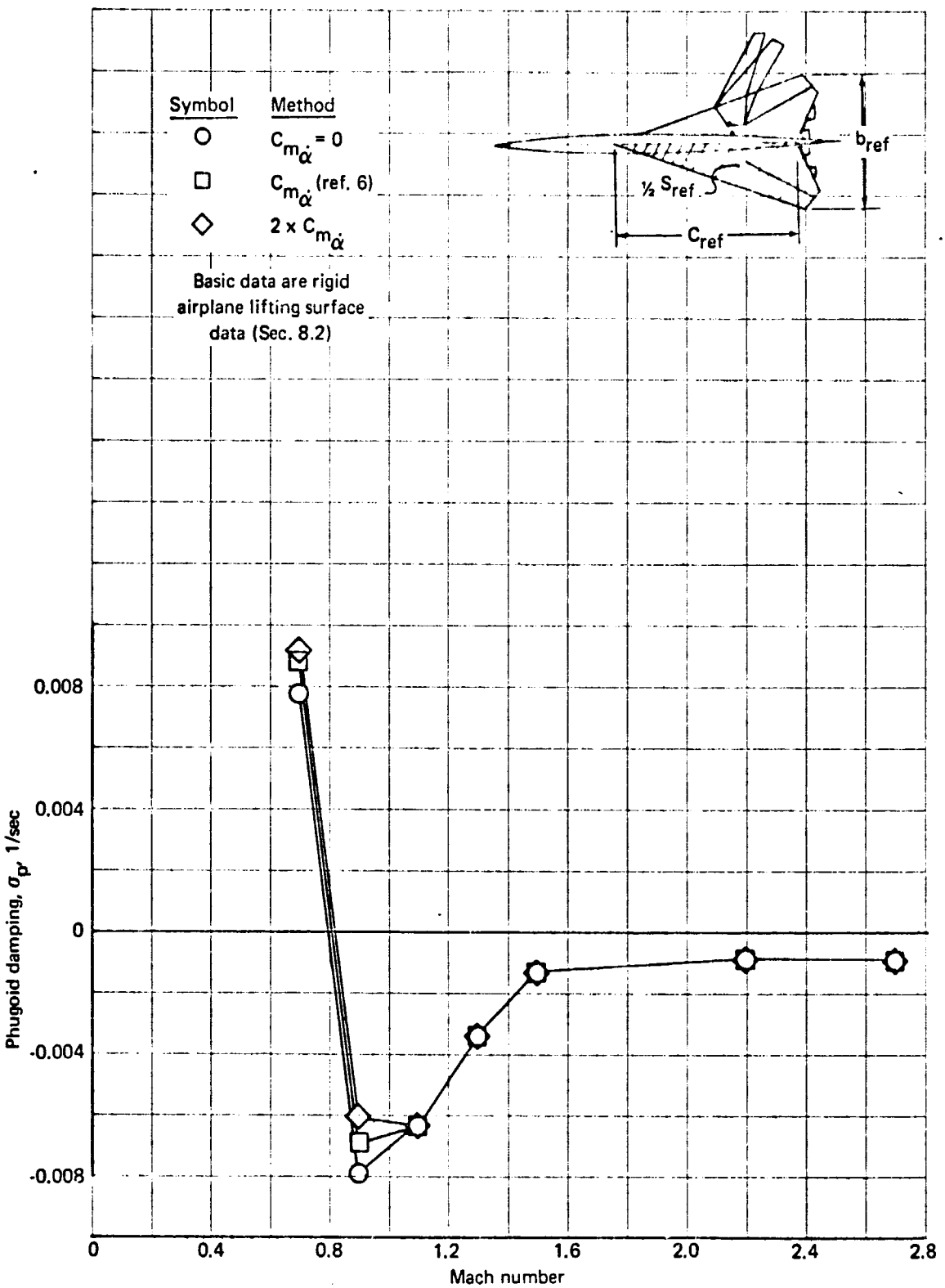

FIGURE 100. CHANGES IN PHUGOID DAMPING DUE TO VARIATIONS IN $C_{m_{\dot{\alpha}}}$ – 72° SST

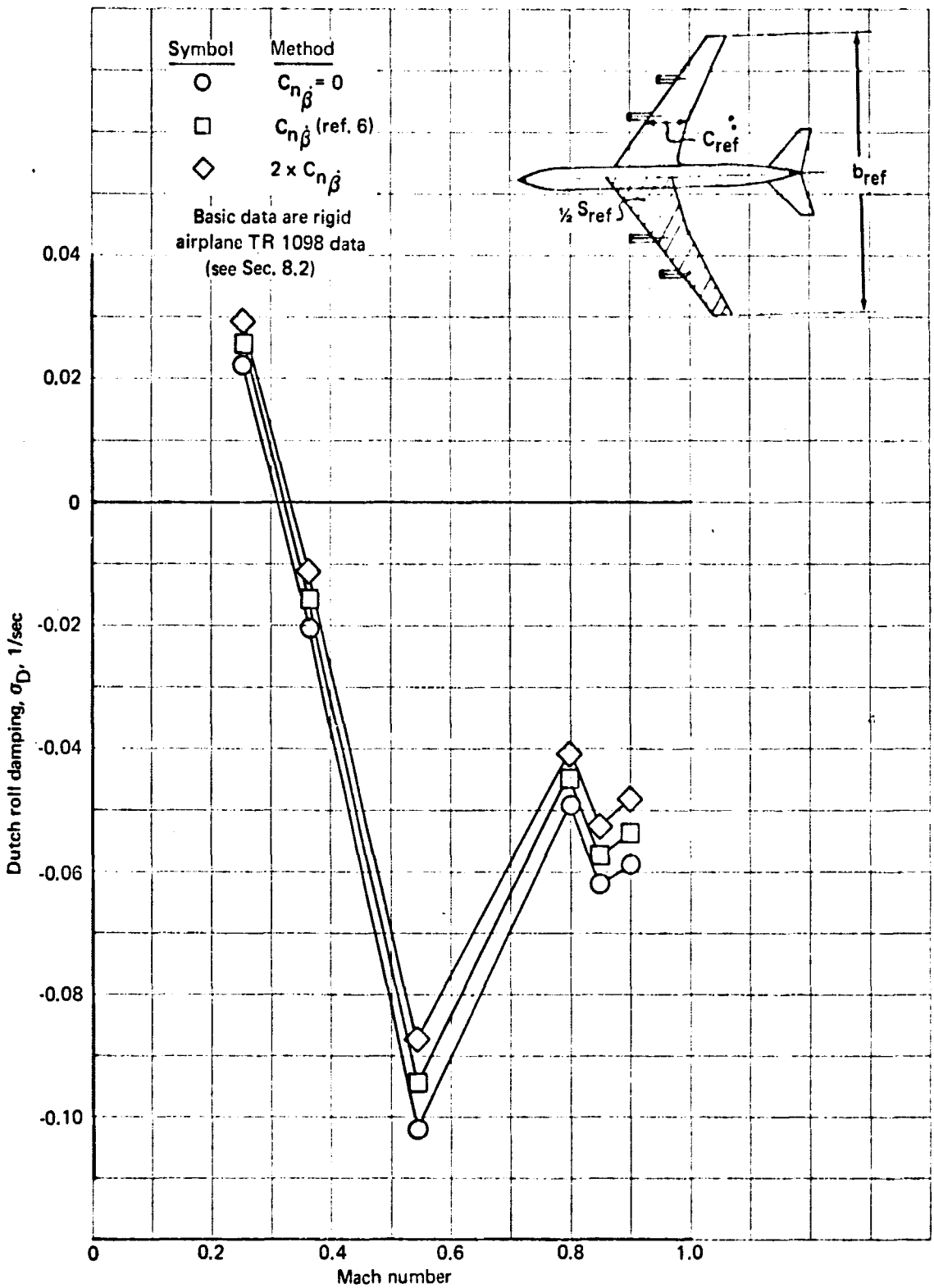

FIGURE 101. CHANGES IN DUTCH ROLL DAMPING DUE TO VARIATIONS IN $C_{n_{\dot{\beta}}}$ – 707-320B

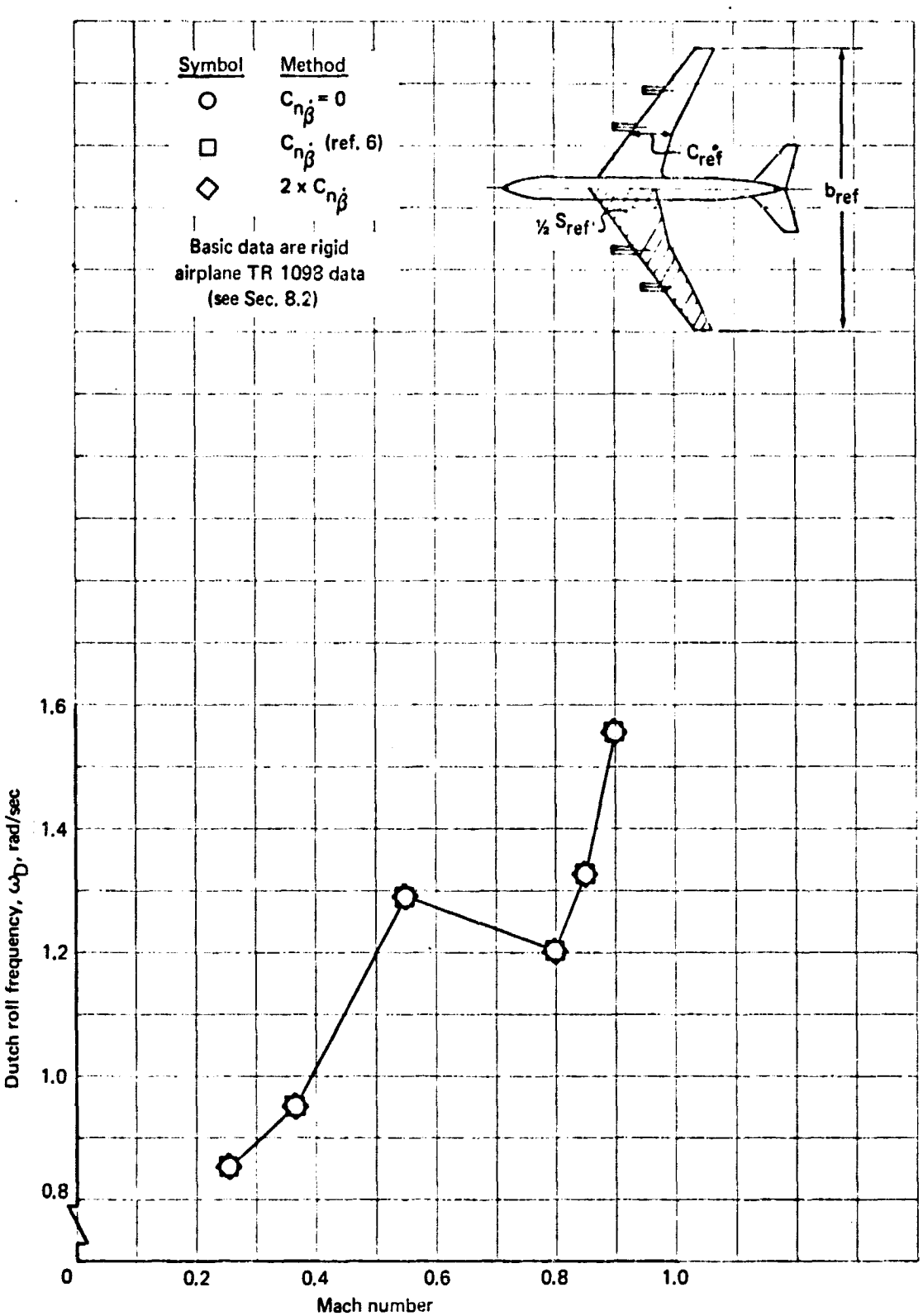

FIGURE 102. CHANGES IN DUTCH ROLL FREQUENCY DUE TO VARIATIONS IN $C_{n_{\dot{\beta}}}$ – 707-320B

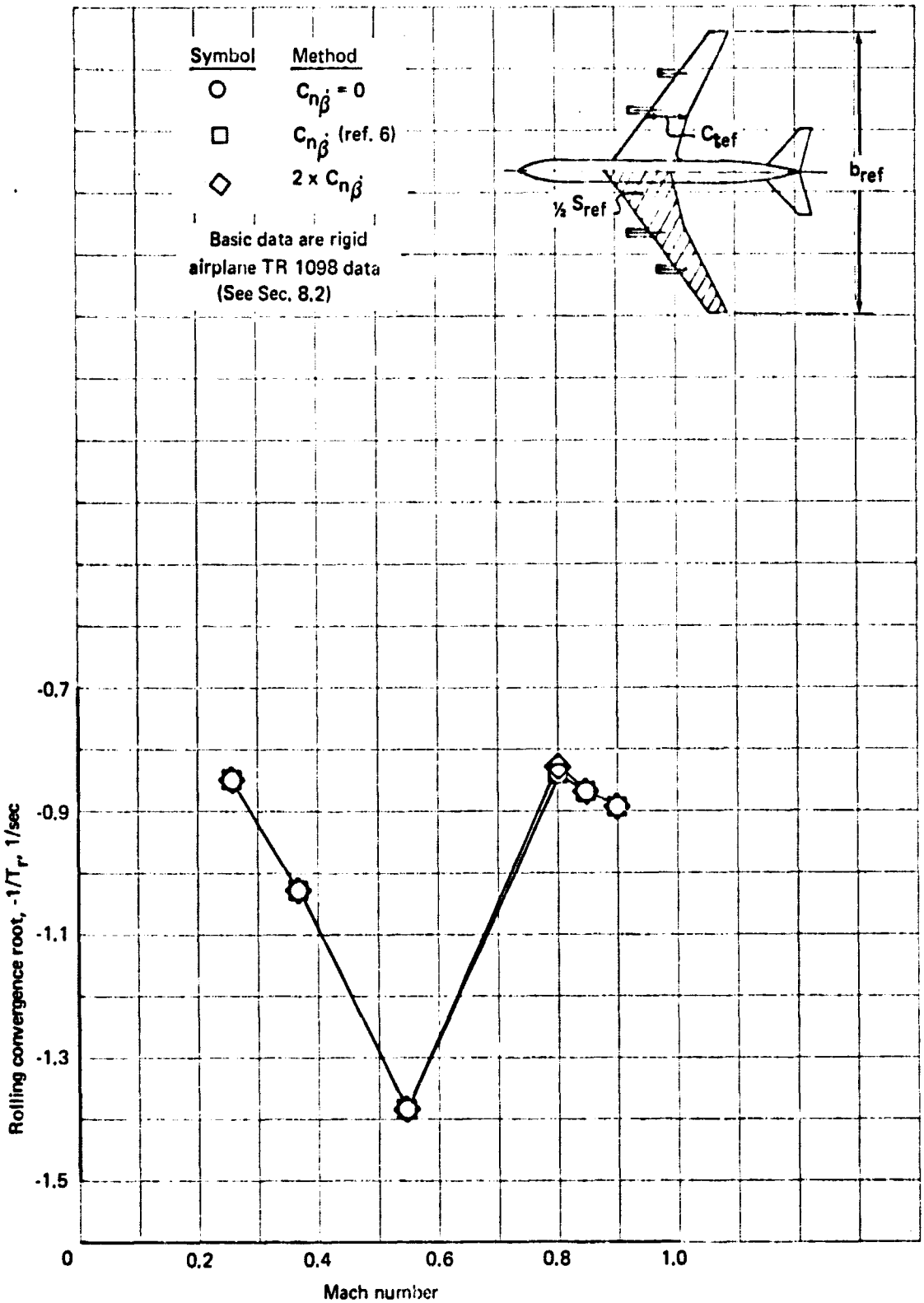

FIGURE 103. CHANGES IN ROLLING CONVERGENCE ROOT DUE TO VARIATIONS IN $C_{n_{\dot{\beta}}}$ – 707-320B

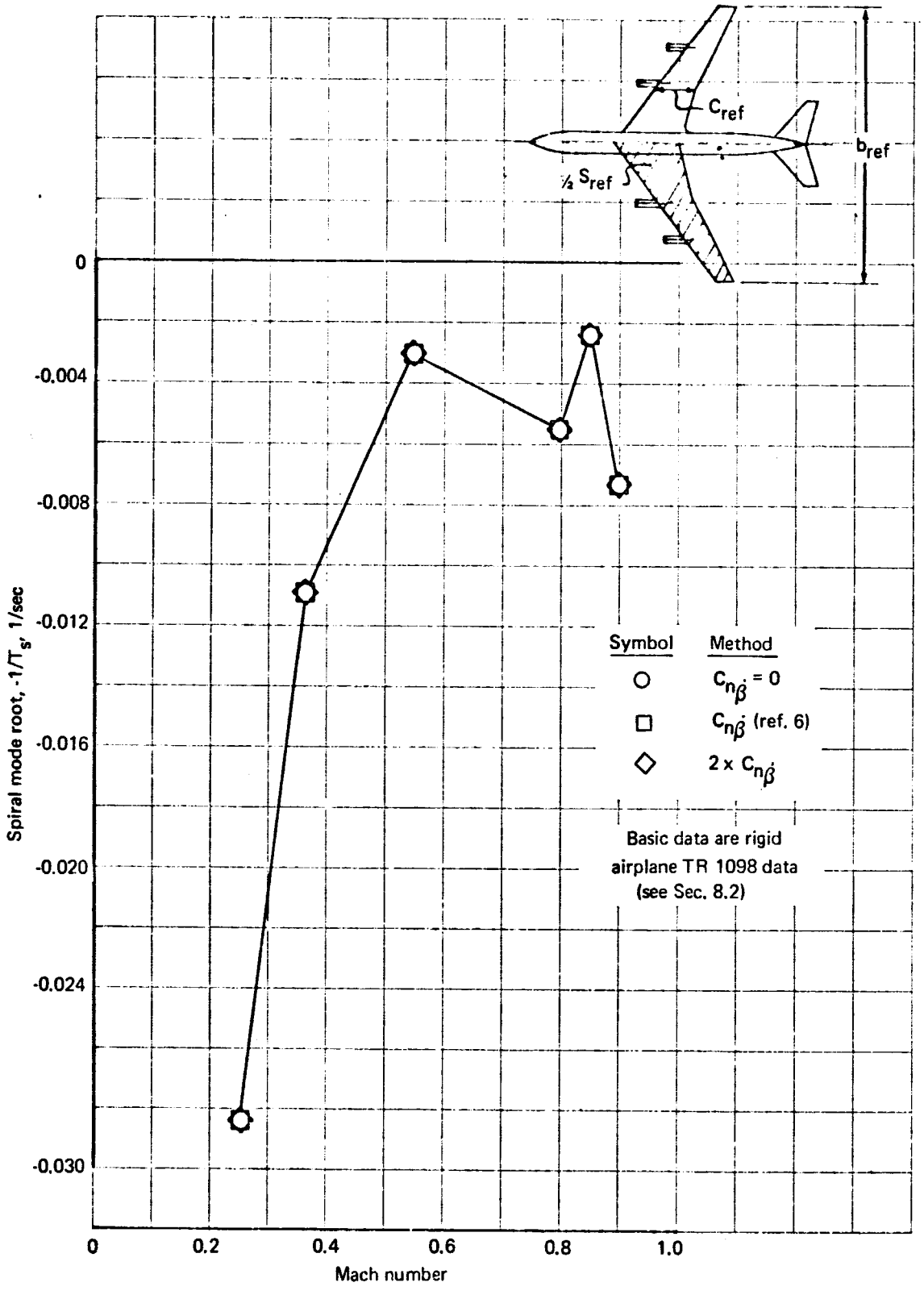

FIGURE 104. CHANGES IN SPIRAL MODE ROOT DUE TO VARIATIONS IN $C_{n_{\dot{\beta}}}$ – 707-320B

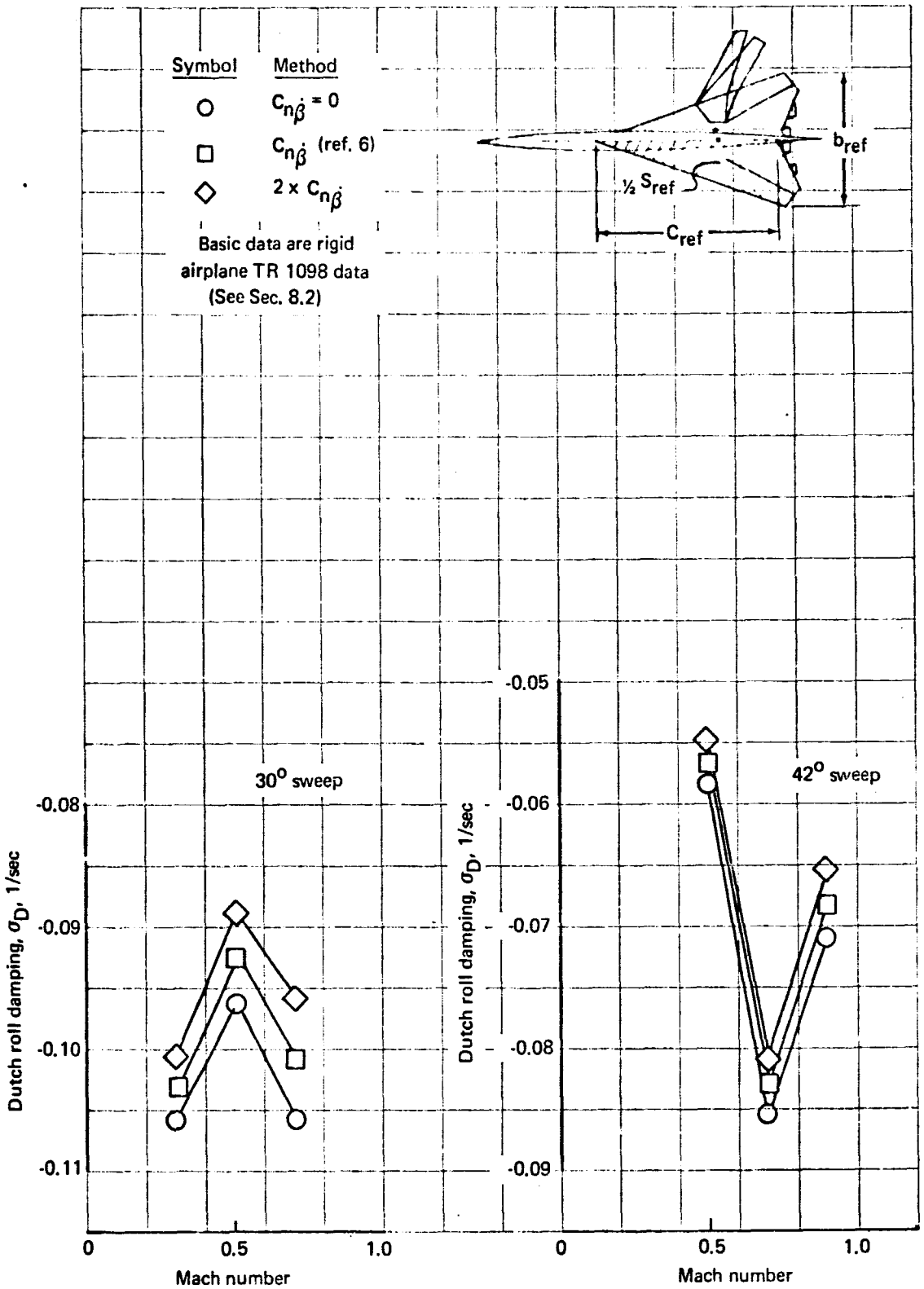

FIGURE 105. CHANGES IN DUTCH ROLL DAMPING DUE TO VARIATIONS IN $C_{n_{\dot{\beta}}}$ – 30° AND 42° SST

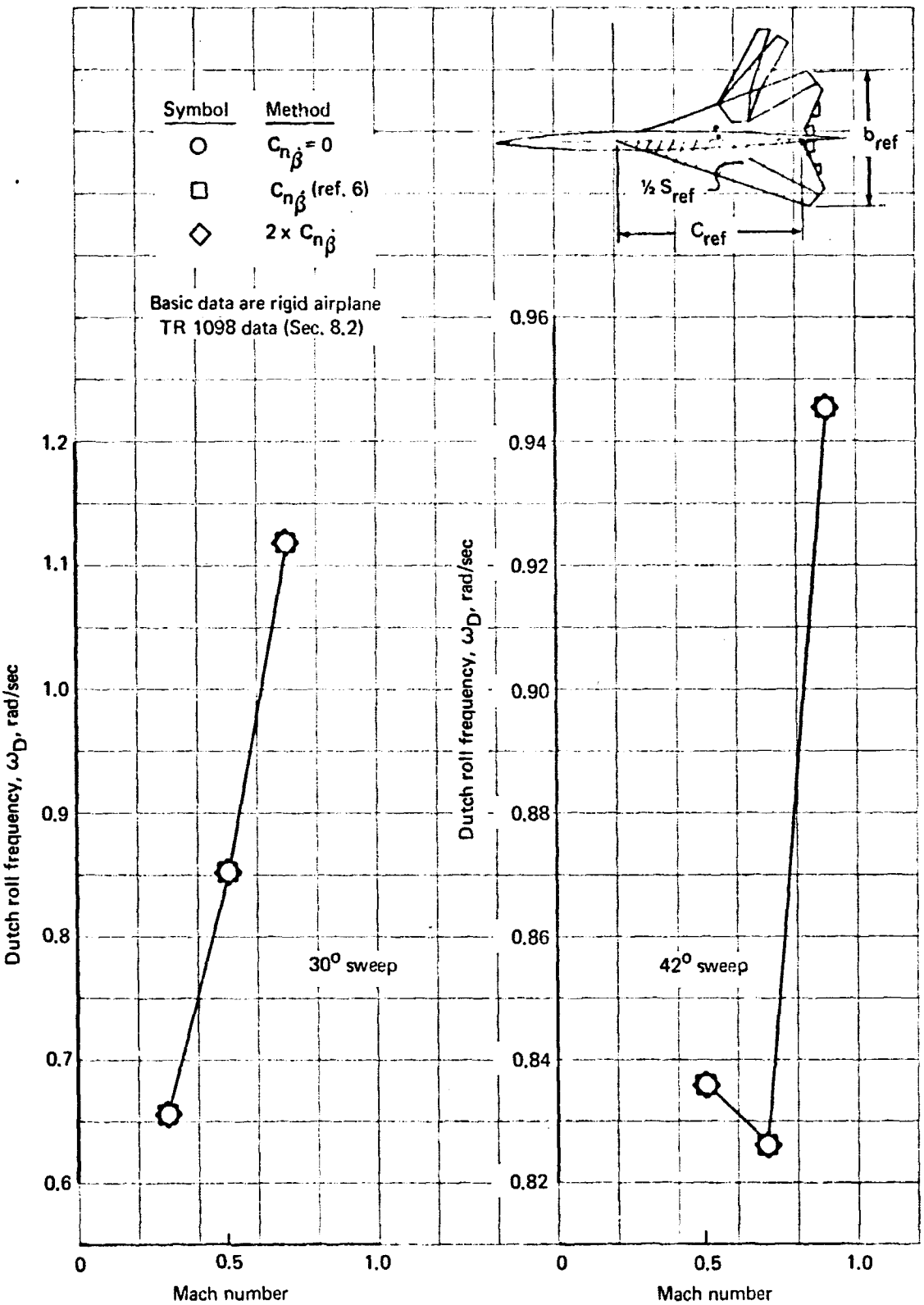

FIGURE 106. CHANGES IN DUTCH ROLL FREQUENCY DUE TO VARIATIONS IN $C_{n_{\dot{\beta}}}$ – 30° AND 42° SST

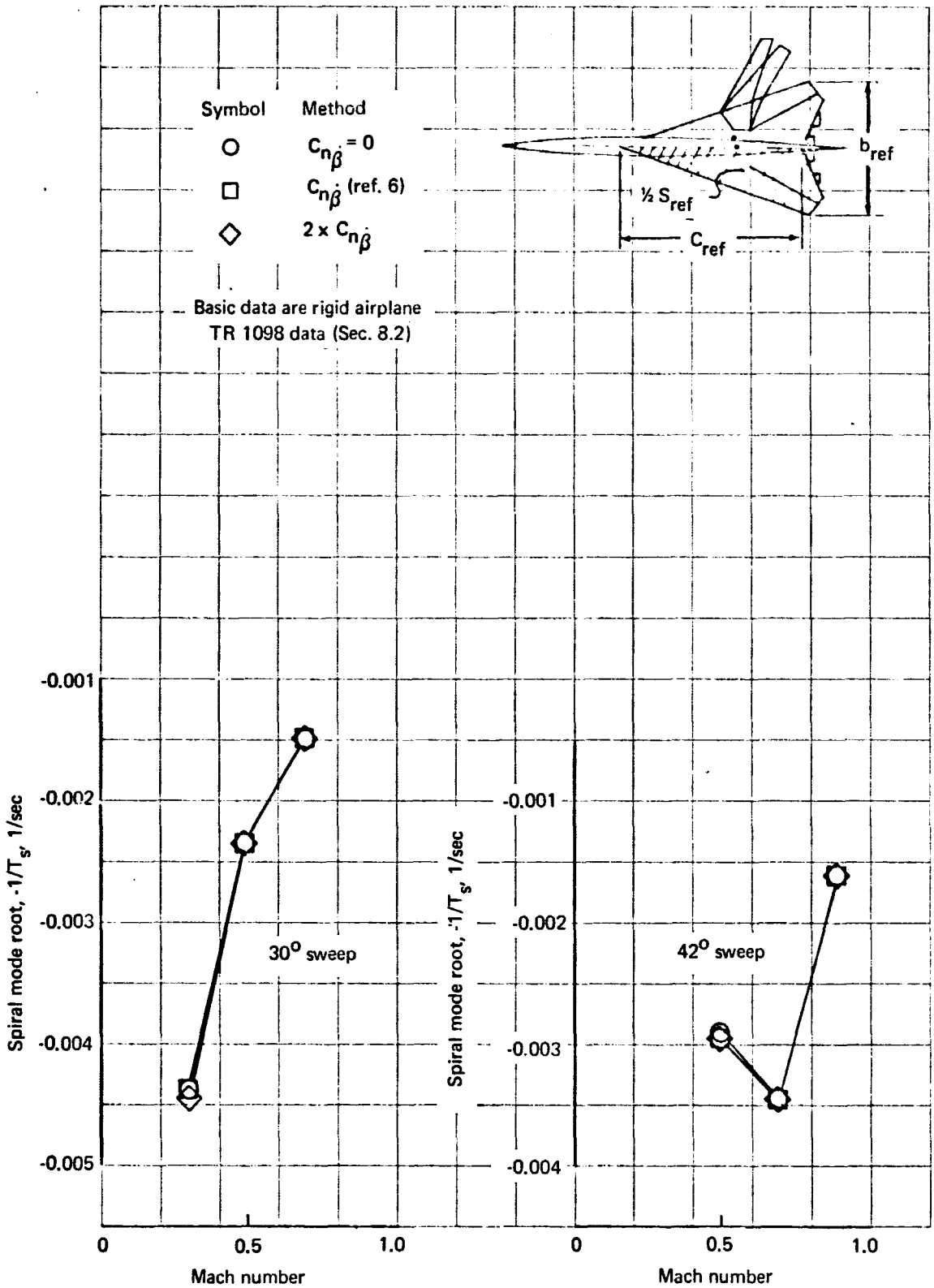

FIGURE 107. CHANGES IN SPIRAL MODE ROOTS DUE TO VARIATIONS IN $C_{n_{\dot{\beta}}}$ – 30° AND 42° SST

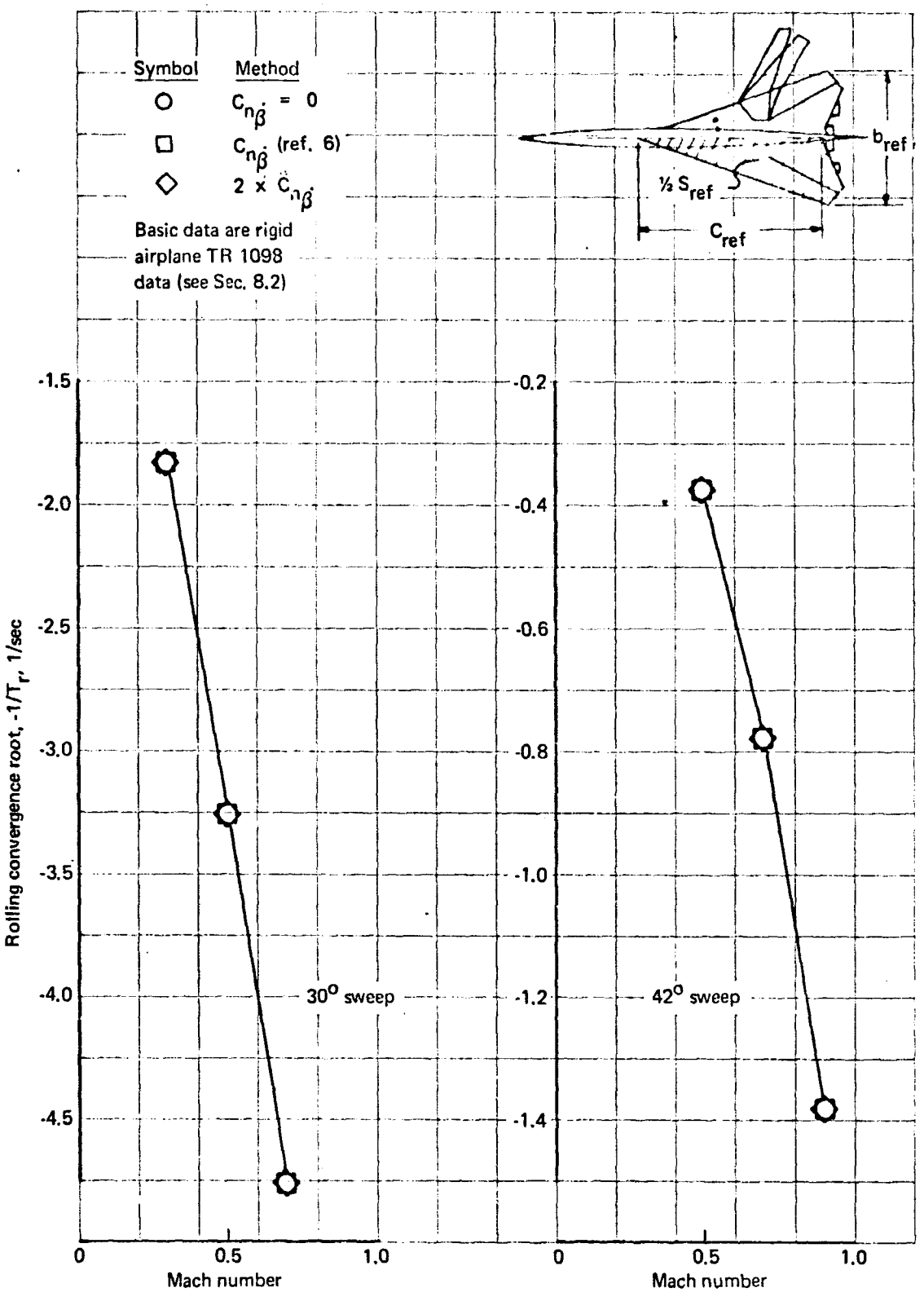

FIGURE 108. CHANGES IN ROLLING CONVERGENCE ROOTS DUE TO VARIATIONS IN $C_{n_{\dot{\beta}}}$ – 30° AND 42° SST

TABLE 23.–VARIATION OF SHORT PERIOD AND PHUGOID ROOTS WITH $C_{L_{\dot{\alpha}}}$ FOR STUDY AIRPLANES

M	$C_{L_{\dot{\alpha}}} = 0$				$C_{L_{\dot{\alpha}}}$ (Ref. 6)				$2 \times C_{L_{\dot{\alpha}}}$			
	σ_p	ω_p	σ_{SP}	ω_{SP}	σ_p	ω_p	σ_{SP}	ω_{SP}	σ_p	ω_p	σ_{SP}	ω_{SP}
	707-320B lifting surface derivatives (Sec. 8.2)											
0.255	0.009572	0.1418	-0.7213	0.8613	0.009680	0.1417	-0.7157	0.8559	0.009789	0.1417	-0.7101	0.8506
0.365	0.002475	0.09774	-1.032	1.234	0.002518	0.09774	-1.024	1.226	0.002561	0.09773	-1.016	1.219
0.548	-0.001226	0.05831	-1.667	1.924	-0.001210	0.05831	-1.657	1.916	-0.001194	0.05831	-1.647	1.907
0.800	0.0006146	0.03535	-1.185	1.982	0.0006100	0.03535	-1.187	1.984	0.0006054	0.03535	-1.188	1.986
0.850	-0.00000491	0.02128	-1.364	2.131	-0.0000186	0.02127	-1.369	2.136	-0.0000323	0.02128	-1.374	2.141
0.900	0.01910[a]	-0.02407[a]	-1.560	2.336	0.01905[a]	-0.02412[a]	-1.581	2.357	0.01901[a]	-0.02418[a]	-1.603	2.377
M/ sweep	SST lifting surface derivatives (Sec. 8.2)											
0.3/30°	-1.289[a]	0.2674[a]	-0.05446	0.1514	-1.278[a]	0.2667[a]	-0.05444	0.1514	-1.268[a]	0.2660[a]	-0.05442	0.1513
0.5/30°	-2.117[a]	0.2933[a]	-0.03555	0.1108	-2.105[a]	0.2928[a]	-0.03556	0.1108	-2.092[a]	0.2923[a]	-0.03557	0.1108
0.7/30°	-2.956[a]	0.2448[a]	-0.06109	0.1150	-2.982[a]	0.2452[a]	-0.06109	0.1150	-3.009[a]	0.2456[a]	-0.06110	0.1151
0.5/42°	-0.6361[a]	0.1940[a]	-0.02284	0.1076	-0.6353[a]	0.1939[a]	-0.02284	0.1076	-0.6345[a]	0.1938[a]	-0.02285	0.1076
0.7/42°	-0.9563[a]	0.1389[a]	-0.07593	0.1059	-0.9563[a]	0.1389[a]	-0.07593	0.1059	-0.9563[a]	0.1389[a]	-0.07593	0.1059
0.9/42°	-0.07159[a]	0.09153[a]	-0.7320[a]	-1.157[a]	-0.07159[a]	0.09153[a]	-0.7323[a]	-1.159[a]	-0.07172[a]	0.09147[a]	-0.7215[a]	-1.208[a]
0.7/72°	0.008866	0.09302	-0.1673	0.1277	0.008875	0.09300	-0.1675	0.1278	0.008885	0.09297	-0.1678	0.1280
0.9/72°	-0.006967	0.08053	-0.3335	0.3240	-0.006955	0.08052	-0.3340	0.3244	-0.006943	0.08052	-0.3346	0.3249
1.1/72°	-0.006369	0.05035	-0.4802	0.9946	-0.00637	0.05035	-0.4808	0.9957	-0.00637	0.05035	-0.4813	0.9969
1.3/72°	-0.003456	0.02882	-0.6323	1.359	-0.00346	0.2882	-0.6333	1.361	-0.003457	0.02882	-0.6344	1.363
1.5/72°	-0.001278	0.005170	-0.8057	1.857	-0.00128	0.00517	-0.8068	1.860	-0.00128	0.005169	-0.8080	1.863
2.2/72°	-0.000824	0.01150	-0.1738	1.108	-0.000825	0.01150	-0.1738	1.108	-0.000825	0.01150	-0.1739	1.108
2.7/72°	-0.000876	0.00721	-0.3209	1.631	-0.000876	0.00722	-0.3212	1.632	-0.000876	0.007215	-0.3212	1.632

a. Real roots

TABLE 24. – CHANGES IN LATERAL-DIRECTIONAL CHARACTERISTICS DUE TO VARIATIONS IN $C_{y_{\dot{\beta}}}$ FOR STUDY AIRPLANES

M	$C_{Y_{\dot{\beta}}} = 0$				$C_{Y_{\dot{\beta}}}$ (ref. 6)				$2 \times C_{Y_{\dot{\beta}}}$ (Not required)			
	σ_D	ω_D	$-1/T_r$	$-1/T_s$	σ_D	ω_D	$-1/T_r$	$-1/T_s$	σ_D	ω_D	$-1/T_r$	$-1/T_s$
707-320B TR 1098 derivatives (Sec. 8.2)												
0.255	0.2599	0.8504	-0.8479	-0.02841	0.02600	0.8506	-0.8480	-0.02841	No Significant Change from $C_{y_{\dot{\beta}}}$			
0.365	-0.01577	0.9517	-1.026	-0.01116	-0.01576	0.9519	-1.026	-0.01116				
0.548	-0.09476	1.286	-1.380	-0.003026	-0.09477	1.286	-1.380	-0.003026				
0.800	-0.04498	1.206	-0.8263	-0.005527	-0.04498	1.206	-0.8263	-0.005527				
0.850	-0.05737	1.325	-0.8629	-0.002444	-0.05737	1.326	-0.8629	-0.002444				
0.900	-0.05363	1.555	-0.8895	-0.0007335	-0.05364	1.555	-0.8895	-0.0007335				
M/ sweep	SST TR 1098 derivatives (Sec. 8.2)											
0.3/30°	-0.1030	0.6567	-1.827	-0.004395	-0.1031	0.6570	-1.827	-0.004446				
0.5/30°	-0.09255	0.8525	-3.260	-0.002307	-0.0926	0.8529	-3.259	-0.002307				
0.7/30°	-0.1008	1.119	-4.774	-0.001472	-0.1009	1.120	-4.774	-0.001472				
0.5/42°	-0.05661	0.8361	-0.3764	-0.003404	-0.05661	0.8362	-0.3764	-0.003404				
0.7/42°	-0.08318	0.8263	-0.7899	-0.003931	-0.08319	0.8264	-0.7899	-0.003931				
0.9/42°	-0.06830	0.9457	-1.393	-0.002098	-0.06832	0.9458	-1.393	-0.002098				

TABLE 25. – CHANGES IN LATERAL-DIRECTIONAL CHARACTERISTICS DUE TO VARIATIONS IN $C_{\ell_{\dot{\beta}}}$ FOR STUDY AIRPLANES

M	$C_{\ell_{\dot{\beta}}} = 0$				$C_{\ell_{\dot{\beta}}}$ (ref. 6)				2 x $C_{\ell_{\dot{\beta}}}$			
	σ_D	ω_D	$-1/T_r$	$-1/T_s$	σ_D	ω_D	$-1/T_r$	$-1/T_s$	σ_D	ω_D	$-1/T_r$	$-1/T_s$
	707-320B TR 1098 derivatives (Sec. 8.2)											
0.255	0.02595	0.8506	-0.8479	0.02841	0.02600	0.8506	-0.8480	-0.02841	0.02606	0.8505	-0.8480	-0.02841
0.365	-0.01590	0.9520	-1.026	-0.01116	-0.01576	0.9519	-1.026	-0.01116	-0.01562	0.9518	-1.026	-0.01116
0.548	-0.09482	1.287	-1.380	-0.003026	-0.09477	1.286	-1.380	-0.003026	-0.09472	1.286	-1.380	-0.003026
0.800	-0.04501	1.206	-0.8262	-0.005527	-0.04498	1.206	-0.8263	-0.005527	-0.04495	1.206	-0.8264	-0.005527
0.850	-0.5738	1.326	-0.8628	-0.002444	-0.05737	1.326	-0.8629	-0.002444	-0.05736	1.326	-0.8629	-0.002445
0.900	-0.05363	1.555	-0.8895	-0.0007335	-0.05364	1.555	-0.8895	-0.0007335	-0.05364	1.555	-0.8896	-0.0007335
M/ sweep	SST TR 1098 derivatives (Sec. 8.2)											
0.3/30°	-0.1034	0.6569	-1.828	-0.004397	-0.1031	0.6570	-1.827	-0.004446	-0.1028	0.6572	-1.826	-0.004394
0.5/30°	-0.09280	0.8528	-3.260	-0.002307	-0.09260	0.8529	-3.259	-0.002307	-0.09240	0.8530	-3.259	-0.002307
0.7/30°	-0.1010	1.120	-4.775	-0.001473	-0.1009	1.120	-4.774	-0.001472	-0.1008	1.120	-4.774	-0.001472
0.5/42°	-0.05661	0.8362	-0.3764	-0.003403	-0.05661	0.8362	-0.3764	-0.003404	-0.05660	0.8362	-0.3764	-0.003404
0.7/42°	-0.08341	0.8263	-0.7899	-0.003931	-0.08319	0.8264	-0.7899	-0.003931	-0.08298	0.8264	-0.7898	-0.003931
0.9/42°	-0.06846	0.9458	-1.393	-0.002098	-0.06832	0.9458	-1.393	-0.002098	-0.06817	0.9459	-1.393	-0.002098
0.7/72°	0.01810	1.230	-0.1537	-0.001944	0.01810	1.230	-0.1537	-0.001944	-0.01811	1.230	-0.1537	-0.001944
0.9/72°	-0.06306	1.460	-0.3447	-0.005353	-0.06306	1.460	-0.3447	-0.005353	-0.06306	1.460	-0.3447	-0.005353

9. COMPLETELY ELASTIC AIRPLANE ANALYSIS

9.1 Introduction

This section presents some of the details of the different approaches used in the completely elastic analysis of the Boeing 707-320B and the SST study airplanes. Two approaches were used to calculate the free-free vibration modes. Both analyses used quasi-steady aerodynamics; however, a subsonic lifting line theory was used for the 707-320B analysis, whereas a subsonic-supersonic lifting surface theory was used for the SST. Several cases were analyzed using lift growth functions with the 707-320B airplane, but in general the analysis (S12) used quasi-steady aerodynamic theory. In addition, both analyses used beam theory to compute the structural influence coefficients.

9.2 707-320B Analysis

9.2.1 General considerations.—The 707-320B is a subsonic jet transport with a high aspect ratio wing. The choice was made to base the equations of motion on lifting line theory for the aerodynamic representation and on simple beam theory for the structural representation. The reference axes for rigid-body motion are stability axes, which are defined as rectangular cartesian axes with origin at the center of mass of the airplane. The stability axes are fixed to the center of mass and the translations and rotations of the axes represent the translations and rotations of the center of mass. The z-axis is positive down and the y-axis is positive toward the right wingtip. The x-axis is positive forward and is oriented so that, in the reference condition of steady, symmetrical flight, the x-axis is parallel to the undisturbed freestream vector.

Generalized coordinates, defined as any set of quantities that completely describe the configuration of a system, are used to describe the perturbed motion of the airplane. The choice of generalized coordinates is arbitrary, with the stipulation that the product of a generalized coordinate with its appropriate generalized force must have units of work. The equations of motion are based (G8) on small perturbation assumptions; therefore, the generalized coordinates that describe rigid-body rotation (rotation of the stability axes) are the Euler angles and Euler rates as described in app. A. The analysis considers the case of zero

climb angle; therefore, the relations between the Euler rates and angular velocity components are simply:

$$\begin{aligned} \dot{\theta} &= q \\ \dot{\phi} &= p \\ \dot{\psi} &= r \end{aligned} \qquad (9.1)$$

The two-degree-of-freedom, rigid-body approximation for the short period motion was made in the present analysis, i.e., velocity perturbations in the x-stability direction were ignored. The equations that relate the velocity perturbations in the stability axes to the velocities in the earth-fixed inertial system (ref. 4) are: (D15)

$$\begin{aligned} \dot{h}_x &= u_o \\ \dot{h}_y &= v + u_o \psi \\ \dot{h}_z &= w - u_o \theta \end{aligned} \qquad (9.2)$$

The generalized coordinates associated with the flexible degrees of freedom are measures of the displacements in the structural modes. The term "structural modes," as used here, refers to the normalized mode shape of the free airplane in free vibration (free-free modes). (S4)

9.2.2 — Structural representation.— The airplane structure was idealized as a set of slender beams with each beam cantilevered at a selected reference station, as shown in fig. 109. The cantilever stations chosen for the wing and stabilizer were the side of the body; for the forebody, the front wing spar; and for the aftbody, the rear wing spar. The influence coefficients were computed for structural displacements relative to the cantilever stations. These coefficients were used to calculate cantilevered modes, which were then coupled to produce the free-free modes. (S12)

Equation (9.3) can be used to write the deflections of selected points on the cantilevered structural members.

$$\{\delta_s\} = [C]\{F\} \qquad (9.3)$$ (S1) (S2)

where [C] is the flexibility influence coefficient matrix. The calculation of [C]

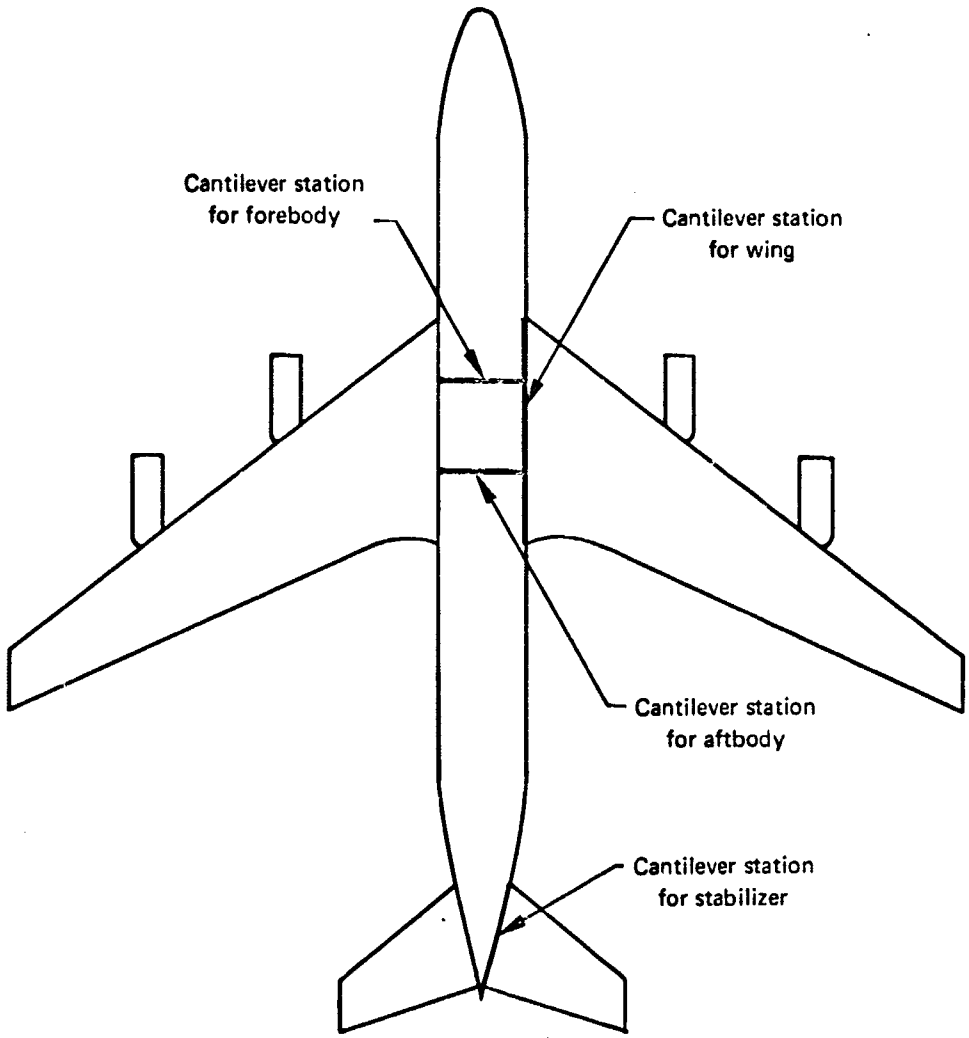

FIGURE 109. TYPICAL CANTILEVER STATIONS FOR AIRPLANE COMPONENTS

from beam theory was described in app. B. The displacements $\{\delta_s\}$ are rotations or translations, or both, depending on what is of interest.

The mass distribution of the airplane was approximated by lumping the system into a finite number of discrete masses. Each discrete mass is located at the center of mass of a grid panel. The displacements of concern, then, are the displacements of the mass centers of each grid. This system can be visualized as a set of springs equivalent to the elastic structure.

G1

S5

Free vibration stipulates that no external forces are acting on the system; therefore, the only forces acting to deform the structure are the inertia reactions acting at the mass centers of the lumped masses. These inertia forces are given by the expression

S9

S3

G2

G3

$$\{F\} = \text{inertia forces} = -[m]\{\ddot{\delta}_s\}$$

The equations of free vibration are then

$$\{\delta_s\} = [C]\{F\} = -[C][m]\{\ddot{\delta}_s\} \qquad (9.4)$$

where $[m]$ = mass matrix

The equations of motion, in this form, are an eigenvalue problem. That is, the equations are satisfied only for particular values of a quantity called λ. Physically, λ is the natural frequency of undamped vibration. Thus, for simple harmonic vibration with all displacements in phase with each other in a manner such that all points reach maximum deflection at the same time and pass through zero at the same time

$$\{\delta_s\} = \{\mu\} e^{i\lambda t}, \quad \{\ddot{\delta}_s\} = \lambda^2\{\mu\} e^{i\lambda t} \qquad (9.5)$$

By substitution into equation (9.4)

$$\frac{1}{\lambda^2}\{\mu\} e^{i\lambda t} = [C][M]\{\mu\} e^{i\lambda t} \qquad (9.6)$$

λ = natural frequency of undamped vibration for a cantilevered component

$\{\mu\}$ = cantilever mode shape - characteristic shape or eigenvector

Note that any scalar multiplication of $\{\mu\}$ would divide from both sides of equation (9.6). Therefore, the mode shape gives information only about the relative amplitudes of the displacements of the masses as they vibrate together, and the mode shape is independent of the amplitude of vibration. The actual motions at any time, t, are the real parts of equation (9.5). Equation (9.6) has a number of solutions, n, equal to the total number of cartesian degrees of freedom of all the masses (equal to the number of rows in $\{\mu\}$.)

The solutions of eigenvalue problems have the property of being orthogonal to each other. Orthogonality relations that can be shown between the i^{th} and j^{th} mode shapes are

$$\begin{aligned} &\{\mu\}_i \, [\mu]_j = 0 \quad , \quad i \neq j \\ &[\mu]_j [C] [m] \{\mu\}_i = 0 \quad , \quad i \neq j \\ &[\mu]_j [m] \{\mu\}_i = 0 \quad , \quad i \neq j \end{aligned} \tag{9.7}$$

The n solutions of equation (9.6) may be written separately

$$[C][m]\{\mu\}_1 = \frac{1}{\lambda_1^2}\{\mu\}_1$$

$$[C][m]\{\mu\}_2 = \frac{1}{\lambda_2^2}\{\mu\}_2$$

$$\vdots$$

$$[C][m]\{\mu\}_n = \frac{1}{\lambda_n^2}\{\mu\}_n$$

Or, the total number of solutions of equation (9.6) written in matrix form is

$$[C][M][\mu] = [\mu]\left[\frac{1}{\lambda^2}\right] \tag{9.8}$$

where $[\mu]$ = matrix whose columns are the eigenvectors $\{\mu\}_1$ through $\{\mu\}_n$

The frequencies of the cantilever modes that were used in computing the free-free modes for the 707-320B are listed in table 26.

The previous paragraphs have discussed the calculation of mode shapes with the cantilever stations fixed in space. When the constraints are removed

TABLE 26. – CANTILEVER MODE FREQUENCIES

	Wing		Forebody	Aftbody	Stabilizer	
Mode number	Bending freq, Hz	Torsion freq, Hz	Bending freq, Hz	Torsion freq, Hz	Bending freq, Hz	Torsion freq, Hz
Symmetrical						
1	1.09	2.53	4.3	2.98	5.66	35.2
2	3.34	5.4	21.3	11.04	23.0	73.2
3	5.87	28.4	N. A.	31.9	N. A.	N. A.

Antisymmetrical							
1	1.09	2.53	4.01	2.33	6.79	4.37	15.0
2	3.34	5.4	19.71	9.4	N. A.	16.09	25.26
3	5.87	28.4	N. A.	23.08	N. A.	N. A.	N. A.

so that the cantilever stations can translate and rotate, the situation is defined as the free airplane in free vibration (that is, if there are no externally applied forces).

Two axis systems were used to describe the free-free vibration state. The G10 X-Y-Z axis set shown in fig. 110 is the master reference system and its origin remains always at the cg of the airplane. A second axis system, X_s-Y_s-Z_s, coincides with X-Y-Z when the structure is quiescent in the reference condition. If the structure near the cg translates or rotates, the motion is represented by a translation and rotation of the X_s-Y_s-Z_s axes and then a displacement relative to the X_s-Y_s-Z_s axes. This sequence is depicted in the three sketches of fig. 110 which are drawn for plane motion. The derivation that follows is for motion in the X-Y plane in order to keep the mathematical expressions less S13 cumbersome. The assumption was made that the grid for lumping the masses is fine enough that the inertia of each mass about its own c.g. is negligible. Also, S11 elongations of the structure in the direction of the X-axis were not considered; therefore, each lumped mass moves only in the Y-direction. These Y displacements can be written in matrix form for all the lumped masses as

S2
$$\{\delta\} = \{1\}\,\sigma_T + \{X\}\,\sigma_R + \{\delta_S\} \qquad (9.9)$$

where:

$\{\delta\}$ = rectilinear displacements relative to the X-Y axes

σ_T = rectilinear displacement of the origin of the X_s-Y_s axes

σ_R = rotation of the origin of the X_s-Y_s axes

$\{\delta_S\}$ = rectilinear displacements of the structure relative to the X_s-Y_s axes = elastic displacements

$\{X\}$ = X coordinates of the reference points along X

The deformations, $\{\delta_S\}$, are the structural displacements relative to the cantilever stations, as discussed previously.

S9 The free-free vibration problem can now be formally constructed. The free vibration state required that there be no external loads acting on the system; G3 therefore, the center of mass and the X-Y axes do not translate or rotate. These two conditions can be expressed in equation form

$$\sum_i m_i \ddot{\delta}_i = \lfloor 1 \rfloor [m] \{\ddot{\delta}\} = 0 \qquad (9.10)$$

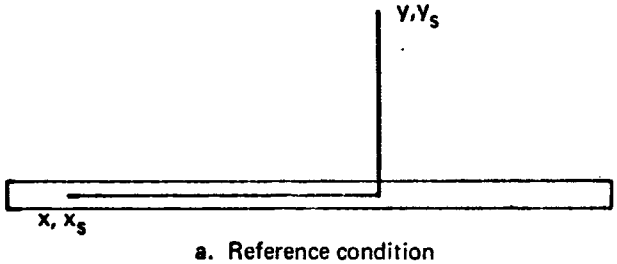

a. Reference condition

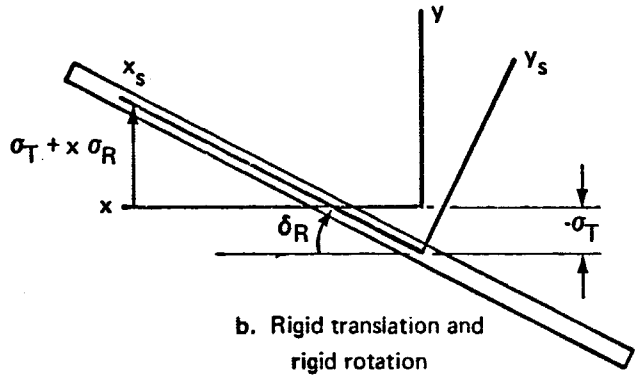

b. Rigid translation and
rigid rotation
(small angle approximations apply)

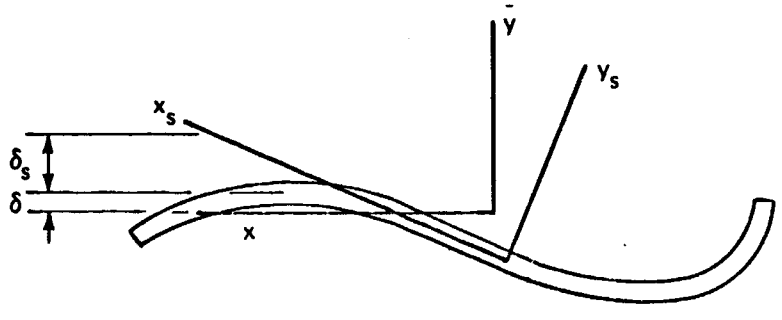

c. Elastic displacement relative to X_s-Y_s

FIGURE 110. STRUCTURAL-INERTIAL AXIS SYSTEM RELATIONSHIPS

and

$$\sum_i m_i x_i \ddot{\delta}_i = [x_i][m]\{\ddot{\delta}\} = 0 \qquad (9.11)$$

Equations (9.10) and (9.11) state that the summations of inertia forces in the Y-direction and inertia moments about the c.g. are zero. The third relationship, which states the connection between inertia forces acting at the lumped mass c.g.'s and elastic displacements relative to the X_s-Y_s axes is

$$\{\delta_s\} = [C]\{F\} = -[C][m]\{\ddot{\delta}\} \qquad (9.12)$$

where [C] = matrix of flexibility influence coefficients for elastic deflection relative to the cantilever stations

In order to establish the eigenvalue problem, simple harmonic motion is assumed. This results in the following relations

$$\{\delta\} = \{\phi\} e^{i\omega t} \; ; \; \{\ddot{\delta}\} = -\omega^2\{\phi\} e^{i\omega t} \qquad (9.13)$$

$$\sigma_T = \bar{\sigma}_T e^{i\omega t} \; , \quad \sigma_R = \bar{\sigma}_R e^{i\omega t} \; , \quad \{\delta_s\} = \{\bar{\delta}_s\} e^{i\omega t}$$

where:

ω = frequency of oscillation

The foregoing relations are substituted into equation (9.9), and $e^{i\omega t}$ is divided from both sides to obtain

$$\{\phi\} = \{1\}\bar{\sigma}_T + \{x\}\bar{\sigma}_R + \{\bar{\delta}_s\} \qquad (9.14)$$

The procedure used in the 707-320B analysis to calculate the free-free modes, equation (9.14), was to apply Lagrange's equations using the cantilever modes as degrees of freedom. Lagrange's equation was used so that the calculations could be systematized to use the same procedures and digital programs to formulate the unforced (free vibration) and forced motion equations. Lagrange's equation for an elastic conservative system is

$$\frac{d}{dt}\left(\frac{\partial T}{\partial \dot{q}_i}\right) + \frac{\partial U}{\partial q_i} = 0 \qquad (9.15)$$

where:

T = kinetic energy

U = strain energy

q_i = generalized coordinates

The relative displacements in the cantilever modes, $\tilde{q}$, and the translations and rotations of the X_S-Y_S axes, σ_T and σ_R, were chosen as generalized coordinates. This includes the assumption that displacements relative to the structural axes are represented by a superposition of deflections in the cantilever modes. The deflections relative to the X-Y axes are described by equation (9.9) and repeated here. (S4)

$$\{\delta\} = \{1\}\sigma_T + \{X\}\sigma_R + \{\delta_S\} \qquad (9.9)$$

If equation (9.9) is rewritten in terms of cantilever modes

$$\{\delta\} = \{1\}\sigma_T + \{X\}\sigma_R + [\mu]\{\tilde{q}\} \qquad (9.16)$$

equation (9.16) can be written in matrix form

$$\{\delta\} = \left[\begin{array}{c:c:c:c:c} [\mu_1] & [0] & [0] & \{1\} & \{X\} \\ \hdashline [0] & [\mu_2] & [0] & & \\ \hdashline [0] & [0] & [\mu_3] & & \end{array}\right] \left\{\begin{array}{c} \{\tilde{q}_1\} \\ \{\tilde{q}_2\} \\ \{\tilde{q}_3\} \\ \{\sigma_T\} \\ \{\sigma_R\} \end{array}\right\} = [G]\left\{\begin{array}{c} \tilde{q} \\ \sigma \end{array}\right\} \qquad (9.17)$$

allowing for three cantilever components in the system. The 707-320B actually had four cantilever components, but three are used in the following discussion. The shorthand notation (to the right of the second equal sign) will be used for equation (9.17) throughout the remainder of this discussion.

The kinetic energy and its contributing term to equation (9.15) is written as

$$T = \frac{1}{2}\sum_i m_i \dot{\delta}_i^2 = \frac{1}{2}\lfloor\dot{\delta}\rfloor[m]\{\dot{\delta}\} = \frac{1}{2}\lfloor\dot{\tilde{q}}\ \dot{\sigma}\rfloor[G]^T[m][G]\begin{Bmatrix}\dot{\tilde{q}}\\ \dot{\sigma}\end{Bmatrix}$$

$$\left\{\frac{\partial T}{\partial \dot{q}}\right\} = [G]^T[m][G]\begin{Bmatrix}\dot{\tilde{q}}\\ \dot{\sigma}\end{Bmatrix} \qquad (9.18)$$

$$\left\{\frac{d}{dt}\left(\frac{\partial T}{\partial \dot{q}}\right)\right\} = [G]\ [m][G]\begin{Bmatrix}\ddot{\tilde{q}}\\ \ddot{\sigma}\end{Bmatrix}$$

The strain energy is

$$U = \frac{1}{2}\sum_i\sum_j k_{ij}\delta s_i \delta s_j = \frac{1}{2}\lfloor\delta s\rfloor[k]\{\delta s\} = \frac{1}{2}\lfloor\tilde{q}\rfloor[\mu]^T[k][\mu]\{\tilde{q}\} \qquad (9.19)$$

where:

$[k]=[C]^{-1}$ = cantilever stiffness influence coefficients

$$\{\tilde{q}\} = \begin{Bmatrix}\{\tilde{q}_1\}\\ \{\tilde{q}_2\}\\ \{\tilde{q}_3\}\end{Bmatrix}$$

From equation (9.8) it is seen that

$$[m][\mu] = [k][\mu]\left[\frac{1}{\lambda^2}\right] \qquad (9.20)$$

For three cantilever stations equation (9.20) has the form

$$\left[\begin{array}{c|c|c} [m_1] & [0] & [0] \\ \hline [0] & [m_2] & [0] \\ \hline [0] & [0] & [m_3] \end{array}\right]\begin{bmatrix}[\mu_1] & [0] & [0]\\ [0] & [\mu_2] & [0]\\ [0] & [0] & [\mu_3]\end{bmatrix}$$

$$= \begin{bmatrix}[k_1] & [0] & [0]\\ [0] & [k_2] & [0]\\ [0] & [0] & [k_3]\end{bmatrix}\begin{bmatrix}[\mu_1] & [0] & [0]\\ [0] & [\mu_2] & [0]\\ [0] & [0] & [\mu_3]\end{bmatrix}\begin{bmatrix}\left[\frac{1}{\lambda_1^2}\right] & [0] & [0]\\ [0] & \left[\frac{1}{\lambda_2^2}\right] & [0]\\ [0] & [0] & \left[\frac{1}{\lambda_3^2}\right]\end{bmatrix}$$

$$[A_2] = [\mu]^T [m] [\{1\} | \{X\}] \tag{9.26}$$

$$[A_3] = \left[\frac{1}{X}\right] [m] [\mu] \tag{9.27}$$

$$[A_4] = \left[\frac{1}{X}\right] [m] [\{1\} | \{X\}] \tag{9.28}$$

$$[B_3] = [\mu]^T [m] [\mu] [\lambda^2] = [A_1] [\lambda^2] = [\mu]^T [C]^{-1} [\mu] \tag{9.29}$$

Equation (9.24) can be put in eigenvalue form by first removing $\ddot{\sigma}_T$ and $\ddot{\sigma}_R$ by multiplying the partitions of equation (9.24), with the result

$$[A_1] \{\ddot{\tilde{q}}\} + [A_2] \begin{Bmatrix} \ddot{\sigma}_T \\ \ddot{\sigma}_R \end{Bmatrix} + [B_1] \{\tilde{q}\} = 0 \tag{9.30}$$

$$[A_3] \{\ddot{\tilde{q}}\} + [A_4] \begin{Bmatrix} \ddot{\sigma}_T \\ \ddot{\sigma}_R \end{Bmatrix} = 0 \tag{9.31}$$

Equation (9.31) can then be solved for $\ddot{\sigma}_T$ and $\ddot{\sigma}_R$

$$\begin{Bmatrix} \ddot{\sigma}_T \\ \ddot{\sigma}_R \end{Bmatrix} = -[A_4]^{-1} [A_3] \{\ddot{\tilde{q}}\} \tag{9.32}$$

which can be substituted into equation (9.30) to obtain

$$\left[[A_1] - [A_2] [A_4]^{-1} [A_3] \right] \{\ddot{\tilde{q}}\} + [B] \{\tilde{q}\} = 0 \tag{9.33}$$

When the assumption of simple harmonic motion is made in which all of the cantilever components of the free airplane are simultaneously in free vibration, equation (9.33) becomes

$$\omega^2 [B]^{-1} \left[[A_1] - [A_2] [A_4]^{-1} [A_3] \right] \{\bar{\tilde{q}}\} = \{\bar{\tilde{q}}\} \tag{9.34}$$

Equation (9.20) can be written as

$$[\mu]^T[m][\mu][\lambda^2] = [\mu]^T[k][\mu] = [\mu]^T[C]^{-1}[\mu] \quad (9.21)$$

which is a diagonal matrix, as can be seen from equation (9.7). Equation (9.21), substituted into equation (9.19), gives

$$U = \frac{1}{2}\lfloor\tilde{q}\rfloor[\mu]^T[m][\mu][\lambda^2]\{\tilde{q}\}$$
$$\left\{\frac{\partial U}{\partial q}\right\} = [\mu]^T[m][\mu][\lambda^2]\{\tilde{q}\} \quad (9.22)$$

When equations (9.22) and (9.18) are substituted into equation (9.15), the following results

$$[G]^T[m][G]\left\{\begin{matrix}\ddot{\tilde{q}}\\ \ddot{\sigma}\end{matrix}\right\} + [\mu]^T[m][\mu][\lambda^2]\{\tilde{q}\} = 0 \quad (9.23)$$

Equation (9.23) can be written in partitioned form as

$$\left[\begin{array}{c:c}[A_1] & [A_2]\\ \hdashline [A_3] & [A_4]\end{array}\right]\left\{\begin{matrix}\{\ddot{\tilde{q}}\}\\ \{\ddot{\sigma}_T\}\end{matrix}\right\} + \left[\begin{array}{c:c}[B_1] & [0]\\ \hdashline [0] & [0]\end{array}\right]\left\{\begin{matrix}\{\tilde{q}\}\\ \{0\}\end{matrix}\right\} = 0 \quad (9.24)$$

From equation (9.17) it is seen that

$$[A_1] = [\mu]^T[m][\mu] \quad (9.25)$$

where:

$$\{\tilde{q}\} = \{\bar{\tilde{q}}\}\, e^{i\omega t}$$

$$\{\ddot{\tilde{q}}\} = -\omega^2 \{\bar{\tilde{q}}\}\, e^{i\omega t}$$

ω = vibration frequency

The eigenvectors, $\{\bar{\tilde{q}}\}$, and eigenvalues, ω, are calculated from equation (9.34), and $\bar{\sigma}_T$ and $\bar{\sigma}_R$ are determined from equation (9.32) as

$$\begin{Bmatrix} \bar{\sigma}_T \\ \bar{\sigma}_R \end{Bmatrix} = -[A_4]^{-1}[A_3]\{\bar{\tilde{q}}\}$$

The free-free mode shape is found by applying equation (9.14) and the following relation between the elastic amplitudes and the eigenvectors

$$\{\bar{\sigma}_s\} = [\mu]\{\bar{\tilde{q}}\} \tag{9.35}$$

to obtain

$$\{\phi\} = [\mu]\{\bar{\tilde{q}}\} + \{1\}\bar{\sigma}_T + \{x\}\bar{\sigma}_R \tag{9.36}$$

The matrix involving all of the free-free mode shapes can be written as

$$[\phi] = [1][\bar{\sigma}_T] + [x][\bar{\sigma}_R] + [\mu][\bar{\tilde{q}}] \tag{9.37}$$

where [1] is a square matrix of all unitary elements.

The symmetrical and antisymmetrical free-free mode frequencies and associated cantilever vectors, $\{\bar{\tilde{q}}\}$, are listed in tables 27 and 28, respectively.

9.2.2.1 Aerodynamic representation: The external aerodynamic forces were represented by a modified quasi-steady lifting line theory. The modifications were corrections for Mach number and three-dimensional effects. The Mach number corrections were from wind tunnel data and the three-dimensional corrections were derived from Weissinger's lifting line theory, as described in ref. 68. The derivation of the strip theory is discussed in chapter 5 of ref. 26. Downwash (A11)

TABLE 27. – CANTILEVER VECTORS FOR SYMMETRICAL FREE-FREE MODES

	Symmetrical Free-Free Modes													
Mode number	1	2	3	4	5	6	7	8	9	10	11	12	13	14
Frequency, Hz	1.24	2.92	3.39	4.50	4.93	6.31	8.75	10.0	17.6	25.4	26.8	31.9	43.9	47.3
Cantilever modes	Cantilever vectors													
1 Wing bending	1.0	0.83	-0.1	-0.61	0.24	-0.09	-0.008	-0.22	0.74	-0.06	-0.40	0.34	0.1	-0.03
2 Wing bending	0.04	0.95	1.0	1.0	0.23	0.10	-0.49	0.10	-0.57	0.10	0.11	0.01	-0.05	0.02
3 Wing bending	-0.01	0.16	-0.07	0.15	0.67	0.02	1.0	-0.09	0.38	-0.08	-0.03	-0.08	0.03	-0.009
1 Wing torsion	-0.08	1.00	-0.20	-0.25	-0.11	-0.009	-0.19	-0.06	-0.10	0.01	-0.13	0.13	0.02	-0.007
2 Wing torsion	0.003	0.02	0.04	0.001	-0.42	0.06	0.25	-0.07	0.10	-0.004	-0.08	0.06	0.01	-0.009
3 Wing torsion	—	—	—	—	—	—	0.006	0.006	-0.04	-0.03	0.75	0.44	0.03	-0.002
1 Forebody bending	-0.008	0.08	0.24	-0.29	-0.18	-0.23	0.53	0.51	-0.57	-0.11	0.89	-0.90	-0.13	0.[illegible]
2 Forebody bending	—	-0.001	-0.001	-0.004	0.002	-0.007	0.04	0.05	-0.28	0.21	-0.96	0.66	0.06	-0.02
1 Aftbody bending	-0.06	-0.11	0.53	-0.51	0.33	-0.14	-0.06	-0.63	0.96	0.15	-0.65	0.65	0.20	-0.07
2 Aftbody bending	0.001	-0.001	0.004	-0.03	0.04	0.03	0.02	-0.08	-0.49	0.12	0.30	-0.24	-0.03	0.008
3 Aftbody bending	—	—	—	—	—	-0.003	0.003	-0.009	0.04	0.04	-0.02	0.17	-0.05	0.02
1 Stabilizer bending	-0.02	-0.08	0.42	-0.96	1.0	1.0	-0.19	1.0	1.0	-0.56	-0.89	1.0	-0.26	-0.04
2 Stabilizer bending	—	0.002	-0.008	0.009	-0.06	0.01	-0.008	0.07	0.46	1.0	1.0	-0.55	0.04	-0.04
1 Stabilizer torsion	-0.002	-0.006	-0.04	-0.08	0.09	0.09	-0.02	0.1	0.13	0.36	0.47	-0.67	1.0	1.0
2 Stabilizer torsion	—	—	—	—	—	0.004	-0.002	0.02	0.13	0.29	0.27	-0.11	-0.04	-0.05

TABLE 28. – CANTILEVER MODES FOR ANTISYMMETRICAL FREE-FREE MODES

	Antisymmetrical free-free modes													
Mode number	1	2	3	4	5	6	7	8	9	10	11	12	13	14
Frequency, Hz	2.22	2.69	2.94	4.30	4.98	5.42	6.84	9.55	10.21	14.57	18.90	20.67	24.30	27.69
Cantilever modes	Cantilever vectors													
1 Wing bending	1.0	0.22	0.276	-0.06	-0.24	-0.6	1.0	-0.473	1.0	-0.02	0.014	0.041	0.02	-0.002
2 Wing bending	0.04	0.15	0.678	0.086	0.16	1.0	-0.68	0.293	0.64	0.01	-0.009	0.013	0.007	—
1 Wing torsion	-0.04	-0.43	0.968	-0.026	-0.12	-0.1	0.05	-0.008	-0.064	—	—	0.02	-0.017	—
2 Wing torsion	0.02	0.013	0.003	0.005	-0.01	-0.32	-0.11	0.034	0.056	0.001	—	-0.004	-0.006	—
1 Forebody bending	-0.007	0.055	0.198	-0.048	1.0	-0.10	0.05	-0.02	0.032	—	—	-0.17	-0.034	—
2 Forebody bending	—	—	—	—	0.012	-0.002	—	0.016	0.008	—	0.001	1.0	0.10	—
1 Aftbody bending	-0.103	1.0	0.781	-0.137	-0.27	-0.04	0.022	-0.028	0.196	-0.019	0.017	0.032	0.034	—
2 Aftbody bending	-0.002	0.008	0.014	0.006	—	-0.007	0.003	-0.085	-0.47	-0.008	—	0.010	0.10	0.002
3 Aftbody bending	—	—	0.001	—	—	—	—	—	0.016	0.003	-0.007	-0.022	0.54	—
1 Aftbody torsion	0.013	-0.025	-0.054	-0.06	-0.025	-0.006	0.081	0.232	-0.54	0.024	-0.032	-0.001	0.037	0.006
1 Fin bending	-0.15	0.777	1.0	1.0	0.259	-0.44	0.927	1.0	-0.97	-0.010	-0.225	0.042	-0.94	0.049
2 Fin bending	0.003	-0.019	-0.018	—	0.005	-0.004	0.031	0.12	-0.108	-0.19	0.268	-0.057	0.85	-0.14
1 Fin torsion	-0.01	0.091	0.10	0.073	0.008	-0.039	0.072	-0.052	-0.47	1.0	1.0	-0.127	0.66	-0.25
2 Fin torsion	0.002	-0.016	-0.015	0.002	0.005	-0.001	0.016	0.076	-0.003	-0.081	0.362	-0.077	1.0	1.0

effects were included by applying an average value of $(1 - \epsilon_\alpha)$ to the rigid-body component of the wing angle of attack. The equation format for the angle of attack of the stabilizer lifting panels is

$$\{\alpha_S\} = \left[\left[(1-\epsilon_\alpha)\right] \vdots \left[1\right]\right] \begin{bmatrix} \{\alpha_{S_R}\} \\ \hdashline \{\alpha_{S_F}\} \end{bmatrix} \tag{9.38}$$

where:

α_{S_R} = rigid-body angle of attack

α_{S_F} = angle of attack from structural deformation

α_S = total angle of attack of stabilizer panels

The equations for the panel lifts and moments take the following forms (ref.26):

$$\{L\}_{CIRC} = 2\rho u_o^2 [\Delta y][S_1]^{-1}[a]\left[\left[\frac{1}{u_o}\{\dot{h}_P\} + \{\theta_S\} + \frac{1}{u_o}\left[\frac{c}{2}\right]\{\dot{\theta}_S\}\right]\right]$$

$$\{L\}_{NC} = \frac{\pi\rho}{4}[\Delta y][c^2]\left[\left[\{\ddot{h}_P\} + \frac{1}{4}[c]\{\ddot{\theta}_S\} + u_o\{\dot{\theta}_S\}\right]\right] \tag{9.39}$$

$$\{M\}_{NC} = \frac{-\pi\rho}{8}[\Delta y][c]\left[\left[.5\{\ddot{h}_P\} + .787[c]\{\ddot{\theta}_S\} + u_o\{\dot{\theta}_S\}\right]\right]$$

where:

Δy = spanwise panel width

$[S_1]$ = matrix of aerodynamic influence (ref. 68)

C = local chord

a = local lift curve slope

θ_S = streamwise rotation of panel

$\dot{h}_p$ = velocity of panel normal to streamwise direction

The subscripts "circ" and "nc" indicate circulatory and noncirculatory components. Lift growth was included for several cases by multiplying the circulatory lift by the Wagner function. The details of how the lift growth functions were handled will be described later.

The velocity of the panels normal to the streamwise direction, $\{\dot{h}_p\}$, can be written by applying equation (9.16)

$$\{\dot{h}_p\} = \{\dot{\delta}\} = \left[\{1\} \vdots \{X\} \vdots [\mu]\right] \begin{Bmatrix} \dot{\sigma}_T \\ \dot{\sigma}_R \\ \dot{q} \end{Bmatrix} \quad (9.40)$$

9.2.2.2 The equations of motion: The equations of motion are the relations between the accelerations, velocities, and displacements. The normal mode shapes for the airplane were used to reduce the number of degrees of freedom required for an adequate approximate representation of the airplane's elastic motion. These normal modes are introduced into the problem by starting the development from the viewpoint of Lagrange's equations of motion and utilizing the concept of generalized coordinates. The use of Lagrange's equation leads to the equations of motion as:

$$[\bar{M}]\frac{d}{dt}\{\dot{q}\} + [M_3]\{\ddot{q}\} + [M_2]\{\dot{q}\} + [\omega_i^2][\bar{M}]\{q\} + [M_1]\{q\} + [\bar{M}][M_4]\{q\} + [\bar{M}][M_5]\{\dot{q}\} = 0 \quad (9.41)$$

This matrix equation constitutes the complete equations of motion for the elastic airplane. In equation (9.41) $[M] = [\Phi]^T [M] [\Phi]$ which is called the generalized mass, where:

$$[\Phi] = [[\Phi_T] \vdots [\Phi_R] \vdots [\Phi_E]]$$

$$[\Phi_T] = \begin{bmatrix} 1 & 0 & 0 \\ 0 & 1 & 0 \\ 0 & 0 & 1 \\ \vdots & & \\ 0 & 1 & 0 \\ 0 & 0 & 1 \end{bmatrix}$$

$$[\Phi_R] = \begin{bmatrix} [\Phi_{R_1}] \\ [\Phi_{R_2}] \\ \vdots \\ [\Phi_{R_n}] \end{bmatrix} \quad \text{where: } [\Phi_{R_i}] = \begin{bmatrix} 0 & r_{ci_z} & -r_{ci_y} \\ -r_{ci_z} & 0 & r_{ci_x} \\ r_{ci_y} & -r_{ci_x} & 0 \end{bmatrix}$$

and

$[\Phi_E]$ are the 3n-6 elastic mode shapes (if three translational degrees of freedom are considered for each lumped mass)

The matrix $[\omega_i^2]$ contains zeros for the first six diagonal elements corresponding to the airplane mass center degrees of freedom. The three

matrices, $[M_1]$, $[M_2]$, and $[M_3]$, contain the generalized aerodynamic stiffness, aerodynamic damping, and apparent mass aerodynamics, respectively. For the 707-320B analysis $[M_3]$ was set equal to zero. The remaining terms are as follows:

$$[M_4] = \left[\begin{array}{ccc|ccc|c} 0 & 0 & 0 & 0 & (g\cos\theta_1) & 0 & 0 \cdots \\ 0 & & & 0 & (g\sin\theta_1 \sin\phi_1) & (-g\cos\theta_1 \cos\phi_1) & 0 \cdots \\ 0 & & & 0 & (g\sin\theta_1 \cos\phi_1) & (g\cos\theta_1 \sin\phi_1) & 0 \cdots \\ \hline 0 & & & & & & \\ \vdots & & & & 0 & & 0 \\ 0 & & & & & & \end{array}\right]$$

$$[M_5] = \left[\begin{array}{ccc|ccc|cccc} 0 & 0 & 0 & 0 & W_1 & -V_1 & 0 & 0 & \cdots & 0 \\ 0 & 0 & 0 & -W_1 & 0 & U & 0 & 0 & \cdots & 0 \\ 0 & 0 & 0 & V_1 & -U & 0 & 0 & 0 & \cdots & 0 \\ \hline 0 & 0 & 0 & & & & & & & \\ \vdots & \vdots & \vdots & & 0 & & & 0 & & \\ 0 & 0 & 0 & & & & & & & \end{array}\right]$$

$$\{q\} = \begin{Bmatrix} \{q_T\} \\ \{q_R\} \\ \{q_E\} \end{Bmatrix}$$

where

$$\{q_T\} = \begin{Bmatrix} x \\ y \\ z \end{Bmatrix}, \quad \{q_R\} = \begin{Bmatrix} \psi \\ \theta \\ \phi \end{Bmatrix}, \quad \{q_E\} = \text{3n-6 generalized coordinates for the elastic degrees of freedom.}$$

The equations of motion (9.41) may be separated into a longitudinal and a lateral-directional set. For longitudinal motion

$$\dot{q}_2 = v = 0$$
$$\dot{q}_4 = p = 0$$
$$\dot{q}_6 = r = 0$$

Therefore, $\{\dot{q}\} = \begin{Bmatrix} u \\ w \\ q \\ \dot{q}_E \end{Bmatrix}$

and the $\{\dot{q}_E\}$ correspond to only the symmetric mode shapes. Also,

$$[\bar{M}] = \left[\begin{array}{cc|c} M & & 0 \\ & M & \\ & & I_{yy} \\ \hline 0 & & [\phi_E^s]^T [M] [\phi_E^s] \end{array}\right]$$

$$[\omega_i^2][\bar{M}] = \left[\begin{array}{c|c} 0 & 0 \\ \hline 0 & [\omega_i^2][\phi_E^s]^T [M] [\phi_E^s] \end{array}\right]$$

and the $[\phi_E^S]$ denotes symmetric mode shapes. The remaining matrices of equation (9.41) for longitudinal motion are given by:

$$[M_1] = \begin{bmatrix} 0 & 0 & f_{Az,\alpha} & f_{Az,q_{E_1}} & \cdots & f_{Az,q_{E_i}} & \cdots \\ 0 & 0 & f_{Az,\alpha} & f_{Az,q_{E_1}} & \cdots & f_{Az,q_{E_i}} & \cdots \\ 0 & 0 & m_{Ay,\alpha} & m_{Ay,q_{E_1}} & \cdots & m_{Ay,q_{E_i}} & \cdots \\ 0 & 0 & f_{i,\alpha} & f_{i,q_{E_1}} & & & \\ 0 & 0 & \vdots & \vdots & & & \\ 0 & 0 & f_{i,\alpha} & f_{i,q_{E_1}} & \cdots & f_{i,q_{E_i}} & \cdots \end{bmatrix}$$

$$[M_2] = \begin{bmatrix} \frac{\partial f_{Az}}{\partial u} & \frac{f_{Az,\alpha}}{u_0} & f_{Az,q} & f_{Az,\dot{q}_{E_1}} & \cdots \\ \frac{\partial f_{Az}}{\partial u} & \frac{f_{Az,\alpha}}{u_0} & f_{Az,q} & f_{Az,\dot{q}_{E_1}} & \cdots \\ \frac{\partial m_{Ay}}{\partial u} & \frac{m_{Ay,\alpha}}{u_0} & m_{Ay,q} & m_{Ay,\dot{q}_{E_1}} & \cdots \\ \frac{\partial f_i}{\partial u} & \cdots & & & \\ \vdots & & & & \end{bmatrix}$$

As stated earlier, $[M_3]$ was set equal to zero for both the longitudinal and lateral-directional analyses. Similar expressions for $[M_1]$ and $[M_2]$ could be shown for the lateral-directional case.

The equations of motion were analyzed in several ways, as listed below.

(1) The roots of the characteristic equation were computed with varying numbers of elastic modes included in the equations.

(2) Roots and time histories were computed with the modes treated in a static elastic manner, as described later in this discussion.

(3) Roots were computed with Wagner lift growth functions applied to the circulator aerodynamic forces.

(4) Terms in rigid-body positions of the matrices were multiplied by the appropriate dimensional constants to reduce them to stability derivatives. The rigid-body derivatives were compared to the comparable terms from the static elastic formulation in order to observe the effects of elasticity on the rigid-body derivatives.

The results of the elastic analysis of the 707-320B were shown and discussed in Sec. 6.

9.2.2.3 The static elastic equations: The static elastic formulation assumes that the designated flexible modes displace in a static manner; therefore, the velocity and acceleration coefficients are set equal to zero. The first step in forming the static elastic equations is to sum the terms of equation (9.41)

$$[A]\{q\} + [B]\{\dot{q}\} + [C]\{\ddot{q}\} = \{0\} \qquad (9.42)$$

where

$$[A] = [\tilde{\omega}^2][\bar{M}] + [M_1] + [\tilde{\bar{M}}][M_4]$$

$$[B] = [M_2] + [\tilde{\bar{M}}][M_5]$$

$$[C] = [\tilde{\bar{M}}] + [M_3] \quad ; \quad [M_3] = [0]$$

Equation (9.42) is written in partitioned form,

$$\left[\begin{array}{c|c} A_{11} & A_{12} \\ \hline A_{21} & A_{22} \end{array}\right] \left\{\begin{array}{c} q_1 \\ \hline q_2 \end{array}\right\} + \left[\begin{array}{c|c} B_{11} & 0 \\ \hline B_{21} & 0 \end{array}\right] \left\{\begin{array}{c} \dot{q}_1 \\ \hline \dot{q}_2 \end{array}\right\} + \left[\begin{array}{c|c} C_{11} & 0 \\ \hline C_{21} & 0 \end{array}\right] \left\{\begin{array}{c} \ddot{q}_1 \\ \hline \ddot{q}_2 \end{array}\right\} = \left\{\begin{array}{c} 0 \\ \hline \end{array}\right\} \qquad (9.43)$$

where

$\{q_1\}$ = generalized coordinates to be retained as dynamic

$\{q_2\}$ = generalized coordinates to be treated as static elastic

The partitions of equation (9.43) are multiplied out

$$[A_{11}]\{q_1\} + [A_{12}]\{q_2\} + [B_{11}]\{\dot{q}_1\} + [C_{11}]\{\ddot{q}_1\} = \{0\} \qquad (9.44)$$

$$[A_{21}]\{q_1\} + [A_{22}]\{q_2\} + [B_{21}]\{\dot{q}_1\} + [C_{21}]\{\ddot{q}_1\} = \{0\} \qquad (9.45)$$

Equation (9.45) is solved for $\{q_2\}$

$$\{q_2\} = [A_{22}]^{-1}([A_{21}]\{q_1\} + [B_{21}]\{\dot{q}_1\} + [C_{21}]\{\ddot{q}_1\}) \qquad (9.46)$$

Equation (9.46) is substituted into equation (9.44) to obtain the final form of the static elastic equations.

$$([A_{11}]-[A_{12}][A_{22}]^{-1}[A_{21}])\{q_1\}+([B_{11}]-[A_{12}][A_{22}]^{-1}[B_{21}])\{\dot{q}_1\} +([C_{11}]-[A_{12}][A_{22}]^{-1}[C_{21}])\{\ddot{q}_1\} \qquad (9.47)$$

Rigid derivatives and elastic corrections from all modes being treated as static elastic were compared in tables 9 and 10.

9.2.2.4 Lift growth functions: Two lift growth (Wagner) functions were selected from ref. 42 and incorporated into the flexible equations for two cases to study their effect. The Wagner functions are indicial (step) response functions for lift growth on an airfoil that has experienced a step input in angle of attack. The exponential functions that are listed in ref. 42 are approximations of the exact solutions. The exact solutions are for incompressible flow for an infinite wing, an aspect ratio 6 wing with elliptical lift distribution and an aspect ratio 3 wing with elliptical lift distribution. The aspect ratio 3 and 6 functions were selected for study and are listed below.

$$\begin{aligned} &AR = 3 \quad \text{approximation} \\ &K(\tau) = 1 - .283\, e^{-.54\tau} \quad ; \qquad \tau = \frac{2V_0}{c}t \\ &AR = 6 \quad \text{approximation} \\ &K(\tau) = 1 - .361\, e^{-.381\tau} \end{aligned} \qquad (9.48)$$

The lift growth functions were incorporated into the equations of motion by applying the convolution (Duhamel's) integral. The equations of motion were written in the form

$$[A_1]\{q\}+[A_2]\{\dot{q}\}+[A_3]\{\ddot{q}\}+[A_4]\{q\}*\dot{K}+[A_5]\{\dot{q}\}*\dot{K}=\{0\} \qquad (9.49)$$

where

$$[A_1] = [\omega^2][M] + [\bar{M}][M_4]$$

$[A_1]$ = generalized structural stiffness and gravity perturbation

$[A_2]$ = noncirculatory aerodynamic velocity coefficients (ref. 26)

$[A_3] = [\bar{M}]$ = generalized inertia coefficients

$[A_4] = [M_2]$ = circulatory aerodynamic displacement coefficients (ref. 26)

$[A_5]$ = circulatory aerodynamic velocity coefficients

$$[A_2] + [A_5] = [M_2] + [\bar{M}][M_5]$$

and the symbol, *, denotes the convolution integral as

$$q * \dot{K} = \int_0^t K(t-\tau)\, q(\tau)\, d\tau$$

The Laplace transformed equations of motion appear as

$$\left[[A_1] + [A_2]s + [A_3]s^2 + [A_4]\bar{K}(s) + [A_5]s\bar{K}(s) \right] \{\bar{q}(s)\} = \{0\} \qquad (9.50)$$

The Laplace transformation of the first time derivative of the Wagner function is

$$\mathcal{L}[\dot{K}] = s\mathcal{L}[K] = \bar{\dot{K}} = 1 - \frac{\alpha s}{s+\beta} = \frac{(1-\alpha)s + \beta}{s+\beta} \qquad (9.51)$$

where

$$\alpha = .283 \quad \text{or} \quad .361$$

$$\beta = .54\,\frac{2U_0}{c} \quad \text{or} \quad .381\,\frac{2U_0}{c}$$

Substituting equation (9.51) into (9.50) and clearing the fraction gives

$$\left[(s+\beta)\left[[A_1] + [A_2]s + [A_3]s^2 \right] + (s + \alpha s + \beta)\left[[A_4] + [A_5]s \right] \right] \{\bar{q}(s)\} = \{0\} \qquad (9.52)$$

Equation (9.52) was solved with the aspect ratio 6 function for a longitudinal case and with the aspect ratio 3 and aspect ratio 6 functions for a lateral-directional case. The rigid-body roots with and without lift growth were listed and discussed in Sec. 6. Caution is in order when interpreting characteristic roots when lift growth functions are included in equations. The clearing of fractions to obtain equation (9.52) is an operation that introduces extraneous roots.

9.3 SST Analysis

For the elastic dynamic analysis of the SST, the airplane was idealized by panels the same as for the calculation of elastic derivatives described in app. B. The completely elastic SST analysis was accomplished only for the longitudinal mode. The longitudinal motion was approximated by two rigid-body degrees of freedom. This approximation does, of course, delete the phugoid motion. The equation of motion for the completely elastic airplane was written in the form

$$[M]\{\ddot{z}\} + [B]\{\dot{z}\} + [K]\{z\} + [K_A]\{\alpha\} = \{0\} \qquad (9.53)$$

where

Z_i = vertical displacement of each panel about equilibrium position

α_i = panel angle of attack consistent with the displacement Z_i

$[M]$ = mass matrix

$[B]$ = matrix of aerodynamic velocity coefficients

$[K]$ = structural stiffness matrix

$[K_A] = \bar{q}[A]$, where $[A]$ is the matrix of aerodynamic influence coefficients as discussed in apps. A and B

Equation (9.53) is changed to generalized coordinates by substituting

$$\{z\} = [\phi]\{q\}$$
$$\{\alpha\} = [\theta]\{q\} \qquad (9.54)$$

The angle mode matrix $[\theta]$ is defined such that the structural deformations, Z_i, are consistent with the twist deformations, α_i. The procedure used to find $[\theta]$ will be described later.

When equation (9.53) is premultiplied by $[\phi]^T$, the following form of the equation of motion results

$$[\bar{M}]\{\ddot{q}\} + [\bar{C}]\{\dot{q}\} + [\bar{K}]\{q\} = 0 \qquad (9.55)$$

Equation (9.55) was rooted by a standard complex eigenvalue routine. Time histories were also determined from equation (9.55) using a standard numerical integration routine. Section 5 presents a discussion of the characteristic equation and time history methods used for the completely elastic airplanes. The discussion of results for the elastic analysis is contained in Sec. 6.

The three coefficient matrices of equation (9.55) are formed as follows:

$$[\bar{M}] = [\phi]^T [M] [\phi] \tag{9.56}$$

$$[\bar{C}] = \frac{\bar{q}}{V} [\phi]^T [A] [\phi] \tag{9.57}$$

where

$[A]$ = aerodynamic influence matrix described in app. B

$\bar{q}$ = dynamic pressure

V = flight velocity

$$[\bar{K}] = [\phi]^T [K] [\phi] + \bar{q} [\phi]^T [A] [\theta] \tag{9.58}$$

where

$[K]$ = structural stiffness matrix

S5 Equation (9.56) needs no explanation, except to say that it is diagonal and that $[M]$ is merely the mass lumped at each panel point.

Equation (9.57) was formed by first considering the relation between panel airloads and the aerodynamic matrix $[A]$.

$$\{P\} = \bar{q} [A] \{\alpha\} \tag{9.59}$$

where

$\{P\}$ = panel airloads

$\{\alpha\}$ = panel incidence

The relation between velocities normal to the freestream, $\{\dot{z}\}$, and the change in incidence is

$$\{\alpha\} = \frac{\{\dot{z}\}}{V} \tag{9.60}$$

(G8)

using small perturbation approximations. Therefore, equation (9.59) becomes

$$\{P\} = \bar{q}\,[A]\,\frac{\{\dot{z}\}}{V} \tag{9.61}$$

Equation (9.61) is equivalent to the second term of equation (9.53), which gives the forces due to panel velocity normal to the freestream. Equating this term and equation (9.61), we get

$$[B] = \frac{\bar{q}}{V}\,[A] \tag{9.62}$$

Therefore, the expression for equation (9.57) follows

$$[\bar{c}] = \frac{\bar{q}}{V}\,[\phi]^T[A][\phi]$$

The term $[\phi]^T[K]\ [\phi]$ is identical to $[\bar{M}][\omega^2]$, which has been shown in par. 9.2, equation (9.21). The matrix $[\omega^2]$ is a diagonal matrix of frequencies associated with the individual mode shapes. The generalized stiffness was computed by the $[\bar{M}][\omega^2]$ formulation since it is so simple and the frequencies have already been calculated.

The components of equations (9.56) and (9.57) were determined by techniques previously described in apps. A and B. The calculation of the term $[\theta]$ has not been described previously and is described in detail in the following paragraphs.

Since the aerodynamic forces are a function of the angle of attack of each panel, it is necessary to convert each structural mode shape to a set of angles of attack corresponding to the mode shape. The problem thus becomes one of defining an angle matrix, $[\theta]$, such that

$$\{\alpha\} = [\theta]\{q\} \tag{9.63}$$

where $\{\alpha\}$ is the column of angles of attack resulting from a defined deflection shape in terms of the generalized coordinates $\{q\}$. The procedure for finding $[\theta]$ is to require the structural deformations, Z_i, to be consistent with the twist deformations, α_i, where

$$\{Z\} = [\Phi]\{q\} \tag{9.64}$$

The total structural influence matrix is generated such that when it is partitioned it appears as

$$\begin{Bmatrix} Z_E \\ \alpha_E \end{Bmatrix} = \left[\begin{array}{c|c} C_{11} & C_{12} \\ \hline C_{21} & C_{22} \end{array}\right] \begin{Bmatrix} F \\ M \end{Bmatrix} \tag{9.65}$$

Since the moments on each panel are zero as generated by the current aerodynamic theory, equation (9.65) can be rewritten as

$$\{Z_E\} = [C_{11}]\{F\} \tag{9.66}$$

and

$$\{\alpha_E\} = [C_{21}]\{F\} \tag{9.67}$$

In equations (9.66) and (9.67), $\{Z_E\}$ and $\{\alpha_E\}$ are displacements and rotations resulting from elastic deformations. To find the total displacement for any particular position of the reference point, one must include the rigid-body motion associated with the reference point displacement. The vertical displacement then becomes

$$\{Z\} = [C_{11}]\{F\} + Z_r\{1\} + \alpha_r\{X\} \tag{9.68}$$

and the angle-of-attack displacement becomes

$$\{\alpha\} = [C_{21}]\{F\} + \alpha_r\{1\} \tag{9.69}$$

Solving equation (9.68) for $\{F\}$ and substituting into equation (9.69) yields

$$\{\alpha\} = [C_{21}][C_{11}]^{-1}\left\{\{Z\} - Z_r\{1\} - \alpha_r\{X\}\right\} + \alpha_r\{1\} \tag{9.70}$$

Substituting equations (9.63) and (9.64) into equation (9.70) for the i^{th} mode shape yields

$$\{\theta\}_i q_i = [C_{12}][C_{11}]^{-1}\{\phi\}_i q_i - [C_{12}][C_{11}]^{-1}\{1\}(\phi_{r_i})\, q_i - [C_{12}][C_{11}]^{-1}\{X\}(\theta_{r_i}) q_i + \{1\}(\theta_{r_i})\, q_i \tag{9.71}$$

where

ϕ_{r_i} = element of $[\phi]$ corresponding to structural reference point, r, and i^{th} structural mode

θ_{r_i} = same definition as above for element from angle mode matrix, $[\theta]$

$(\phi_{r_i})q_i$ = displacement at the structural reference point, r, due to mode i

$(\theta_{r_i})q_i$ = rotation of the point r due to mode i

Since q_i is a nonzero constant it can be divided out of equation (9.71), yielding $\{\theta\}$ for the i^{th} mode shape. Equation (9.71) can be written for many mode shapes by an expansion resulting in

$$[\theta] = [C_{12}][C_{11}]^{-1}\left[[\phi] - \{1\}\,\lfloor\phi\rfloor_r - \{X\}\,\lfloor\theta\rfloor_r\right] + \{1\}\,\lfloor\theta\rfloor_r \tag{9.72}$$

The $\lfloor\phi\rfloor_r$ and $\lfloor\theta\rfloor_r$ matrices are from the r^{th} row corresponding to the structural reference mass point and have m elements, where m is the number of modes considered. The matrices $[\phi]$ and $[\theta]$ are of order n x m, where n is the number of mass points and m the number of structural modes. Equation (9.72) was used for determining the angle mode shapes during the current study.

The sequencing of computer programs used for the SST completely elastic dynamic analysis is shown schematically in fig. 111.

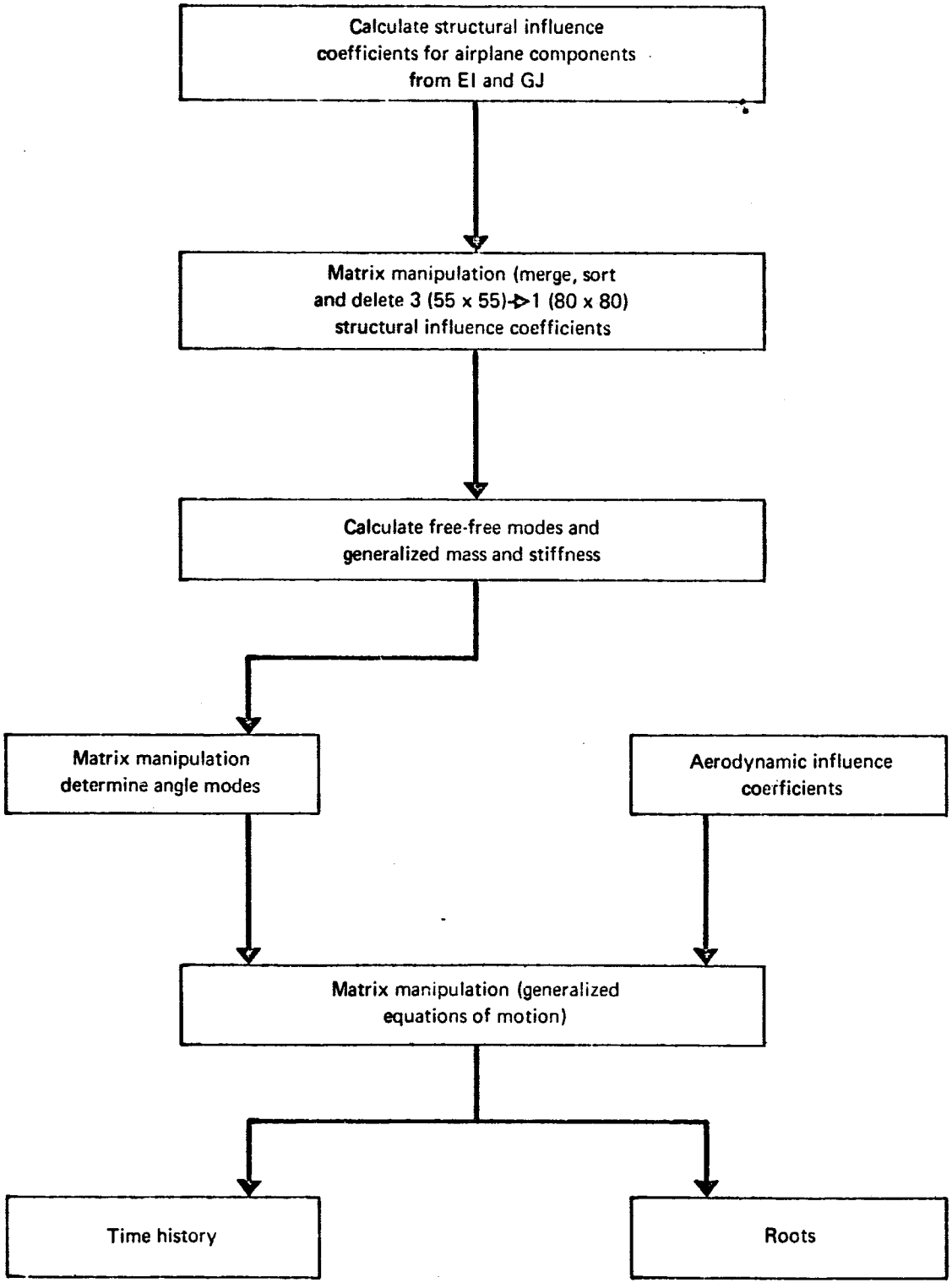

FIGURE 111. SCHEMATIC OF PROGRAM SEQUENCING FOR SST DYNAMIC ANALYSIS

10. CONCLUSIONS AND RECOMMENDATIONS

10.1 Conclusions

The airplanes used in the method comparisons are subsonic and supersonic jet transport types. Most of the conclusions could be applied to similar airplane types that fly within the study flight envelope. However, nearly all the conclusions regarding static elastic and dynamic elastic effects are highly configuration dependent and care should be followed. A general conclusion is that the effects of aeroelasticity appear to be more significant for the static than the dynamic stability characteristics.

Results of the static stability investigation (Sec. 4) show the following.

(1) The lifting surface theory (aerodynamic influence coefficient method) gives better predictions than handbook methods for some cases (using rigid wind tunnel data as the basis for comparison). Changes in the lifting surface theory mechanization program are expected to improve the predictions, as discussed in app. B.

(2) The lifting surface theory (aerodynamic influence coefficient method) gives direct, acceptable results for some stability characteristics for equivalent elastic and rigid airplanes. However, if wind tunnel data are available, a more accurate way of predicting elastic effects would be to compute an elastic-to-rigid ratio or increment that is referenced to the wind tunnel value (app. B). For example,

$$Cm_{\alpha_{eq\ el}} = \left.\frac{Cm_{\alpha_{elastic}}}{Cm_{\alpha_{rigid}}}\right|_{ls} \cdot \left. Cm_{\alpha_{rigid}}\right|_{WT}$$

The results of the longitudinal dynamic stability investigation are listed below in their approximate order of importance.

(1) Dynamic stability characteristics are more sensitive to aerodynamic derivative accuracy than to elastic effects.

(2) Elastic effects on the dynamic stability characteristics are relatively small.

(3) Quasi-static treatment of aeroelastic effects can predict more significant changes in stability characteristics than does the inclusion of many dynamically participating elastic degrees of freedom.

(4) Considering only a few (less than about 10) elastic degrees of freedom can produce results that are misleading as to the trends and significance of the effects of aeroelasticity.

(5) Adding many elastic degrees of freedom consistently decreased the damping for the study airplanes.

(6) No consistent trends appear in the variation of frequency due to adding many elastic degrees of freedom.

(7) No consistent trends appear as to the adequacy of either lifting surface derivatives or handbook derivatives in predicting the dynamics. A method that is satisfactory for one configuration may not be for another.

(8) Approximate formulas for frequency and damping for longitudinal dynamics are very satisfactory for some configurations where C_{m_α} is dominant. Approximate expressions would be useful mainly for preliminary design. Time history methods find their use mainly when nonlinear aerodynamic data are available or when the response to arbitrary control inputs is desired. Also, time history programs can show the response to extreme conditions — engine-out conditions, for instance. Characteristic equation methods can be used to analyze the stability of an airplane only if linear equations are used.

(9) The adequacy of a particular mathematical model (structural or aerodynamic) for the longitudinal dynamics would be an important consideration of a handling-qualities study.

The results of the lateral-directional dynamic stability investigation are listed below in their approximate order of importance.

(1) For many cases the variations in dynamic characteristics for the rigid airplane from using different methods of calculating the stability derivatives are as large as any elastic effects. This points to the fact that a sophisticated, completely elastic airplane mathematical model is only as good as the basic rigid stability derivatives.

(2) The elastic effects on the Dutch roll period are quite small. A good equivalent elastic analysis will predict the period of this mode accurately enough for stability and control purposes. The structural modes have a very small effect on the period.

(3) For the Boeing 707-320 the damping of the Dutch roll mode decreases with the addition of the first few elastic modes, but then increases very slightly as more elastic degrees of freedom are added. A static elastic analysis would appear to predict the damping with sufficient accuracy.

(4) The truncated, completely elastic airplane model gave good correlation with flight test data for the Dutch roll mode. The static elastic representation tends to overpredict the amount of damping present, but the difference is considered unimportant.

(5) The equivalent elastic handbook as developed in app. B for the lateral-directional modes is incapable of accurately predicting the dynamics.

(6) Lifting surface aerodynamic methods are not mechanized at the present time for predicting the lateral-directional stability derivatives. Handbook techniques and wind tunnel data were used almost exclusively to generate the rigid stability derivatives.

(7) Approximate expressions for frequency and damping are accurate enough for some configurations for the Dutch roll mode; however, since these formulas tend to be unreliable, characteristic equation methods are recommended.

10.2 Recommendations

10.2.1 Longitudinal dynamic analyses. — For longitudinal dynamic stability analyses within the scope of the various stages of airplane development, the following procedures and improvements are recommended.

(1) Preliminary Design: Use small perturbation-type programs or approximate techniques utilizing wind tunnel or lifting surface derivative data as available and supplement with handbook data. A mechanized, analytical approach to generating rate derivatives ($C_{m_{\dot{\alpha}}}$, C_{m_q}, C_{L_q}, etc.) in conjunction with the current lifting surface methods would be an invaluable tool. A rigid or equivalent elastic analysis of this type should be adequate.

(2) Product Development: Use wind tunnel data supplemented by handbook data plus elastic increments/ratios determined by using lifting surface methods. Here again, a more detailed mechanization of lifting surface derivative methods is desirable. An analysis using dynamically

participating elastic modes should be accomplished in order to ascertain what is an "adequate" mathematical model. Addition of the effects of elastic modes to the time history (nonlinear aerodynamic data) capability would generate another invaluable tool.

(3) End Product or Flight Test: Use the same analysis as in (2) above. Here, however, it would be very desirable to incorporate the "corrector matrix" technique* of app. B into the additions already mentioned in (2) (that is, mechanization of more sophisticated derivative and coefficient techniques and the capability of accounting for dynamic modes).

10.2.2 Lateral-directional dynamic analyses. — For modern, transport-type airplanes, the proximity of lateral-directional dynamic stability boundaries and characteristics and their sensitivity to both aerodynamic and structural representations demand more sophisticated analytical techniques. It appears that nothing short of the capabilities available or recommended for longitudinal analyses (lateral-directional lifting surface methods) will suffice.

*The corrector matrix technique utilizes experimental data to modify aerodynamic influence coefficients generated using lifting surface methods to account for nonlinear aerodynamic effects.

11. REFERENCES

This section includes all of the references for the Summary Report and the three appendixes.

1. Bisplinghoff, R. L.; and Ashley, H.: Principles of Aeroelasticity. John Wiley and Sons, Inc., 1962.

2. Milne, R. D.: Dynamics of the Deformable Airplane, Parts I and II. Her Majesty's Stationery Office, London, 1964.

3. Frazer, R. A.; Duncan, W. J.; and Collar, A. R.: Elementary Matrices. Cambridge University Press, 1952.

4. Etkin, Bernard: Dynamics of Flight. John Wiley and Sons, Inc., 1962.

5. Schwendler, R. G.; and MacNeal, H.: Optimum Structural Representation in Aeroelastic Analysis. ASD-TR-61-680, Computer Engineering Associates, March 1962.

6. Anon.: USAF Stability and Control Handbook. AF33(616)-6460, Douglas Aircraft Company, 1960.

7. Lamb, H.: Hydrodynamics. Second ed., Dover Publications, 1945.

8. Sokolnikoff, I. S.: Mathematical Theory of Elasticity. McGraw-Hill Book Company, Inc., 1956.

9. Hildebrand, F. B.: Advanced Calculus for Engineers. Prentice-Hall, Inc., 1957.

10. Anon.: Military Specification Flying Qualities of Piloted Airplanes. MIL-F-8785 (ASG), April 17, 1959.

11. Anon.: British Civil Airworthiness Requirements. Section D Aeroplanes, Air Registration Board, Issue 8, February 1, 1966.

12. Anon.: Proposal for a Revised Military Specification, Flying Qualities of Piloted Airplanes. MIL-F-8785 (ASG), with Substantiating Text. Bureau of Naval Weapons, Washington, D.C., Report No. NADC-ED-6282, January 18, 1963.

13. Seckel, E.: Stability and Control of Airplanes and Helicopters. Academic Press, Inc., 1964.

14. Babister, A. W.: Aircraft Stability and Control. Pergamon Press, Inc., 1961.

15. Perkins, C. D.; and Hage, R. E.: Airplane Performance, Stability and Control. John Wiley and Sons, Inc., 1957.

16. Kolk, W. R.: Modern Flight Dynamics. Prentice-Hall, Inc., 1961.

17. Abramson, H. N.: The Dynamics of Airplanes. The Ronald Press Company, 1958.

18. Chestnut, H.; and Mayer, R. W.: Servomechanisms and Regulating System Design. Second ed., John Wiley and Sons, Inc., 1963.

19. Graham, D.; and McRuer, D.: Analysis of Nonlinear Feedback Control Systems. John Wiley and Sons, Inc., 1961.

20. Pastel, M. P.; and Thaler, G. J.: Analysis and Design of Nonlinear Feedback Control Systems. McGraw-Hill Book Company, Inc., 1962.

21. Levinson, Emanuel: Nonlinear Feedback Control Systems. Electro-Technology, July through December 1962.

22. Davis, Harold T.: Introduction to Nonlinear Differential and Integral Equations. Government Printing Office, September 1960.

23. Roskam, J.: On Some Linear and Nonlinear Stability and Response Characteristics of Rigid Airplanes and a New Method to Integrate Nonlinear Ordinary Differential Equations. PhD Dissertation, University of Washington, July 1965.

24. Jaffe, Peter: A Generalized Approach to Dynamic-Stability Flight Analysis. JPL Technical Report No. 32-757, July 1965.

25. Hahn, Wolfgang, ed. and trans.: Theory and Application of Liapunov's Direct Method. Prentice-Hall, Inc., 1963.

26. Bisplinghoff; Ashley; and Hoffman: Aeroelasticity. Addison-Wesley Publishing Company, Inc., 1955.

27. Ashley; and Landahl: Aerodynamics of Wings and Bodies. Addison-Wesley Publishing Company, Inc., 1965.

28. Miles, J. W.: The Potential Theory of Unsteady Supersonic Flow. Cambridge University Press, 1959.

29. Chester, W.: Supersonic Flow Past Wing-Body Combinations. The Aeronautical Quarterly, Vol. IV, August 1953, pp. 287-314.

30. Ward, G. N.: Linearized Theory of Steady High-Speed Flow. Cambridge University Press, 1955.

31. Van Dyke, Milton D.: Supersonic Flow Past Oscillating Airfoils Including Nonlinear Thickness Effects. NACA Report 1183, 1954.

32. Bryson, Arthur E.: Stability Derivatives for a Slender Missile with Application to a Wing-Body-Vertical Tail Configuration. J. Aeron. Sci., Vol. 20, May 1953.

33. Landau; and Lifshitz (J. B. Sykes and J. S. Ball, trans.): Mechanics. Addison-Wesley Publishing Company, Inc., 1960.

34. Hayes, W. D.: and Probstein, R. F.: Hypersonic Flow Theory. Academic Press, Inc., 1959.

35. Woodward, F.; LaRowe, E.; and Love, J. E.: Analysis and Design of Supersonic Wing-Body Combinations, Including Flow Properties in Near Field. Part I and II, NASA Report CR-73107, 1967.

36. Anon.: Flight Control and Fire Control System Manual. Vol. II, AE-61-4 II, Bureau of Aeronautics (prepared by Northrop Corporation), September 1952.

37. Francis, J. G. F.: The QR Transformation. Part I. The Computer Journal, Vol. 4, No. 3, October 1961, pp. 263-271. Part II, IBIO, January 1962, pp. 332-345.

38. Wilkinson, J. H.: The Algebraic Eigenvalue Problem. Clarendon Press, Oxford, 1965.

39. Pearce, B. F.; Johnson, W. A.; and Siskind, R. K.: Analytical Study of Approximate Longitudinal Transfer Functions for a Flexible Airframe. ASD-TDR-62-279, June 1962.

40. Samson, F. J.; and Petersen, Harry E.: MIMIC Programming Manual, SEG-TR-67-31, July 1967.

41. Van Dyke, M.: Perturbation Methods in Fluid Mechanics. Academic Press, Inc., 1964.

42. Fung, Y. C.: An Introduction to the Theory of Aeroelasticity. John Wiley and Sons, Inc., 1955.

43. Milne, R. D.: Some Remarks on the Dynamics of Deformable Bodies. AIAA Journal, Vol. 6, March 1968.

44. Anon.: Air Worthiness Standards, Transport Category Airplanes. FAR, Part 25 Federal Aviation Administration.

45. Kuo, B. C.: Automatic Control Systems. Prentice-Hall, Inc., 1962.

46. Korn, G. A.; and Korn, T. M.: Mathematical Handbook for Scientists and Engineers. McGraw-Hill Book Company, Inc., 1961.

47. Hamming, R. W.: Numerical Methods for Scientists and Engineers. McGraw-Hill Book Company, Inc., 1962.

48. Anon.: International Dictionary of Applied Mathematics. D. van Nostrand Company, Inc., 1960.

49. Duncan, W. J.: The Principles of the Control and Stability of Aircraft. Cambridge University Press, 1956.

50. Rheinfurth, Mario H.; and Swift, Frederick W.: A New Approach to the Explanation of the Flutter Mechanism. NASA TN D-3125, 1966.

51. Haus, F. C.; Czinczenheim, J.; and Moulin, L.: The Use of Analog Computers in Solving Problems of Flight Mechanics. Agardograph 44, June 1960.

52. Chetayev, N. G.: The Stability of Motion. Pergamon Press, Inc., 1961.

53. Malkin, I. G.: Theory of Stability of Motion. AEC-TR-3352, translated from the publication of the State Publishing House of Technological-Theoretical Literature, Moscow-Leningrad, 1952.

54. Lefferts, Eugene J.: A Guide to the Application of the Lyapunov Direct Method to Flight Control Systems. NASA CR-209, 1966.

55. Bryan, G. H.: Stability in Aviation. The Macmillan Company, 1911.

56. Milne-Thomson, L. M.: Theoretical Aerodynamics. The Macmillan Company, 1948.

57. Green, A. E.; and Zerna, W.: Theoretical Elasticity. Clarendon Press, Oxford, 1960.

58. Pearce, B. F.: Topics on Flexible Airplane Dynamics, Part I. ASD-TDR-63-334, Systems Technology, Inc., Inglewood, California, 1963.

59. Heaslet, Max A.; Lanar, Harvard; and Jones, Arthur L.: Volterra's Solution of the Wave Equation as Applied to 3-Dimensional Supersonic Airfoil Problems. NASA Report No. 889, Ames Aeronautical Laboratory, Moffett Field, California, April 14, 1947.

60. Pope, A.: Basic Wing and Airfoil Theory. McGraw-Hill Book Company, Inc., 1952.

61. Nelson, H. C.; and Berman, J. H.: Calculations on the Forces and Moments for an Oscillating Wing-Aileron Combination in Two-Dimensional Potential Flow at Sonic Speeds. NACA TN 2590, 1952.

62. Rubbert, P. E.; et al.: A General Method for Determining the Aerodynamic Characteristics of Fan-in-Wing Configurations. Vol. I - Theory and Application. USAAVLABS Technical Report 67-61A, 1967.

63. Campbell, J. P.; Johnson, J. L., Jr.; and Hewes, D. E.: Low-Speed Study of the Effect of Frequency on the Stability Derivatives of Wings Oscillating in Yaw with Particular Reference to High Angle-of-Attack Conditions. NACA RM L55H05, 1955.

64. Weissinger, J.: The Lift Distribution of Swept Back Wings. NACA TM 1120, 1947.

65. Tekhonov; and Samarskii (A.R.M. Robson and P. Basu, trans.): Equations of Mathematical Physics. Pergamon Press, Inc., 1963.

66. Royal Aeronautical Society Data Sheets, 1955.

67. Anon.: Aerodynamic Characteristics of Non-Straight-Taper Wings. AFFDL-TR-66-73, General Dynamics, Fort Worth Division, October 1966.

68. Gray, W. L.; and Schenk, K. M.: Method for Calculating the Subsonic Steady-State Loading on an Airplane with a Wing of Arbitrary Planform and Stiffness. NACA TN 3030, 1953.

69. Johnson, J. L., Jr.: Low-Speed Measurements of Static Stability, Damping in Yaw, and Damping in Roll of a Delta, a Swept and an Unswept Wing for Angles-of-Attack from 0° to 90°. NACA RM L56B01, 1956.

70. Wiley, H. G.: The Significance of Nonlinear Damping Trends Determined for Current Aircraft Configurations. NASA U-59-15, September 1966.

71. Flack, Nelson D.: AFFTC Stability and Control Techniques. USAF Flight Test Center, Edwards Air Force Base, California, AFFTC-TN-59-21, 1959.

72. Campbell, J. P.; and McKinney, M. O.: Summary of Methods for Calculating Dynamic Lateral Stability and Response and for Estimating Lateral Stability Derivatives. NACA TR 1098, 1952.

73. Kohlman, D. L.; and Drake, L. R.: Handbook for Estimating C_{l_β} for Rigid and Elastic Airplanes at Subsonic and Supersonic Speeds. Center for Research Inc., Engineering Science Division, The University of Kansas, Lawrence, Kansas, 1966.

74. Pearce, B. F.; and Siskind, R. K.: Topics on Flexible Airplane Dynamics, Part II. The Application of Flexible Airframe Transfer Function Approximations and the Sensitivity of Airframe Transfer Functions to Elastic Mode Shapes. ASD-TDR-63-334, Part II, July 1963.

75. Pass, H. R.; Pearce, B. F.; and Wolkovitch, J.: Topics on Flexible Airplane Dynamics, Part III. Coupling of the Rigid and Elastic Degrees of Freedom on an Airframe. ASD-TDR-63-334, Part III, July 1963.

76. Pass, H. R.; and Pearce, B. F.: Topics of Flexible Airplane Dynamics, Part IV. Coupling of the Rigid and Elastic Degrees of Freedom of an Airframe-Autopilot System. ASD-TDR-63-334, Part IV, July 1963.